ABSTRACT

Title of Dissertation: 5′-MODIFIED LIPOPHILIC G-QUADRUPLEXES: STRUCTURAL STUDIES AND APPLICATIONS AS SCAFFOLDS FOR [2+2]PHOTOCYCLOADDITIONS

Keith Brandon Sutyak, Doctor of Philosophy, 2019

Dissertation directed by: Professor Jeffery T. Davis
Department of Chemistry and Biochemistry

Guanosine self-assembly is a powerful tool for constructing nanostructures and materials with intriguing properties. Guanosine's nucleobase has a hydrogen bond donor and acceptor face that in the presence of an appropriate templating cation can self-assemble to form larger G-quadruplex structures. Through the addition of a nonpolar solubilizing group on the 2′, 3′, or 5′ position of guanosine's ribose sugar, the G-quadruplex may be formed in organic solvents. Not surprisingly, any modification made to the guanine nucleobase can have a substantial effect on the self-assembly of the G-quadruplex core. These alterations can significantly alter or destroy the ability of the guanine base to form larger H-bond structures. For this reason, a major target for the synthetic modification of the G-quadruplex is the ribose sugar. Modifications to the sugar can be used to add new functionality or groups capable of modulating the G-quadruplexes stability and structure.

The 5′-position is easily esterified and is an ideal target for incorporating new functionality to the G-quadruplex, not not much was known about how esterification of the 5′-position of guanosine impacted self-assembly. In this thesis, a series of 5′-modified aryl esters of guanosine were synthesized G **21**-G **25**, comprising either activating or de-activating substituents on the aromatic rings, to systematically investigate how the addition of an ester to the 5′- position of guanosine affects the self-assembly G-quadruplex. The identity of the 5′-aryl ester was found to have a direct impact on the molecularity (how many Gs are in each assembly) and stability of the G-quadruplexes. The information gained from these experiments was applied to rationally design a new G-quadruplex capable of templating a [2+2] photocycloaddition reaction.

With an increased knowledge of how modifications to the 5′-position affect the structural integrity of the G-quadruplex, we applied this information to rationally design a new G-quadruplex system capable of templating a [2+2] photocycloaddition reaction. To achieve this goal a series of 5′-cinnamate esters G **26**-G **29** were synthesized and studied. Each derivative G **26**- G **29** when self-assembled into a G-quadruplex an photoirradiated underwent a photocycloadditon reaction ins high yields with good stereoselectivity. These same compounds when disassembled only underwent *trans-cis* photoisomerization. Highlighting the need for the G-quadruplex self-assembly.

5′-MODIFIED LIPOPHILIC G-QUADRUPLEXES: STRUCTURAL STUDIES AND APPLICATIONS AS SCAFFOLDS FOR [2+2] PHOTOCYCLOADDITIONS

by

Keith Brandon Sutyak

Dissertation submitted to the Faculty of the Graduate School of the
University of Maryland, College Park, in partial fulfillment
of the requirements for the degree of
Doctor of Philosophy
2019

Advisory Committee:
Professor Jeffery T. Davis, Chair
Professor Daniel E. Falvey
Assistant Professor Osvaldo Gutierrez
Associate Professor Paul J. Paukstelis
Associate Professor Ian M. White

© Copyright by
Keith Brandon Sutyak
2019

Acknowledgements

There are many people that have contributed to my success in graduate school over the years, and to them I owe my gratitude.

First and foremost, I would like to thank Professor Jeffery T. Davis for allowing me to develop my chemistry skills in his lab for the last 6 years. Thank you for all your guidance during my time at Maryland. Thank you for your patience and for constantly motivating me to improve. You have taught me many valuable lessons that will remain with me for the rest of my scientific career and life.

I would like to thank my thesis committee members, Prof. Daniel Falvey, Prof. Osvaldo Gutierrez, Prof. Paul Paukstelis, and Prof. Ian White, for your time and for all that I have learned from you over the course of my graduate school career.

There are many amazing facilities at the University of Maryland and they would be useless without the amazing staff. I would like to thank Dr. Yui-Fai Lam and Dr. Yinde Wang for teaching me the ways of the NMR. My time spent as your NMR TA has been an invaluable and will prove beneficial in my future endeavors. Thanks also to Dr. Fu Chen for your help in the NMR lab. Thanks to Dr. Peter Zavalij, who helped solve difficult crystal structures for me and my undergraduate mentees. Dr. Yue Li, thank you, you have always been very helpful in the mass spectrometry facility. Dr. Yan Wang in proteomics thank you for all your mass spectrometry help.

I'd like to special thanks to Wes Lee and Dr. Osvaldo Gutierrez whose calculations were instrumental to my understanding of G-quadruplex structure. Their

contributions really helped to shine a light on the structure and reactivity of photoreactive G-quadruplexes. Thank you to the Falvey's group for allowing me to bogart their light box for days at a time; Steve, Matt, Andrea, and Donald thanks. Thank you to Dr. Monique Koppel, you are selfless, are always there for me when I need a letter of recommendation and I will never be able to repay you.

During my time in graduate school my research was funded by the Office of Basic Energy Sciences of the U.S. Department of Energy by grant DE-FG02-98ER14888. I was also supported by: a GAANN Fellowship from the U.S. Department of Education, travel funds from The University of Maryland Jacob K. Goldhaber Travel Grant, and International Conference Student Support Award. Thank you for your support.

Thanks to all my lab mates for their helpful discussion and making lab a great place to work. To Taylor, Gretchen, Songjun, Luke, and Soumya thank you for all your knowledgeable insight and helpful suggestions. To Mitchell and Deiaa thanks for all the work you did in the lab. I hope I could teach you something that you can bring with you to graduate school to make you a better scientist from the jump. Big shout-out to Michael Robinson whose crystal growing prowess is second to none.

Thank you to all of my Grad school friends. Natalie thanks for always putting up with my shenanigans and dealing with me when I am stressed out and not at my best. I love you.

To my family, you are the best. Mom, Dad, Kristen, Bryan, Jairo, and Maritza thanks for always believing in me.

Table of Contents

List of Figures

Chapter 1: Factors that Influence G-Quadruplex Self-Assembly and G-Quadruplex Promoted Chemical Reactions

1.1 Introduction

Self-assembly is a powerful tool for building highly-ordered nanostructures. Complex structures can be made rapidly in near quantitative yields using only non-covalent interactions. The G-quadruplex is a supramolecular structure that depends on non-covalent interactions to drive its assembly. The G-quadruplex depends on a high degree of cooperativity between all of the non-covalent interactions holding it together: ion-dipole interactions, H-bonding, and π-stacking. Any alterations made to the guanosine nucleotide or self-assembly environment can greatly influence the outcome of the guanosine assemblies. Additionally, the pre-organization offered by the G-quadruplex can be used to control the reactivity of molecules. This thesis describes recent advances on the influence that modifications to the 5′-position of lipophilic guanosine derivatives can have on self-assembly and the use of lipophilic G-quadruplexes to pre-organize reactive groups for [2+2] photocycloadditions.

1.2 Thesis Organization

This thesis is organized into five chapters. The goal of the research in this thesis was to 1) examine how modifications to the 5′-hydroxyl group of lipophilic guanosine derivatives affects the self-assembly, molecularity, thermodynamic, and kinetic

stability of G-quadruplexes in organic solvents and 2) investigate whether these types of 5′-structural modifications can be used to pre-organize reactive groups to undergo regioselective and stereoselective organic reactions. **Chapter 1** introduces background information on the factors that influence G-quadruplex self-assembly, structure, and dynamics. Towards the end of **Chapter 1**, reactive G-quadruplexes will be presented that utilize the G-quadruplex to perform organic reactions. **Chapter 2** delves into how synthetic modifications to the 5′-position of guanosine impacts the self-assembly properties, molecularity, and thermodynamic and kinetic stability of G-quadruplexes made from 5′-modified guanosine nucleosides. This information proved vital for the design of a G-quadruplex system capable of catalyzing [2+2] photocycloadditions at the periphery of the G-quadruplex. **Chapter 3** assesses the G-quadruplexes' capability to act as a template for the [2+2] photocycloaddition of a series of 5′-cinnamate modified guanosine derivatives. **Chapter 4** examines the [2+2] photocycloaddition reaction of a 5′-cinnamate G-quadruplex that is highly regio- and stereoselective, as well as catalytic. Structural information is provided through an x-ray crystal structure and high-level calculations. Finally, **Chapter 5** contains experimental protocols and spectra for the research described in **Chapters 2-4**.

The aim of this introduction is not to provide an exhaustive review of the field of G-quadruplex self-assembly, but highlight important representative examples for the rational design, control, and application of G-quadruplexes and their applications towards stimuli-responsive and reactive G-quadruplex assemblies.

1.3 Guanosine Self-Assembly and G-Quadruplex Structure: The Basics

Guanosine (G 1), a versatile building block for a wide range of diverse assemblies, is a major contributor to the genetic make-up of living organisms, and an important synthon in supramolecular chemistry for the design of functionalized self-assemblies. Guanosine is comprised of two major components: 1) the guanine nucleobase and 2) the sugar. The guanine nucleobase contains a self-complementary hydrogen bond donor and acceptor face that can H-bond to give higher-ordered structures. Guanosine self-associates into one of two structures depending on the assembly conditions: 1) H-bonded G-ribbons or 2) H-bonded G_4-quartet stacks known as G-quadruplexes.[1] When in solution, devoid of any cations, guanosine favors H-bonded G-ribbons. In the presence of suitable cations guanosine forms a hydrogen bonded macrocycle known as a G_4-quartet, which further stack to provide G-quadruplexes.[2] The cation acts as a template to pre-organize the guanine nucleobases through ion-dipole interactions between the central cation and the guanine nucleobase's O^6 carbonyl oxygen (**Figure 1.1**).[4] Each component of the assembly is important; minor alterations to any of the G-quadruplex components can have a significant influence over self-assembly.

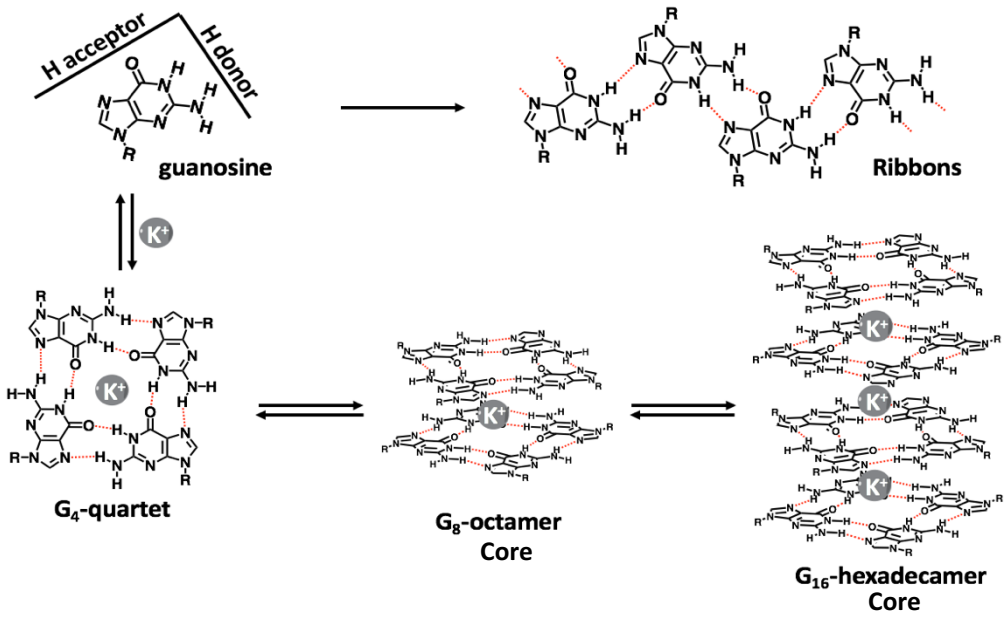

Figure 1.1. Illustration of guanosine self-assembly. In the presence of a cation, guanosine forms a self-assembled macrocyclic "core" through a series of H-bonding and ion-dipole interactions. These G_4-quartets further self-assemble into stacked G-quadruplex structures. Absent of any cations, guanosine favors H-bonded ribbons. The R group is considered the periphery to the G-quadruplex structure.

1.4 A Brief History of the G-Quadruplex: From the First G_4-Quartet to the Advent of Lipophilic G-Quadruplexes and Beyond

The G-quadruplex structure took many years and combined efforts to fully elucidate. The foundations of G-quadruplex chemistry were built with contributions made by multiple researchers over many decades (**Figure 1.2**). The G_4-quartet was first proposed in 1962 by Gellert *et al.* during their investigation of guanosine monophosphate (GMP **2**) hydrogels. By examining the X-ray diffraction patterns from fibers of 3′- and 5′-GMP **2** gels they were able to correctly propose that four guanine units self-assembled to form a G_4-tetramer and that stacking between these structures

had interlayer distance between 3-4 Å.[2] Around the same time Fresco and Massoulié found that poly G-DNA self-associated to form extremely stable G-stacked structures, presumably caused by G-quadruplexes.[3]

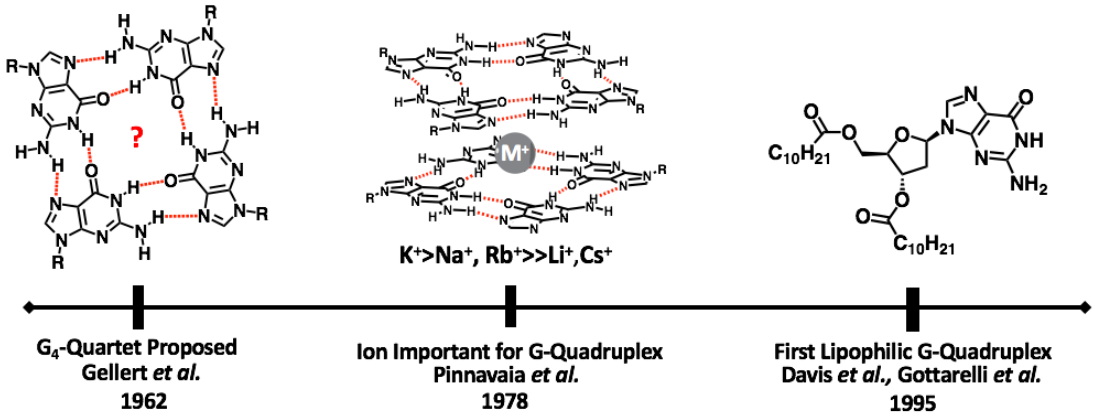

Figure 1.2. A timeline highlighting advancements of the G-quadruplex.[2,4,6]

Stacks of G-tetramers were discovered in both 5′-GMP **2** and polyG ribonucleic acids, and these structures were hypothesized to form through a series of cooperative H- bonding interactions and π-stacking, but not much was known about the role of the cation. It wasn't until 1978 when Pinnavaia and colleagues discovered that 5′-GMP **2** self-assembly depended on the nature of the alkali cation sandwiched between the G_4-quartet layers.[4] Their study provided a hierarchy for alkali templated G-quadruplex stability: $K^+ > Na^+$, $Rb^+ >> Li^+$, Cs^+. Pinnavaia *et al.* also found that 5′-GMP **2** could form discrete self-assemblies that could be monitored by ^1H NMR.[5]

It wasn't until much later that organic soluble G-quadruplexes were developed. The poor solubility of guanosine in organic solvents hindered the study of guanosine assemblies in organic solvents. To circumvent solubility issues and form organic

soluble G-quadruplexes, Gottarelli and colleagues synthesized a 5′, 3′-didecanoyl-2′-deoxy guanosine derivative (G 3**)**. In the presence of an organic K^+ picrate salt a G-quadruplex formed composed of 8 guanosine nucleosides (G_8-octamer) (**Figure 1.3**).[6] At approximately the same time the Davis group showed that an analogous isoguanosine compound, 5′-tert-butyldimethylsilyl-2′, 3′-isopropylidene isoguanosine (isoG 4), formed an $isoG_8$-octamer in the presence of KI.[7]

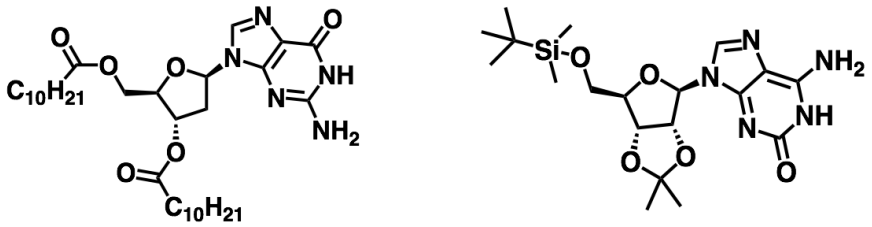

G **3** isoG **4**

Figure 1.3. Illustration of the first guanosine nucleosides to self-assemble in organic solvents. The modifications made to the sugar region are necessary to solubilize the guanosine derivative in organic solvents.[6,7]

G-quadruplex research is still a hot area of research, almost 60 years after the initial G-quadruplex paper from Gellert and Davies, and has witnessed an explosion in research publications in the last twenty years (**Graph 1.1**). Recent efforts are focused on understanding guanosine self-assemblies in biological systems, how they influence the transmission of genetic information, and the role that these G aggregates have on diseases, such as cancer. Drug compounds are being developed to target G-quadruplexes for the treatment of disease.[8-12] There is still much fundamental research aimed at understanding structural factors that affect guanosine's self-assembly. My main interests and the topics of this thesis are: 1) the synthesis of non-natural lipophilic

guanosine derivatives, 2) how structural modification to the guanosine nucleoside influence G-quadruplex self-assembly and stability, and 3) novel applications of these functionalized G-quadruplexes to promote organic reactions. The rest of this introduction will examine structural and extrinsic factors (e.g. cation, anion, solvent, temperature) that have an impact on self-assembly, investigate how these factors modulate G-quadruplex molecularity and stability, and survey organic reactions that have been achieved using the G-quadruplex. These topics are all relevant for the discussion of my research.

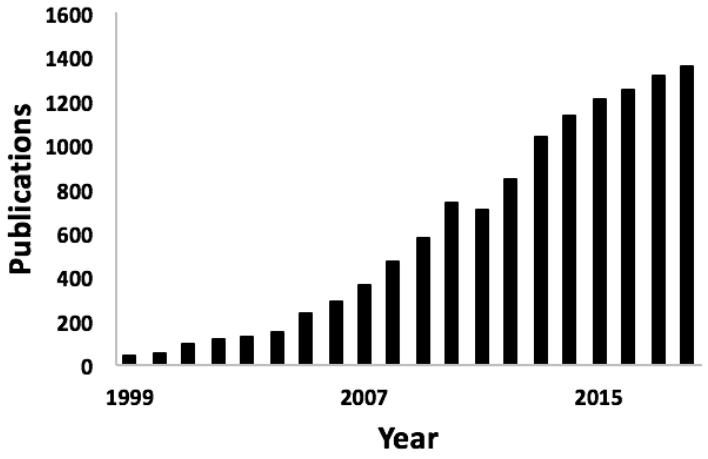

Graph 1.1. Graph displaying the number of G-quadruplex publications over the last 20 years (1999-2019) using a SciFinder search with the phrase "G-quadruplex". The field of G-quadruplex research has grown significantly and continues to grow.

1.5 Structural Diversity of Guanosine: The Impact of Guanosine's Structural Identity on G-Quadruplex Self-Assembly

There are many structural derivatives of guanosine (DNA, RNA, monomeric nucleotides, and functionalized nucleosides) each with their own self-assembly properties (**Figure 1.4**). The guanosine nucleotide is naturally found in genetic materials, DNA and RNA, covalently linked through phosphodiester bonds between the 3′ and 5′ hydroxyls of the sugar. Monomeric guanosine monophosphate (GMP **2**) nucleotides make up the backbone of DNA and RNA. In addition to these natural guanosine derivatives, synthetic derivatives exist. Guanosine nucleosides are easily modified and can be altered at multiple positions on the sugar and guanine nucleobase. Modifications to the structure of the nucleoside influence G-quadruplex structure and properties.

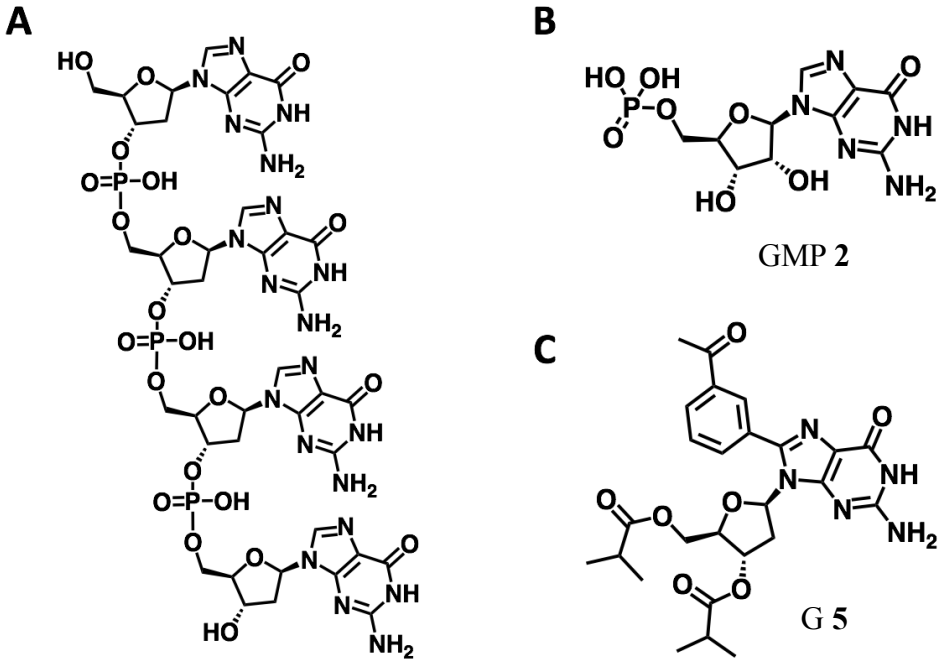

Figure 1.4. Illustration of a few of the structural diverse forms of guanosine that can self-assemble into G-quadruplex structures. A) G4-DNA strand, B) 5′-guanosine monophosphate GMP **2**, and C) a lipophilic guanosine nucleoside, 8-acetylphenyl-3′,5′-isobutyryl-2′-deoxy guanosine G **5**.

1.5.1 Guanosine Monophosphate Assembles into G-Quadruplexes

The discovery of the G-quartet was made during the investigation of guanosine monophosphate (GMP **2**) based hydrogels in the 1960s. Examination of G-quadruplexes made from GMP derivatives is still ongoing today. Guanosine can be modified at the sugar hydroxyl groups (2′, 3′, or 5′) with a phosphate group. The structure and stability of 5′-GMP assemblies were examined by Wu and Kwan through a series of ^{1}H NMR experiments. Their results suggest a G-quadruplex structure that is stabilized by a 5′-phosphate H-bonding interaction with the next G-quartets layer's C2′

hydroxyl group (**Figure 1.5**).[13] This interlayer H-bonding between the 5′-phosphate and the next G_4-layer was further corroborated by Mudronova and colleagues when they reported that ribo-5′-GMP was more stable than 2′-deoxyribose 5′-GMP (dGMP **6**).[14] The phosphate modification at the 5′-hydroxyl has a significant influence on the stability of the G-quadruplex self-assembly.

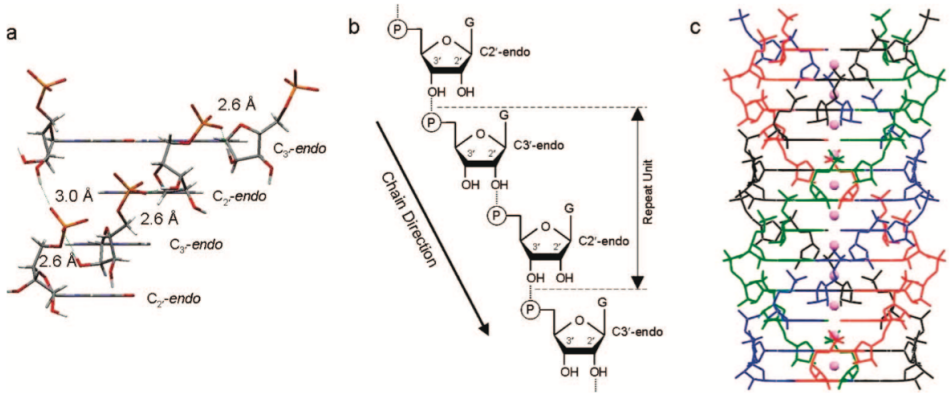

Figure 1.5. Computer generated model showing stabilizing H-bonding between G_4-layers of 5′-GMP **2** quadruplexes. The H-bonding interaction occurs between the 5′-phosphate of 5′-GMP **2** with the next layer's C2′ hydroxyl group.[13]

Covalently linked cyclic diguanosine monophosphates can also form G-quadruplex structures in the presence of K^+ cations. Cyclic diguanosine monophosphate (diGMP **7**) is a cyclic compound formed by a reciprocal bonding between the 3′- and 5′-phosphodiester group of two guanosine nucleotides. Zheng e*t al.* have found that cyclic diGMP **7** can form tetramolecular G-quadruplex structures and octamolecular G-quadruplex structures (**Figure 1.6**).[15]

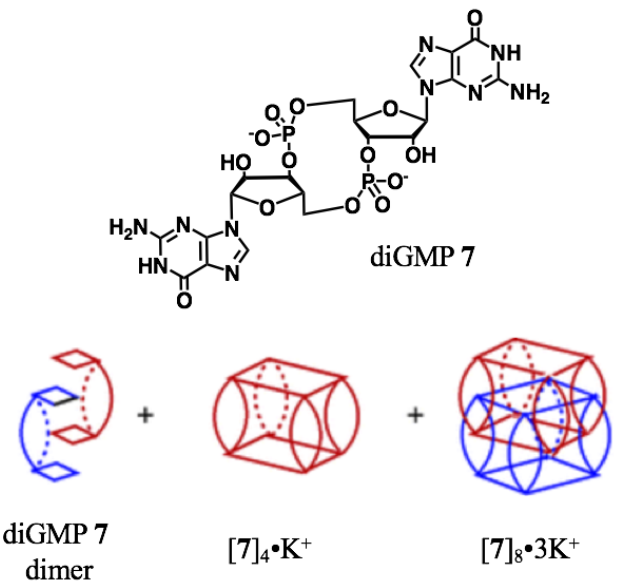

Figure 1.6. Illustration of the self-assembly of 3′, 5′-cyclic diGMP **7**. Bimolecular complex of two cyclic diGMP **7** molecules B) cartoon of the tetramolecular G-quadruplex structure. C) Cartoon of the octamolecular G-quadruplex.[15]

1.5.2 G-Rich DNA/RNA Self-Assembles into G-Quadruplexes

G-rich DNA and RNA self-assembles into G-quadruplex structures. These G-quadruplexes are prevalent in biology.[8-11] This field is immense so this introduction will only focus on the basics of nucleic acid G-quadruplex structure. DNA and RNA are covalently linked through a series of 3′ to 5′ phosphodiester bonds and as a result are much more thermodynamically stable in solvents that usually disfavor G-quadruplex formation. G-rich nucleic acids can take many different tertiary structures depending on the assembly environment, this is known as polymorphism. G-rich nucleic acids can form G-quadruplexes from one nucleic acid strand (unimolecular) or multiple strands. These strands can take either a parallel form, anti-parallel form or

some combination of parallel and antiparallel (**Figure 1.7**).[16-18] Depending on the environmental conditions different G-quadruplex polymorphs can be favored.[19-20]

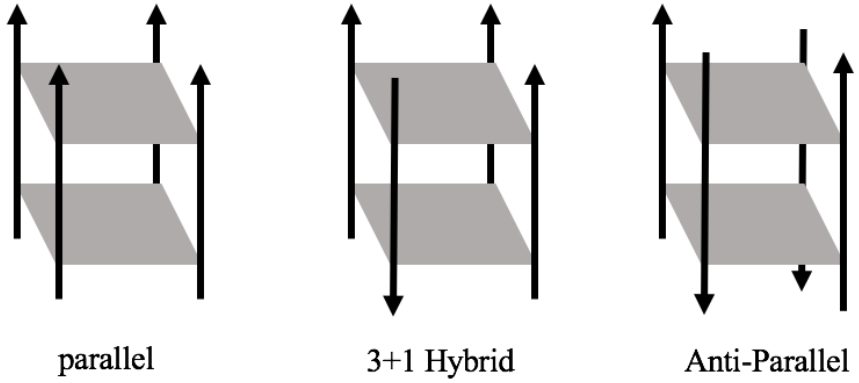

Figure 1.7. Illustration of a few of the possible G-quadruplex polymorphs that DNA G-quadruplexes can form: parallel stranded G-quadruplex, 3+1 hybrid G-quadruplex, anti-parallel stranded G-quadruplex.

1.5.3 Synthetically Modified Guanosine Nucleoside Derivatives Self-Assemble into G-Quadruplexes

Nature often inspires breakthroughs in chemistry. Synthetically modified guanosine nucleosides have been investigated as a way to incorporate new functionality and properties into G-quadruplex nanostructures. Analogous to the naturally occurring guanosine monophosphate and G-rich nucleic acid strands, synthetically altered guanosine derivatives self-assemble into G-quadruplexes. Adding a non-polar group to the guanosine nucleoside allows for organic soluble G-quadruplexes to be generated. These alterations to the G-quadruplex open the door to novel structures with intriguing new functionalities.

Guanosine G **1** can be synthetically modified at multiple positions making it a versatile building block for constructing functional nanostructures. The guanine nucleobase and the sugar (deoxyribose or ribose) are the main targets for synthetic modifications. The guanine nucleobase contains three modifiable positions that can be altered without disrupting G self-assembly: the H^8 position, the N^9 position, and the N^2H exocyclic amine. The sugar unit can be modified at any of the hydroxyl groups: 2′, 3′, or 5′ (**Figure 1.8**).

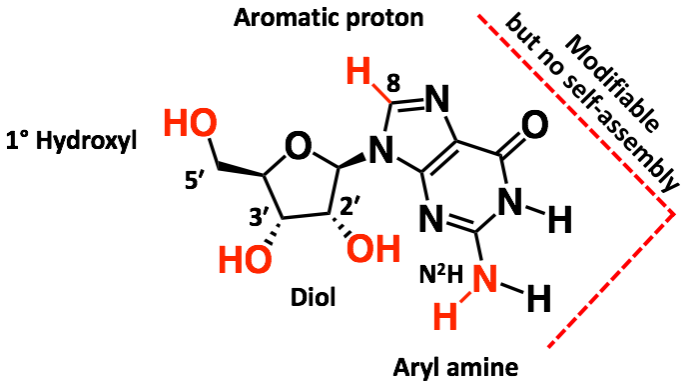

Figure 1.8. Illustration of sites that can be synthetically modified on guanosine G **1**. Guanosine's nucleobase can be altered at the aromatic H8 proton or the outer N^2H amine. Changes made to the inner N^1H, N^7 nitrogen, or C^6 carbonyl destroy guanosine's capacity to self-assemble. The sugar can be modified at the 2′/3′ diol or the 5′ hydroxyl group.

Modifications can be made to the N^9 position to completely replace the sugar unit of a nucleoside. An N^9 modified guanine derivative, N^9-(3,5-*bis*(tert-butyldimethylsilyloxy)-benzyl) guanine (G **8**), was synthesized by McCallum *et al.* and this derivative was found to self-assemble into D_4-symmetric G_8-octamers in the presence of K^+ picrate (**Figure 1.9**). This result suggests that the sugar is not always

required for G_4-quartet aggregates to form.[21] N^9-modifications have also been exploited for the design of stimuli-responsive hydrogels. Ghoussoub and Lehn synthesized a polyethylene oxide linked *bis*-guanine derivative (G **9**), that forms a highly cross-linked hydrogel in the presence of KCl. G_4-quartet complexes are responsible for the gel formation (**Figure 1.9**).[22] Mixing in [2.2.2] cryptand, a compound that chelates K^+, to the hydrogel resulted in a gel-sol conversion, demonstrating the importance of the K^+ ion to gel formation.

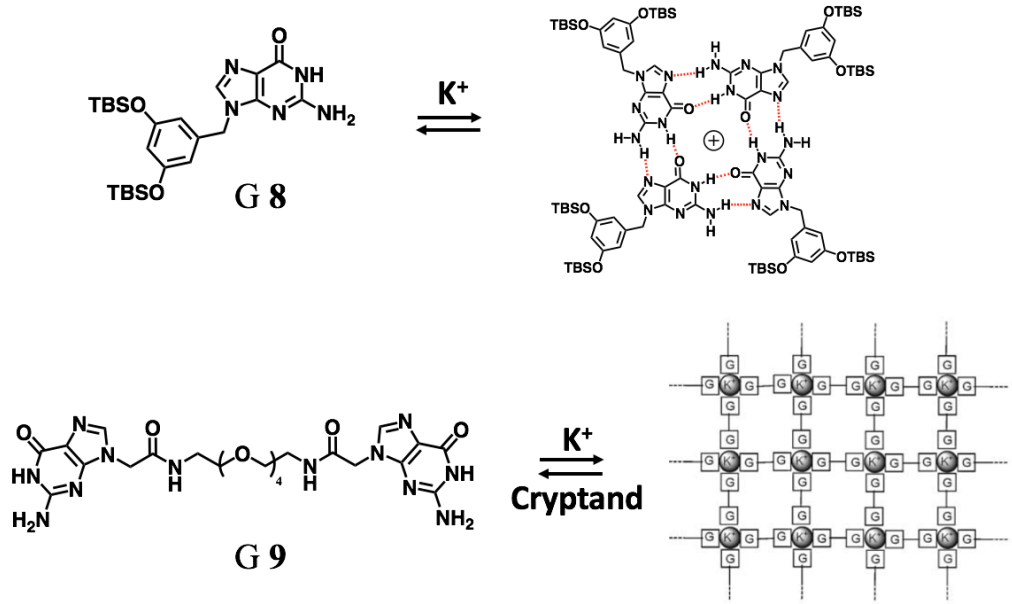

Figure 1.9. Illustration showing selected N^9 modified guanosine derivatives. Top) N^9-(3,5-*bis*(tert-butyldimethylsilyloxy)-benzyl) guanine G **8** self-assembles into G_4-quartet structures that stack into G_8-octamers.[21] Bottom) Lehn's N^9-modified *bis*-guanine hydrogelator G **9**. A network of G-quadruplex assemblies is presumably responsible for the gelation. [2.2.2] Cryptand can reverse the gelation.[22]

Guanosine modified at the C^8 position has also been demonstrated to self-assemble and alter thermodynamic stability of the G-quadruplex. The Rivera group has

designed a C^8 modified guanosine derivative, 8-(3-acetylphenyl)-3′,5′-isobutyryl guanosine (G **10**), with an 8-acetylphenyl group that extends the Hoogsteen bonding face of the guanine nucleobase. In the presence of K^+ cations the modified nucleoside G **10** forms G_{16}-quadruplexes that are more thermodynamically stable than non-C^8 acetylphenyl modified G-quadruplexes.[23] Further work was performed to understand this stabilizing effect. The acetyl group and the aryl ring were found to increase the stability of the G-quadruplex through increasing the number of H-bonding and π-stacking interactions (**Figure 1.10**).[24,25] Recent work by the Shi group examined the self-assembly of a bis-guanosine derivative (G **11**), that covalently attaches two guanosine nucleosides together through a C^8-(3-ethylenephenyl) linker.[26] The ethylene linked bis-guanosine G **11** forms extraordinarily stable G_8-octamers. These G_8-otamers are thermodynamically stable enough to form in polar solvents (DMSO and MeOH), solvents that often favor complete disassembly of the G-quadruplex.

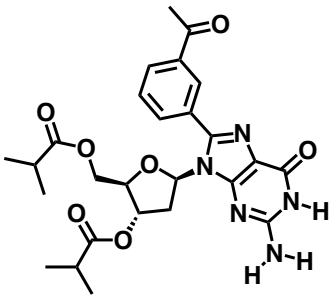

G **10**

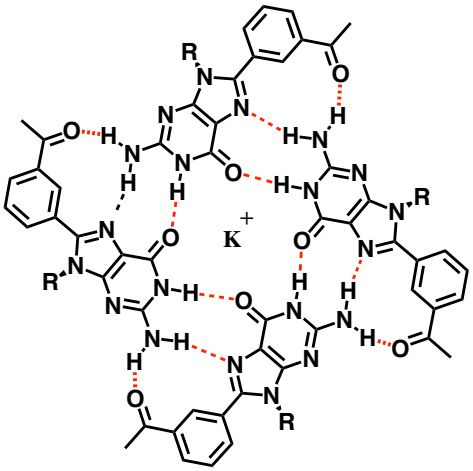

one [G **10**]$_4$-quartet
of a G$_{16}$-hexadecamer

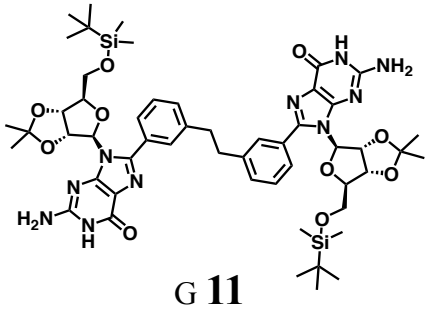

G **11**

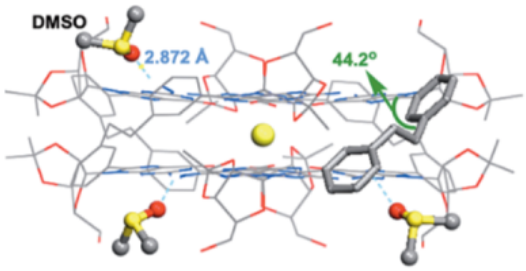

[G **11**]$_4$•K$^+$

Figure 1.10. Illustration providing examples of C^8-modified guanosine derivatives. Top) Rivera's 8-phenylacetyl guanosine derivative G **10** that forms stable G$_{16}$-hexadecamers promoted by an extended Hoogsteen face.[23-25] Bottom) Phenylethylene linked *bis*-guanosine derivative G **11** that forms robust G$_8$-octamers. An X-ray crystal structure of the guanosine assembly.[26]

The N^{2}H amine protons provide another site for synthetic modification. The N^{2}H amino protons are directly involved in G$_4$-quartet formation and are vital to the H-bonding responsible for self-assembly of the G-quadruplex. There are two N^{2}H amino protons located on each guanosine: an endocyclic proton, that forms a G$_4$-quartet by H-

bonding to an N^7 H-bond acceptor of a neighboring guanosine, and an exocyclic N^2H amino proton located on the periphery of the quadruplex core. Kaucher and Davis discovered that modifying the exocyclic N^2H amine proton of a lipophilic guanosine derivative doesn't preclude G-quadruplex assembly. An N^2-(4-pentenyl)-8-vinyl-2',3′-isopropylidene-5′-TBMDS guanosine (G **12**) was synthesized and self-assembled in a G_8-octamer in the presence of $Ba(DNP)_2$ (**Figure 1.11**).[27] Around the same time Martic and colleagues synthesized two new N^2-modified guanosine derivatives containing aromatic ring systems capable of π-stacking, N^2-(4-*n*-butylphenyl)-2′,3′,5′-triacetylguanosine (G **13**) and N^2-(4-pyrenyl-phenyl-2′,3′,5′-triacetylguanosine (G **14**) (**Figure 1.11**). These N^2 modified G derivatives self-assemble into G_8-octamers in CD_3CN. It was hypothesized that the larger pyrene group on the periphery of the assembly might stabilize the G-quadruplex assembly through π-stacking interaction, however experiments were not performed to prove this hypothesis.[28]

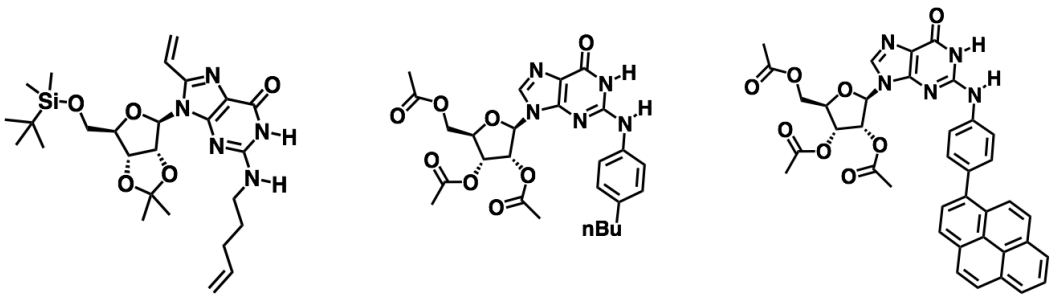

G **12** G **13** G **14**

Figure 1.11. Illustration of N2-modified guanosine derivatives. Left to right) N^2-(4-pentenyl)-8-vinyl-2',3′-isopropylidene-5′-TBMDS guanosine G **12**,[27] N^2-(4-n-butylphenyl)-2′,3′,5′-triacetylguanosine G **13** and N^2-(4-pyrenyl-phenyl-2′,3′,5′-triacetylguanosine G **14**.[28]

The sugar moiety is another position for altering the guanosine nucleoside so as to modulate the properties and function of G-quadruplex nanostructures. The hydroxyl groups (2′, 3′, and 5′) are easily modified. The sugar unit is often modified to increase the organic solubility of guanosine in order to form G-quadruplexes in organic solvents. The first example of an organic soluble G-quadruplex came from Gottarelli and colleagues when they modified the 3′ and 5′ hydroxyl group of 2′-deoxyguanosine with dodecanoyl chains to form G **3**. The long straight chain acyl groups promoted the solubilization of the guanosine derivative in CH_2Cl_2. G_8-octamers formed in CH_2Cl_2 in the presence of K^+ picrate.[6] Since then many others have used the same strategy to solubilize G-quadruplexes into organic solvents and build functional assemblies.[29] My research has focused on examining how modifications to the 5′-position of the ribose sugar of a 2′,3′-isopropylidene guanosine derivative influences self-assembly. This work is presented in **Chapter 2.**[33] The Davis group has pioneered the design of functional G-quadruplex assemblies through modifications to the sugar. Work by Peters and Davis found that modifying the 2′ and 3′ position of guanosine with a borate ester formed a stable hydrogel based on G-quadruplex structures (**Figure 1.13**).[30,31] Xiao and Davis designed a 5′-hydrazinoguanosine (G **15**) nucleoside that formed G-quadruplex hydrogels that were capable of sequestering toxic electrophiles from the local environment (**Figure 1.12)**.[32] More examples of these sugar modifications will be discussed in subsequent sections.

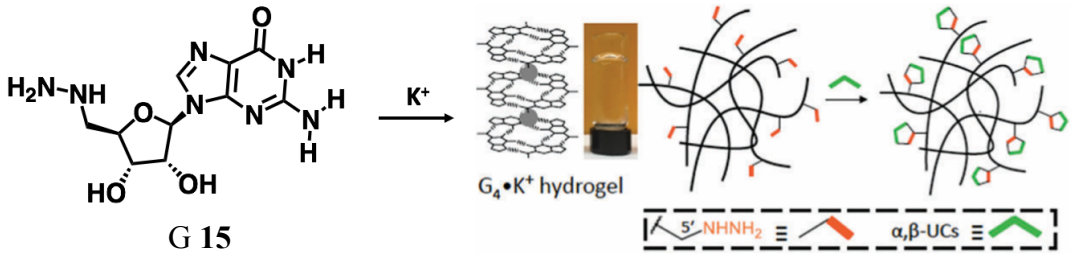

Figure 1.12. Illustration of Xiao's 5′-hydrazinoguanosine hydrogel. 5′-Hydrazinoguanosine G **15** forms hydrogels in the presence of KCl. These hydrogels can remediate α,β-unsaturated carbonyls (α,β-UCs).[32]

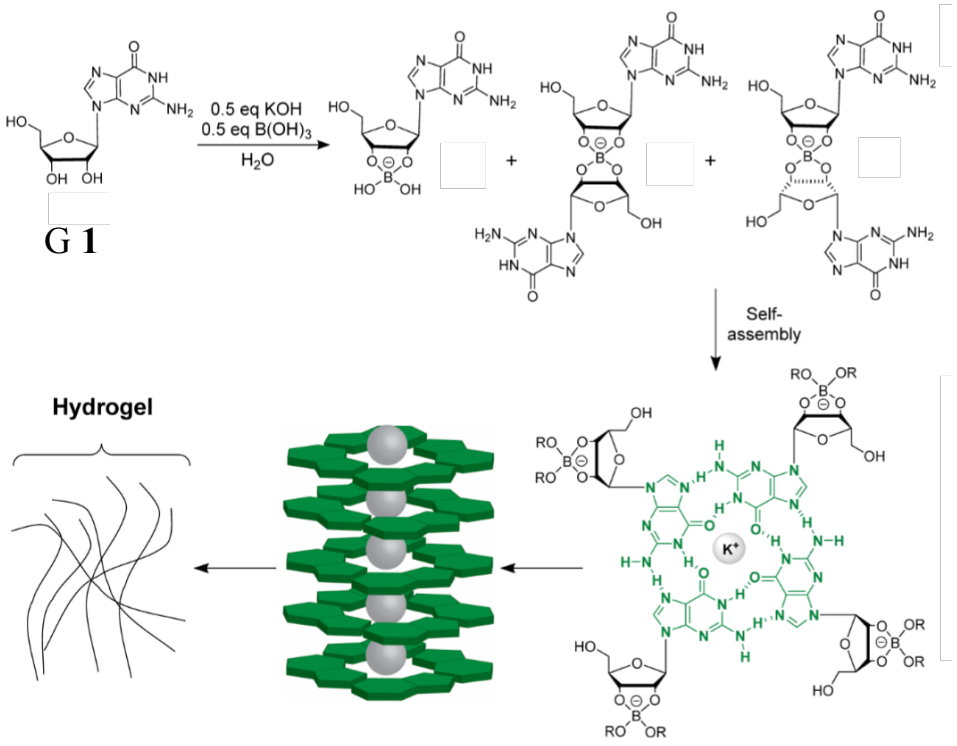

Figure 1.13. Illustration of a 2′,3′-borate ester guanosine that self-assembles to form crosslinked hydrogel networks. Guanosine (G **1)** in the presence of KOH and $B(OH)_2$ forms borate esters. The guanosine borate esters undergo self-assembly to form G-quadruplex based hydrogels.[30,31]

1.6 Extrinsic Factors that Control G-Quadruplex Structure and Stability

Structural changes to the guanosine nucleotide clearly have an influence over the self-assembly and properties of the resulting G-quadruplexes. Many other components are vital for G-quadruplex self-assembly: cation, counter-anion, solvent, and temperature. The G-quadruplex relies on many cooperative noncovalent interactions to stabilize the assemblies: ion-dipole interactions, solvation, solvophobic effects, H-bonding, and π-stacking. Each of these factors contribute to the thermodynamic and kinetic stability of the G-quadruplex.

1.6.1 The Identity of the Cation Influences G-Quadruplex Self-Assembly

The G-quadruplex is built from a cooperative array of noncovalent interactions and each component helps to thermodynamically or kinetically stabilize the self-assembly. Multiple interactions are responsible for stabilizing the self-assembly, but arguably none are more important for forming G-quadruplexes than the central cation that templates the formation of G-quartets (**Figure 1.14**). Ion-dipole interactions between the central cation and the coordinated guanine nucleobase provide the thermodynamic stability necessary to overcome the entropic penalty for self-assembly. Many types of cations can stabilize the G-quadruplex structure: alkali cations, ammonium cations, alkaline earth cations, lanthanides, and post-transition metal cations. Many factors influence the cation's ability to form G-quadruplexes, including the ionic radius and charge state of each cation.

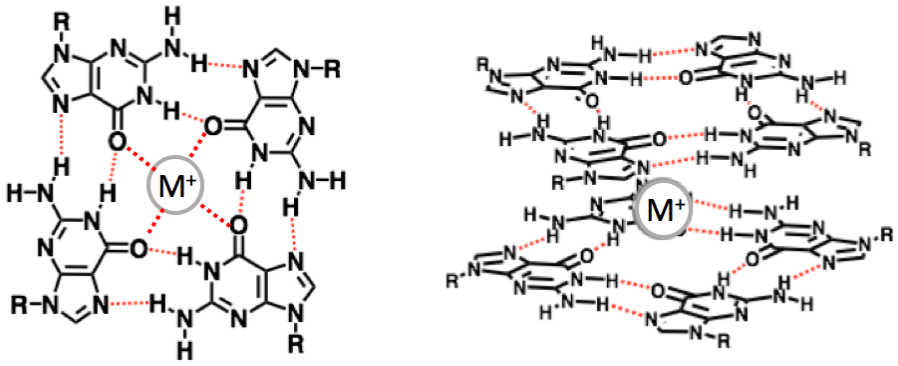

Figure 1.14. Illustration showing the location of a central cation between two G-quartet layers (right). The cation may also sit in the plane of the G-quadruplex (left).

Alkali Metal Cations Template G-Quadruplex Assembly

Pinnavaia *et al.* were the first to recognize that the identity of the cation influenced G-quadruplex formation.[4] In their seminal paper, they discovered that the self-assembly of 5′-guanosine monophosphate into [GMP **7**]$_{12}$•2M$^+$ dodecamers was directly influenced by the monovalent alkali cation used (M$^+$= Li$^+$, Na$^+$, K$^+$, Cs$^+$, Rb$^+$). Using variable temperature ^{1}H NMR experiments they analyzed the stability of G-quadruplex self-assemblies and found the following stability series for the alkali cations: K$^+$ > Na$^+$, Rb$^+$ >> Li$^+$, Cs$^+$. Assemblies built from K$^+$ are the most thermodynamically stable. They proposed that the size of the cation dictates the stability of self-assembly. Cations that can properly fit within the G-quadruplex cavity exhibit greater stabilization. Potassium is the goldilocks cation for forming G-quadruplexes, it has the perfect dehydration energy and ionic radius (r = 1.33 Å) to fit within the central core of two G$_4$-quartets. Whereas, lithium and cesium cations (r= 0.6 Å and 1.69 Å respectively), are too small and large respectively, to fit in the central guanine core and template the self-assembly (**Figure 1.15**).

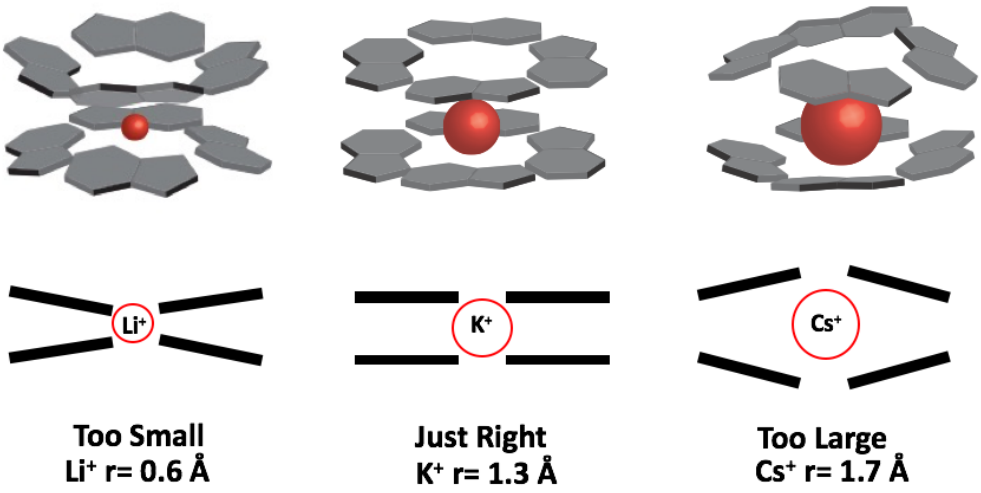

Figure 1.15. Illustration demonstrating the influence that cation size can have on G-quadruplex self-assembly. Cations that are too small or large to fit in the central G-quadruplex cavity likely destabilize G_4-quartet formation and prohibit further organization into higher ordered structures.

The cation used to template assemblies can also have a significant impact on biologically relevant DNA G-quadruplex structure. Research by Sen and Gilbert examined the influence of alkali cations on the formation of tetramolecular G_4-DNA self-assembles from short-strand G-rich DNA oligomers. The quadruplex architecture formed from G-rich DNA strands was dependent on the identity of the alkali cation used. Tetramolecular G-quadruplexes, bringing together 4 separate strands of DNA through intermolecular quadruplex formation, were favored in the presence of Na^+ while bimolecular "fold-back" structures between two DNA strands formed in the presence of K^+ ions.[34] In this example, the G-quadruplex polymorph formed could be directly controlled by the alkali cation used (Na^+ vs. K^+).

The Spada group showed that guanosine can behave as an ionophore and form G-quadruplexes in organic solvents. Spada revealed that the lipophilic guanosine

derivative 3′,5′-dodecanoyl guanosine G **3** formed a [G **3**]$_8$-octamer in CH_2Cl_2 in the presence of an organic alkali salt, K^+ Pic^-. Depending on the K^+ concentration, G-quadruplexes are formed having varying molecularities from G_8-octamers to extended higher-ordered G_4-quartet based structures.[6] Ma *et al*. further examined the influence that alkali ions have on the G-quadruplex by investigating the binding affinity and exchange mechanism of alkali cations within a G_{16}–hexadecamer. A lipophilic guanosine derivative was used in this study: 5′-TBDMS-2′, 3′-isopropylidene guanosine (G **16**) . Ma found that by adding K^+ to a G_{16}•3Na^+ hexadecamer that the Na^+ is replaced by the more thermodynamically favored cation.[35]

Alkaline Earth Metal Cations-Divalent Salts

Divalent alkaline earth cations template the formation of G-quadruplex structures in DNA/RNA and lipophilic G-quadruplex systems. The stability of G-quadruplex formation from the alkaline earth metal cations follows the series Sr^{2+} >> Ba^{2+} > Ca^{2+} > Mg^{2+}, with the G-quadruplexes containing Sr^{2+} being the most stable.[36,37] Similar to K^+ (r=1.33 Å), Sr^{2+} (r= 1.26 Å) has the ideal size to fit in the G-quadruplex cavity and stabilize the structure. In general, the divalent cations form more stable G-quadruplex structures than the monovalent cations due to greater ion-dipole charge stabilization between guanine and the divalent cation.[38]

Martin-Hidalgo and Rivera exploited the G-quadruplex's preference for the thermodynamically more stable alkaline earth metal Sr^{2+} to design a metalloresponsive G-quadruplex that can switch between a [G]$_{16}$•3K^+ quadruplex and a [G]$_8$•Sr^{2+}

quadruplex in organic solvents. The guanosine derivative used was a lipophilic 8-(3-phenylacetyl)-3′,5′-butyryl-2′-deoxy guanosine G **10**. By adding K^+ or Sr^{2+} the molecularity of the G-quadruplex could be switched between [G **10**]$_8$ octamer and a [G **10**]$_{16}$ hexadecamer (**Figure 1.16**).[39]

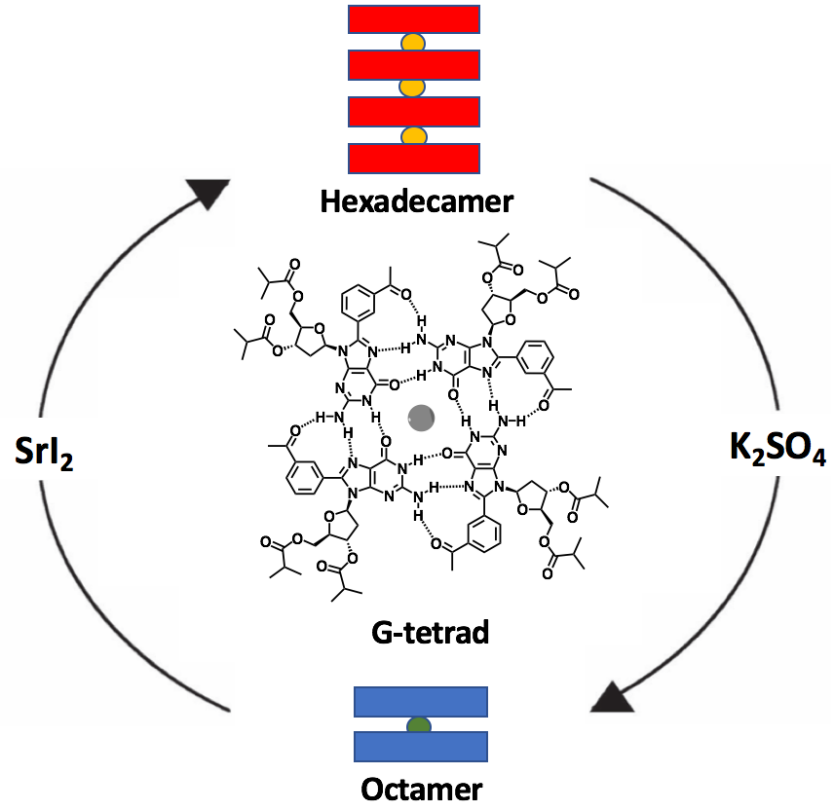

Figure 1.16. Illustration showing the metallo-responsive G-quadruplex designed by Rivera *et al*. In the presence of K^+ a [G **10**]$_{16}$•3K^+ quadruplex is formed. If Sr^{2+} is added to [G **10**]$_{16}$•3K^+ the molecularity changes to form [G **10**]$_8$•Sr^{2+}.[39]

In another interesting example of the influence of alkaline earth metals over G-quadruplex self-assembly, Shi *et al.* discovered that an enantiomeric mixture of D- and L-5′-TBDMS-2′,3′-isopropylidene guanosine could be resolved into discrete

enantiomeric G_{16} assemblies using a Ba^{2+} picrate salt. When K^+ picrate was used the D- and L- guanosine derivatives formed mixed assemblies (**Figure 1.17**).[40]

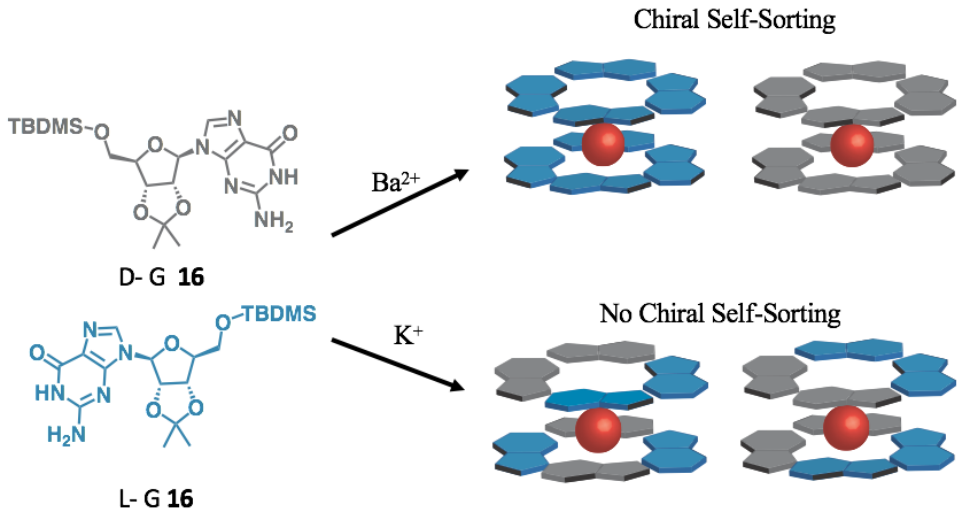

Figure 1.17. Illustration of the chiral resolution of D- and L- 5′-TBDMS-2′,3′-isopropylidene guanosine G **16** by Ba^{2+}, a divalent alkaline earth cation. The alkali cation K^+ does not resolve the enantiomers.[40]

Other Metal Ions that Form G-Quadruplexes

G-quadruplexes have been formed from Pb^2+ in both DNA and lipophilic G-quadruplex systems. Kotch *et al.* showed that Pb^{2+} picrate templated the self-assembly of 5′-TBDMS-2′,3′-isopropylidene guanosine into a G_{16} quadruplex in $CDCl_3$. An X-ray crystal structure was obtained and revealed that the G-quadruplex was composed of two G_8-octamers with an empty central G-quadruplex core providing [G **16**]$_{16}$•2Pb^{2+}.[41]

G4-DNA G-quadruplexes have also been formed from thallium cations (Tl^+). Using a d(TTGGGGTT) G4-DNA strand Strobel and colleagues demonstrated that Tl^+

formed G-quadruplex structures in water. It was found that Tl^+ quadruplexes formed more efficiently than analogous K^+ or Na^+ assemblies.[42,43]

Lanthanide Ions Template G-Quadruplex Formation

Ions from the lanthanide series can also template the formation of G-quadruplex assemblies. The Wu group has shown that lipophilic guanosine 2′,3′-5′-triacetylguanosine (G **17**) forms G-quadruplexes from trivalent lanthanide ions La^{3+}, Eu^{3+}, Tb^{3+}, Dy^{3+}, and Tm^{3+}.[44] The molecularity of the structure is controlled by the lanthanide cation: lanthanum and europium cations resulted in [G **17**]$_{12}$•M^{3+} dodecamers, while terbium, dysprosium, and thulium cations formed mixtures of [G **17**]$_{12}$•M^{3+} and [G **17**]$_8$•M^{3+}. La^{3+} (r= 1.17 Å) and Eu^{3+} (r= 1.08 Å) have the appropriate size to sit in between the G_4-quartet plane and promote formation of the larger aggregate, as shown in **Figure 1.18**.

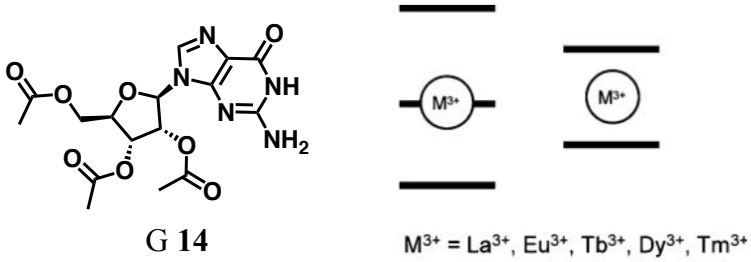

G **14**

Figure 1.18. Cartoon illustration showing hypothetical G-quadruplex formation of 2′, 3′, 5′-triacetylguanosine proposed by Wu *et al.* Lanthanum and europium cations have ionic radii that allow them to sit in the plane of a central G-quadruplex and promote [G]$_{12}$•M^{3+} dodecamer formation. Terbium (r= 1.06 Å), dysprosium (r= 1.05 Å), and thulium (r= 1.02 Å) cations are smaller and form a mixture of [G **14**]$_{12}$•M^{3+} dodecamer and [G **14**]$_8$•M^{3+}octamer.[44]

Lanthanide ions can also stabilize G-quadruplex DNA formed from the DNA human telomere repeat sequence (hTel21). Galezowska *et al.* have shown that hTel21 in the presence of europium or terbium cations form DNA G-quadruplex assemblies. Interestingly, in a buffered H_2O solution of NaCl in the absence of Tb^{3+} a circular dichroism spectrum showed Na^+ parallel-stranded quadruplexes. After the addition of Tb^{3+}, and exchange of the Na^+ ions the G-quadruplex structure changed to anti-parallel.[45] This is another example of a G-quadruplex structure switching between polymorphs in the presence of different salts.

1.6.2 The Identity of the Anion Influences G-Quadruplex Self-Assembly

Although the cation is arguably the most important contributor to G-quartet formation and the construction of higher-ordered structures, the counter-anion also has a significant impact on self-assembly. A prime example of the anion's influence on G-quadruplex assembly was demonstrated by Shi et al.[46] Shi examined the stabilizing effect that a series of organic anions (picrates and dinitrophenolates) had on the kinetic stability of 5′-TBDMS-2′,3′-isopropylidene guanosine [G **16**]$_8$ octamers built with Ba^{2+} or Sr^{2+}. Kinetic exchange experiments were performed monitoring Ba^{2+} and Sr^{2+} exchange between G-quadruplexes formed from a series of their corresponding nitrophenolate salts. It was found that the 2,6-dinitrophenolate anion stabilized the G-quadruplex by H-bonding between the nitro and phenolate functional groups and the exocyclic N^2H amino proton. The 2,5-dinitrophenolate anion did not have the same stabilizing effect (**Figure 1.19**).[46] A follow up experiment by Davis et al. also showed

that 2,6-dinitrophenolate formed more kinetically stable G-quadruplexes compared to 2,4,6-trinitrophenolate. This difference in kinetic stability was due to differences in the coordinating H-bonding capacity of the anion.[47]

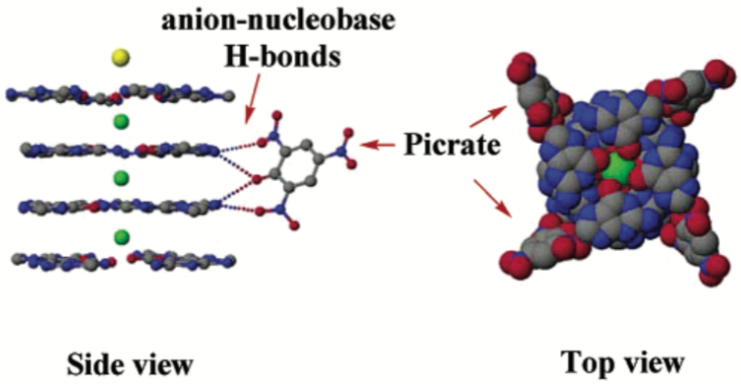

Figure 1.19. Illustration of G-quadruplex stabilization by 2,4,6-trinitrophenolate. The nitro groups and phenolate ion coordinate to the exocyclic N^2H amine protons from adjacent G_4-quartets to stabilize the structure.[46]

Coulombic interactions between the central G_4-cation and the counter-anion also have a significant impact over G-quadruplex self-assembly. Gonzaléz-Rodriguez *et al.* examined the formation of G-quadruplex structures made from lipophilic 8-bromo-5′-*tert*-butyldimethylsilyl-2′,3′-isopropylidene guanosine (G **18**) in organic solvents with different non-templating anions $I^- > Br^- > Cl^-$ and templating nitrophenolates 4-Me-2,6-DNP^- >2,6-DNP^- >Picrate. Assemblies made from K^+ salts containing templating and non-templating anions (K^+A^-) are in dynamic equilibrium between G_8-octamers and G monomers. This equilibrium was monitored by ^1H NMR and indicated that the templating anions all stabilized G_8-octamer formation, while the only non-templating anion that favored G-quadruplexes was the I^- anion.[48]

1.6.3 The Solvent Can Influence G-Quadruplex Self-Assembly

The solvent has a tremendous impact on G-quadruplex self-assembly. There is a structural diverse collection of G-quadruplex forming compounds: G-rich DNA, monomeric water soluble G, lipophilic guanosine derivatives. The solvent helps to not only solvate the guanosine analogs for self-assembly, but also has a direct influence over the coulombic interactions between the cation and anions in the self-assembly.[48]

G-Rich DNA and guanosine monophosphate are found in biological systems and their self-assembly takes place primarily in H_2O. To form organic soluble G-quadruplexes the nucleoside must be modified with nonpolar, organic solubilizing groups. Gonzaléz-Rodriguez et al. examined the formation of G-quadruplex structures of lipophilic 8-bromo-5′-tert-butyldimethylsilyl-2′, 3′-isopropylidene guanosine G **18** in different organic solvents.[48] They found that the polarity of the solvent could directly control the molecularity of the G-quadruplex by regulating Coulombic interactions between the cation and anion of the assembly. There is a delicate balance between solvation of the monomer, cation, and anion on lipophilic G-quadruplexes. They proposed that the solvent modulated the structure though Coulombic interactions between the central cation in the G-quadruplex self-assembly and the counter-anion.[48] A more recent study by the González-Rodríguez group studied $[G\ \mathbf{18}]_{12}\bullet 2K^{+}2BPh4^{-}$ G-quadruplex structures in apolar toluene. The self-assemblies formed in toluene were found to have remarkably high thermodynamic and kinetic stabilities.[49] This increased stability is likely due to increased hydrogen-bonding strength due to solvophobic effects.

1.6.4 Temperature Influences G-Quadruplex Self-Assembly

Temperature has a direct influence on G-quadruplex self-assembly.[50] Temperature can be used to compare G-quadruplex thermodynamic stability.[51] The G-quadruplex is in rapid equilibrium between assembly and monomeric G. At increased temperatures the G-quadruplex melts favoring disassembled G monomers. At low temperatures G-quadruplexes are favored. The temperature dependence on G-quadruplex assembly can be exploited to control G-quadruplex structure and function.

A recent example that exploits temperature's control on G-quadruplex self-assembly was presented by Harraz and Davis. Harraz examined the reactivity of a 5′-GMP G-quadruplex hemin complex that catalyzes the peroxidation of a dye compound, 2,2′-azino-bis-(3-ethylbenzothiazoline-6-sulphonic acid) (**ABTS**) (**Figure 1.20**). At low temperatures 5′-GMP self-assembled into G-quadruplex structures in the presence of excess Na^+. Heme can bind to G-quadruplex to form a catalyst for peroxidation reactions of **ABTS**. At high temperatures, the catalytic hemin G-quadruplex was disassembled and no ABTS oxidation was observed. At lower temperatures that favor G-quadruplex formation, hemin was bound, and the oxidation of **ABTS** proceeded. This example illustrates how temperature can be used to modulate G-quadruplex structure and function, in this case resulting in a catalytic system that exhibits an apparent anti-Arrhenius dependence on reactivity. [52]

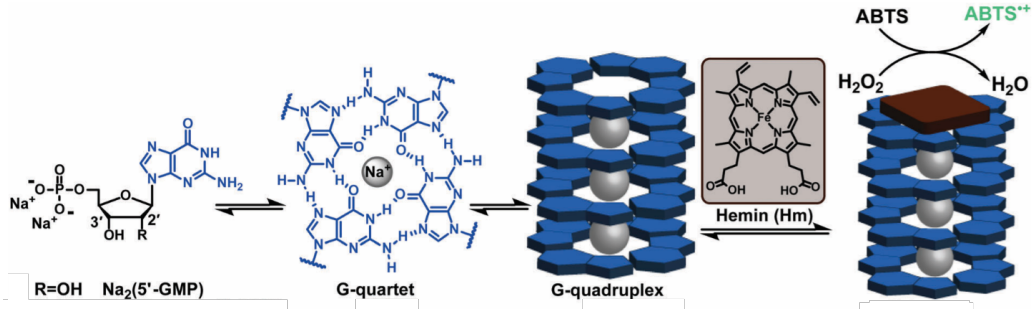

Figure 1.20. Illustration of the self-assembly of 5′-GMP **2** into a G-quadruplex that catalyzes the oxidation of **ABTS**.[52]

1.7 Organic Reactions Promoted by G-Quadruplexes

One of the goals of my doctoral research has been to examine lipophilic G-quadruplexes as templates to perform organic reactions. There have been many examples of DNA G-quadruplexes catalyzing organic reactions. Covalently linked nucleic acid G-quadruplexes, 5′-GMP, and lipophilic guanosine G-quadruplex systems have all been found to promote stereocontrolled organic reactions.

1.7.1 G-Quadruplex Hemin Complexes Catalyze Peroxidation Reactions

One major class of reactions that are catalyzed by the G-quadruplex result from the formation of hemin/G-quadruplex complexes. The G-quadruplex hemin complex mimics a horseradish peroxidase. Travascio and Sen pioneered this work in 1998 when they examined the reactivity of a G-rich DNA sequence (5′-GTG GGT CAT TGT GGG TGG GTG TGG-3′) that formed a G-quadruplex and bound N-methylmesoporphyrin IX (NMM IX). This complex catalyzed the peroxidation reaction of 2, 2′-azino-bis-(3-ethylbenzothiazoline-6-sulphonic acid) **ABTS**.[53] Recent work by Harraz has shown

that the same reaction can be carried out using a 5′-GMP quadruplex/hemin complex, showing that the DNA backbone is not necessary to catalyze the oxidation (shown in **Figure 1.20**).[52] Additionally, Sen found that two electron oxidations can also be catalyzed by hemin G-quadruplex complexes. These complexes were shown to oxidize thioanisole to thioanisole sulfoxide and styrene to styrene oxide.[54] Sens' work led to the expansion of G-quadruplex hemin peroxidation reactions to include the oxidation of a thiol to a disulfide bond (**Figure 1.21**).[55]

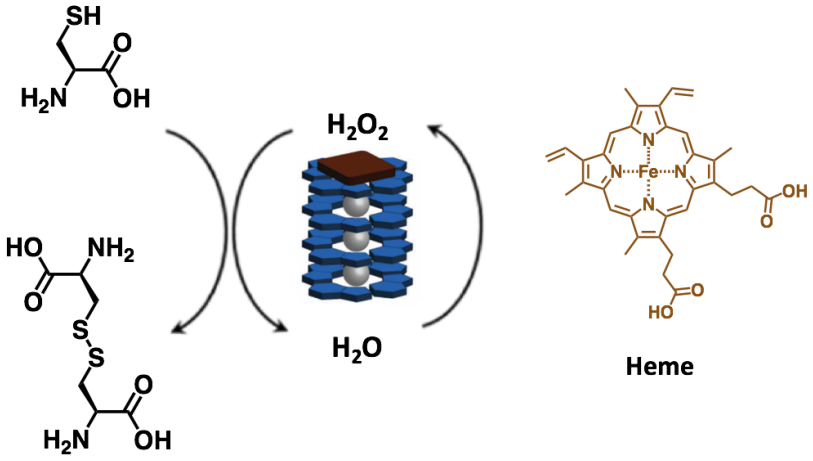

Figure 1.21. Illustration showing a G-quadruplex hemin catalyst promoting the peroxidation of a thiol to disulfide bond.[55] The hemin is represented as a brown block.

1.7.2 Diels-Alder, Friedel-Crafts, and Aldol Reactions Catalyzed by the G-Quadruplex

The G-quadruplex has long been known to bind heme ligands and catalyze oxidation reactions. Roe *et al.* expanded this catalytic ligand binding strategy to a series of bis-pyridyl Cu^{2+} ligands (**Figure 1.22**). G-quadruplexes formed from G_4-rich DNA,

the human telomere DNA hTel or cKit, were used as scaffolds to bind the catalytic ligands and promote asymmetric Diels-Alder reactions. They investigated the Diels-Alder reaction between aza-chalcone derivatives and cyclopentadiene. The Diels-Alder reaction proceeded with high diastereoselectivities and moderate *ee*. [56] A similar Cu^{2+} ligand system was examined for the sulfoxidation of thioanisoles to thioanisole sulfoxides.[57] The G-quadruplex ligand complexes provided greater conversions than the reactive species alone. This work prompted the Li group to examine the reactivity of a human telomere G-quadruplex/Cu^{2+} mixture, absent of any binding ligand. Li found that a DNA G-quadruplex/Cu^{2+} complex promoted the same Diels-Alder reactions with high levels of conversion, high diastereoselectivity and modest enantionselectivity.[58]

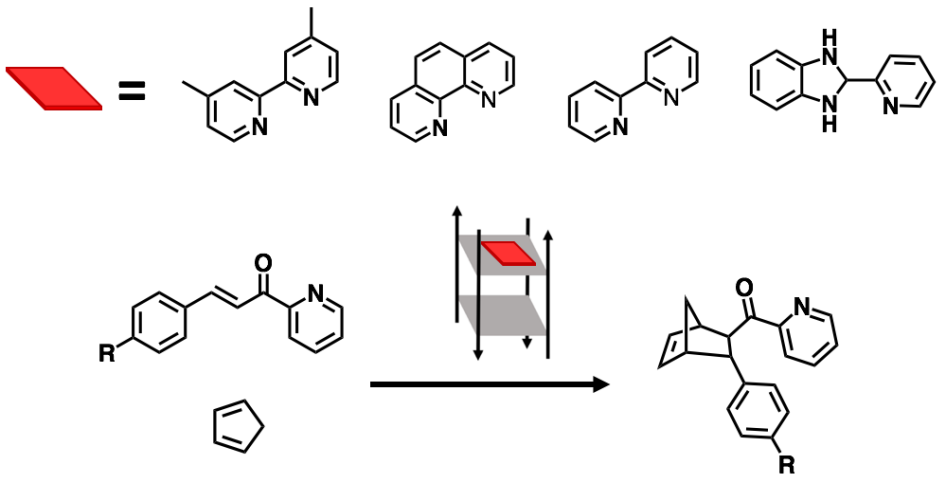

Figure 1.22. Roe *et al.'s* catalytic G-quadruplex. A series of ligands (1-4) that bound to the G-quartet's π-stacking surface were investigated to perform a Diels-Alder reaction between an *aza*-chalcone and cyclopentadiene.[56]

The G-quadruplex has also acted as a template to promote a proline catalyzed aldol reaction. Tang *et al.* demonstrated that a G-quadruplex formed from a partial DNA sequence of the Thrombin Binding Aptamer with a covalently tethered proline catalyst could promote an aldol reaction between acetone and an aldehyde functionalized porphyrin (tris(4-pyridyl)-(4-Aminophenyl)porphyrin (**TMPyP4**)). The G-quadruplex bound the porphyrin in close proximity to the proline organocatalyst, thus promoting the aldol reaction (**Figure 1.23**). The G-quadruplex was required to catalyze the aldol reaction.[59]

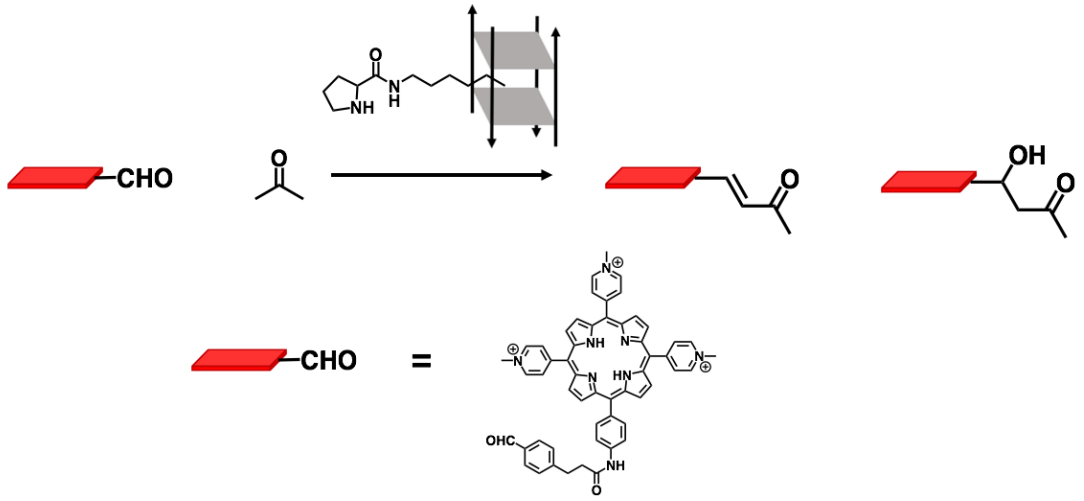

Figure 1.23. Illustration of Tang *et al.*'s G-quadruplex templated aldol reaction between acetone and an aldehyde functionalized porphyrin (tris(4-pyridyl)-(4-aminophenyl)porphyrin (**TMPyP4**)).[59]

Wang and colleagues performed a Friedel-Crafts reaction using a G-quadruplex Cu^{2+} complex. The G-quadruplex Cu^{2+} complex could catalyze a Friedel-Crafts

reaction between a series of substituted 2-acylimidazoles and 5-methoxyindoles with high conversion and moderately high enantiomeric excesses. (**Figure 1.24**).[60]

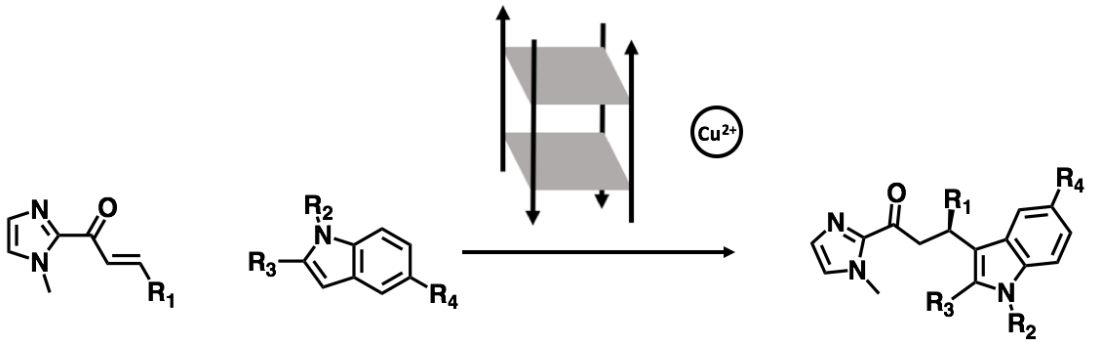

Figure 1.24. Illustration of Wang *et al.*'s G-quadruplex/Cu^{2+} catalyzed Friedel-Crafts reaction between substituted 2-acylamidazole and 5-methoxyindole.[60]

1.7.3 Organic Reactions Promoted by Lipophilic G-Quadruplexes: Olefin Metathesis and [2+2] Cycloaddition of Chalconyls

There are limited examples of lipophilic G-quadruplexes that template or promote organic reactions. Kaucher *et al.* used G-quadruplex self-assembly to align multiple olefin groups for metathesis (**Figure 1.25**).[61] Kaucher synthesized a new guanosine derivative, 5′-(3,5-bis(allyloxy)benzoyl)-2′,3′-isopropylidene guanosine (G **19**), that incorporated reactive π-bonds. When self-assembled, the olefins were brought in close proximity to undergo olefin metathesis to form a covalently linked unimolecular G-quadruplex. The resulting G-quadruplex is capable of transporting Na^+ cations across phospholipid membranes. Rivera and colleagues synthesized a guanosine derivative, 8-chalconyl-3′,5′-butyryl-2′-deoxy guanosine (dG **20**), that when self-assembled aligned the photoreactive olefins of the chalconyl groups in close enough proximity to

photocyclize.[62] Recent work that I performed has shown that the G-quadruplex can catalyze a synthetically useful [2+2] photocycloaddition reaction by using 5′-cinnamate modified guanosine derivatives (as discussed in **Chapter 3** and **Chapter 4**).[63]

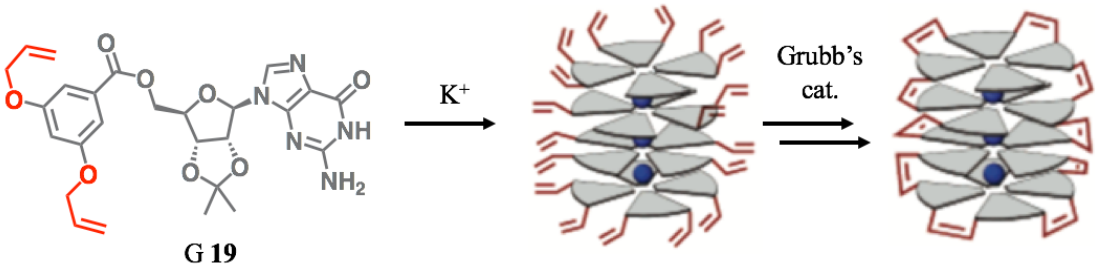

Figure 1.25. Illustration of Kaucher's G-quadruplex templated olefin metathesis.[61]

1.8 Summary

This chapter has introduced some of the factors that can impact G-quadruplex self-assembly. These factors include intrinsic structural factors (e.g. DNA/RNA nucleic acids, GMP nucleotides, and synthetically altered nucleosides) and extrinsic factors (e.g. cation, anion, solvent, temperature). By adjusting any of the factors above the G-quadruplex structure and stability can be fine-tuned. Having greater control over the G-quadruplex allows for the design of novel applications for these systems. One such application and the topic of my thesis is the use of the G-quadruplex as a scaffold to perform organic reactions. As more information about the G-quadruplex is uncovered new applications should be realizable.

Chapter 2: Controlling the Molecularity and Stability of H-Bonded G-Quadruplexes by Modulating the Structure's Periphery

The majority of this chapter has been published in reference 33:

•Sutyak, K.B.; Zavalij, P.Y., Robinson, M.P.; Davis, J.T. "Controlling the molecularity and stability of hydrogen bonded G-quadruplexes by modulating the structure's periphery" *Chem. Comm.* **2016**, 74,11112-111153.

Michael Robinson, an undergraduate student under my supervision, grew the crystals of ***[G21]***$_{16}$•$3K^{+}3I^{-}$. *Dr. Peter Zavalij solved the X-ray crystal structure of* ***[G21]***$_{16}$•$3K^{+}3I^{-}$. *I performed all synthetic and NMR experiments involved in* ***Chapter 2***.

2.1 Research Goals

The goal of the research in this chapter was to examine how synthetic modifications to the 5′-hydroxyl group of a series of lipophilic guanosine (G) derivatives influences the molecularity and self-assembly of G-quadruplex nanostructures. To examine the consequence that these alterations have on self-assembly, 5′-modified aryl esters of guanosine were synthesized. 5′-benzoyl-2′,3′-isopropylidene guanosine (G **21**), 5′-para-nitrobenzoyl-2′,3′-isopropylidene guanosine

(G **22**), 5′-para-methoxybenzoyl-2′, 3′-isopropylidene guanosine (G **23**), 5′-naphthoyl-2′,3′-isopropylidene guanosine (G **24**), and 5′-(2,3,4,5,6) pentafluorobenzoyl-2′,3′-isopropylidene guanosine (G **25**) were examined (**Figure 2.1**). The aromatic esters synthesized were modified with substituents, comprising either activating or de-activating groups, to systematically investigate how the electronics of the aromatic ring and the basicity of the ester carbonyl influence self-assembly. The naphthoyl derivative G **24** was synthesized to gauge the impact of the aromatic surface and π-π stacking interactions on G-quadruplex assembly. The structure and stability of the resulting guanosine architectures were examined using x-ray crystallography, 1D- and 2D- ^{1}H NMR experiments, ESI-MS, DMSO-d_6 NMR titrations, and H/D exchange NMR experiments. The aryl substitutions have a significant influence on the self-assembly of the G monomer (G **21**-G **25**) into its respective G-quadruplex. After examining the self-assembly of 5′-aryl modified G derivatives, the next logical step was to investigate mixed G-quadruplexes formed between 5′-aryl modified G derivatives. Mixing studies were performed between the electron-rich 5′-benzoyl G **21** and electron-poor 5′-pentafluorobenzoyl G **25** to investigate how aromatic-aromatic dispersion interactions might play a role in the assembly.

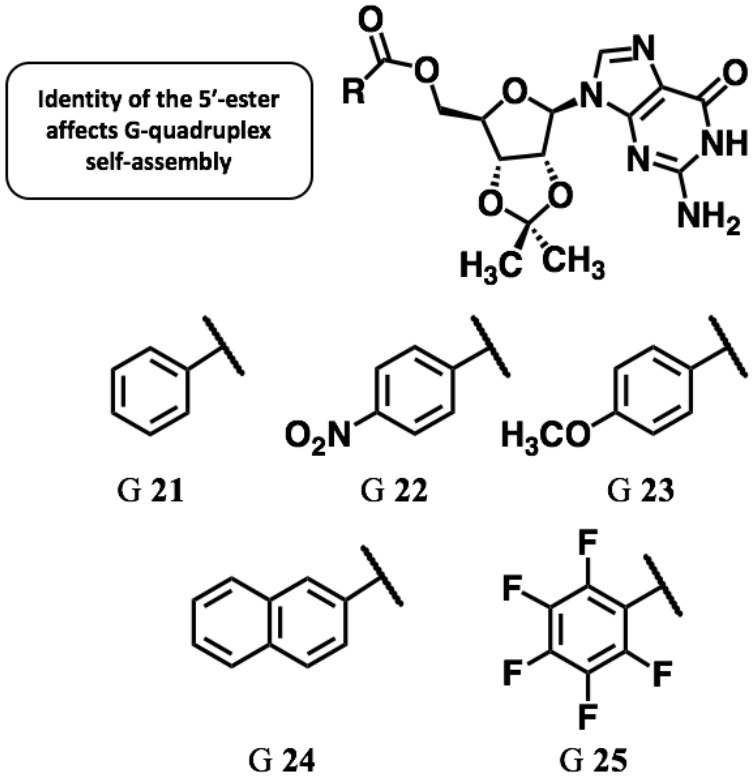

Figure 2.1. Illustration of the 5′-modified guanosine derivatives examined in this chapter: 5′-benzoyl-2′,3′-isopropylidene guanosine (G **21**), 5′-*para*-nitrobenzoyl-2′, 3′-isopropylidene guanosine (G **22**), 5′-*para*-methoxybenzoyl-2′,3′-isopropylidene guanosine (G **23**), 5′-napthoyl-2′,3′-isopropylidene guanosine (G **24**), 5′-(2,3,4,5,6)-pentafluorobenzoyl-2′,3′-isopropylidine guanosine (G **25**).[33]

2.2 Background and Hypothesis: Peripheral Stabilization of G-Quadruplex Structures

Self-assembly is a powerful method for building well-defined nanoscale structures. With the right building blocks, discrete assemblies with new functionalities and tailored properties can be constructed rapidly and in high yields. The nucleotide guanosine (G 1) has unique self-assembly properties and multiple synthetically

modifiable groups. The ease of assembly and synthetic modifications of guanosine makes it an ideal system for designing functional systems and studying self-assembly process. Although synthetic functionalization is easily achieved, the influence that it has over G-quadruplex self-assembly has never been thoroughly examined. Herein we examine how modifications to the 5′-position of guanosine with aryl esters impacts self-assembly.

The G-quadruplex is comprised of a central guanine core and peripheral sugar units extending from the core. In the presence of an appropriate cation the guanine nucleobase forms macrocyclic G-quartets, composed of 4 guanine units that are hydrogen-bonded around a central cation.[5] This hydrogen-bonded G4-quartet is stabilized by ion-dipole interactions between guanosine's C6 carbonyl oxygen and the central cation. The quartets further aggregate together through π-stacking interactions to form the central core of $G_8 \bullet M^+$ octamers and higher ordered G-quadruplexes (**Figure 2.2**).[29] The G-quadruplex nucleobase core is essential for the self-assembly into higher-ordered aggregate structures. The "core" only refers to the central guanine macrocycle, and does not include the ribose sugar that is located on the periphery of the "core". We hypothesized that non-covalent interactions on the periphery of the G-quadruplex, far from the central guanine core, might also have a significant influence on the self-assembly properties of guanosine and be used to modulate structure and dynamics. We tested this hypothesis by systematically investigating how modifications to the

5′-position of guanosine influenced the overall molecularity and stability of the self-assemblies.

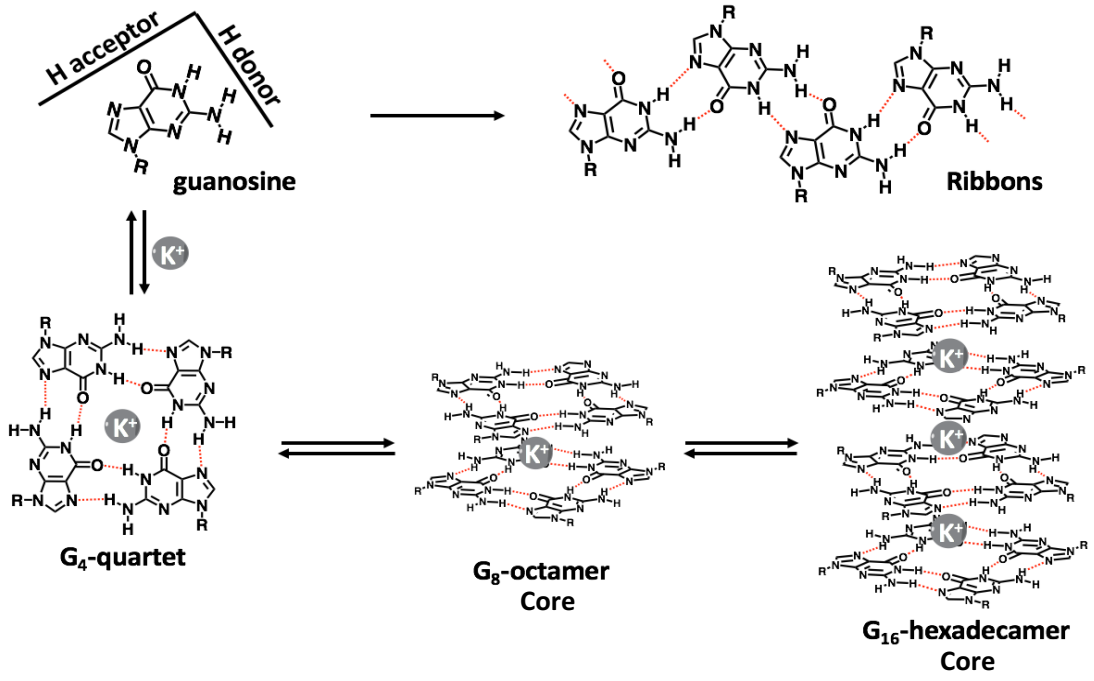

Figure 2.2. Illustration of guanosine self-assembly. In the presence of a cation, guanosine forms a self-assembled macrocyclic "core" through a series of H-bonding and ion-dipole interactions. These G_4-quartets further self-assemble into stacked G-quadruplex structures. Absent of any cations, guanosine favors H-bonded ribbons. The R group is considered the periphery to the G-quadruplex structure.

2.3 Synthetic Targets for Guanosine Functionalization

There are multiple functional groups on guanosine that can be synthetically altered using basic organic reactions. There are two main sites for synthetic modification on guanosine: the guanine nucleobase and the sugar unit. The guanine nucleobase is the primary component responsible for self-assembly into higher ordered

structures; as previously discussed, it is responsible for the assembly of the main π-stacking core of the G-quadruplex. Guanine can be modified at the N^1H amide, N^2H amine, N^3 aryl amine, C^6 carbonyl, N^7 aryl amine, or C^8 aryl H (**Figure 2.3**). Modifications made to the H-bonding donor face (N^1H amide or N^2H amine) or the H acceptor face (C^6 carbonyl or N^7 aryl amine) presumably prevent G-quadruplex self-assembly by impeding the formation of the H-bonded G-quartet core.

The sugar unit is another target for synthetic modification. Depending on whether a DNA or RNA nucleotide is being used, the sugar unit is a 2′-deoxyribose or ribose respectively. The deoxyribose sugar has a primary 5′-hydroxyl group and a secondary 3′-hydroxyl group that are available for functionalization. Ribose also contains a primary 5′-hydroxyl group, but has an additional hydroxyl group at the 2′-position yielding a diol at the 2′/3′ positions.

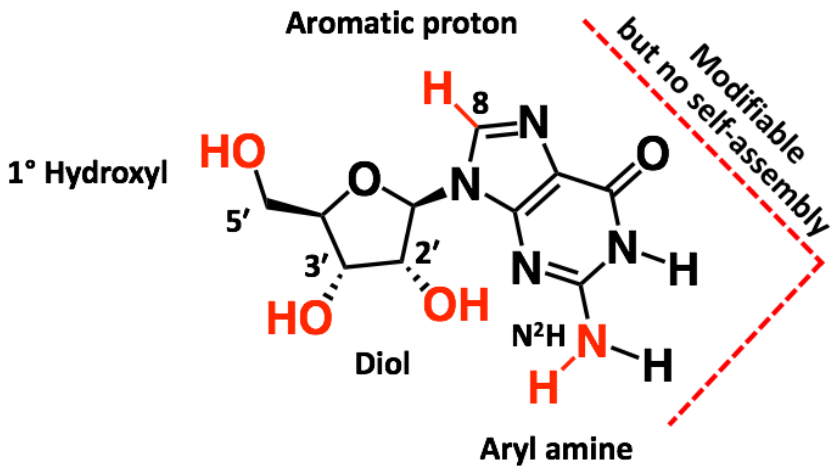

Figure 2.3. Illustration of sites that can be synthetically modified on guanosine G **1**. Guanosine's nucleobase can be altered at the aromatic H8 proton or the outer N^2H amine. Changes made to the inner N^1H, N^7 nitrogen, or C^6 carbonyl destroy guanosine's capacity to self-assemble. The sugar can be modified at the 2′/3′ diol or the 5′ hydroxyl group.

The 5′-position is a favorite location to incorporate new functionality to the G-quadruplex. Lehn developed stimuli-responsive hydrogels from guanosine 5′-hydrazides.[64] By extending chains from the 5′-OH, G-quartet polymers and dendrimers have been made.[65,66] The Sherman, DeFrancq, and Monchaud groups have all used the 5′-OH to graft guanosine units onto macrocycles, generating template-assisted G-quartets.[67-69] The Spada and Masiero group has attached porphyrins, spin labels, thiophenes and ferrocenes to the 5′-position so that arrays of electroactive groups are generated upon G_4-quartet formation.[70-72] Dash's group and the Davis group have linked lipophilic groups to the 5′-OH to make synthetic transmembrane channels for transport of Na^+ and K^+.[73,74]

Although 5′-groups have been used to design synthetic G-quartet architectures, little is known about whether the sidechain itself might help control the structure and stability of the G-quadruplex. Previous work by the Rivera group has shown that G-quadruplex stability can be enhanced by attaching a meta-acetylphenyl (mAG) substituent to guanosine's C8 position on the nucleobase.[23-25] The mAG carbonyl hydrogen bonds with an accessible amino proton N^2H_B within a G_4-quartet layer. Their studies demonstrated that a well-positioned H-bonding acceptor could increase the stability and specificity of the G-quadruplex by strengthening H-bond and π-π interactions. The mAG carbonyl was directly attached to the core of the G-quadruplex, which is primarily responsible for G-quadruplex formation. At first glance, the 5′-position seems too far from the nucleobase G-quartet core at C1′ to influence G-quartet formation. Gellert and Davies, in their landmark paper, suggested that the 5′-phosphate group could stabilize G-quartet layers in 5′-GMP **2** hydrogels through non-covalent interactions.[2] The Wu group used 1D and 2D NMR experimentation to solve a 5′-riboGMP G-quadruplex structure and observed that the 5′-phosphate group from one layer interacts with the next G-quartet's 2′-hydroxyl group to stabilize self-assembly.[13] It has also been shown that eliminating the 2′-hydroxyl group significantly alters the self-assembly properties of guanosine monophosphate in the presence of K^+ or Na^+. Although this H-bonding interaction is on the periphery of the G-quadruplex core, it is apparently still directly involved in stabilizing the self-assembled structures formed from guanosine.[14]

Herein, we explore how modifications made to the 5′-position of lipophilic guanosine derivatives alter guanosine's self-assembly. Throughout this study, we found that the 5′-ester helps control the molecularity and stability of the G-quadruplex by varying H-bonding and dispersion interactions between G-quartet layers. We report on the self-assembly of synthetically modified guanosine derivatives G **21**-G **25** incorporating a series of aromatic esters at their 5′-position. Depending on the basicity, electronics of the ring, and π-surface area of the 5′-aromatic ester the molecularity of the structures is altered, resulting in either discrete $[G]_8 \bullet K^+I^-$ octamers or $[G]_{16} \bullet 3K^+3I^-$ hexadecamers. The thermodynamic and kinetic stabilities of the G-quadruplex are also influenced by interlayer hydrogen-bonding and dispersion interactions on the assembly's periphery. The following sections describe the impact that structural changes at the periphery of the assembly, far from the central H-bonding core, have on the overall stability of the G-quadruplex. The remainder of this chapter, will focus on the structural, thermodynamic, and kinetic aspects of these synthetically modified self-assemblies. X-ray crystallography, 1D and 2D NMR, ^{1}H NMR titrations, and ^{1}H/^{19}F NMR mixing experiments were used to illuminate our findings.

2.4 Synthesis of 5′-Aryl-2′, 3′-Isopropylidene Guanosine Derivatives G 21-G 25

We began by synthesizing the 5′-aryl-2′,3′-isopropylidene G compounds G **21**-G **25** (**Figure 2.4**). Our initial target was the 5′-benzoyl-2′,3′-isopropylidine guanosine derivative G **21**, but after examining G **21**'s self-assembly and the x-ray crystal structure for $[G\ \mathbf{21}]_{16} \bullet 3K^+3I^-$ we synthesized compounds G **22**-G **25** to analyze the 5′-

position's influence over quadruplex assembly. Compounds G **21**-G **25** were prepared in one step from an acetonide protected 2′,3′-isopropylidene guanosine (IspG **26)** and the respective acid chloride. The high reactivity of the acid chloride posed some synthetic challenges, resulting in side product formation of the N2, O5′-diacylated guanosine products. G **21**-G **25** could be isolated through silica gel column purification.

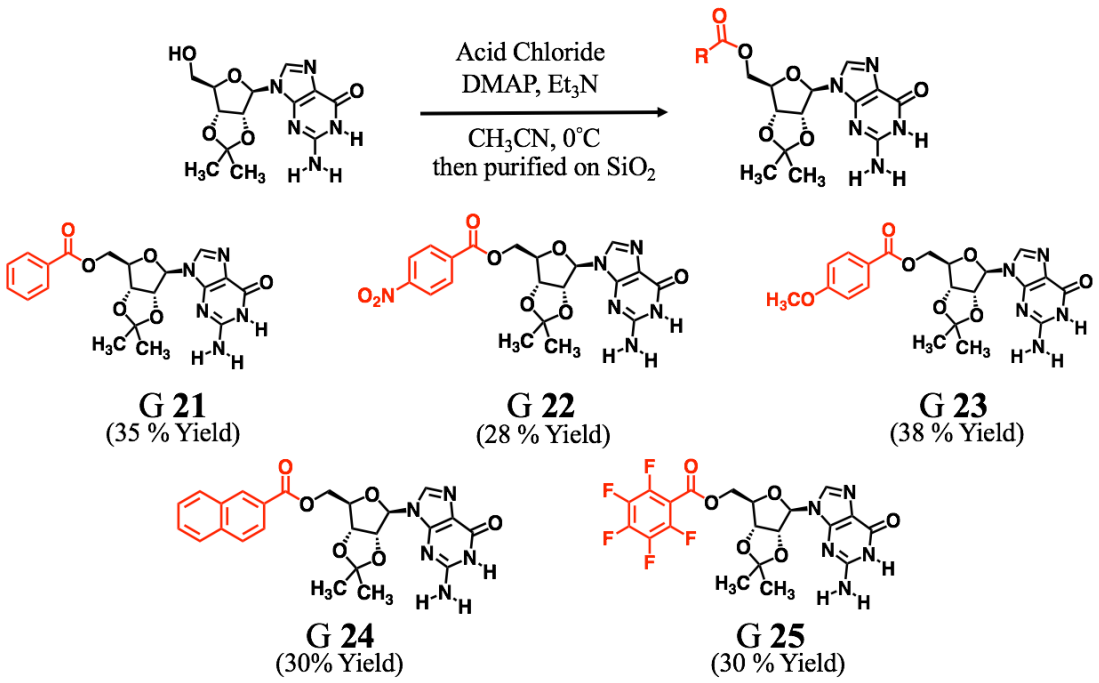

Figure 2.4. Synthesis of compounds G **21-G 25**.

2.5 X-Ray Crystal Structure and ^{1}H-^{1}H Nuclear Overhauser NMR of [G **21**]$_{16}$•3K^{+}3I^{-} Show Highly Cooperative Interlayer H-Bonding and π-Stacking Interactions in Solid State and Solution

The motivation for looking at the 5′-position's influence on quadruplex stability came from the examination of a crystal structure of [G **21**]$_{16}$•3K^{+}3I^{-}. The crystal structure is unique, showing highly-coordinated non-covalent interactions on the periphery of the structure. Single crystals, grown from $CDCl_3$, had a large unit cell: a = 31.601(7) Å, b= 53.211(12) Å and c = 30.881(7) Å. The solid-state structure confirmed that 16 units of **G1** and 3 equivalents of KI form a D_4-symmetric hexadecamer. This G-quadruplex has two D_4-symmetric [G **21**]$_8$•K^{+}I^{-} octamers with an outer G_4-quartet stacking in a tail-to-tail orientation on an inner G_4- quartet. The two co-axial [G **21**]$_8$•K^{+}I^{-} octamers are held together in a head-to-head manner by a central K^{+}. The iodide anions do not make any close contacts with the G-quadruplex. All sugars adopt a *syn* conformation (**Figure 2.5**).

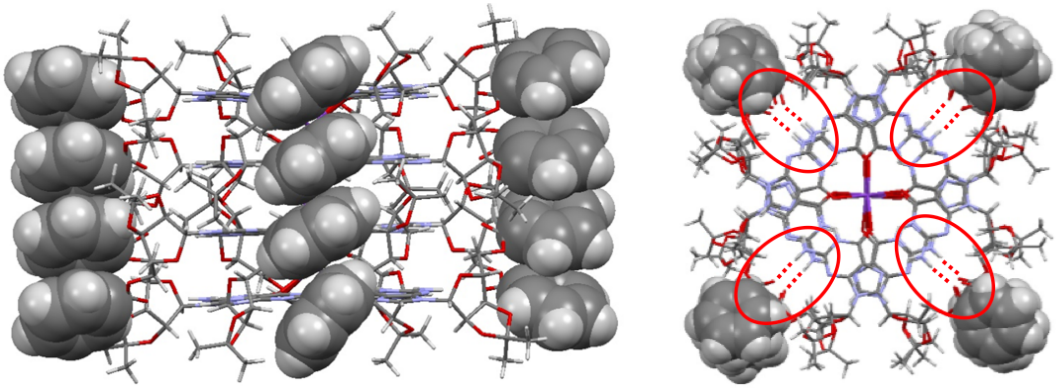

Figure 2.5. X-ray crystal structure for [G **21**]$_{16}$•3K^{+}3I^{-}. Left: Side-view showing organized columns of π-stacking 5′-benzoyls on the periphery of the assembly. Right: red dashed lines illustrate hydrogen bonding interactions between the 5′-carbonyl and exocyclic N^{2}H$_{2}$ amines.

In terms of its H-bonded core, sugar conformation and organization [G **21**]$_{16}$•3K^{+}3I^{-} is similar to other G-quadruplex crystal structures previously reported in the literature.[41,75,76] However, the 5′-benzoate esters on the periphery of [G **21**]$_{16}$•3K^{+}3I^{-} display unique structural attributes that we believe to be crucial for controlling the fidelity and stability of this G-quadruplex. First, all the 5′-ester carbonyls form interlayer H-bonds with exocyclic amines (N^{2}H$_{B}$ donors) in neighboring G$_{4}$-quartets. The outer N^{2}H$_{B}$ hydrogen bonds with the benzoate carbonyl from the inner G-quartet (avg. $d_{N\cdots O}$=3.059 Å) and the inner N^{2}H$_{B}$ forms H-bonds with the outer benzoate (avg. $d_{N\cdots O}$=3.109 Å). These 16 N^{2}H$_{B}$•••O=C H-bonding interactions clamp the outer and inner G-quartets together in [G **21**]$_{16}$•3K^{+}3I^{-}. Another important feature of [G **21**]$_{16}$•3K^{+}3I^{-} are columns of vertically aligned π stacking benzoyl rings involving benzoates from each layer. The 5′-benzoates adopt face-to-face π-stacking orientations with aryl rings extending from neighboring G-quartets, with

centroid-to-centroid distances of 3.7-4.4 Å. We reasoned that these 4 columns of π-stacked benzoates, like interlayer N^2H_B hydrogen bonds, would stabilize the [G **21**]$_{16}$•3K^+3I^- architectures in solution through π-stacking interactions. NMR analysis confirmed that [G **21**]$_{16}$•3K^+3I^- has a similar structure in solution as in the crystal. Strong H8-H1′ nuclear Overhauser effects (nOe) indicate that all sugars are in the *syn* conformation. Signature NOE signals between 5′ and 5″ from one G-quartet with N^2H_2 of the neighboring G-quartet, are consistent with interlayer N^2H_B•••O=C H bonds (**Figure 2.6**). NOes observed between the benzoyl H_{ortho} and H_{meta} of the inner G-quartets verify close π-π stacking distances (**Figure 2.7**). Upfield ^{1}H NMR chemical shifts for 5′-benzoyl protons in [G **21**]$_{16}$•3K^+3I^- in $CDCl_3$, when compared to monomeric G **21** in d_6-DMSO, are also consistent with π-π contacts between neighboring 5′-aromatics. Thus, 5′-benzoyl hydrogens (H_{ortho}, H_{meta}, and H_{para} in both layers) in [G **21**]$_{16}$•3K^+3I are more shielded than in the monomer, with Δδ values ranging from 0.08 to 0.90 ppm.

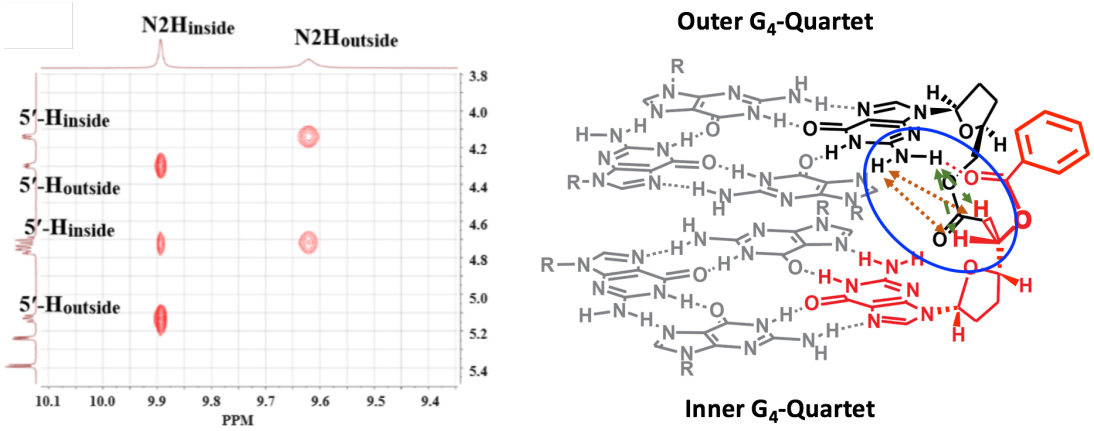

Figure 2.6. ^{1}H-^{1}H NOESY spectrum of [G **21**]$_{16}$•3K^{+}3I^{-} (0.625 mM) in $CDCl_3$ providing evidence for interlayer H-bonding in solution. Nuclear Overhauser effects occur between the 5′ and 5″ hydrogens of the ribose with the next layer's exocyclic N^{2}H amino protons of the guanine nucleobase. The nOes are circled above with double-sided arrows highlighting the through-space interactions. This is significant because it shows that the 5′ hydrogens and N^{2}H protons are close together, providing evidence for interlayer H-bonding interactions in solution.

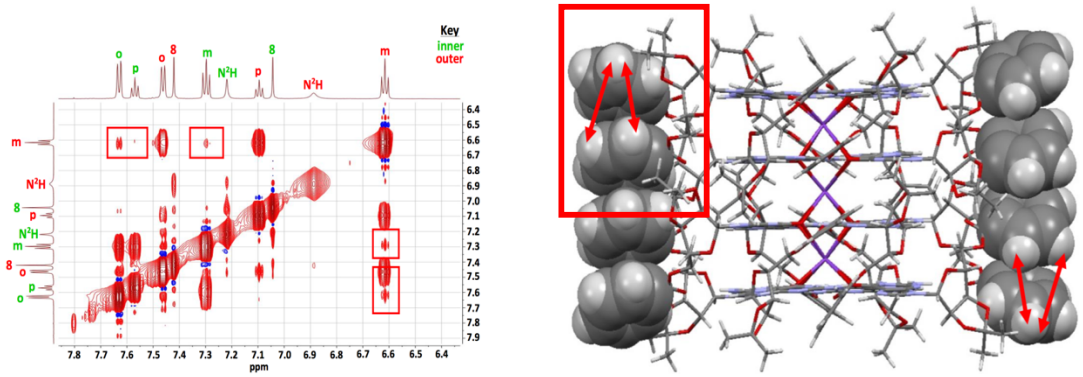

Figure 2.7. ^{1}H-^{1}H NOESY spectrum of [G **21**]$_{16}$•3K^{+}3I^{-} (0.625 mM) in $CDCl_3$ showing the interlayer π-stacking interactions between one layer and the next neighboring layer. The *meta* protons of an aromatic ring in one layer show NOE signals to the neighboring layer's *ortho* and *meta* protons.

2.6 G-Quadruplex Self-Assembly of 5′-Aryl-2′, 3’-Isopropylidene Guanosine

2.6.1 Self-Assembly of 5′-Benzoyl- 2′, 3′- Isopropylidene Guanosine G 21

Benzoate ester G **21**, insoluble in $CDCl_3$, dissolved in the presence of KI (0.125 eq.) to give a ^{1}H NMR spectrum consistent with a D_4-symmetric octamer [G **21**]$_8$•K^+I^- (**Figure 2.8**). We made this assignment based on precedent with related analogs that we, and others, have described.[36] The ^{1}H NMR spectrum for [G **21**]$_8$•K^+I^- had one set of resonances, with a singlet for amide N^1H (δ 12.35 ppm) and two broader signals for N^2H_2 amino protons, δ 9.55 ppm for the proton involved in the G-quartet's N^2H_A•••N^7 H-bond and one at δ 6.40 ppm for the exocyclic N^2H_B. Addition of another 0.125 eq. of KI (to give 0.25 eq.) resulted in disappearance of octamer [G **21**]$_8$•K^+I^- and formation of a new species that we assigned as hexadecamer [G **21**]$_{16}$•$3K^+3I^-$, based on the crystal structure, splitting of its ^{1}H NMR signals into pairs of signals of equal intensity, and mass spectrometry. Using 2D NMR experiments we assigned these sets of signals to the outer and inner G_4-quartets of a D_4-symmetric hexadecamer. Further evidence for formation of [G **21**]$_{16}$•$3K^+3I^-$ was confirmed by mass spectrometry and X-ray crystallography. Electrospray ionization mass spectrometry (ESI-MS) of a $CDCl_3$ sample containing G **21** and 0.25 eq. of KI showed the major, triply charged peak at 2318.43 m/z, indicating a molecular weight of 6955.3 for the hexadecamer [G **21**]$_{16}$•$3K^+3I^-$ (**Figure 2.9**).

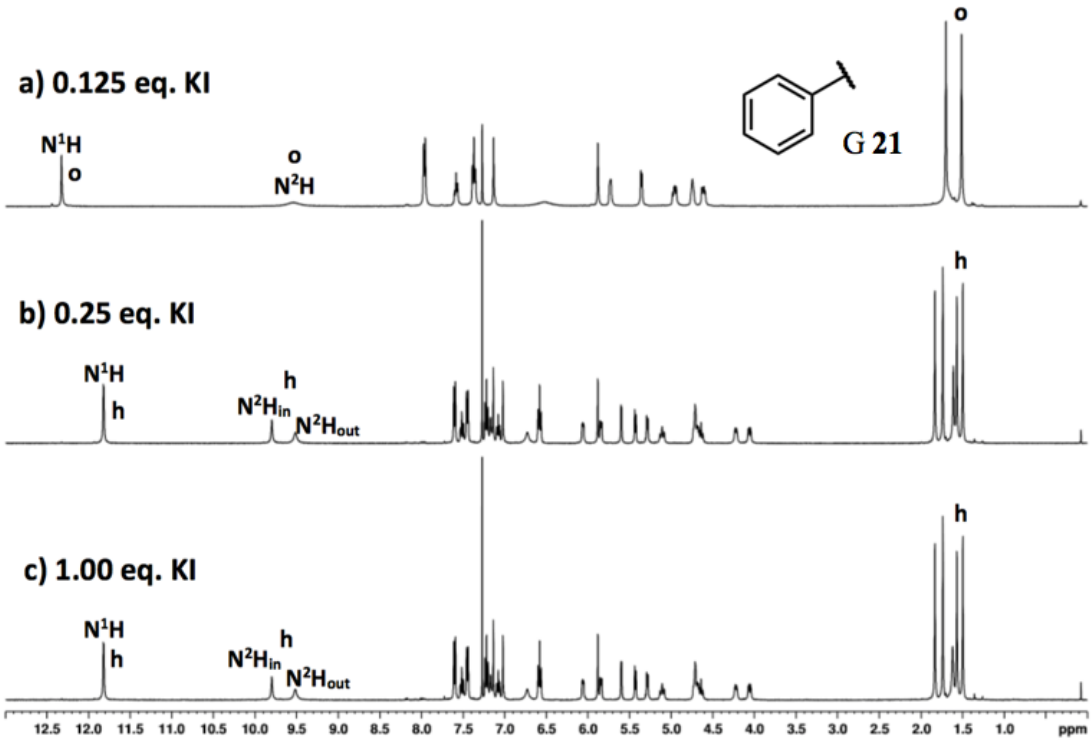

Figure 2.8. A series of ^{1}H NMR spectra showing G **21** self-assembly as a function of KI concentration. A) G **21** (10 mM) in $CDCl_3$ at 25 °C in the presence of 0.125 eq KI (1.25 mM). A single set of ^{1}H NMR resonances are observed, consistent with [G **21**]$_8$•K^+I^- formation. B) G **21** (10 mM) in $CDCl_3$ at 25 °C in the presence of 0.25 eq KI (2.5 mM). Two sets of ^{1}H NMR resonances of equal intensity are present, consistent with [G **21**]$_{16}$•$3K^+3I^-$ formation. C) G **21** (10 mM) in $CDCl_3$ at 25°C in the presence of 1.00 eq KI (10 mM). Two sets of ^{1}H NMR resonances of equal intensity are present, consistent with [G **21**]$_{16}$•$3K^+3I^-$ formation. Selected signals for the octamer are labeled (o) and hexadecamer are labeled (h).

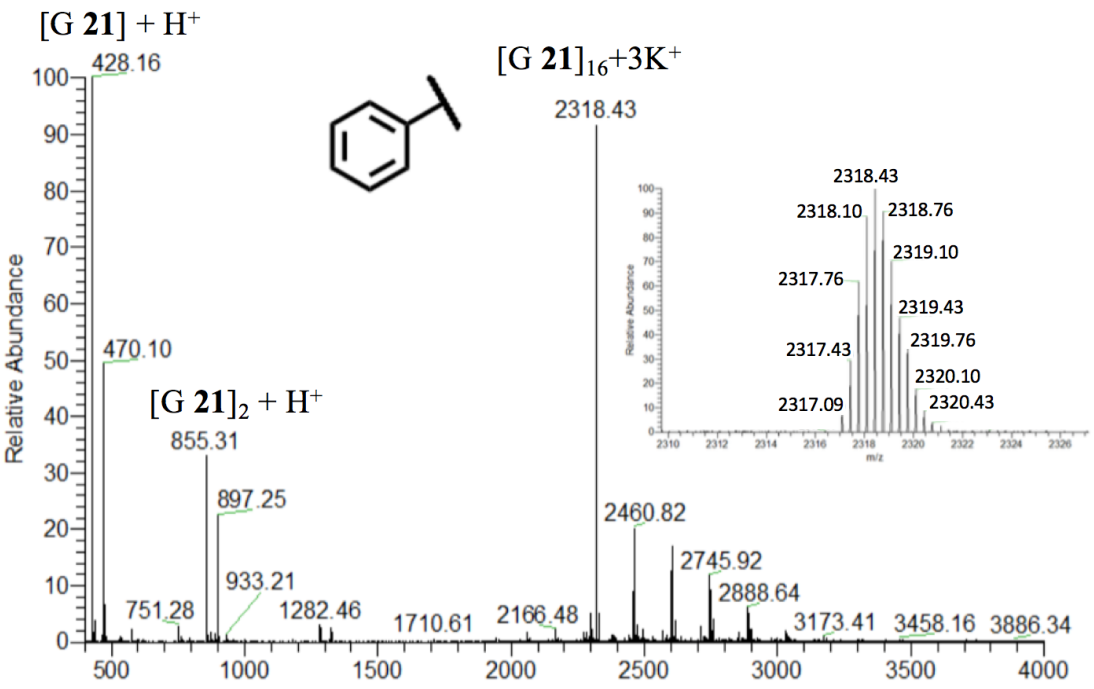

Figure 2.9. ESI-MS of [G **21**]$_{16}$•3K$^+$3I$^-$(0.625 mM) from $CDCl_3$. The inset shows an expanded region for the peak at m/z= 2318.43.

2.6.2 Self-Assembly of 5′-*para*-Nitrobenzoyl-2′,3′-Isopropylidene Guanosine G 22, 5′-*para*-Methoxybenzoyl-2′, 3′-Isopropylidene Guanosine G 23, and 5′-Napthoyl-2′, 3′-Isopropylidene Guanosine G 24

Having characterized [G **21**]$_{16}$•3K$^+$3I$^-$ we sought to determine if altering the N^2H_B•••O=C interlayer H-bonds and π-π stacking on the periphery could control the structure and stability of the G-quadruplex. To gauge the importance of interlayer N^2H_B•••O=C bonds we compared the assembly of 5′-benzoyl G **21** with 5′-*para*-nitrobenzoyl ester G **22** and 5′-*para*-methoxy benzoyl ester G **23**. *Para* substituents on the benzoyl ring might modulate the carbonyl's basicity through resonance and influence its ability to H-bond with the next layer. Thus, the electron-withdrawing *p*-

NO_2 in G **22** should decrease 5′-ester basicity, make it a poorer H-bond acceptor relative to G **21**, and destabilize the G-quadruplex. In contrast, the electron-donating *p*-OMe group in G **23** should make the ester carbonyl more basic, enhance its H-bonding capability, and stabilize the G-quadruplex. With 4 layers of G-quartets in the hexadecamer [G **21**]$_{16}$•3K^+3I^- there are 12 possible π-π stacking interactions on the G-quadruplexes periphery. We probed the importance of π-π stacking interactions by comparing the stability of G-quadruplexes made from 5′-benzoyl G **21** and 5′-naphthoyl G **24**.

Self-assembly of *p*-NO_2Ph G **22** and *p*-OMePh G **23** in the presence of KI was compared to G **21** using ^{1}H NMR and ESI-MS. Like the 5′-benzoate G **21**, G **22** and G **23** were poorly soluble in $CDCl_3$, but dissolved upon addition of KI. At lower K^+ concentrations (0.125 eq.), where there is not enough cation to template [G]$_{16}$•3K^+3I^- hexadecamer formation, G **22** and G 2**3** each formed D_4-symmetric octamers [G]$_8$•K^+I^-, signified by a single set of ^{1}H NMR resonances. Addition of more KI (0.25 eq.) to p-MeO-benzoyl G **23** gave a [G **23**]$_{16}$•3K^+3I^- hexadecamer (**Figure 2.10**), as evidenced by (1) the characteristic doubling of signals in the ^{1}H NMR spectrum and (2) an ESI-MS spectrum that showed a triply charged peak at 2478.48 m/z (**Figure 2.11**). Strikingly, ^{1}H NMR indicated that the p-NO_2 benzoyl G **22** remained an octamer [G **22**]$_8$•K^+I^- even after addition of excess KI (1.00 eq. KI per monomer G **22**) (**Figure 2.12**). ESI-MS of this sample of G **22** and 1 equivalent of KI showed a small peak for a doubly charged ion at 1908.03 m/z, consistent with a molecular weight of 3816 for

[G **22**]$_8$•K^+(**Figure 2.13**). No peaks for any putative hexadecamer [G **22**]$_{16}$•3K^+3I^- were observed in the ESI-MS. Apparently, the p-nitrobenzoate carbonyl is not a strong enough H-bond acceptor to complete hexadecamer formation in $CDCl_3$ and self-assembly stops at the [G **22**]$_8$•K^+I^-. Changing the H-bond strength of the 5′-ester may not be the only factor involved in controlling the molecularity of the G-quadruplex, as it is also possible that dipole-dipole interactions between the 5′-aryl groups influence the supramolecular assembly of G **21**-G **23**. Differences in structure for G **22**, which gives an octamer, and G **21** and G **23**, which form hexadecamers, might be due in part to the greater electrostatic repulsion expected for the nitro substituted G **22**. Clearly, mutation from H in G **21** to a NO_2 group in G **22** results in a dramatic change in molecularity. The molecularity of this class of G-quadruplex can be controlled by (1) toggling the electronics of the peripheral 5′-benzoate and (2) varying the amount of KI in solution.

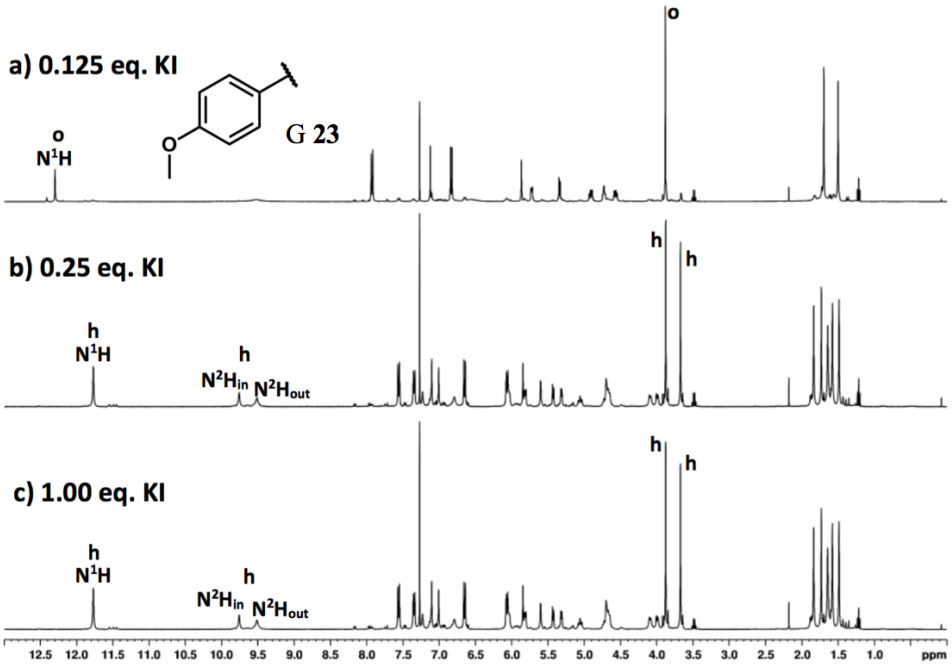

Figure 2.10. A series of ^{1}H NMR spectra showing G **23** self-assembly as a function of KI concentration. A) G **23** (10 mM) in $CDCl_3$ at 25 °C in the presence of 0.125 eq KI (1.25 mM). A single set of ^{1}H NMR resonances are observed, consistent with [G **23**]$_8$•K^+I^- formation. B) G **23** (10 mM) in $CDCl_3$ at 25 °C in the presence of 0.25 eq KI (2.5 mM). Two sets of ^{1}H NMR resonances of equal intensity are present, consistent with [G **23**]$_{16}$•$3K^+3I^-$ formation. C) G **23** (10 mM) in $CDCl_3$ at 25 °C in the presence of 1.00 eq KI (10 mM). Two sets of ^{1}H NMR resonances of equal intensity are present, consistent with [G **23**]$_{16}$•$3K^+3I^-$ formation. Selected signals for the octamer are labeled (o) and hexadecamer are labeled (h).

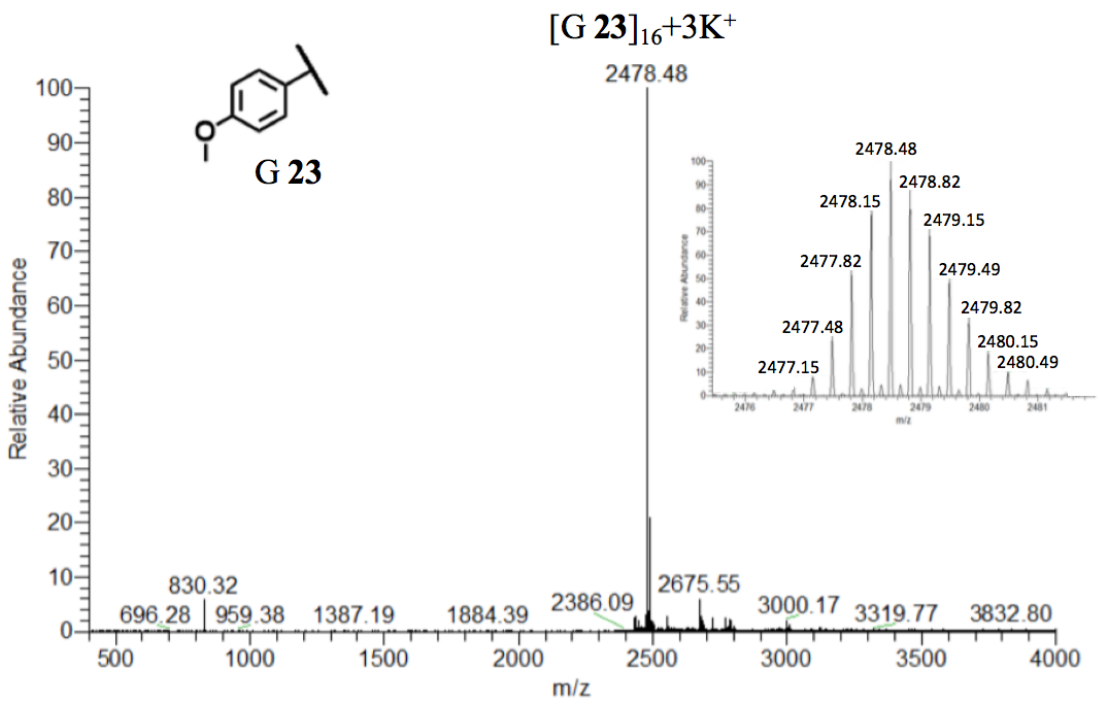

Figure 2.11. ESI-MS of [G **23**]$_{16}$•3K+3I-(0.625 mM) from $CDCl_3$. The inset shows an expanded region for the peak at m/z= 2478.48.

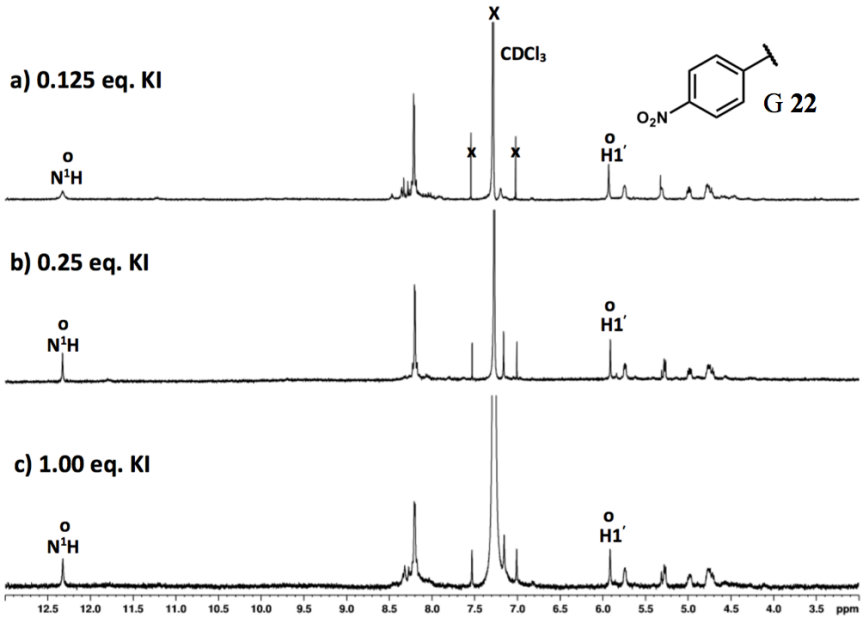

Figure 2.12. A series of ^{1}H NMR spectra showing G **22** self-assembly. A) G **22** (10 mM) in $CDCl_3$ at 25 °C in the presence of 0.125 eq KI (1.25 mM). A single set of ^{1}H NMR resonances are observed, consistent with [G **22**]$_8$•K^+I^- formation. B) G **22** (10 mM) in $CDCl_3$ at 25 °C in the presence of 0.25 eq KI (2.5 mM). A single set of ^{1}H NMR resonances are observed, consistent with [G **22**]$_8$•K^+I^- formation. C) G **22** (10 mM) in $CDCl_3$ at 25 °C in the presence of 1.00 eq KI (10 mM). [G **22**]$_8$•K^+I^- formation is observed.

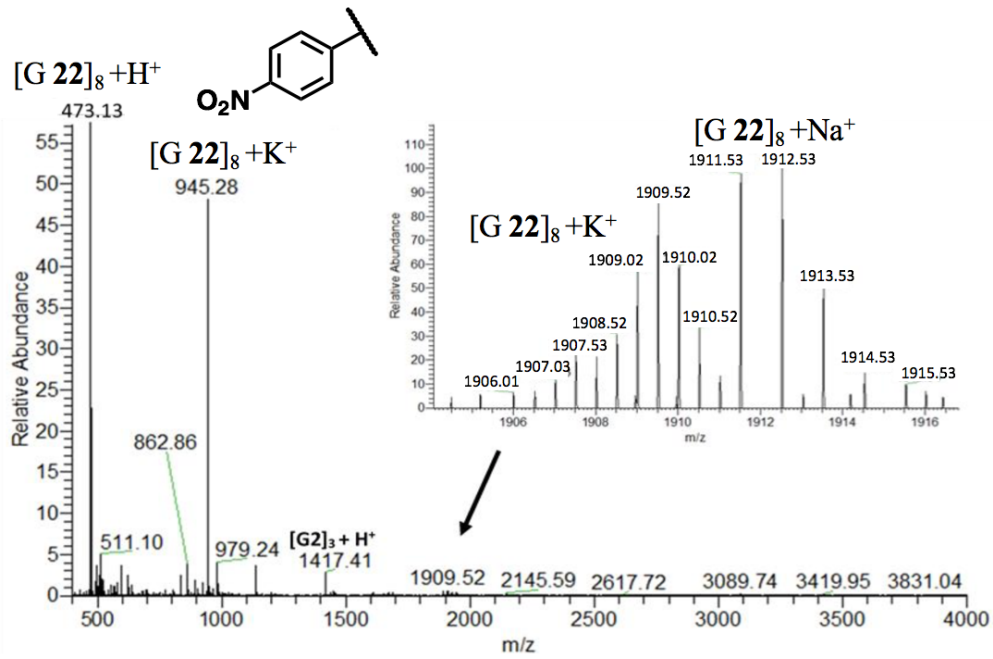

Figure 2.13. ESI-MS of [G **22**]$_8$•K^+I^- (1.25 mM) from $CDCl_3$. The inset shows an expanded region for the peak at m/z= 1909.52.

Self-assembly of naphthoyl G **24** in the presence of KI was also examined using ^{1}H NMR. Like the 5′-benzoate G **21**, G **24** was poorly soluble in $CDCl_3$, but dissolved upon addition of KI. Similar to compounds G **21**-G **23**, at lower K^+ concentrations (0.125 eq.) G **24** formed D_4-symmetric octamers [G]$_8$•K^+I^-, signified by a single set of ^{1}H NMR resonances. Addition of more KI (0.25 eq.) to naphthoyl G **24** gave a [G **24**]$_{16}$•$3K^+3I^-$ hexadecamer (**Figure 2.14**), as evidenced by the characteristic doubling of signals in the ^{1}H NMR spectrum. Having shown that G **23** and G **24** form G_{16} hexadecamers in solution in the presence of K^+, further work was performed to compare

the thermodynamic and kinetic stability of G-quadruplex hexadecamers made from G **21**, G **23**, and G **24**.

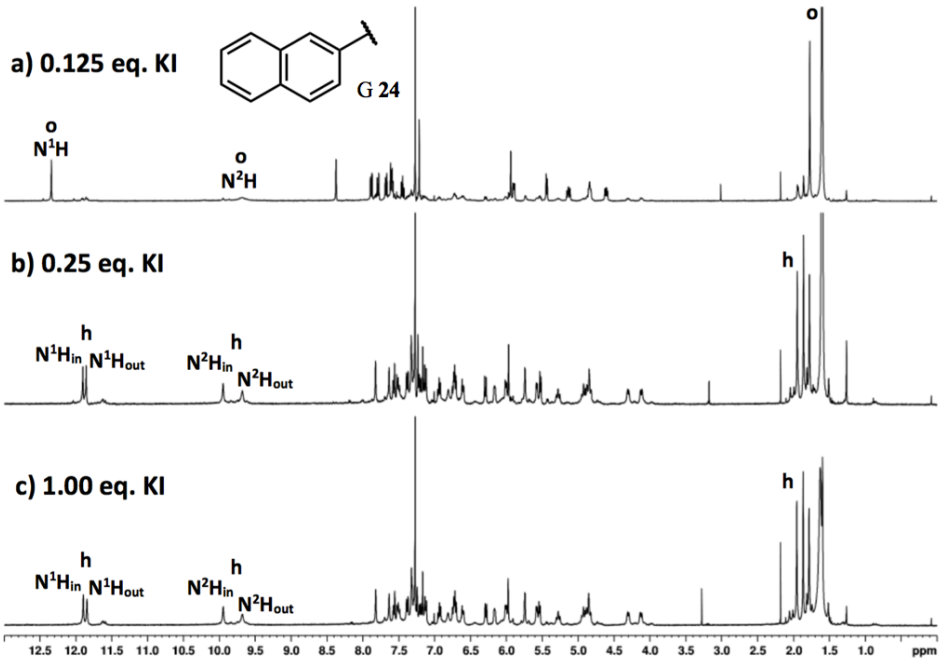

Figure 2.14. A series of ^{1}H NMR spectra showing G **24** self-assembly as a function of KI concentration. A) G **24** (10 mM) in $CDCl_3$ at 25 °C in the presence of 0.125 eq KI (1.25 mM). A single set of ^{1}H NMR resonances are observed, consistent with [G **24**]$_8$•K^+I^- formation. B) G **24** (10 mM) in $CDCl_3$ at 25 °C in the presence of 0.25 eq KI (2.5 mM). Two sets of ^{1}H NMR resonances of equal intensity are present, consistent with [G **24**]$_{16}$•$3K^+3I^-$ formation. C) G **24** (10 mM) in $CDCl_3$ at 25 °C in the presence of 1.00 eq KI (10 mM). Two sets of ^{1}H NMR resonances of equal intensity are present, consistent with [G **24**]$_{16}$•$3K^+3I^-$ formation. Selected signals for the octamer are labeled (o) and hexadecamer are labeled (h).

2.7 Thermodynamic Stability of 5′-Aryl Modified G_{16}-Hexadecamers: DMSO Titrations

To evaluate how the 5′-ester's identity impacts the thermodynamic stability of G_{16}-hexadecamers we used ^{1}H NMR spectroscopy to follow how addition of DMSO-d_6 changes the hexadecamer-monomer equilibrium in CD_3CN. DMSO-d_6 competes for H-bond formation and reduces the thermodynamic stability of the G-quadruplex,[77] shifting the equilibrium towards monomer. Since the signals for the hexadecamer and the dissociated "monomer" are in slow exchange on the chemical shift time scale one can determine the equilibrium concentration of the two species as a function of added DMSO-d_6. We prepared samples in CD_3CN of the 3 different G_{16}•K^+ hexadecamers (0.625 mM) made from G **21**, G **23**, and G **24** by mixing the G derivative (10 mM) and 0.25 eq. of KI (2.5 mM). We measured ^{1}H NMR spectra (600 MHz) of these samples over a DMSO-d_6 co-solvent range from 0% to 50% at 25 °C (**Figure 2.15**). Data in **Figure 2.15** shows that G-quadruplexes made from p-OMe benzoate G **23** and 5′-naphthoate G **24** are more stable than the G-quadruplex made from 5′-benzoate G **21**. Thus, at 20% DMSO-d_6 no hexadecamer [G **21**]$_{16}$•3K^+3I^- remained in solution; the assembly had "melted" to give only dissociated G **21**. In contrast, a significant amount of G **23** (51.5 %) and G **24** (55.5 %) remained bound in their respective G-quadruplexes at 20% DMSO-d_6. We attribute the enhanced stability of [G **23**]•3K^+3I^- relative to that of [G **21**]$_{16}$•3K^+3I^-, to stronger interlayer hydrogen bonding because of the increased basicity of the p-OMe benzoate in G **23**. This interpretation is supported by the fact that

both N^2H_B protons in [G **23**]$_{16}$•3K$^+$I$^-$ (δ_o=6.96 and δ_i=7.30) are shifted downfield relative to the same protons in [G **21**]$_{16}$•3K$^+$3I$^-$ (δ_o=6.88 and δ_i=7.22), consistent with stronger N^2H_B•••O=C H bonds. We attribute greater stability for 5′-naphthoyl [G **24**]$_{16}$•3K$^+$3I$^-$, to enhanced interlayer π-π dispersion interactions for the larger naphthoyl groups that cooperatively stabilize the assembly's H-bonded core. Cockroft and colleagues have demonstrated that increasing the surface area available for dispersion interaction in π-stacked systems can stabilize H-bonded assemblies in organic solvents.[78]

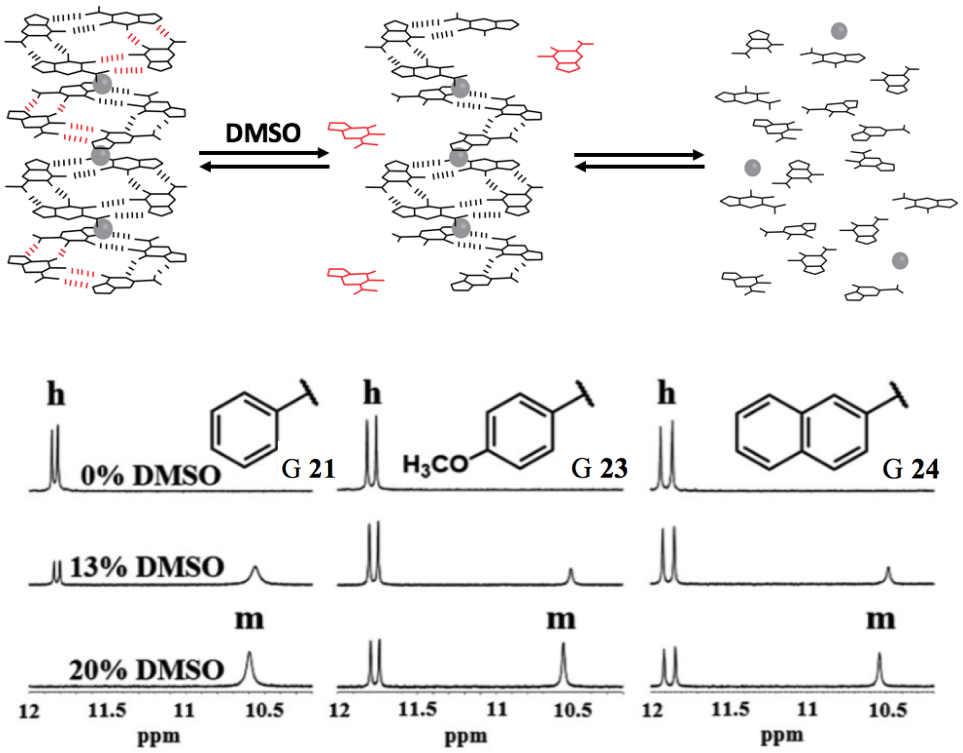

Figure 2.15. ^{1}H NMR spectra of N^{1}H region for [G]$_{16}$•3K$^+$3I$^-$ (0.625 mM) made from G **21**, G **23**, and G **24** upon addition of DMSO-d_6 in CD_3CN. The 2 signals near δ 11.8 ppm belong to hexadecamers (h) and the signal at δ 10.6 ppm is from dissociated monomer (m).

2.8 Kinetic Stability of 5′-Aryl Modified G_{16}-Hexadecamers: Deuterium Exchange Experiments

The G-quadruplex system is in dynamic and rapid equilibrium between monomer and assemblies. To compare the kinetic stability of individual H-bonds in these G-quadruplex variants, we conducted NMR hydrogen-deuterium (H/D) exchange experiments on the N^1H and N^2H protons involved in the core and interlayer H-bonding interactions. The H/D exchange, under equilibrium conditions, reports on the dynamics and solvent accessibility of individual H-bonds within the outer and inner G-quartets (**Figure 2.16**).

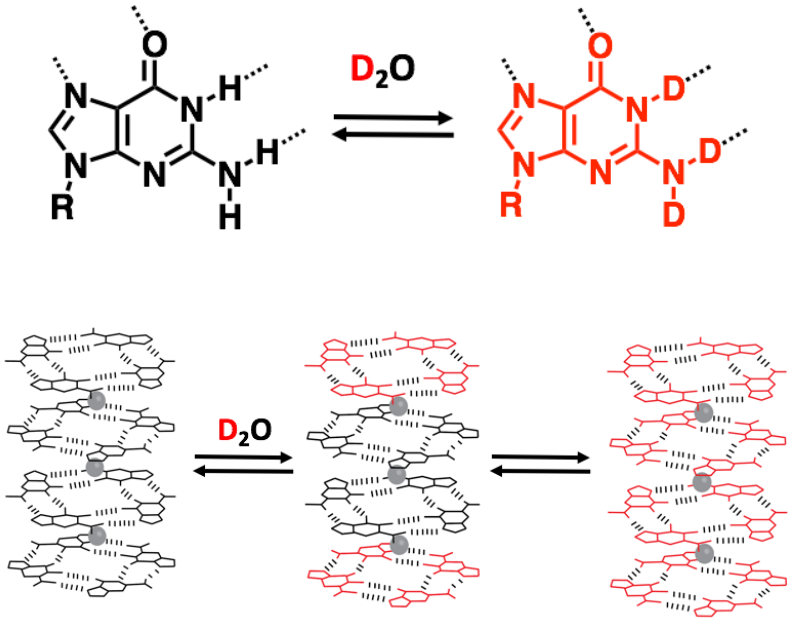

Figure 2.16. Top) Illustration showing H/D exchange of the guanine N^1H and N^2H_2 protons. The guanine nucleobases are color coded red to represent deuteration. Bottom) Illustration showing the process of proton/deuterium exchange in the G-quadruplex in the presence of a deuterium source, in this example D_2O. Deuteration occurs at the outside G_4-quartets first, since they are more weakly held together and are more accessible to solvent. The inner G_4-quartets are less accessible to added D_2O resulting in a slower rate of H/D exchange.

We prepared solutions of G-quadruplexes [G **21**]$_{16}$•3K^+3I^-, [G **23**]$_{16}$•3K^+3I^-, and [G **24**]$_{16}$•3K^+3I^- (0.625 mM) in CD_3CN (0.5 mL), added 10 μL of D_2O and recorded ^1H NMR (600 MHz) spectra of G-quadruplexes over time. One important observation is that in all 3 G-quadruplexes the N^1H and N^2H in the outer G-quartets (o) exchange much faster than do the N^1H and N^2H in the inner G-quartets (i). This is consistent with the inner G-quartets being more protected from solvent and H/D exchange occurring more readily with the exposed outer G-quartets. The second significant finding is that

H/D exchange for N^1H and N^2H protons in the inner G-quartet is significantly slower for both the 5′-p-OMe benzoate [G **23**]$_{16}$•3K$^+$3I$^-$ and the 5′-naphthoyl [G **24**]$_{16}$•3K$^+$3I$^-$ than for the parent [G **21**]$_{16}$•3K$^+$3I$^-$ G-quadruplex. **Figure 2.17** shows that H/D exchange of N^1H_i is complete after 1 h for [G **21**]$_{16}$•3K$^+$3I$^-$, but only 71% exchange has occurred for that same proton in [G **23**]$_{16}$•3K$^+$3I$^-$ after 1 h. Both [G **23**]$_{16}$•3K$^+$3I$^-$ and [G **24**]$_{16}$•3K$^+$3I$^-$ are kinetically more stable (with H/D exchange half-lives on the order of hours) than [G **21**]$_{16}$•3K$^+$3I$^-$ (which has a H/D exchange half-life of about 10 min), consistent with the fact that complexes made from G **23** and G **24** have stronger H-bonds and tighter structures than the G-quadruplexes made from 5′-benzoate G **21**.

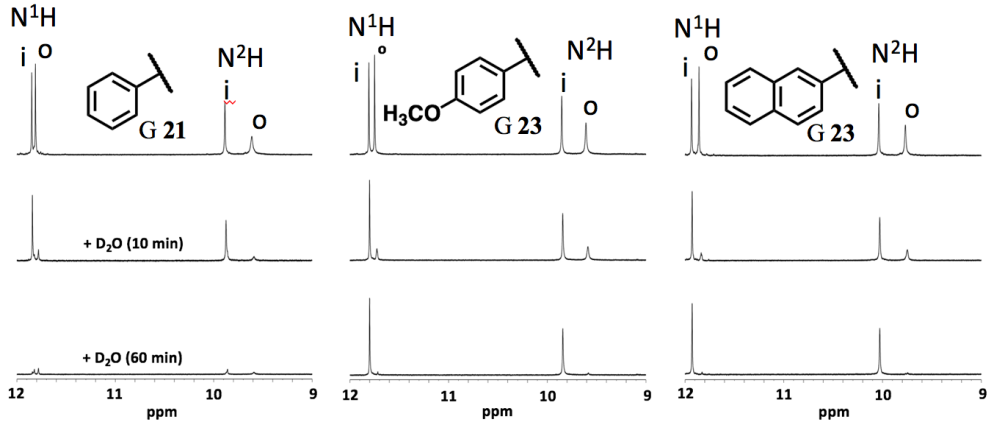

Figure 2.17. ^{1}H NMR spectra of amide N^1H and amino N^2H_2 region for [G **21**]$_{16}$•3K$^+$3I$^-$, [G **23**]$_{16}$•3K$^+$3I$^-$, and [G **24**]$_{16}$•3K$^+$3I$^-$ (0.625 mM, 25°C) after addition of D_2O (10 μL) in CD_3CN. Signals in the outer G-quartets are labeled (o) and inner G-quartets (i).

Through a series of DMSO-d_6 titration ^{1}H NMR and H/D NMR exchange experiments we were able to directly compare the thermodynamic and kinetic stabilities of G-quadruplexes formed from the new 5′-modified guanosine derivatives G **21**, G **23**,

and G **24**. The 5′-aryl modification had a significant impact on the thermodynamic and kinetic stability of the assemblies. The 5′-(4-methoxy)benzoyl G **23** and 5′-naphthoyl **G 24** are more thermodynamically and kinetically stable than the 5′-benzoyl G **21**. This stabilization is presumably due to increased interlayer H-bonding interactions and π-stacking interactions between the substituted 5′-aryl groups as compared to the non-substituted aromatic derivative.

2.9 Mixed Self-Assemblies of 5′-(2,3,4,5,6)-Pentafluorobenzoyl-2′,3′-Isopropylidene Guanosine G 25 and 5′-Benzoyl-2′, 3′-Isopropylidene Guanosine G 21

The next logical step after studying the self-assembly of the 5′-aryl guanosine derivatives, G **21-G 24**, was to investigate the formation of G-quadruplexes containing mixtures of 5′-substituted electron-rich and electron-poor aryl derivatives. A binary mixture of 5′-benzoyl-2′, 3′-isopropylidene guanosine G **21** and 5′-(2,3,4,5,6)-pentafluorobenzoyl-2′, 3′-isopropylidene guanosine G **25** was investigated for G-quadruplex formation. We hypothesized that mixed G-quadruplexes comprised of G **21** and electron-poor aromatic G **25** might self-sort based on the increased enthalpic stability of arene-perfluoroarene π-π stacking interactions (**Scheme 2.18**). There is precedent for self-sorting in mixed quadruplex systems. Previous work on mixed G-quadruplexes between guanosine enantiomers has shown self-sorting based on chirality. Mixtures of D- and L- guanosine G **16** have been shown to self-separate based

on the chirality of the guanosine ribose unit.[40] If stereochemistry can promote self-sorting we figured that the identity of the 5′-aryl group may also promote self-sorting. ^{1}H and ^{19}F NMR experiments were performed to examine the self-assembly of these binary mixtures.

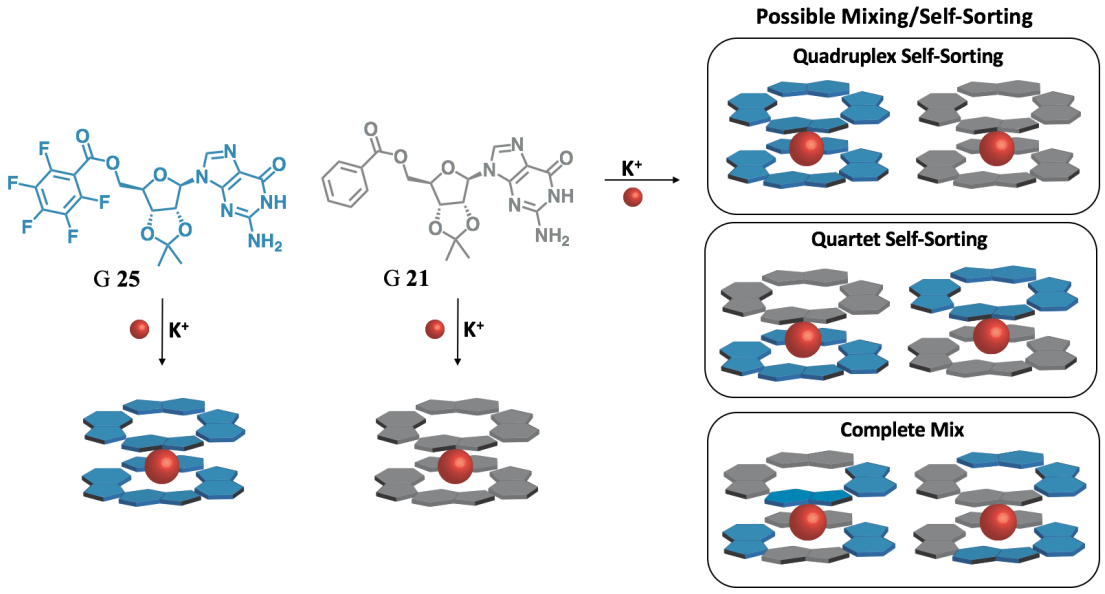

Figure 2.18. Illustration of the hypothetical self-sorting of mixed G-quadruplexes of G **21** and G **25** in the presence of templating K^{+}. There are three possible outcomes when forming quadruplexes from G **21** and G **25** 1) self-sorting of G **21** and G **25** into homomeric quadruplexes, 2) self-sorting of G **21** and G **25** quartets within each quadruplex, or 3) formation of completely mixed assemblies.

We focused on the formation of binary G-quadruplexes composed of 1:1 equimolar mixtures of 5′-benzoyl-2′,3′-isopropylidene guanosine (G **21**) and 5′-(2,3,4,5,6)-pentafluorobenzoyl-2′,3′-isopropylidene guanosine (G **25**). The arene-perfluoroarene is the classic example highlighting π-π stacking interactions between electron-rich and electron-poor aromatic rings. Work by Patrick and Prosser in the early

1960's, found that a 1:1 dimer of benzene-perfluorobenzene had a significantly higher melting point (23.7 ℃) than each compound by itself (C_6H_6 = 5.0 ℃; C_6F_6 = 5.4 ℃),[79] providing early evidence for increased binding affinity between the two aromatics. In theory, mixing G **21** with G **25** in the presence of excess KI might lead to the formation of a highly stable or self-sorted G-quadruplex or not. The arene-perfluoroarene π-stacking interaction is a relatively strong non-covalent interaction, and can offer increased thermodynamic stability through favorable quadrupole moment interactions or dispersion forces, shown in **Figure 2.19**.[80-83] We were interested in examining whether these interactions could be exploited to control G-quadruplex structure, placing the benzoyl G **21** in one G_4-quartet and the pentafluorobenzoyl G **25** in a neighboring layer (**Figure 2.19 left**).

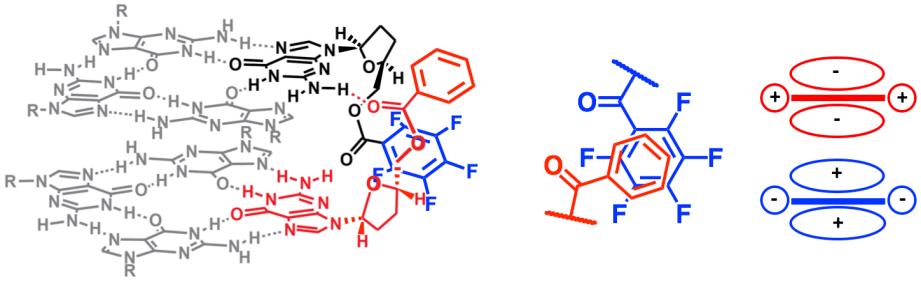

Figure 2.19. Left) Illustration showing hypothetical pentafluorobenzoyl-benzoyl π-stacking interactions between layers of a G-quadruplex. Right) Illustration showing the interaction between the quadrupole moments of the pentafluorobenzoate-benzoate aromatic groups.

2.9.1 Self-Assembly of 5′-(2,3,4,5,6)-Pentafluorobenzoyl-2′,3′-Isopropylidene Guanosine G 25

Encouraged by results from the self-assembly experiments described earlier in this chapter, we examined the homomeric G-quadruplex formation by 5′-(2,3,4,5,6)-pentafluorobenzoyl-2′,3′-isopropylidene (G **25**) using ^{1}H and ^{19}F NMR. The pentafluorobenzoyl ester, G **25,** was insoluble in $CDCl_3$, but dissolved upon the addition of 0.125 eq. KI and gave an ^{1}H NMR spectrum consistent with a D_4-symmetric octamer [G **25**]$_8$•K^+I^- (**Figure 2.20**). This assignment was based on the chemical shifts of previously described ^{1}H NMR spectra of the self-assemblies of other 5′-modified guanosines. The ^{1}H NMR spectrum for [G **25**]$_8$•K^+I^- has one set of resonances, with a singlet for the amide N^1H (δ 12.40 ppm). The N^2H amino protons were not visible, likely due to rapid rotation of the N^2H σ-bond. The addition of another 0.125 equivalents of KI gave a mixture of [G **25**]$_8$•K^+I^- and [G **25**]$_{16}$•$3K^+3I^-$. The complete formation of G_{16}-hexadecamer did not occur even at excesses of up to 1:1 G **25**:K^+ (10 mM:10 mM), which is more than 4 times the theoretical amount of K^+ cation required to form [G **25**]$_{16}$•$3K^+3I^-$ assemblies. Assignment of [G **25**]$_{16}$•$3K^+3I^-$ was made based on the splitting of the ^{1}H NMR signals into pairs of signals with equal intensity. ^{19}F NMR was also used to analyze the self-assemblies (**Figure 2.21**). The ^{19}F NMR of [G **25**]$_8$•K^+I^- showed three separate peaks for the *ortho, meta,* and *para* fluorine atoms. The ^{19}F NMR of [G **25**]$_{16}$•$3K^+3I^-$ showed a doubling of signals, that is typically associated with G_{16}-quadruplex formation.

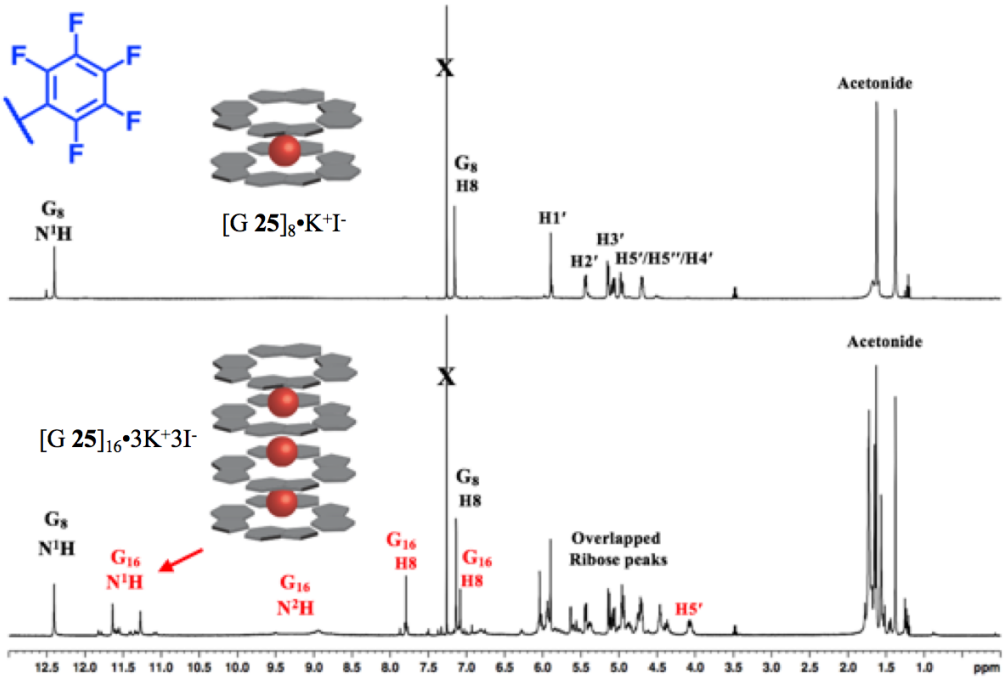

Figure 2.20. ^{1}H NMR spectra of the self-assembly of G **25**. Top) [G **25**]$_8$•K$^+$I$^-$ (1.25 mM) in $CDCl_3$ and Bottom) G **25** in the presence of 1.00 eq. KI (10 mM) in $CDCl_3$ results in a mixture of [G **25**]$_8$•K$^+$I$^-$ and [G **25**]$_{16}$•3K$^+$3I$^-$.

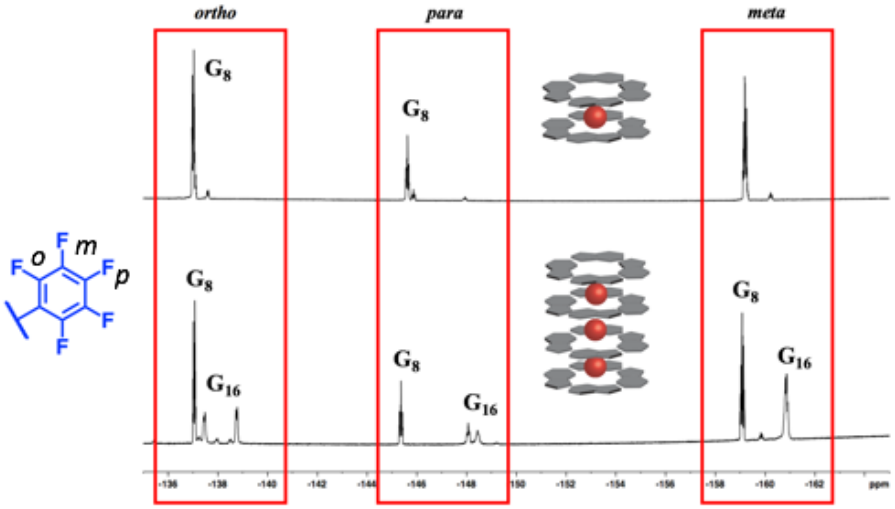

Figure 2.21. ^{19}F NMR spectra of the self-assembly of G **25**. Top) [G **25**]$_8$•K$^+$I$^-$ (1.25 mM) in $CDCl_3$ and Bottom) G **25** in the presence of 1.00 eq. KI (10 mM) in $CDCl_3$ results in a mixture of [G **25**]$_8$•K$^+$I$^-$ and [G **25**]$_{16}$•3K$^+$3I$^-$.

One plausible explanation for the mixture of [G **25**]$_8$•K^+I^- and [G **25**]$_{16}$•$3K^+3I^-$ assemblies in this system is that the strongly electron-withdrawing fluorine atoms decrease the basicity of the 5′-carbonyl, weakening the interlayer N^2H•••O=$C^{5'}$ hydrogen bond. The G-quadruplex structure is stabilized by a highly-cooperative balance of H bonding and π-stacking. Evidence for this explanation comes from line shape analysis of the N^2H protons. G_8-octamers usually show weak ^1H NMR signals for the N_2H protons due to relatively fast rotation about the N^2H σ-bond. Typically, G_{16}-hexadecamers ^1H NMR spectra display sharp peaks for their N^2H protons likely due to restricted σ-bond rotation from interlayer H-bonding. The [**G5**]$_{16}$•$3K^+3I^-$ has weak N^2H signals indicating diminished interlayer H-bonding. Purely electronic effects through the 5′-position would disfavor interlayer H-bonding by decreasing the basicity of the ester carbonyl. The fact that any G_{16}-hexadecamer forms suggests that π-π stacking may be stabilizing the assemblies, this weakened H-bonding is likely counteracted by the perfluoroarene π-stacking interactions.

2.9.2 Mixed G-Quadruplexes Containing 5′-(2,3,4,5,6)-Pentafluorobenzoyl-2′,3′-Isopropylidene Guanosine G 25 and 5′-Benzoyl-2′, 3′-Isopropylidine Guanosine G 21

Having demonstrated that G **25** forms G-quadruplex assemblies in $CDCl_3$, we sought to determine if binary mixtures of 5′-benzoyl-2′, 3′-isopropylidene guanosine G

21 and G **25** might form mixed assemblies under similar conditions. There are multiple types of mixed assemblies that can form, as shown in (**Figure 2.18**). These can include assemblies that are completely scrambled or it can be mixed assemblies where one G-quartet is completely made of G **21** and the neighboring G-quartet is composed of all G **25**. We examined binary G_8-octamer and G_{16}-hexadecamers in $CDCl_3$**.** The G_8-octamer is comprised of two G_4-quartet layers with 4 possible π-stacking arrangements that could provide additional enthalpic stabilization to the structures. The G_{16}-hexadecamer has 12 mixed stacking interactions resulting in an even greater enthalpic driving force for assembly. This additional energetic contribution might help to provide stabilization to counteract the entropic penalty for bringing together guanosine units in one highly-organized assembly. Our goal was to examine mixed G-quadruplex formation. We wondered if self-sorting of discrete G_4-layers or G_8-octamer units would occur, or if mixed G-quadruplexes containing statistical mixtures of G **21** and G **25** would form.

To evaluate how mixing influenced G-quadruplex formation, ^1H and ^{19}F NMR experiments were performed to follow self-assembly. We began by investigating G_8-octamer formation. A 1:1 equimolar mixture of G **21**: G **25** with 0.125 equivalents of added KI in $CDCl_3$ showed signs for G_8-octamer self-assembly. ^1H NMR chemical shifts for the mixed G-quadruplex occur in approximately the same region as the homomeric G_8-octamers [G **21**]$_8$•K^+I^- and [G **25**]$_8$•K^+I^-, except the line shape is broad. Conveniently, the fluorine atoms in G **25** are invisible to ^1H NMR and allow a clear

examination of the 5′-benzoyl aromatic protons of G **21**. Two clear sets of benzoyl aromatic protons for G **21** appear in the ^{1}H NMR, one set with a broad line shape similar in chemical shift to the homomeric [G **21**]$_8$•K^+I^- and one new set of protons shifted downfield by 0.2 ppm (**Figure 2.22**). This new set of resonances shifted downfield provides some evidence for mixed octamer formation where one G-quartet is completely made of G **21** and the neighboring G-quartet is composed of all G **25**.

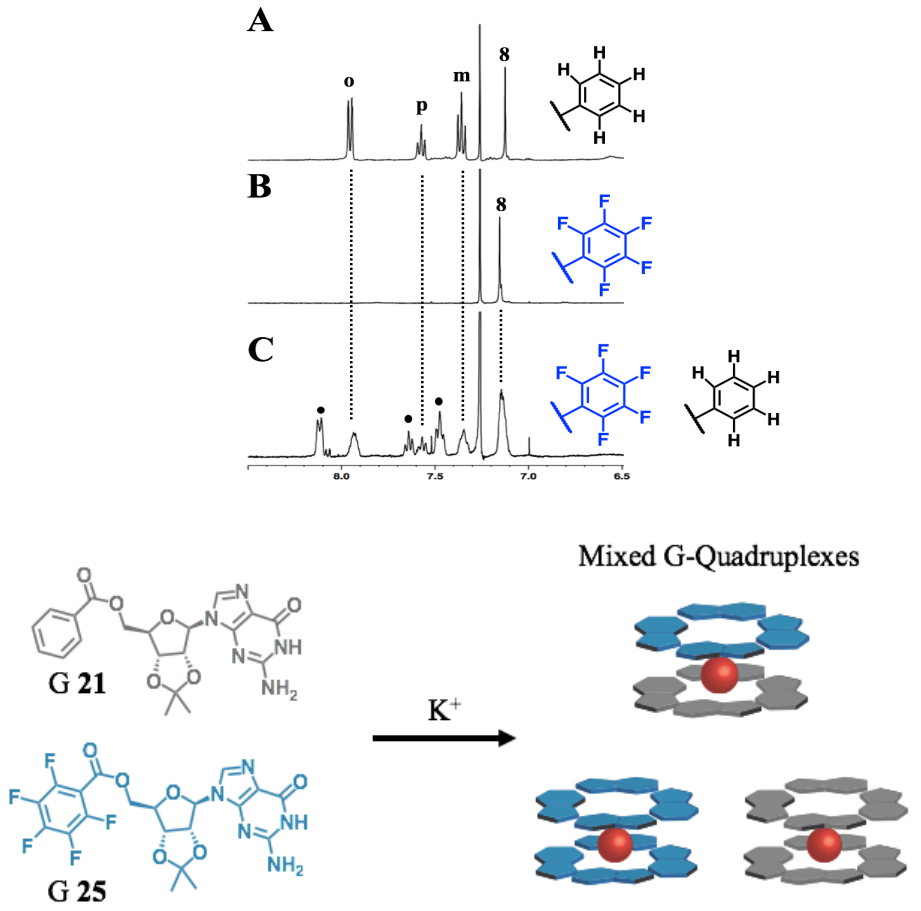

Figure 2.22. Top) ^{1}H NMR spectra of the aromatic region of a) [G **21**]$_8$•K^+I^- (1.25 mM) in $CDCl_3$ b) [G **25**]$_8$•K^+I^- (1.25 mM) c) and a mixture of G **21** (5mM) and G **25** (5 mM) in the presence of KI (1.25 mM) in $CDCl_3$. The labeled peaks (•) are resonances attributed to mixed assemblies. Bottom) One new sets of peaks of equal intensity are observed when G **21** and G **25** are mixed. These signals might arise from the formation of mixed G-quadruplex assemblies where homogenous G_4-quartet layers composed of all G **21** and all **G25** make up the new assembly.

To gain a clearer picture of the mixed self-assemblies ^{19}F NMR was used (**Figure 2.23**). The pentafluorobenzoyl fluorine atoms provide a clear analytical handle to monitor G-quadruplex formation. [G **25**]$_8$•K^+I^- (1.25 mM) was visible by ^{19}F NMR in $CDCl_3$, providing a single set of three individual peaks for the *ortho*, *meta*, and *para* fluorine atoms. A mixture of G **21** (5 mM) and G **25** (5 mM) in the presence of 1.25

mM KI gave a new set of signals. The original fluorine peaks were still present, but a new set of peaks grew in, presumably for a mixed G **21**/G **25** G_8-quadruplex.

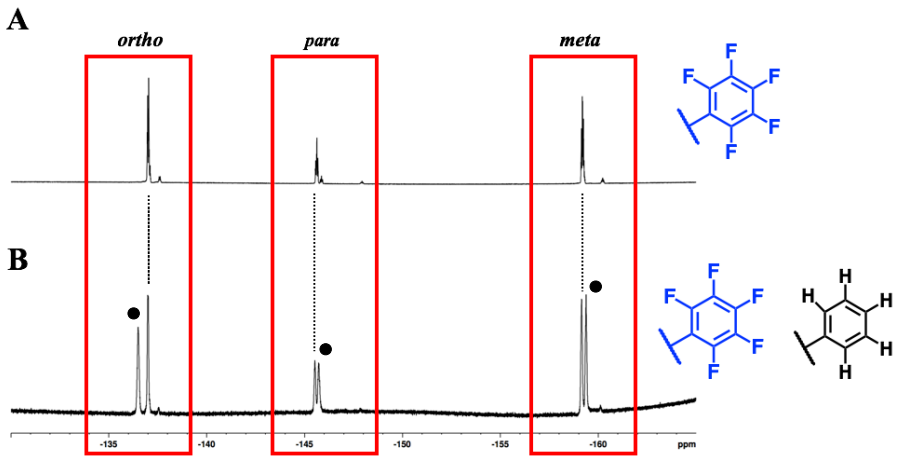

Figure 2.23. ^{19}F NMR spectra of a) [G **25**]$_8$•K^+I^- (1.25 mM) in $CDCl_3$ and b) a mixture of G **21** (5mM) and G **25** (5 mM) in the presence of 1.25 mM KI. A new set of signals appear for a mixed G_8-quadruplex. New NMR signals are denoted by (•).

Low temperature ^1H NMR experiments were performed in an attempt to slow down molecular motion in the system to decrease line broadening caused by assembly/dis-assembly processes. The experiments provided similar results to the room temperature experiments (**Figure 2.24**). ^1H NMR chemical shifts for the mixed G-quadruplex line up approximately in the same region as the homomeric G_8-octamers of each derivative, except again the line shape is broad. Two clear sets of benzoyl aromatic protons for **G1** appear in the ^1H NMR at -30 ℃, one set with a broad line shape similar in chemical shift to the homomeric [G **21**]$_8$•K^+I^- and one new set of protons shifted downfield.

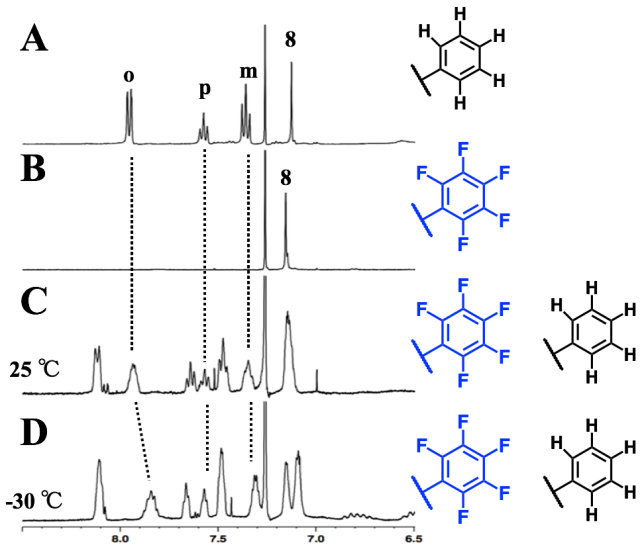

Figure 2.24. Variable temperature ^{1}H NMR spectra of the aromatic region of a) [G **21**]$_8$•K^+I^- (1.25 mM) in $CDCl_3$ b) [G **25**]$_8$•K^+I^- (1.25 mM) in $CDCl_3$ c) a mixture of G **21** (5mM) and G **25** (5 mM) in the presence of KI (1.25 mM) in $CDCl_3$ at 25°C d) and a mixture of G **21** (5mM) and G **25** (5 mM) in the presence of KI (1.25 mM) in $CDCl_3$ at -30°C.

After examining the self-assembly of binary G **21**/G **25** octamers we turned our attention towards the formation of binary G_{16}-hexadecamers. Again ^{1}H and ^{19}F NMR experiments were used to analyze self-assembly. One-to-one equimolar mixtures of G **21** (5 mM) to G **25** (5 mM) were investigated in the presence of 1 eq. of KI. The ^{1}H NMR of the sample was very broad, although the chemical shifts of the broad peaks did somewhat align with closely related peaks for the homomeric assemblies (**Figure 2.25**). It looks as though both mixed G_8 and G_{16} assemblies are forming based on the chemical shifts of the broad peaks.

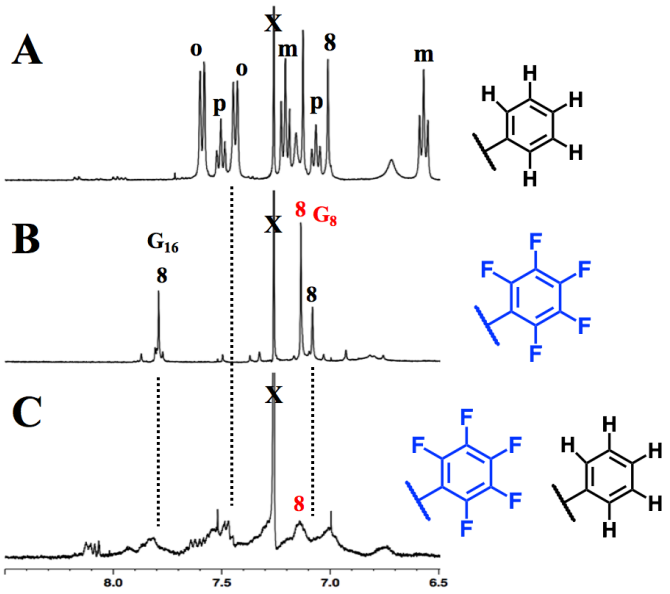

Figure 2.25. ^{1}H NMR spectra of the aromatic region of a) [G **21**]$_{16}$•3K^{+}3I^{-} (0.625 mM) in $CDCl_3$ b) a mixture of [G **25**]$_8$•K^{+}I^{-} and [G **25**]$_{16}$•3K^{+}3I^{-} assemblies c) and a mixture of G **21** (5mM) and G **25** (5 mM) in the presence of KI (10 mM) in $CDCl_3$.

The ^{1}H NMR results from the mixed G_{16}-hexadecamers were difficult to analyze due to signal broadening so the system was studied by ^{19}F NMR (**Figure 2.26**). The pentafluorobenzoyl fluorine atoms provide a clearer NMR spectrum to analyze. We began by examining homomeric [G **25**]$_{16}$•3K^{+}3I^{-}. The G_{16}-hexadecamer was visible by ^{19}F NMR in $CDCl_3$, giving two sets of peaks for the *ortho*, *meta*, and *para* fluorine atoms of the pentafluorobenzoyl. One set of resonances arise from the inner G_4-quartet layers of the G_{16}-hexadecamer and the other set of signals is from the outer G_4-quartet layers. [G **25**]$_8$•K^{+}I^{-} was still visible in this NMR spectrum. In a mixture of G **21** (5 mM) and G **25** (5 mM) in the presence of 10 mM KI a new set of signals

became visible. The original fluorine signals for [G **25**]$_{16}$•3K$^+$3I$^-$ broadened significantly, collapsing into the baseline. Surprisingly, peaks for both [G **25**]$_8$•K$^+$I$^-$ and the mixed G **21**/G **25** G$_8$-quadruplex were present. Taking into consideration the ^{1}H NMR broadening and the ^{19}F signal decrease, mixed G$_{16}$-hexadecamers seem to be forming.

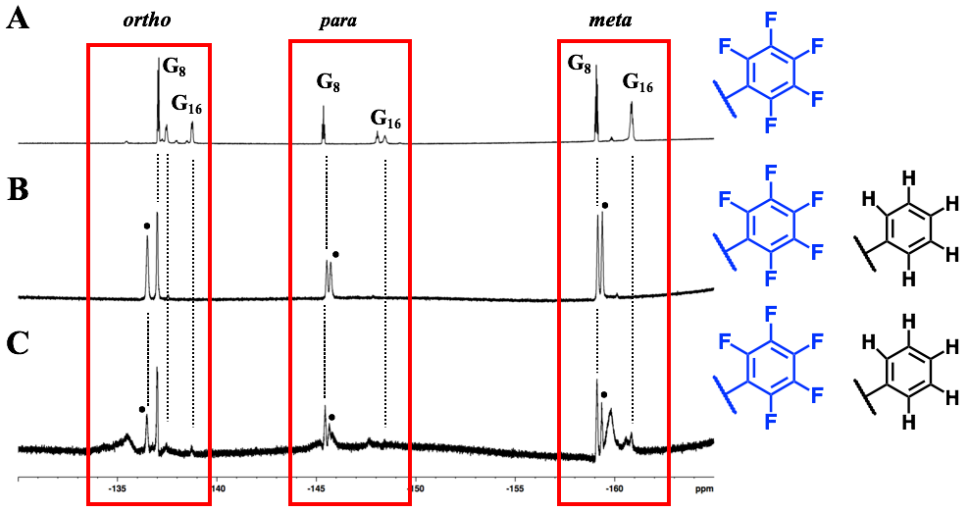

Figure 2.26. ^{19}F NMR spectra of a) mixture of [G **25**]$_8$•K$^+$I$^-$ and [G **25**]$_{16}$•3K$^+$3I$^-$ in $CDCl_3$ b) a mixture of G **21** (5mM) and G **25** (5 mM) in the presence of KI (1.25 mM) in $CDCl_3$ C) a mixture of G **21** (5 mM) and G **25** (5 mM) in the presence of KI (10 mM) in $CDCl_3$. Peaks labeled with (•) are mixed G$_8$•K$^+$I$^-$ assemblies.

Low temperature ^{1}H NMR experiments were performed to slow down the molecular motion within the assembly to resolve the peaks. The NMR at -30 ℃ provided a slightly more resolved spectrum, but was still too broad to fully analyze. The results were comparable to the room temperature experiments (**Figure 2.27**). Again, it appears that self-assemblies are forming, as determined by comparison of the homomeric G-quadruplexes and mixed G-quadruplexes chemical shift.

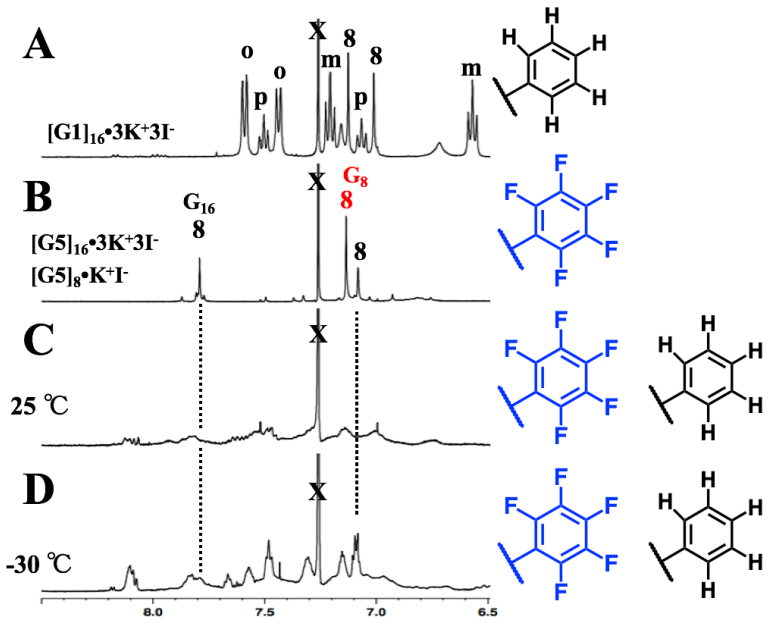

Figure 2.27. Variable temperature ^{1}H NMR spectra of the aromatic region of a) [G **21**]$_{16}$•3K^{+}3I^{-} (0.625 mM) in $CDCl_3$ b) a mixture of [G **25**]$_8$•K^{+}I^{-} and [G **25**]$_{16}$•3K^{+}3I^{-} c) a mixture of G **21** (5mM) and G **25** (5 mM) in the presence of KI (10 mM) in $CDCl_3$ at 25°C d) and a mixture of G **21** (5mM) and G **25** (5 mM) in the presence of KI (10 mM) in $CDCl_3$ at -30 °C.

2.9.3 Conclusion: Mixed Assemblies from 5′-Benzoyl-2′, 3′-Isopropylidene Guanosine G 21 and 5′-(2,3,4,5,6)-Pentaflurobenzoyl-2′, 3′-Isopropylidene Guanosine G 25

Self-assembly of mixed G **21**/G **25** quadruplexes were studied using ^{1}H and ^{19}F NMR. It appears that mixed G_8-octamers and G_{16}-hexadecamers are forming, as shown by line shape and chemical shift analyses, but the exact compositions of such assemblies are not known. The broad line shape is not surprising, given the number of possible arrangements the monomers can take in the G-quadruplex. Although, the

signals were broad for the formation of G_8-octamers two clear signals were present, which might be attributable to self-sorting of the G **21** and G **25** in assemblies. Further experiments are needed to fully characterize the binary G-quadruplex assemblies. ESI-MS experiments to determine the composition of these mixed G-quadruplexes are currently underway. Thermodynamic stability could be gauged through DMSO titrations and variable temperature experiments

2.10 Conclusion-The Identity of the 5′-Functionalization Impacts Self-Assembly

This chapter has focused on the synthesis and self-assembly of a series of 5′-aryl modified guanosine derivatives. This work has led to important insights into the self-assembly and stability of lipophilic 5′-aryl modified G-quadruplexes. This information may be applied in the future to rationally design G-quadruplex assemblies for new applications (see **Chapter 3** for one such application based on this work). We have shown that the 5′-sidechain is crucial for controlling the molecularity and stability of assemblies formed from 5′-aryl modified guanosine analogs. Guanosine derivatives with 5′-aryl groups modified with activating substituents (G **21** and G **23**) or extended π-surface areas (G **24**) favored larger assemblies ($[G]_{16}\bullet 3K^{+}3I^{-}$), while the G derivatives containing de-activating groups (G **22** and G **25**) favored smaller aggregates ($[G]_8\bullet K^{+}I^{-}$). A crystal structure of $[G\ \mathbf{21}]_{16}\bullet 3K^{+}$ revealed a highly cooperative network of interlayer H-bonds and π-stacks on the periphery of the G-quadruplex. The 5′-ester carbonyl of one G-quadruplex layer H-bonds with the neighboring G_4-layers exocyclic

N^2H amino proton. Two-dimensional ^1H NMR experiments confirm the G-quadruplex structure and peripheral interactions in solution. A series of DMSO-d_6 ^1H NMR titrations and H/D kinetic exchange ^1H NMR experiments were performed. G_{16}-hexadecamers formed from the 5′-*para*-methoxy aryl guanosine derivative G **21** and the 5′-naphthoyl G **24** were found to be more thermodynamically and kinetically stable than G **21**. Based on comparative ^1H NMR data, our working hypothesis is that the electronics and surface area of the 5′-aryl esters modulate the structure and stability of these assemblies. Investigating mixed stacking between electron poor and electron rich aromatic rings was the next logical step, and mixed G-quadruplex assemblies seem to be forming. Self-sorting may be occurring, but further experimentation needs to be performed. A better understanding of how such sidechain hydrogen bonding and dispersion interactions cooperate to influence G-quadruplex structure, stability and dynamics will be useful for designing functional structures and possible catalytic scaffolds for organic reactions. Thus, our efforts are focused on trying to better understand the mechanism of self-assembly involved in formation of this class of 5′-modified G-quadruplex.

Chapter 3: Utilizing the G-Quadruplex as a Scaffold for [2+2] Photocycloaddition Reactions of Lipophilic 5′-Cinnamate Modified Guanosine

3.1 Research Goal

The goal of the research in this chapter was to utilize G-quadruplex self-assembly to template the [2+2] photocycloaddition of a series of 5′-modified cinnamate guanosine derivatives. The cinnamate group's reactivity is highly dependent on the orientation and local environment of the reactants. While free in solution cinnamates undergo *trans-cis* isomerization about their π-bond when irradiated with an appropriate wavelength of light. When the reactive olefins are constrained within 3.3-4.2 Å and irradiated the reaction pathway that is favored is a [2+2] photocycloaddition reaction yielding cyclobutane products.[83,84] The interlayer distances between G_4-quartet layers is approximately 3.3 Å, well within the distance necessary for [2+2] cycloaddition to occur. The G-quadruplex is an ideal system for performing this topologically controlled [2+2] cycloaddition since its self-assembly can bring together up to sixteen reactive units and align them within the required distance to react. We reasoned that the G-quadruplex might align the reactive olefin units in a favorable orientation to undergo photodimerization. To achieve this goal, a series of 5′-modified guanosine derivatives were synthesized: 5′-cinnamoyl-2′,3′-isopropylidene guanosine (G **26**), 5′-*ortho*-methoxycinnamoyl-2′,3′-isopropylidene guanosine (G **27**), and 5′-*para*-

methoxycinnamoyl-2′, 3′-isopropylidene guanosine (G **28**) (shown in **Figure 3.1)**. The 5′-*meta*-methoxycinnamoyl-2′,3′-isopropylidene guanosine (G **29**) is discussed in detail in **Chapter 4**. The self-assembly and photoreactivity of G **26**, G **27**, and G **29** were examined. As expected, irradiation of free monomers G **26**-G **29** resulted in only *trans-cis* isomerization. Irradiation of self-assembled G **26**- G **29** derivatives resulted in an efficient [2+2] photocycloaddition with high regioselectivity, stereoselectivity, and yields (**Figure 3.2**).

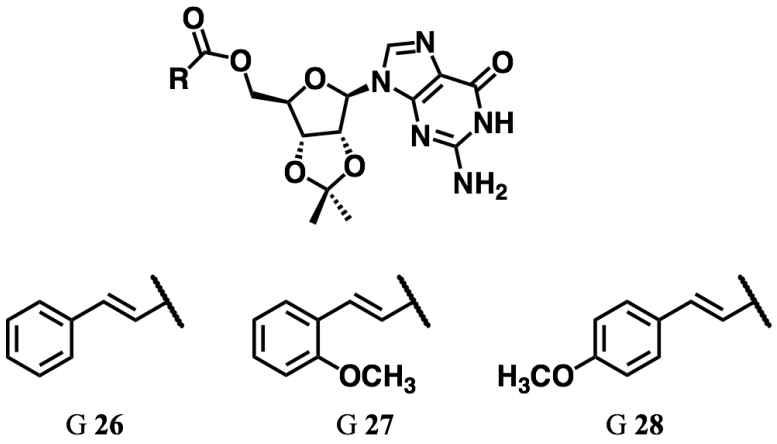

Figure 3.1. Synthesized photoreactive guanosine derivatives: 5′-cinnamoyl-2′,3′-isopropylidene guanosine (G **26**), 5′-*ortho*-methoxycinnamoyl-2′,3′-isopropylidene guanosine (G **27**), and 5′-*para*-methoxycinnamoyl- 2′, 3′-isopropylidene guanosine (G **28**).

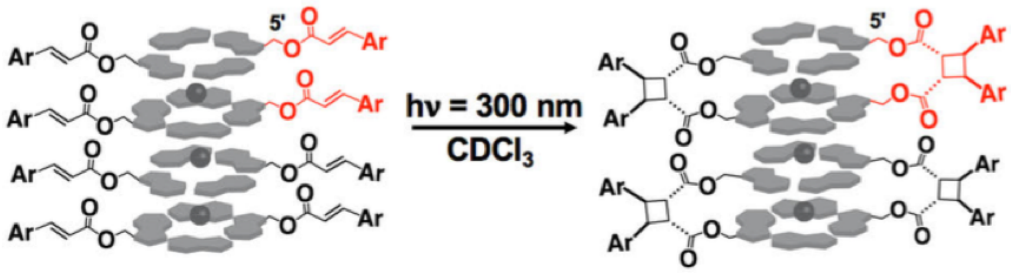

Figure 3.2. General scheme for the G-quadruplex templated [2+2] photocycloaddition of lipophilic 5′-cinnamate ester guanosine derivatives G **26**-G **28**.

3.2 Background and Hypothesis: 5′-Cinnamate Modified Guanosine [2+2] Photocycloaddition

The [2+2] photocycloaddition of cinnamic acids and cinnamate esters provides an efficient method to access strained cyclobutane products. Photocycloaddition reactions are one of the most studied methods for cyclobutane ring formation.[85] The olefin of the cinnamate readily undergoes photodimerization with another cinnamate when exposed to the appropriate wavelength of light. Dimerization of two cinnamic acids (**CA**) results in the formation of truxinate and/or truxillate cyclobutanes (**Figure 3.3**).[83,84] The truxinates and truxillates are cyclobutane structures that are formed from cinnamic acid and its derivatives. The truxinate and truxillate cyclobutanes are regio-isomers of one another: the truxinate cyclobutanes are formed by head-to-head dimerization, while the truxillate cyclobutanes are formed by head-to-tail dimerization (**Figure 3.4**). There are 17 possible isomers that can form from the [2+2] cycloaddition of cinnamate derivatives. Methods to promote and control the regio- and stereochemical outcome of the reaction are of value and an area of ongoing research.[85]

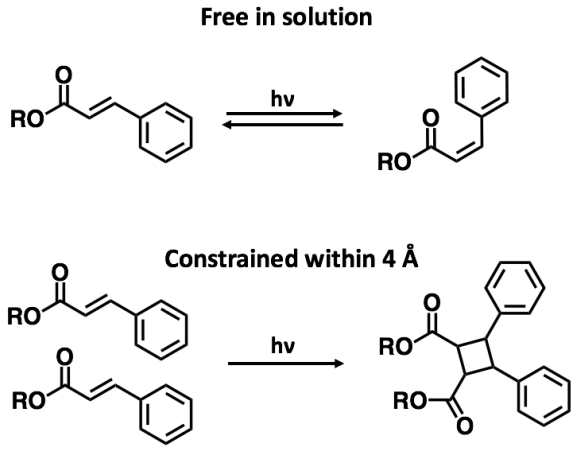

Figure 3.3. Illustration of the general reactivity of the cinnamate group. While free in solution the major photoreaction is *trans-cis* isomerization. When constrained within 4 Å, irradiation results in photodimerization yielding cyclobutanes.

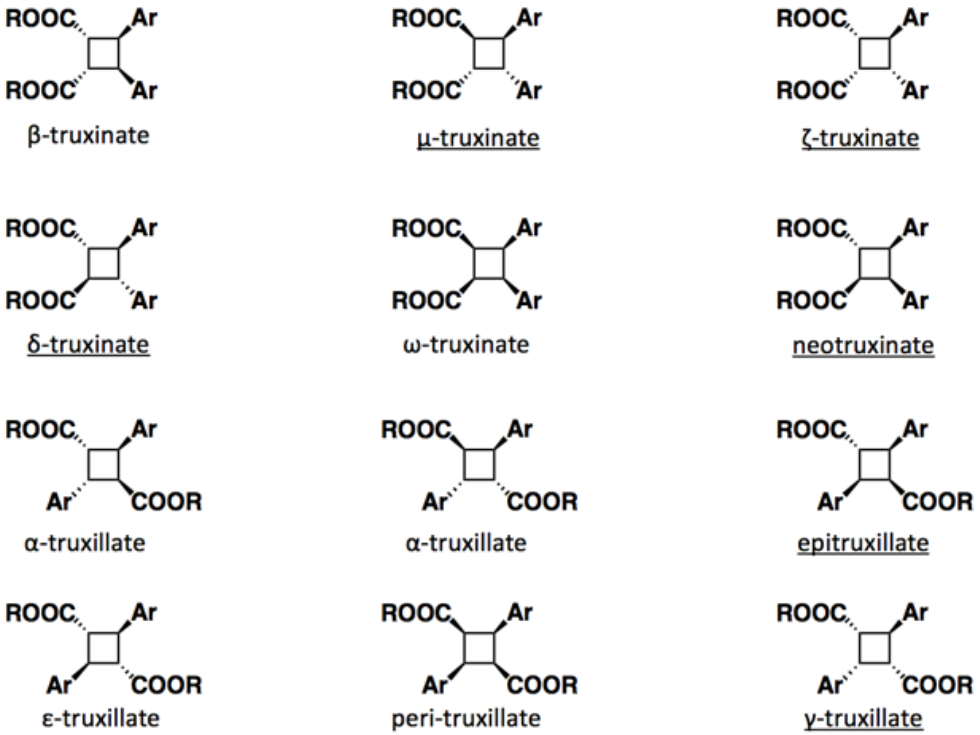

Figure 3.4. Structures of the truxinate and truxillate isomers formed from cycloaddition of 2 cinnamate esters. Compounds that are underlined also possess an enantiomer. There are 17 different stereoisomers possible.

The truxinate and truxillate four-membered rings are the building blocks for many natural products with promising biological activity.[86] These cyclobutane containing natural products are found in many plants, often arising from the dimerization of substituted cinnamate building blocks originating in the biosynthesis of plant cell walls: ferulic acid, chlorogenic acid, and coumaric acid.[87,88] **Figure 3.5** highlights the structure of selected pharmacologically active truxinates and truxillates. Incarvillateine (**30**), containing a truxillate cyclobutane, has found use in Chinese folk medicine as a pain reliever for rheumatoid arthritis. Incarvillateine **30** has been shown to have potent antinociceptive (pain relief) properties.[89] Caracasandiamide (**31**), a guanidinium containing truxinate derivative, has promising activity as an anti-hypertensive compound for regulating blood pressure.[90] Another truxinate derivative, piperaborenine D (**32**), containing a dihydropyridone ring has shown anticancer properties against cancerous cells.[91] Similarly, eucommacin A (**33**), a truxinate derivative formed from the dimerization of chlorogenic acid, has activity against cancer stem cells.[92] New methods to control the synthesis of truxinate and truxillate derivatives might lead to the development of valuable drug candidates.[63]

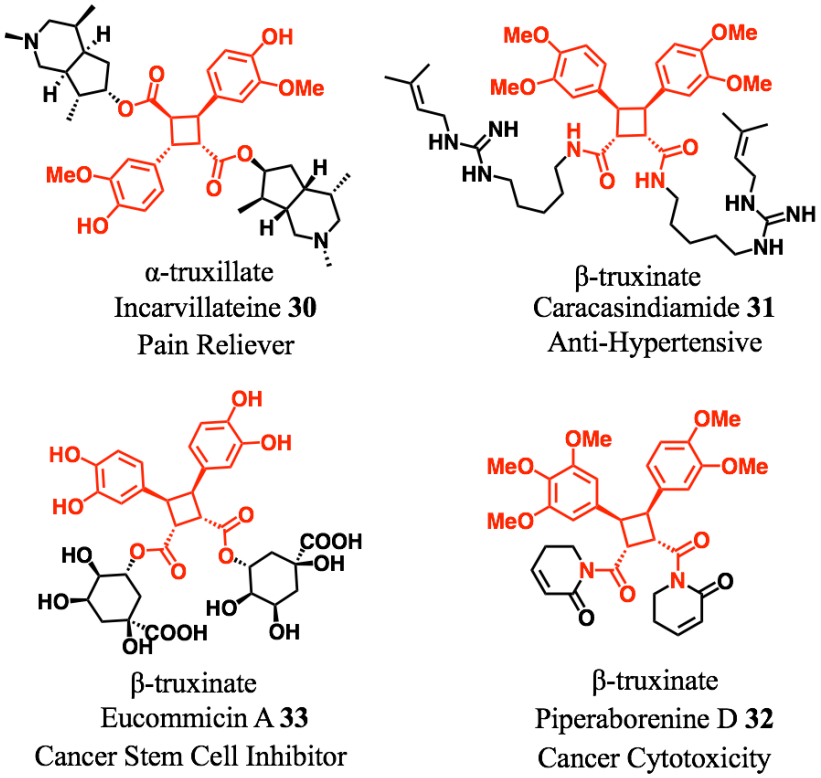

Figure 3.5. Structures of selected pharmacologically active truxillate and truxinate compounds.[89-92]

3.2.1 General Photoreactivity of Cinnamic Acids and Cinnamate Esters

Cinnamic acid derivatives undergo one of two reactions when exposed to light: 1) *trans-cis* isomerization about the olefin or 2) [2+2] cycloaddition to yield cyclobutane products (shown in **Figure 3.3**). The reaction that occurs depends on the spatial arrangement and orientation of the reactive alkenes; this is referred to as topochemical control. While free in solution the primary reaction that occurs upon irradiation is the *trans-cis* isomerization of the cinnamate π-bond. When the reactive olefins are constrained within 3.3-4.5 Å photodimerization is the dominant reaction. To address the spatial constraints of the [2+2] photocycloaddition reaction,

traditionally the reaction has been performed in the solid state due to the proximity of the reactants in the crystalline state. Recently new synthetic methods have been developed to move the reaction into solution in an attempt to increase reaction yields and improve stereocontrol over the reaction.

3.2.2 Solid-State Photocycloaddition of Cinnamic Acid Derivatives

To address the spatial restrictions for the cycloaddition, reactions have traditionally been performed in the solid-state to promote the dimerization of cinnamic acid derivatives.[83,84,93]When in the solid-state, some cinnamic acid derivatives pack so that their reactive olefins are properly aligned in orientations capable of undergoing photocycloadditions. The photodimerization of cinnamic acids has been well documented since the early 1900s. In the early 1960s, Schmidt *et al.* released a series of seminal papers that fully examined the solid-state reactivity of cinnamic acid crystals and selected derivatives.[83,84] Studying the photocycloaddition of substituted cinnamic acids, Schmidt deduced that solid-state dimerization is contingent on the alignment of the cinnamates in the crystal and the intermolecular distance required for the photocyloaddition must be less than 4.2 Å.

Since the early work by Schmidt, many others have designed new crystal engineering strategies to align cinnamates in the solid-state. Notable examples are presented here. Coates and Grubbs exploited π-stacking interactions between a 2,3,4,5,6-pentafluorocinnamic acid (**pfCA**) and cinnamic acid (**CA**) to align olefins in the solid state. When these crystals were irradiated photocycloaddition formed the β-

truxinate product (**Figure 3.6A**).[94] Sharma *et al* also employed π-donor/acceptor interactions to control the photodimerization of a 1:1 co-crystal containing 3,5-dinitrocinnamic acid (**3,5-diNO_2CA**) and 2,5-dimethoxycinnamic acid (**2,5-diMeOCA**) (**Figure 3.6B**).[95]Again the π-stacking interaction aligned the aryl groups in a head-to-head orientation to provide the β-truxinate photodimer. Ito *et al.* designed an approach that relied on ionic interactions between a series of diamines and cinnamic acids in a crystalline solid (**Figure 3.6C**).[96] Although the solid-state reaction of cinnamates has been well studied there are still many drawbacks to these methods that limit their synthetic utility, including limited reactant scope, poor control over the stereochemical outcome of the reactions, and low yields. As described below, new solution-based methods have been devised to widen the scope of reactants, increase yields, and gain greater control over the stereochemistry of the reaction.

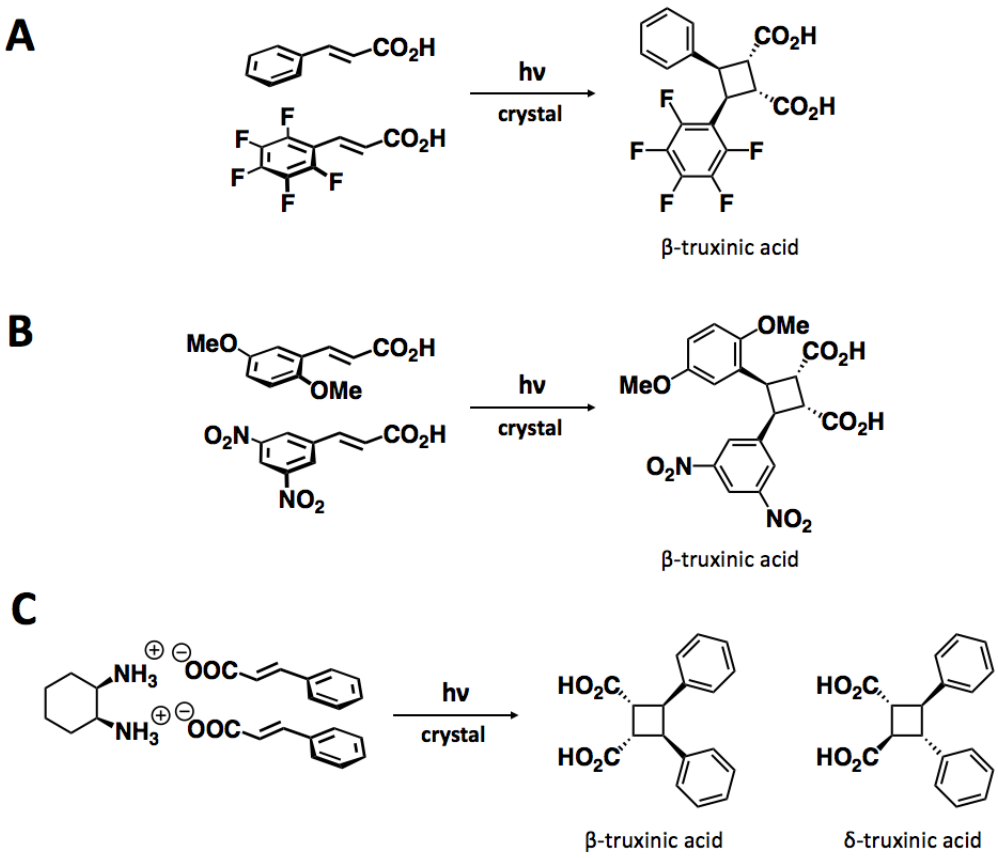

Figure 3.6. Selected examples of solid state [2+2] photocycloaddition reactions. [2+2] Photocycloaddition of: A) 1:1 co-crystals of (2,3,4,5,6)-pentafluorocinnamic acid: cinnamic acid B) 1:1 co-crystals of 2,5-dimethoxycinnamic acid: 3,5-dintrocinnamic acid C) 1:2 co-crystals of cyclohexane-1,2-*cis*-diamine: cinnamic acid.[94-96]

3.2.3 [2+2] Photocycloaddition of Cinnamic Acids in Solution

Methods have been developed to transfer the cycloaddition of cinnamic acids from the solid-state into solution. Performing the reaction in solution allows for the design of more dynamic systems that can address some of the limitations encountered in the solid-state photocycloadditions. A variety of strategies have been implemented to control the photoreaction. Covalent templates, non-covalent interactions, and self-

assembly have been used to pre-organize cinnamates at the proper distance and orientation for dimerization in solution.

To address the spatial restriction of the reaction in solution, researchers have covalently attached cinnamate units next to each other on neighboring atoms within the same compound. The covalent scaffolds anchor the olefins close together with specific orientations aiding in the regio- and stereoselectivity of the photodimerization reaction. In addition to increased stereochemical control over the reaction, the substrate scope can be broadened and is no longer reliant on the crystallization efficiency of each individual cinnamic acid derivative. Zitt *et al.* attached two cinnamates on neighboring aromatic rings of a cyclophane scaffold **34** (**Figure 3.7A**). When irradiated, the cyclophane system yielded the β-truxinate product (76 % yield).[97] Ghosn and Wolf used a 1,8-bis(anilino)naphthalene **35** as a scaffold to attach two cinnamates in a reactive orientation. Irradiation of the cinnamate bis(aniline)naphthalene **35** system resulted in the formation of the β-truxinate product (87 % yield) (**Figure 3.7B**).[98] Another prime example of this tethering strategy is the work performed by Yuasa *et al.* using a β-xylopyranoside **36** to template a photocycloaddition between cinnamates taking a 1,3-diaxial alignment on the sugar. Irradiation of the sugar-cinnamate compound resulted in the formation of the β-truxinate (75% yield) as the major product with the δ-truxinate (7% yield) and ζ-truxinate (5 % yield) also forming (**Figure 3.7C**).[99] Each of the 3 previous covalent methods used hydrolysable covalent linkages to anchor the reactant olefins for photolysis, and then the linkages could be subsequently cleaved to release the desired cyclobutane product.

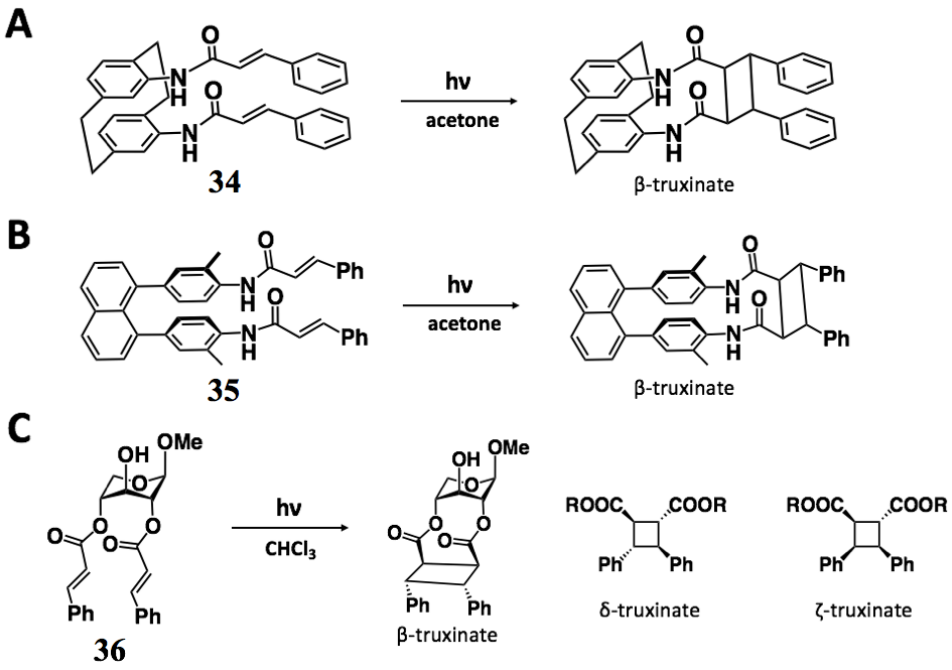

Figure 3.7. Selected examples of covalent scaffolds for [2+2] photocycloaddition reactions of cinnamates. [2+2] Photocycloaddition of: A) a 4,15-diamino-[2.2]paracyclophane cinnamide **34** B) a 1,8-(bis)4′-anilino naphthalene cinnamide template **35** C) β-xylopyranoside cinnamate template **36**.[97-99]

Supramolecular structures and containers have been investigated as templates for the [2+2] photocycloadditions of cinnamates.[100] Supramolecular approaches rely on non-covalent interactions such as solvophobic effects, hydrogen bonding, and π-stacking to properly orient the reactive alkenes in solution. The Ramamurthy group has pioneered the use of molecular containers to template [2+2] photocycloaddition reactions in solution. They showed that cucurbiturils **37**,[101] cyclodextrins,[102] and "Fujita cages" can trap 2 cinnamic acids and cinnamate derivatives in their central cavities, and then when irradiated the caged cinnamates could react to give truxinates and truxillates in high yields (**Figure 3.8A**).[103] Beak and Zeigler focused on hydrogen

bonding interactions between two pyrimidone units **38** to template photodimerizations, although their method proceeded with low yields (9.9 % δ-truxinate and 1.9% β-truxinate) (**Figure 3.8B)**.[104] Bassani *et al.* designed a barbiturate-melamine H-bonded complex **39** to dimerize a pair of cinnamates resulting in the β-truxinates, neotruxinates, and α-truxillates (**Figure 3.8C**).[105] A thiourea catalyst **40** was employed by the Beeler group to promote the cycloaddition of a diverse set of cinnamate esters in a flow reactor, yielding primarily the δ-truxinate and the β-truxinate (**Figure 3.8D**).[106]

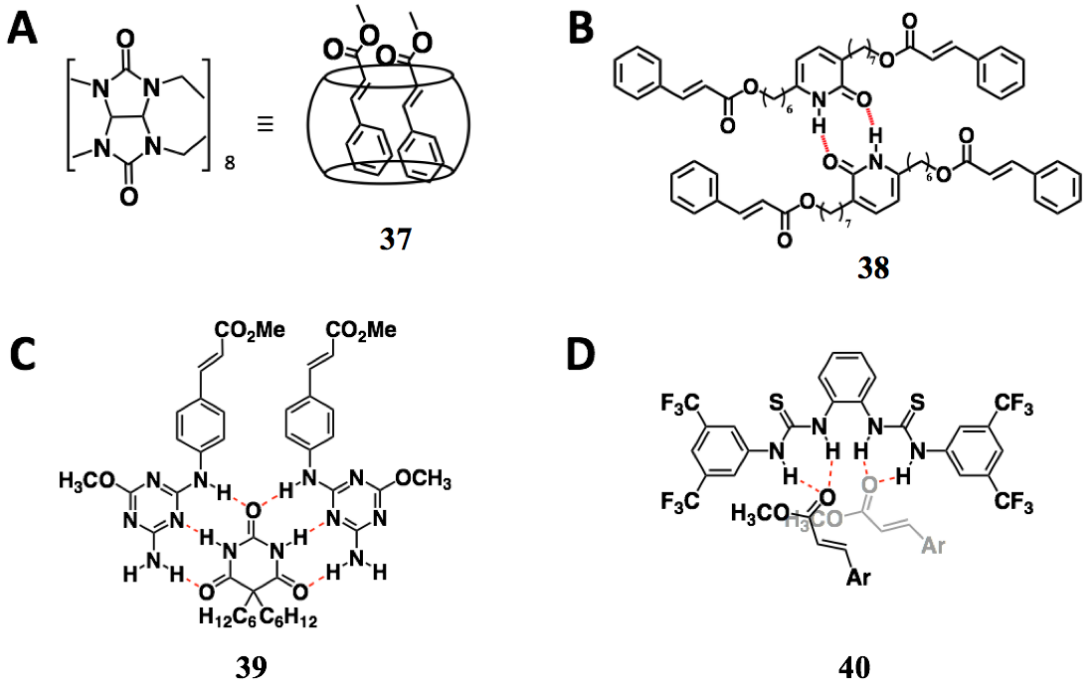

Figure 3.8. Selected examples of non-covalent scaffolds for [2+2] photocycloaddition reactions of cinnamates. A) a cucurbit[8]uril **37**, B) a pyrimidone template **38**, C) barbiturate-melamine template **39**, and D) a thiourea catalyst **40** scaffold.[101,104-106]

3.2.4 Hypothesis: The G-Quadruplex can be Used to Template [2+2] Photocycloadditions

Gaining inspiration from 1) previously reported supramolecular photodimerizations and 2) structural information gained from the crystal structure of a 5′-aryl modified G_{16}-quadruplex (discussed in **Chapter 2**), we hypothesized that the G-quadruplex might be able to pre-organize cinnamate groups within the topological requirements necessary to cyclize. Additionally, the highly-organized structure of the G-quadruplex might encourage the reaction to go with high regioselectivity and stereoselectivity. The interlayer distance between the G-quadruplex layers is ≈3.3 Å, well within the topological requirements for cyclization to occur.[33] This led us to propose that the G-quadruplex could be used to pre-organize and promote the proper alignment of the photoreactive guanosine esters.

Herein, we introduce a non-covalent templating strategy that enables photochemical dimerization of a guanosine cinnamic acid derivative using the G-quadruplex as a scaffold (**Figure 3.2**). We began by synthesizing a new series of guanosine derivatives: 5′-cinnamoyl-2′, 3′-isopropylidene guanosine (G **26**), 5′-*ortho*-methoxycinnamoyl-2′, 3′-isopropylidene guanosine (G **27**), and 5′-*para*-methoxycinnamoyl-2′, 3′- isopropylidene guanosine (G **28**). We found that the reactivity of G **26**-G **28** can be controlled by self-assembly. When the guanosine derivative is free in solution *trans-cis* isomerization is the only reaction that occurs upon photoirradiation, but when assembled the reactive groups are pre-organized

within the necessary distance to undergo dimerization to the four-membered rings. The G-quadruplex was found to also have an influence on the stereochemical outcome of the [2+2] cycloaddition.

3.4 Synthesis of 5′-Cinnamoyl-2′,3′-Isopropylidene Guanosine (G 26), 5′-*ortho*-Methoxycinnamoyl-2′,3′-Isopropylidene Guanosine (G 27), and 5′-*para*-Methoxycinnamoyl-2′,3′-Isopropylidene Guanosine (G 28)

We began this work by synthesizing a series of 5′-cinnamate ester guanosine derivatives: 5′-cinnamoyl-2′,3′-isopropylidene guanosine (G **26**), 5′-*ortho*-methoxycinnamoyl-2′,3′-isopropylidine guanosine (G **27**), and 5′-*para*-methoxycinnamoyl-2′, 3′-isopropylidine guanosine (G **28**). 5′-Cinnamoyl- (G **26**) and 5′-*ortho*-methoxycinnamoyl-2′,3′-isopropylidene (G **27**) were synthesized using dicyclohexyl carbodiimide (DCC). The use of DCC as a coupling agent versus the previously employed acid chloride method for modifying the 5′-position of G (in **Chapter 2**) prevented the formation of N2,5′-diacyl guanosine side products. Although DCC thwarted side-product formation it was quite difficult to remove from the reaction mixture and required column chromatography. A new synthetic method using 1-ethyl-3-(3-dimethylaminopropyl) carbodimide (EDC) as a coupling agent was used to synthesize 5′-*para*-methoxycinnamoyl-2′,3′-isopropylidene guanosine (G **28**) (**Figure 3.9**). Using EDC eliminated the time-consuming column chromatography step with the DCC coupling. EDC is water soluble and easily removed from the reaction products by

a series of water washes. Compounds G **26** and G **27** were purified by column chromatography followed by a series H_2O washes to rid the samples of excess cationic impurities. G **28** was purified through a sequence of H_2O washes followed trituration with hot isopropanol. The resulting products were found to be analytically pure by ^{1}H NMR, ^{13}C NMR, UV-vis spectroscopy, and ESI-MS (see experimental details in **Chapter 5**).

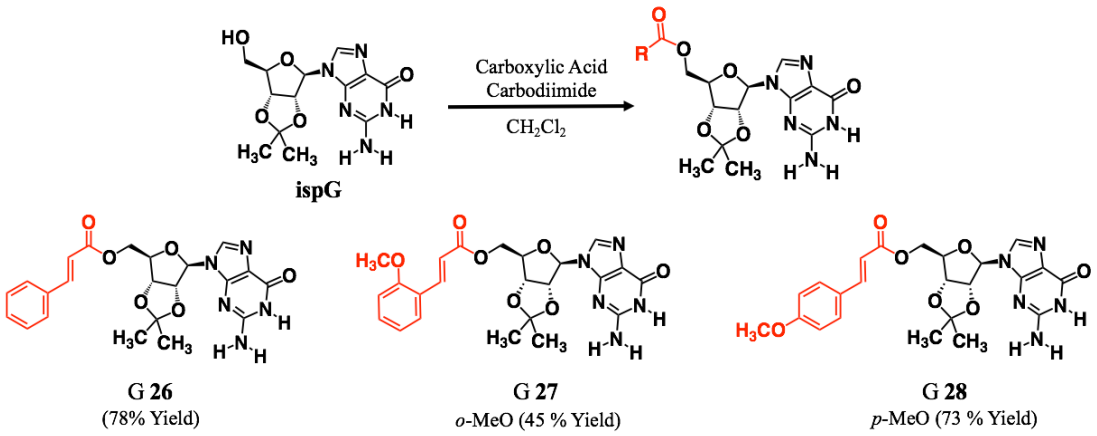

Figure 3.9. Scheme for the synthesis of 5′-cinnamoyl-2′, 3′-isopropylidene guanosine (G **26**), 5′-*ortho*-methoxycinnamoyl-2′, 3′- isopropylidine guanosine (G **27**), and 5′-*para*-methoxycinnamoyl-2′, 3′-isopropylidine guanosine (G **28**)

3.5 Self-Assembly and Photochemistry of 5′-Cinnamoyl-2′,3′-Isopropylidene Guanosine (G 26)

To test the ability of the G-quadruplex to act as a scaffold in the [2+2] photocycloaddition of cinnamic acid derivatives we began by examining the self-assembly and reactivity of the 5′-cinnamoyl-2′, 3′- isopropylidene guanosine G **26**.

3.5.1 UV-Vis Spectroscopy of 5′-Cinnamoyl-2′,3′-Isopropylidene Guanosine G 26

We began this study by examining the photochemical properties of monomeric G **26** in $CDCl_3$. We compared the absorbance of G **26** against 2′, 3′-isopropylidene guanosine (**IspG**) to determine if there would be a direct competition for absorbance of photons with the guanine nucleobase. Guanosine was found to absorb at a λ_{max} of 256 nm. UV-vis spectroscopy studies of G **26** show a λ_{max} of 278 nm corresponding to the π-π* transition of the cinnamate group (**Figure 3.10**). Cinnamic acid (**CA**) absorbs at a similar λ_{max} of 278 nm. We decided to irradiate all subsequent photochemical reactions of G **26** using 300 nm light as this wavelength is outside of the absorbance range of isopropylidene guanosine **IspG** while remaining within G **26**'s absorbance range as shown in **Figure 3.10**.

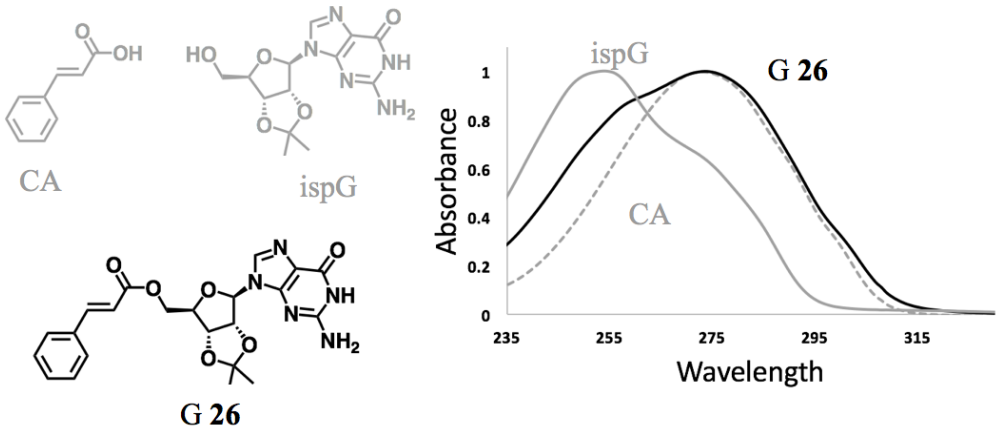

Figure 3.10. Normalized UV-vis absorbance spectra for 2′,3′-isopropylidene guanosine **ispG**, cinnamic acid **CA**, and 5′-cinnamoyl-2′, 3′-isopropylidene guanosine G **26** in $CDCl_3$.

3.5.2 Photoisomerization of 5′-Cinnamoyl-2′, 3′-Isopropylidene Guanosine G 26

Guanosine, while free in solution, is in rapid equilibrium between free monomer and hydrogen-bonded ribbons.[49,107] As a control experiment for the [2+2] photocycloaddition of G **26** we tested the photoreactivity of monomeric G **26**. To ensure that no G-quadruplex assemblies were present the reaction was performed in DMSO-d_6 because 1) DMSO-d_6 prevents G-quadruplex formation by disrupting H-bonding within the assembly and 2) G **26** has poor solubility in other organic solvents. When monomeric *trans*-G **26** (10 mM) was irradiated at 300 nm in DMSO-d_6 only *trans-cis* photoisomerization of the olefin side-chain occurred (**Figure 3.11**). No cycloaddition product was observed. The photoisomerization was also performed in CD_3CN. In this solvent, [2.2.2] cryptand was added to sequester any rogue cations (such as Na^+ or K^+) that may be present. Again, *trans-cis* isomerization occurred upon irradiation. Under these cation free conditions, no photocycloaddition product was observed in CD_3CN after irradiation (**Figure 3.12**).

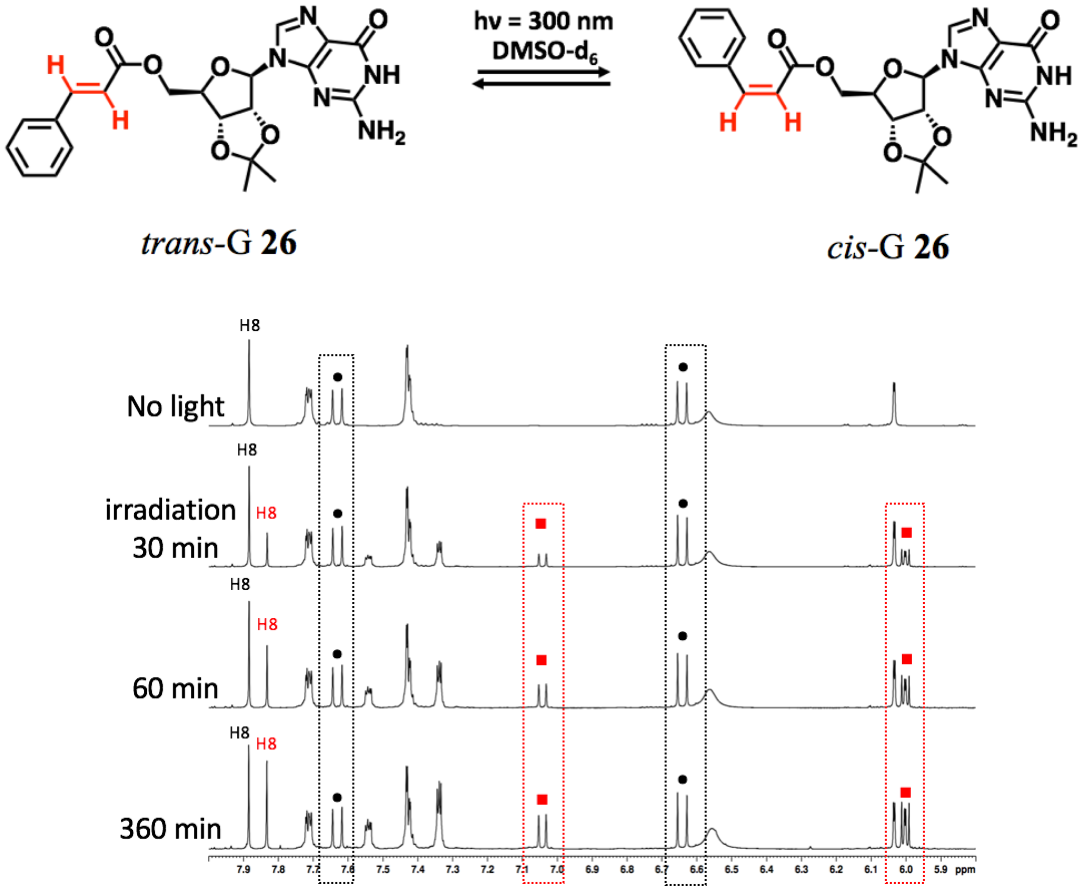

Figure 3.11. ^{1}H NMR spectra highlighting the olefinic protons of G **26** (10 mM) during photoirradiation with 300 nm light in DMSO-d_6. DMSO-d_6 disrupts G-quadruplex formation so that only the monomeric *trans*-G **26** is in solution. Under these conditions *trans-cis* isomerization of the double bond in G **26** was observed, there was no cycloaddition. The olefin protons for *trans*-G **26** are labeled with •. The olefin protons for *cis*-G **26** are labeled with ■.

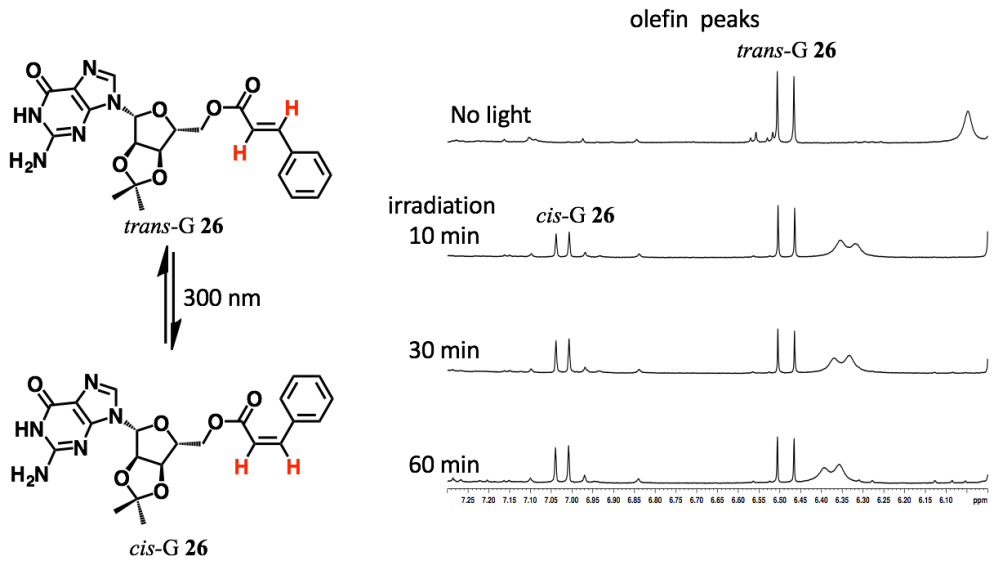

Figure 3.12. ^{1}H NMR spectra of the olefinic protons of G **26** (10 mM) at certain timepoints during photoirradiation at 300 nm in CD_3CN. [2.2.2] cryptand (80 mM) was added to sequester cation impurities that might template G-quadruplex formation. Under these conditions *trans-cis* isomerization of the double bond in G **26** was observed, there was no cycloaddition.

3.5.3 G-Quadruplex Self-Assembly of 5′-Cinnamoyl-2′,3′-Isopropylidene Guanosine G 26

We next examined the self-assembly properties of G **26**. 5′-Cinnamoyl G **26** in the presence of KI (0.125 eq.) gave a ^{1}H NMR spectrum consistent with a D_4-symmetric octamer [G **26**]$_8$•K^+I^-. We made this assignment based off previously reported analogs that we and others have described.[33] The ^{1}H NMR spectrum for [G **26**]$_8$•K^+I^- displayed one set of resonances; a singlet is present for the N^1H amide proton (δ 12.30 ppm) and another set of two broader signals for the N^2H_2 amino protons were visible, δ 9.61 ppm for the protons involved in the G-quartets N^2H_A•••N^7 H-bond and one at δ 6.59 ppm for the exocyclic N^2H_B protons. Addition of an excess of KI (1.00

eq.) resulted in the formation of a new assembly that we designated as a D_4-symmetric G_{16}-hexadecamer [G **26**]$_{16}$•3K$^+$3I$^-$ (Figure 3.13). This assignment was made based on previously reported G_{16}-hexadecamers, as well as the characteristic N_1H/N_2H regions and doubling of ^{1}H resonances.

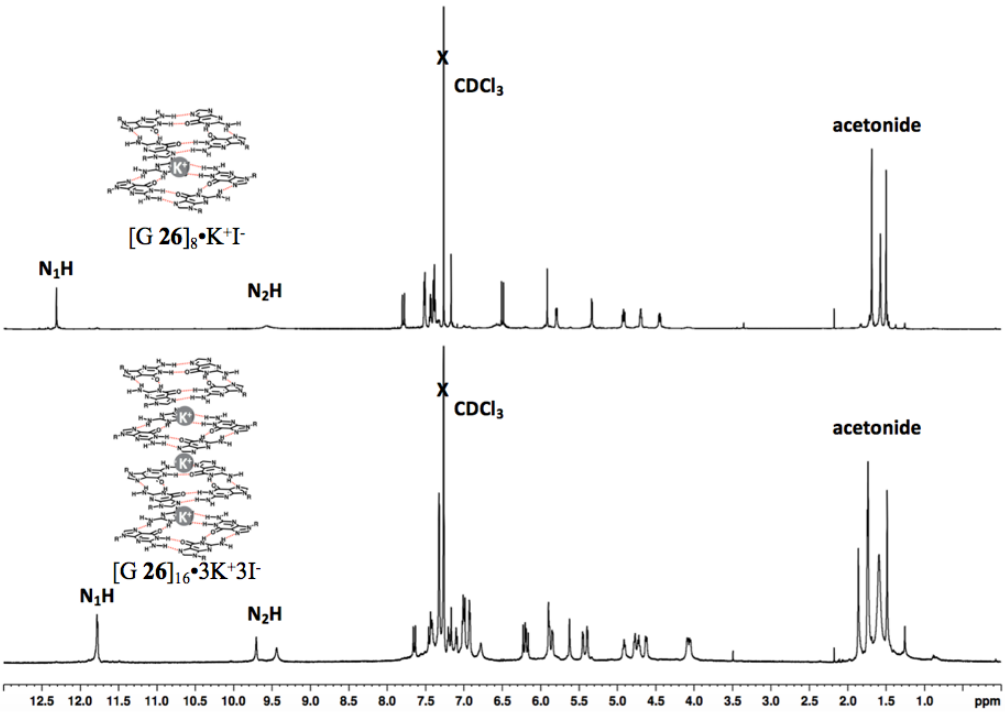

Figure 3.13. ^{1}H NMR spectra showing G **26** self-assembly. Top) ^{1}H NMR spectrum of [G **26**]$_8$•K$^+$I$^-$ (1.25 mM) in $CDCl_3$. Bottom) ^{1}H NMR spectrum of [G **26**]$_{16}$•3K$^+$3I$^-$ (0.625 mM) in $CDCl_3$.

3.5.4 [2+2] Photocycloaddition Promoted by [G 26]$_{16}$•3K$^+$3I$^-$

Irradiation of [G **26**]$_{16}$•3K$^+$3I$^-$ with 300 nm UV light resulted in photocycloaddition of G **26** to give cyclobutane products. To analyze the rate of

product formation and monitor the reaction for completion, aliquots were taken at t = 0 h, 1 h, 6 h, and 24 h, the solvent was evaporated, and the samples were re-dissolved in DMSO-d_6 and investigated by ^{1}H NMR (**Figure 3.14**). DMSO-d_6 disrupts H-bonding and can be used to disassemble the G-quadruplex. The olefinic protons of the cinnamate group were monitored as the reaction progressed. Two reactions appear to occur simultaneously: *trans-cis* isomerization of the π-bond and [2+2] photocycloaddition. After 24 h the signals for the alkene double-bonds have almost completely disappeared. The reaction is complete after 24 hours, yielding cyclobutane guanosine products (84% yield). ESI mass spectrometry provided additional evidence that photocycloaddition occurred. The ESI mass spectrum gives a major mass to charge peak at 907.727 m/z, corresponding to the molecular weight of the G **26** photodimers (**cbG 26**) (**Figure 3.15**).

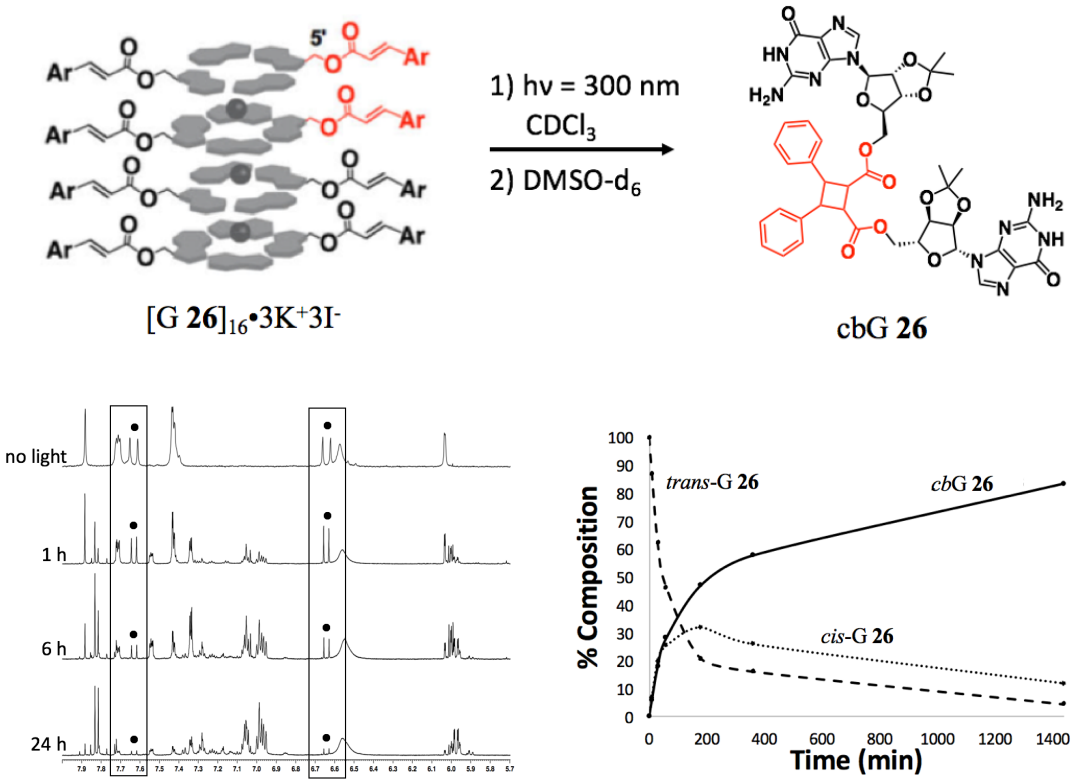

Figure 3.14. Top) Illustration showing the general photoreaction of [G **26**]$_{16}$•3K^{+}3I^{-} followed by G-quadruplex disassembly to provide **cbG 26** cyclobutanes. Bottom left) A series of ^{1}H NMR spectra highlighting the olefinic and aromatic protons during irradiation of [G **26**]$_{16}$•3K^{+}3I^{-} (0.625 mM) in $CDCl_3$. Reaction aliquots were taken out at time= 0 h, 1 h, 6 h, and 24 h, the solvent was evaporated, and re-dissolved in DMSO-d_6. The olefin protons are labeled (•), as the reaction proceeds the double bond protons gradually disappear as the photocycloaddition reaction occurs. Bottom right) A graph showing reaction composition as a function of time. As the reaction proceeds two reactions occur: *cis-trans* isomerization and [2+2] photocycloaddition resulting in G **26** cyclization products.

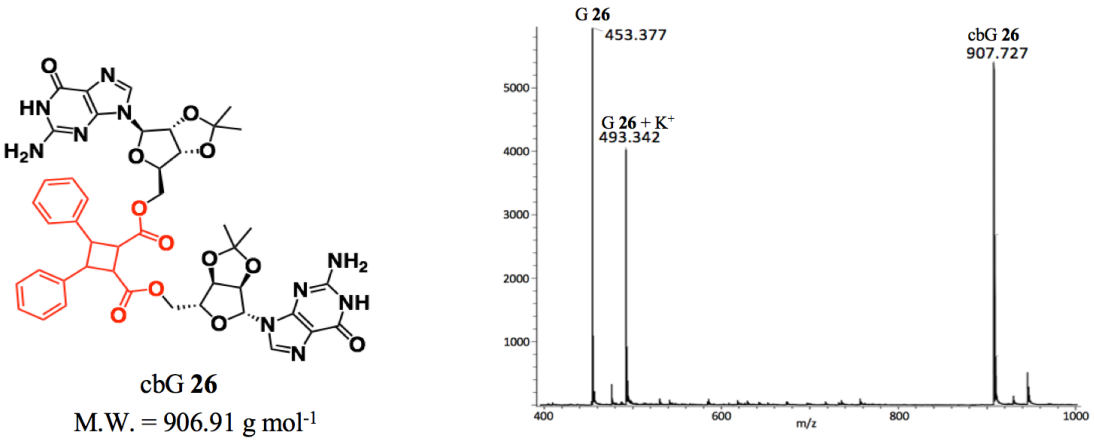

Figure 3.15. ESI mass spectrum of **cbG 26** (10 mM) showing a singly charged peak at 907.727 m/z corresponding to the molecular weight of the photodimer.

To characterize the products of the [G **26**]$_{16}$•3K^{+}3I^{-} templated photocycloaddition, the photoproducts were transesterified to the corresponding methyl esters and the ^{1}H NMR and MS data was compared to literature values. One major methyl ester product was observed, along with two minor methyl ester cyclobutanes. The cyclobutane methyl esters were analyzed by ^{1}H NMR and the data was compared with literature values of known cyclobutane methyl esters. Three products were isolated: β-truxinate (β-trux **41**),[108] δ-truxinate (δ-trux **42**),[109,110] and what we believe to be the ε-truxillate (ε-trux **43)** (**Figure 3.16**). The β-truxinate methyl ester **41** and δ-truxinate **42** have been reported in the literature.[108,109] Assignment of the ε-truxillate derivative **43** was made based on the number of NMR resonances observed, ^{1}H NMR splitting pattern, and chemical shifts. There are two NMR signals for the proton in question, this eliminates a few of the cyclobtuane steroisomers: ζ-truxinate, neotruxinate, epitruxillate, and γ-truxillate, for which we would expect 4 signals. The

^{1}H NMR splitting pattern is a triplet, so the neighboring protons observed must have similar *J*- coupling values. The triplet suggests that the neighboring protons are in similar environments (or symmetrically equivalent). This leaves only the ε-truxillate and peri-truxillate derivatives; based on the upfield shift of the protons, we made the assignment as ε-truxillate.

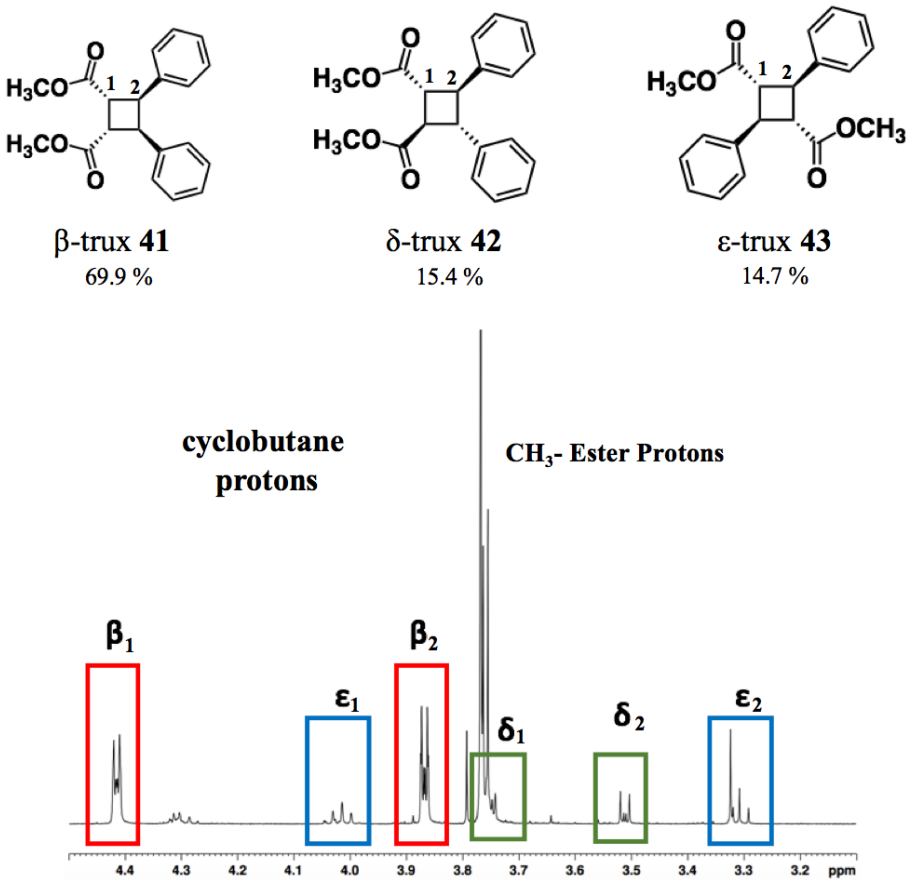

Figure 3.16.^{1}H NMR of the cyclobutane protons of the transesterified cycloaddition products from the photodimerization of G **26**. β-truxinates, δ-truxinates, and ε-truxillate G **26** derivatives formed during the irradiation of [G **26**]$_{16}$•3K^{+}3I^{-}.

3.5.5 Conclusions of 5′-Cinnamoyl-2′, 3′-Isopropylidene Guanosine

In conclusion, we have synthesized a new guanosine derivative G **26** with a 5′-cinnamoyl group and demonstrated that G-quadruplex self-assembly can be used to template [2+2] cycloaddition reactions in high yields. The cycloaddition is highly dependent on G-quadruplex assembly, free G **26** only undergoes *trans-cis* isomerization. Three products are formed during the photoirradiation, and when transesterified provide β-truxinate **41**, δ-truxinate **42**, and the ε-truxillate **43**. The G-quadruplex $[G\ \mathbf{26}]_{16}\bullet 3K^{+}3I^{-}$ exhibits moderate diastereoselectivity (β **41**:δ **42**:ε **43** *d.r.* 70:15:15) and high yields of cyclobutane product formation during irradiation (84 %). This system exhibits impressively high yields for a supramolecular system achieving yields on par with the covalent scaffolds **34**, **35**, and **36**.

3.6 Self-Assembly and Photochemistry of 5′-*ortho*-Methoxycinnamoyl-2′, 3′-Isopropylidene Guanosine (G 27)

The next logical step after examining the photoreactivity of 5′-cinnamoyl-2′, 3′-isopropylidene guanosine (G **26**) was to investigate how functionalization of the cinnamate impacts the G-quadruplexes' ability to template the [2+2] photocycloaddition. We started these studies with 5′-*ortho*-methoxycinnamoyl-2′, 3′-isopropylidene guanosine G **27**. The photochemical and self-assembly properties of G **27** were evaluated and are discussed in the subsequent sections.

3.6.1 UV-Vis Spectroscopy of 5′-*Ortho*-Methoxycinnamoyl-2′,3′-Isopropylidene Guanosine G 27

We began by studying the photochemical properties of 5′-*ortho*-methoxycinnamoyl-2′, 3′-isopropopylidene guanosine G **27** in $CDCl_3$ (**Figure 3.17**). We compared the absorbance of G **27** with the guanine nucleobase of 2′, 3′-isopropylidene guanosine (**IspG**) to determine if there would be direct competition for photon absorption. Guanosine absorbs at a λ_{max} of 254 nm UV-vis spectroscopy studies of G **27** show a λ_{max} of 275 nm corresponding to the π-π* transition of the cinnamate group, with an absorbance stretching up to 361 nm. *Ortho*-methoxycinnamic acid (***o*MeOCA**) absorbs at a similar UV range. A significant peak is observed at 324 nm for the cinnamate π-π* transition. All subsequent photochemical reactions of G **27** used 300 nm UV-light as it is outside of the absorbance range of isopropylidene guanosine **IspG** while remaining within G **27**'s absorbance range.

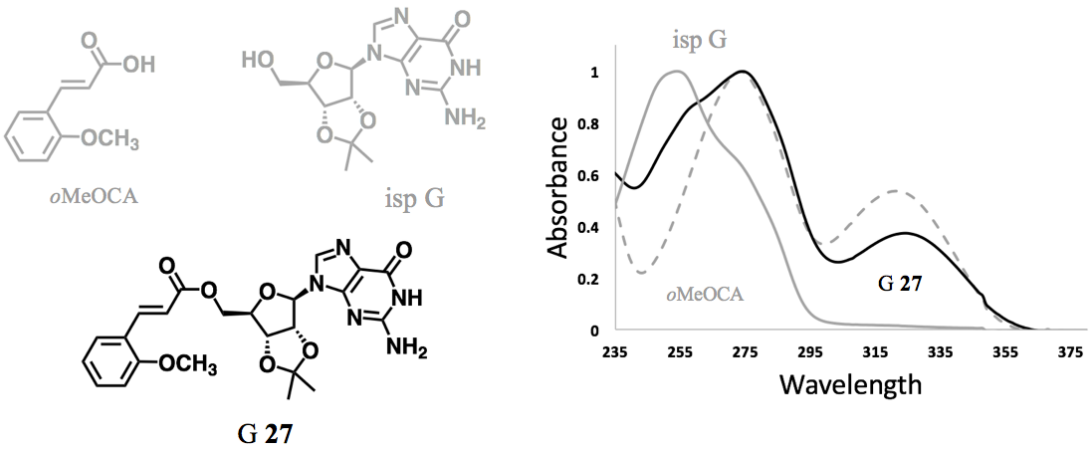

Figure 3.17. Normalized UV-vis absorbance spectra for 2′, 3′-isopropylidene guanosine **ispG**, *ortho*-methoxycinnamic acid (***o*MeOCA)**, and 5′-*ortho*-methoxycinnamoyl-2′, 3′-isopropylidene guanosine **G 27** in $CDCl_3$.

3.6.2 Photoisomerization of 5′-*Ortho*-Methoxycinnamoyl-2′, 3′-Isopropylidene Guanosine (G 27)

As a control experiment to the G-quadruplex facilitated [2+2] photocycloaddition of [G **27**]$_{16}$•3K$^+$3I$^-$ we tested the photoreactivity of monomeric G **27**. To ensure that no self-assembly was occurring we examined the photoisomerization of G **27** in DMSO-d_6, a solvent that disfavors G-quadruplex formation. When *trans*-G **27** (10 mM) was irradiated at 300 nm in DMSO-d_6 only *trans-cis* isomerization of the alkene π-bond occurred, no cycloaddition was observed (**Figure 3.18**). The *ortho*-methoxy derivative G **27** reaches a photostationary state of 34% *trans*-G **27**: 66% *cis*-G **27** after 6 h.

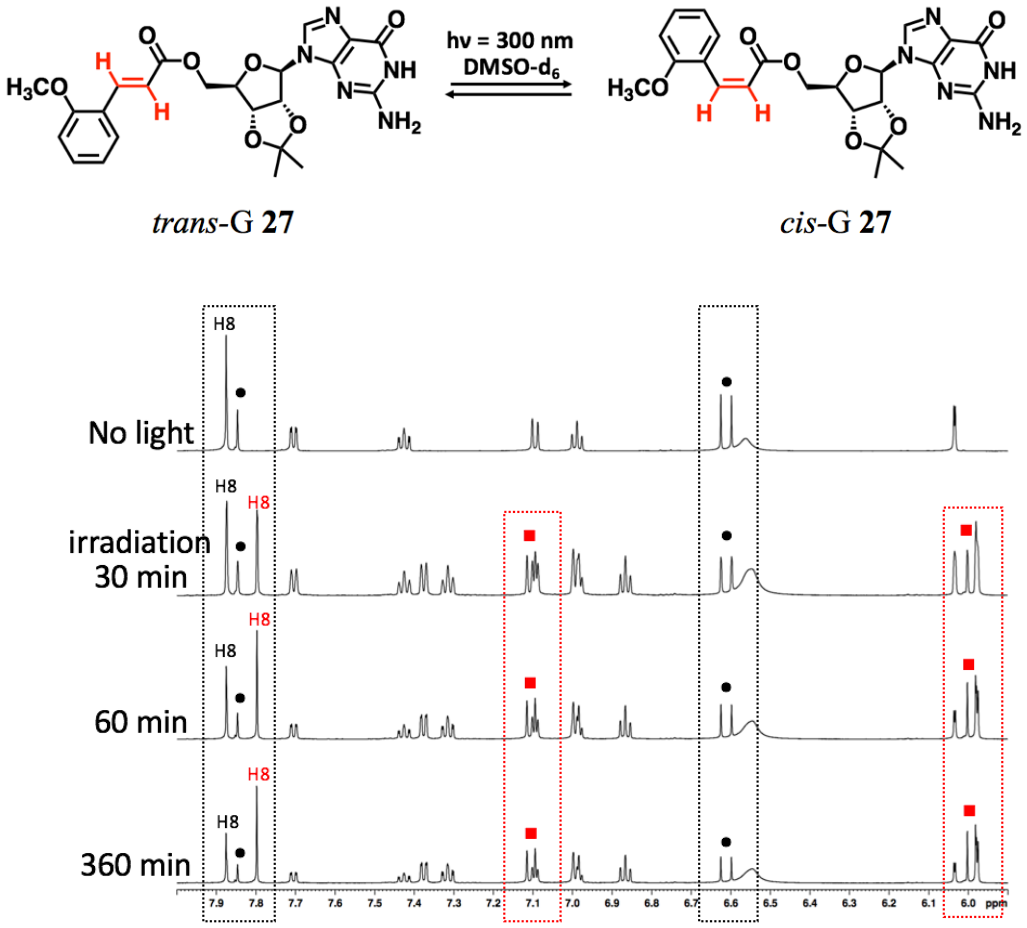

Figure 3.18. ^{1}H NMR spectra highlighting the olefinic protons of G **27** (10 mM) during photoirradiation with 300 nm light in DMSO-d_6. DMSO-d_6 disrupts G-quadruplex formation so that only the monomeric *trans*-G **27** is in solution. Under these conditions *trans-cis* isomerization of the double bond in *trans*-G **27** was observed, there was no cycloaddition. The olefin protons for *trans*-G **27** are labeled with •. The olefin protons for *cis*-G **27** are labeled with ■.

3.6.3 G-Quadruplex Self-Assembly of 5′-*Ortho*-Methoxycinnamoyl-2′, 3′-Isopropylidene Guanosine G 27

The guanosine derivative *ortho*-methoxycinnamate **G 27** (10 mM) self-assembles into a D_4-symmetric octamer [**G 27**]$_8$•K^+I^- in the presence of 0.125 eq. KI (1.25 mM) in $CDCl_3$. We made this assignment based on previously reported G-quadruplex self-assemblies. The ^{1}H NMR spectrum for [**G 27**]$_8$•K^+I^- displayed one set of resonances, a singlet is present for the N^1H amide proton (δ 12.37 ppm) and another set of two broader signals for the N^2H_2 amino protons were visible, δ 9.50 ppm for the protons involved in the G-quartets N^2H_A•••N^7 H-bond and one at δ 6.52 ppm for the exocyclic N^2H_B protons. Addition of an excess of KI (1.00 eq.) resulted in the formation of a new assembly that we characterized as a D_4-symmetric G_{16}-hexadecamer [**G 27**]$_{16}$•$3K^+3I^-$ (**Figure 3.19**). Similar to other G_{16}-hexadecamers, two sets of resonances appear: one set of resonances for the inner G_4-quartet layers and another set of resonances for the outer G_4-quartet layers.

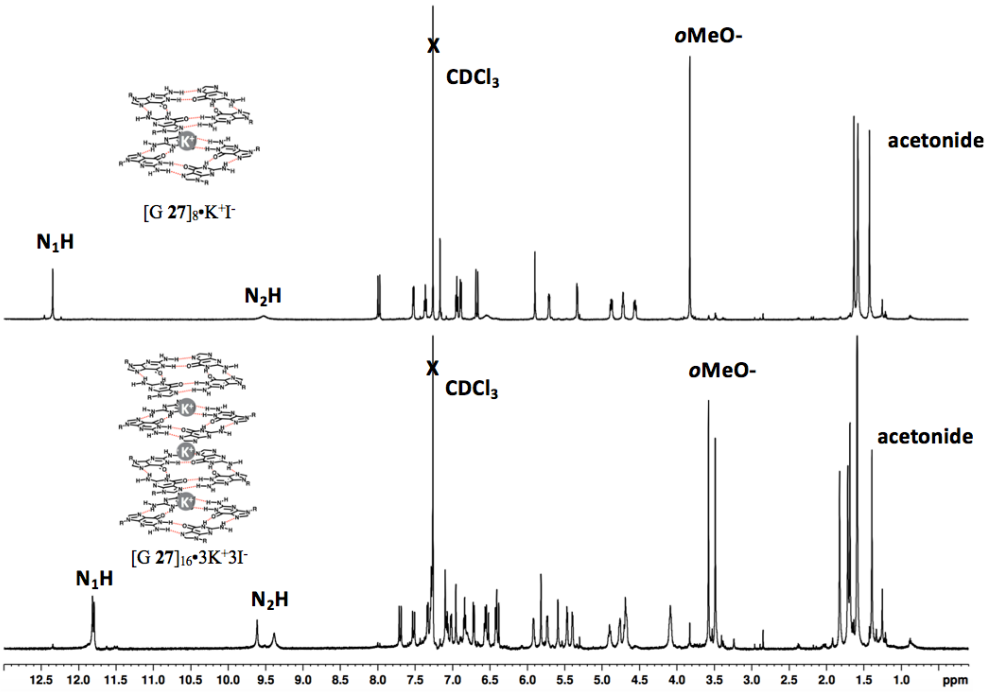

Figure 3.19. ^{1}H NMR spectra showing **G 27** self-assembly. Top) ^{1}H NMR spectrum of [**G10**]$_8$•K$^+$I$^-$ (1.25 mM) in $CDCl_3$. Bottom) ^{1}H NMR spectrum of [**G 27**]$_{16}$•3K$^+$3I$^-$ (0.625 mM) in $CDCl_3$.

3.6.4 [2+2] Photocycloaddition Templated by [G 27]$_{16}$•3K$^+$3I$^-$

Irradiation of [**G 27**]$_{16}$•3K$^+$3I$^-$ with 300 nm UV light resulted in the formation of cyclobutane products. The reaction was monitored by taking aliquots at different time points, evaporating the solvent, re-dissolving the sample in DMSO-d_6 and analyzing the samples by ^{1}H NMR. The *ortho*-methoxy protons provide a clear analytical handle to monitor the reaction progress (**Figure 3.20**). Two simultaneous reactions occur during the G-quadruplex templated reaction: *trans-cis* isomerization of the olefin and [2+2] photocycloaddition. As the reaction progressed two new sets of methoxy protons appeared for the cycloaddition products, while the peaks that

corresponded to the *trans*-G **27** and *cis*-G **27** methoxy protons and olefin protons gradually disappeared. The reaction is complete after 24 h, yielding 89% cyclobutane products **cbG 27a** and **cbG 27b**. To further analyze the products, the cyclobutanes formed were transesterified to their corresponding *ortho*-methoxy cyclobutane esters.

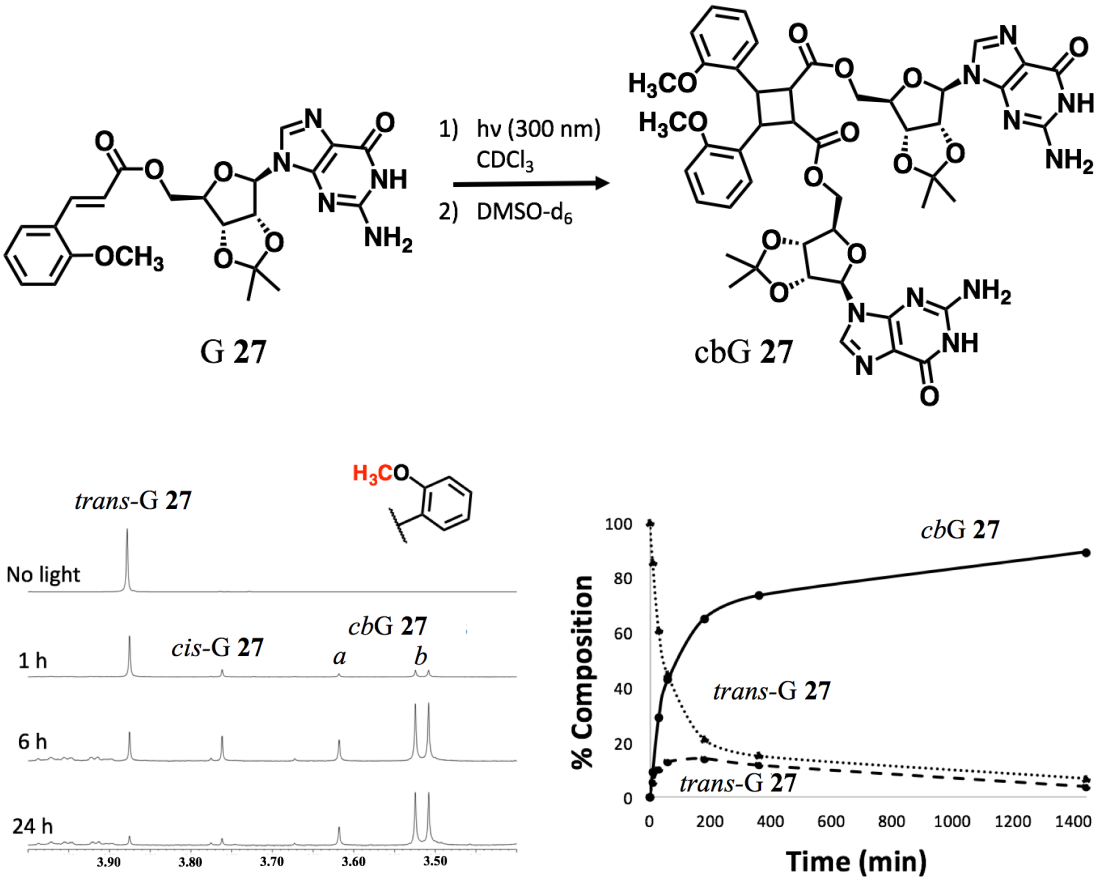

Figure 3.20. Left) A series of ^{1}H NMR spectra highlighting the *ortho*-methoxy protons during irradiation of [**G 27**]$_{16}$•3K^{+}3I^{-} (0.625 mM) in $CDCl_3$. Reaction aliquots were taken out at time= 0 h, 1 h, 6 h, and 24 h, solvent was evaporated, and re-dissolved in DMSO-d_6. Right) A graph showing reaction composition as a function of time. As the reaction proceeds two reactions occur: *cis-trans* isomerization and [2+2] photocycloaddition resulting in **G 27** cyclization products.

Transesterification of the [2+2] cycloaddition products to the methyl esters allowed for a direct comparison of the products with known *ortho*-methoxytruxinate and truxillate methyl esters.[111] The cyclobutane esters were analyzed by ^{1}H NMR and compared to known compounds. Two products were isolated, which we assigned to be the μ-*ortho*-methoxy truxinate (μ-trux **44**) and ω-*ortho*-methoxy truxinate (ω-trux **45**) methyl esters (**Figure 3.21**). The μ-*ortho*-methoxy truxinate has been previously reported in the literature.[111] Assignment of the ω-*ortho*-methoxy truxinate methyl ester was made based on the number of NMR resonances observed, ^{1}H NMR splitting pattern, and chemical shifts. There are only two NMR signals for the compound in question, this eliminates the cyclobutane stereoisomers: ζ-truxinate, neotruxinate, epitruxillate, and γ-truxillate; as they should have 4 separate signals. The ^{1}H NMR splitting pattern observed is a doublet of doublets, thus eliminating the ε-truxillate and peri-truxillates which would be expected to have a triplet splitting pattern. We made the assignment as ω-truxinate, by examining the chemical shifts of known, analogous cyclobutanes to eliminate the remaining α-truxillate and δ-truxinate from contention. There are 17 possible stereoisomers that can form, the [**G 27**]$_{16}$•3K$^+$3I$^-$ templates the formation of only two products. Both truxinates form from the head-to-head orientation of ***c****is*-G **27**. This is in stark contrast to the cinnamoyl derivative G **26** which reacts out of the *trans* conformation. It seems that the *trans*-G **27** in the G-quadurplex [G **27**]$_{16}$•3K$^+$3I$^-$ might not be able to orient itself in such a way to undergo photocycloaddition with a neighboring alkene. One possible explanation is that steric

interactions between the *ortho*-methoxycinnamate groups of neighboring layers in the G-quadruplex might prevent proper alignment for reactivity of the *trans* isomer.

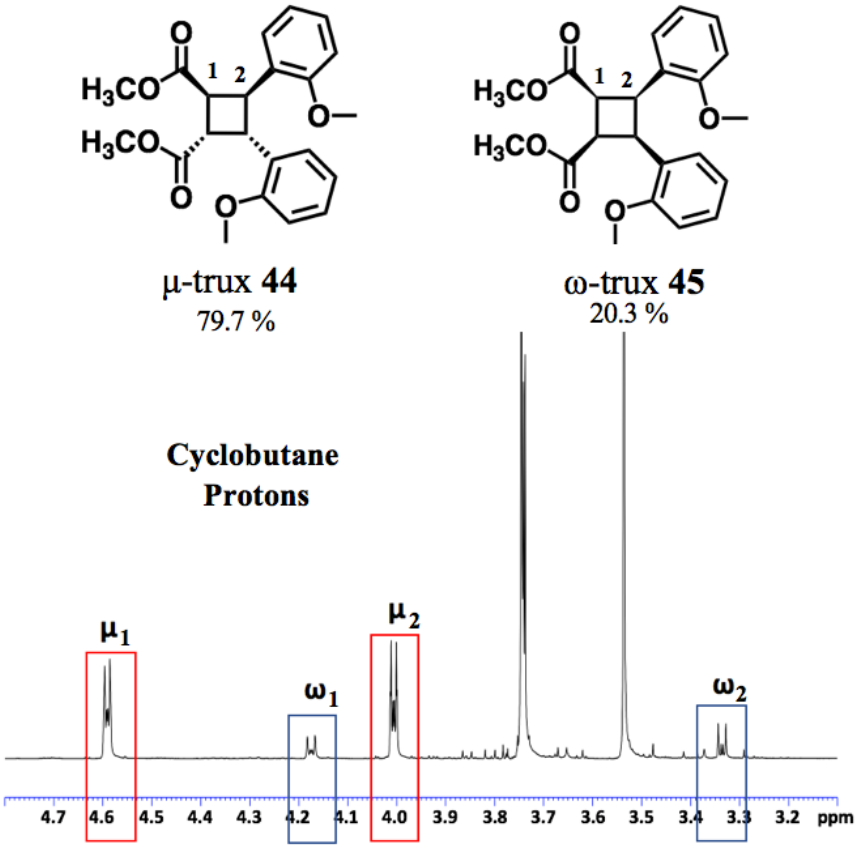

Figure 3.21. ^{1}H NMR of the cyclobutane protons of the transesterified cycloaddition products from the photodimerization of G **27**. μ-truxinates and ω-truxinate of **G 27** derivatives formed during the irradiation of [**G 27**]$_{16}$•3K^{+}3I^{-}.

3.6.5 Conclusions of 5′-*Ortho*-Methoxycinnamoyl-2′, 3′-Isopropylidene Guanosine G 27

We have synthesized a G derivative with a 5′-*ortho*-methoxycinnamoyl group **G10** and demonstrated that G-quadruplex self-assembly is necessary to template the

[2+2] cycloaddition reaction of this compound. The [2+2] photocycloaddition is reliant on K^+ templated G-quadruplex assembly; free *trans*-G **27** in DMSO-d_6 only undergoes *trans-cis* isomerization. Two products form during the G-quadruplex templated photocycloaddition, and upon transesterification provide μ-*ortho*-methoxy truxinate **44** and ω-*ortho*-methox*y* truxinate **45**. Surprisingly, the addition of the methoxy functional group at the *ortho* position significantly altered the outcome of the reaction as compared to the 5′-cinnamoyl G **26** derivative. This difference in reactivity might be due to steric interactions between neighboring *ortho*-methoxycinnamates and highlights the importance of the functionalization on the preorganization of the olefins on the periphery of the quadruplex (**Figure 3.21**). [G **27**]$_{16}$•3K^+3I^- exhibits high diastereoselectivity (μ **44**:ω **45** *d.r.* 80:20) and high yields (89 %).

3.7 Self-Assembly and Photochemistry of 5′-*Para*-Methoxycinnamoyl-2′, 3′-Isopropylidene Guanosine (G 28)

We next examined the self-assembly and photochemistry of the 5′-*para*-methoxycinnamoyl-2′,3′-isopropylidene guanosine G **28**. We conjectured that the *para*-methoxy aryl group might alter the alignment of the cinnamate olefin and provide a different photocycloaddition product than that of the *ortho*-methoxycinnamoyl derivative G **27** and the cinnamoyl derivative G **26**. The self-assembly and photochemistry of G **28** was evaluated and is discussed in the following section.

3.7.1 UV-Vis Spectroscopy of 5′-*Para*-Methoxycinnamoyl-2′,3′-Isopropylidene Guanosine G 28

We began our investigation by examining the photochemical properties of monomeric G **28**. The UV-vis absorbance of G **28** was examined in $CDCl_3$. We compared the absorbance of G **28** with the guanine nucleobase 2′, 3′-isopropylidene guanosine (**IspG**) to determine if there would be a direct competition for photon absorbance. Guanosine absorbs UV light at a λ_{max} of 256 nm. UV-vis spectroscopy studies of G **28** show a λ_{max} of 315 nnm corresponding to the π-π* transition of the cinnamate group (**Figure 3.22**). *Para*-cinnamic acid (**CA**) absorbs at a similar λ_{max} of 315 nm. Based on the absorbance profile of G **28** we decided on 300 nm UV-light for all subsequent photochemical reactions.

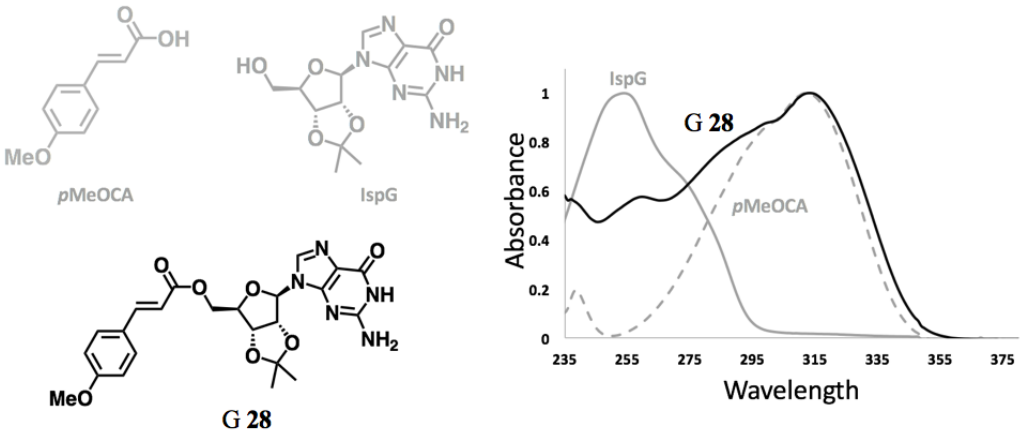

Figure 3.22. Normalized UV-vis absorbance spectra for 2′, 3′-isopropylidene guanosine **IspG**, *ortho*-methoxycinnamic acid (***p*MeOCA)**, and 5′-*para*-methoxycinnamoyl-2′,3′-isopropylidene guanosine **G 28** in $CDCl_3$.

3.7.2 Photoisomerization of 5′-*Para*-Methoxycinnamoyl-2′, 3′-Isopropylidene Guanosine G 28

As with the other 5′-cinnamoyl G derivatives, when 5′-*para*-methoxycinnamoyl G **28** is exposed to 300 nm light in DMSO-d_6 *trans*-*cis* isomerization about the alkene π-bond is the only reaction that occurs. No cycloaddition was observed. A photostationary state is reached within 6 h. The photostationary state provided a *trans*-G **28**: *cis*-G **28** ratio of 45%: 55% (**Figure 3.23**).

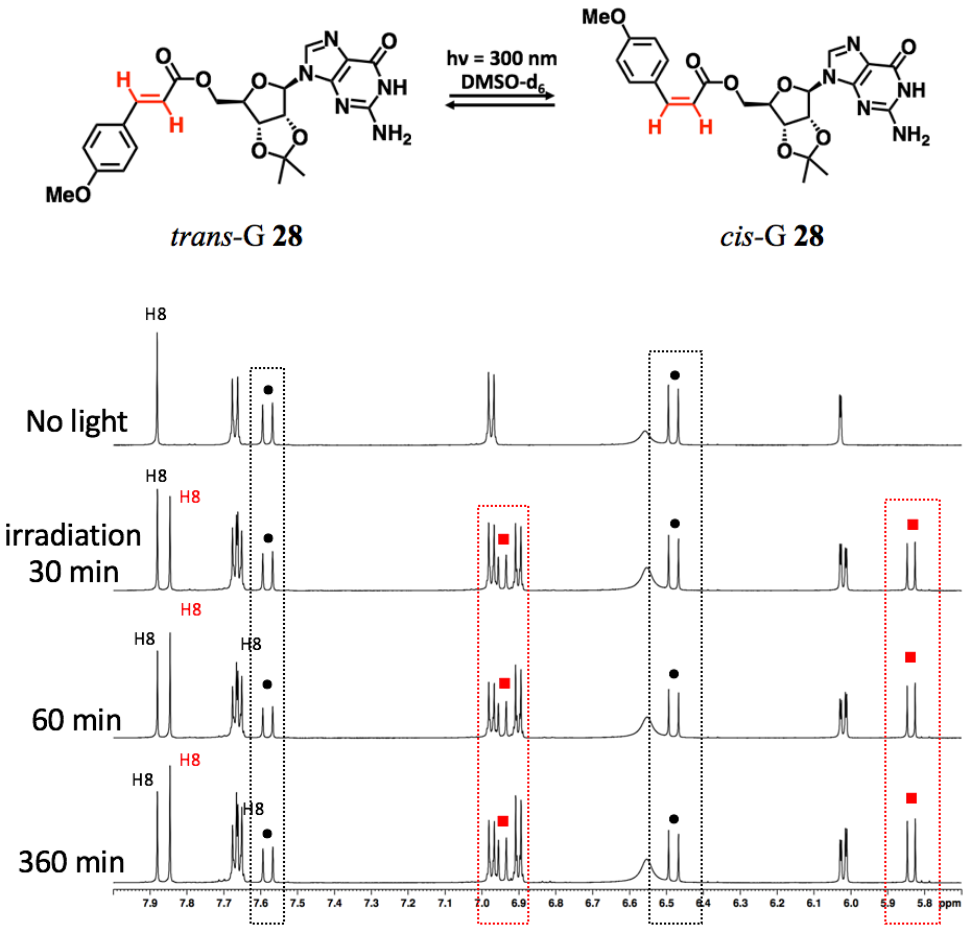

Figure 3.23. ^{1}H NMR spectra highlighting the olefinic protons of **G 28** (10 mM) during photoirradiation with 300 nm light in DMSO-d_6. DMSO-d_6 disrupts G-quadruplex formation so that only the monomeric **G 28** is in solution. Under these conditions *trans-cis* isomerization of the double bond in **G 28** was observed, there was no cycloaddition. The olefin protons for *trans*-G ***28*** are labeled with •. The olefin protons for *cis*-G ***28*** are labeled with ■.

3.7.3 G-Quadruplex Self-Assembly of 5′-*Ortho*-Methoxycinnamoyl-2′,3′-Isopropylidene Guanosine G 28

We next examined the self-assembly of **G 28**. *Para*-methoxy cinnamate **G 28** in the presence of KI (0.125 eq.) gave a ^{1}H NMR spectrum consistent with a D_4-

symmetric octamer [G **28**]$_8$•K^+I^-. This assignment was based on previously reported G-quadruplex ^{1}H NMR. The ^{1}H NMR spectrum for [G **28**]$_8$ •K^+I^- displayed one set of resonances, a singlet is present for the N^{1}H amide protons (δ 12.31 ppm) and another set of two broader signals for the N^{2}H$_2$ amino protons were visible, δ 9.60 ppm and one at δ 6.59 ppm for the exocyclic N^{2}H$_B$ protons. Addition of an excess of KI (1.00 eq.) resulted in the formation of a new assembly that we designated as a D_4-symmetric G_{16}-hexadecamer [G **28**]$_{16}$•$3K^+3I^-$ (**Figure 3.24**). This ^{1}H NMR shows the characteristic doubling of resonance peaks and N_1H/N_2H hydrogen bonding region (δ 9.40-11.71 ppm) of analogous G_{16}-quadruplexes.

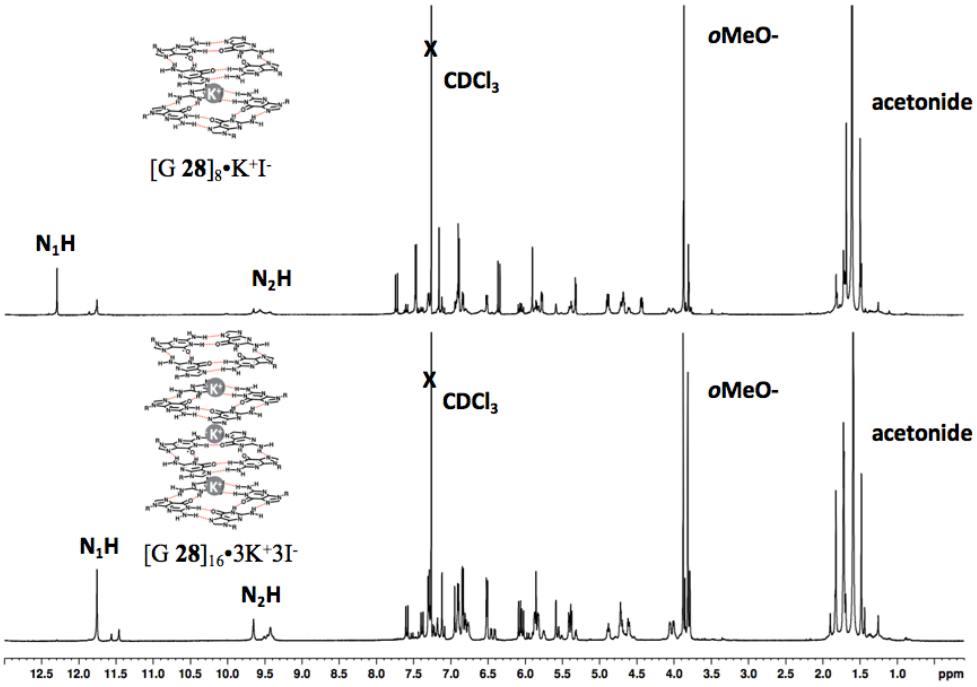

Figure 3.24. ^{1}H NMR spectra showing G **28** self-assembly. Top) ^{1}H NMR spectrum of [G **28**]$_8$•K^+I^- (1.25 mM) in $CDCl_3$. Bottom) ^{1}H NMR spectrum of [G **28**]$_{16}$•$3K^+3I^-$ (0.625 mM) in $CDCl_3$.

3.7.4 [2+2] Photocycloaddition Templated by $[G\ \mathbf{28}]_{16}\bullet 3K^{+}3I^{-}$

Irradiation of $[G\ \mathbf{28}]_{16}\bullet 3K^{+}3I^{-}$ with 300 nm UV light resulted in the formation of only one cyclobutane product **cbG 28**. To monitor the [2+2] photocycloaddition as the reaction progressed, aliquots were taken at t= 0 h, 1 h, 3 h, and 6 h, the solvent was evaporated, and the resulting samples were re-dissolved in DMSO-d_6 for ^{1}H NMR analysis. The cinnamate's *para*-methoxy protons provide a clear analytical handle to monitor the reaction progress by ^{1}H NMR (**Figure 3.25**). Our results indicate that two reactions occurred simultaneously: *trans-cis* isomerization of the olefin and [2+2] photocycloaddition between two G **28** cinnamates in the quadruplex. As the reaction progressed one new sets of methoxy protons appeared for the cycloaddition product, while the peaks that corresponded to the *trans*-G **28** and *cis*-G **28** methoxy protons gradually disappeared. The reaction is complete at 3 h, yielding one guanosine cyclobutane product in 93% yield. This cycloaddition is much faster than the other two cinnamate guanosine derivatives cinnamoyl G **26** and *ortho*-MeO G **27** which take 24 h to go to completion. To further analyze the product that formed the cyclobutane was transesterified to the corresponding methyl ester and compared against known *para*-methoxycinnamoyl cyclobutane methyl esters.

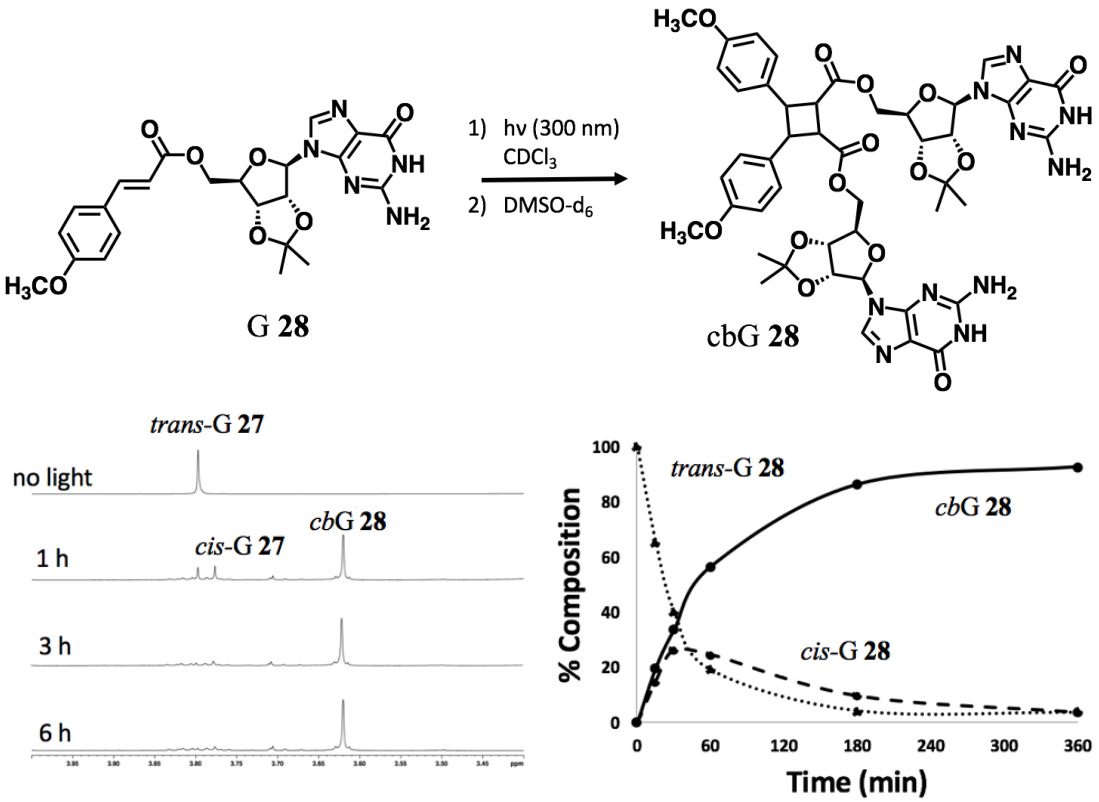

Figure 3.25. Left) A series of ^{1}H NMR spectra highlighting the *para*-methoxy protons during irradiation of [**G 28**]$_{16}$•3K^{+}3I^{-} (0.625 mM) in $CDCl_3$. Reaction aliquots were taken out at time= 0 h, 1 h, 6 h, and 24 h, solvent was evaporated, and re-dissolved in DMSO-d_6. Right) A graph showing reaction composition as a function of time. As the reaction proceeds two reactions occur: *cis-trans* isomerization and [2+2] photocycloaddition resulting in **G 28** cyclization products.

Transesterification of the [2+2] cycloaddition products to the methyl ester allowed for a direct comparison of the product with known *para*-methoxy truxinate methyl esters. The resulting methyl ester was analyzed by ^{1}H NMR and compared to known compounds. The major product was identified as the β-*para*-methoxy truxinate methyl ester (β-trux **46**) (**Figure 3.26**). The β-*para*-methoxy truxinate methyl ester **46** has been previously reported in the literature.[112] The β-truxinate arises from the [2+2] cycloaddition reaction of two *trans* cinnamates aligned in a head to head arrangement.

It is astounding that through a collection of non-covalent interaction that a single product is formed in this reaction.

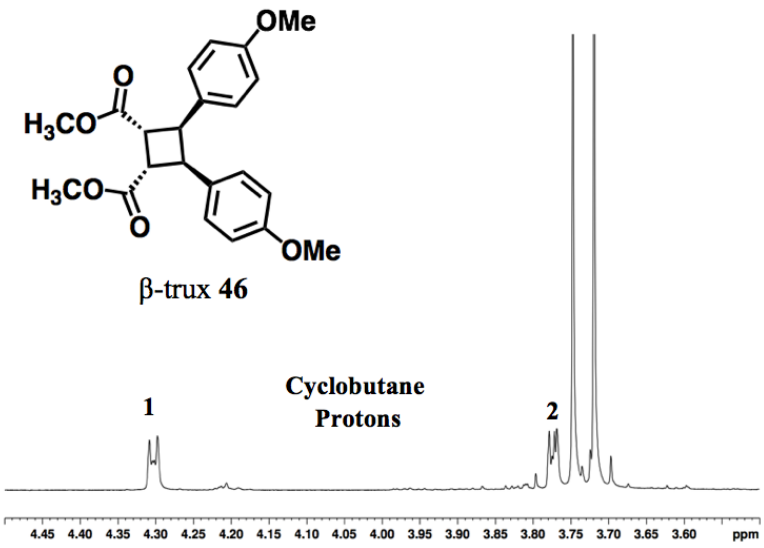

Figure 3.26. ^{1}H NMR of the cyclobutane protons of the transesterified cycloaddition product from the photodimerization of G **28**. β-truxinate derivative formed during the irradiation of [G **28**]$_{16}$•3K^{+}3I^{-}.

3.7.5 Conclusions of 5′-*Para*-Methoxycinnamoyl-2′, 3′-Isopropylidene Guanosine G 28

In conclusion, we have synthesized a new lipophilic G derivative with a 5′-*para*-methoxycinnamoyl appended at the 5′-position. This compound undergoes [2+2] photocycloaddition reactions when self-assembled into a G-quadruplex. The cycloaddition is highly dependent on G-quadruplex assembly, free *trans*-G **28** only undergoes *trans-cis* isomerization. One major product forms during the photocyloaddition, the β-truxinate G **46** derivative, confirmed through analysis of the

transesterified methyl esters. [G **28**]$_{16}$•3K^{+}3I^{-} photoirradiation exhibits impressively high diastereoselectivity and yields during irradiation. This is an exciting system showing the prospects of using the G-quadruplex as a scaffold for controlling the stereochemical outcome for topochemically restricted organic transformations.

3.8 Conclusion: Utilizing the G-Quadruplex as a Scaffold for Photochemical [2+2] Cycloaddition Reactions

We have developed a new method that utilizes G-quadruplex self-assembly to template the [2+2] photocycloaddition reaction of 5′-cinnamate ester derivatives G **26**-G **28**. The G-quadruplex templated reaction proceeds with high yields and stereoselectivities as compared to other self-assembled photocycloaddition templates.[63] While free in solution the monomeric G derivatives only undergo *trans-cis* isomerization. The identity of the 5′-cinnamate has a significant influence over the outcome of the reaction. The substituent on the cinnamate might affect how the olefins align when self-assembled in the G-quadruplex nanostructures. The different reaction outcomes suggest that steric interactions between cinnamates on adjacent G_4-layers might influence the regioselectivity and stereoselectivity of the reaction. The methoxy groups attached to the aryl rings promotes higher regioselectivities and stereoselectivities. This new method might be useful in synthesizing new cyclobutane based drugs that have been difficult to construct through other currently available methods.

To gain a greater understanding of the reactivity of the 5′-cinnamate guanosine derivatives, *meta*-methoxycinnamoyl-2′,3′-isopropylidene guanosine (G **29**), was chosen for an in-depth study and is presented in **Chapter 4**. G **29** was chosen for analysis because: 1) a crystal structure of the reactive self-assembly [G **29**]$_{16}$•3K^{+}3I^{-} was obtained illuminating structural information about the active olefin on the periphery of the structure and 2) the reaction is highly regioselective and stereoselective, providing 1 product in high yields (> 90%).

Chapter 4. Templating and Catalyzing [2+2] Photocycloaddition in Solution Using a Dynamic G-Quadruplex

The majority of this chapter has been published in reference 63:

•Sutyak, K.B.; Lee, W; Zavalij, P.V.; Gutierrez, O.; Davis, J.T. "Templating and Catalyzing [2+2] Photocycloaddition in Solution Using a Dynamic G-Quadruplex" *Angew. Chemie.* **2018**, 57, 17146-17150.

Wes Lee and Dr.Osvaldo Gutierrez provided all ONIOM calculations and invaluable discussion on this project. Dr. Peter Zavalij performed all X-ray crystallography and solved the ***[G12]***•$3K^+3I^-$ *crystal structure.*

4.1 Research Goals

The goal of the research in this chapter was to gain a better understanding of the regioselectivity, stereoselectivity and catalytic capability of the G-quadruplex promoted [2+2] photocycloaddition reaction. **Chapter 3** highlighted a series of cinnamate guanosine derivatives that are capable of dimerizing to produce cyclobutane truxinate and truxillate products. Questions remained about the structure and reactivity of the G-quadruplex promoted [2+2] photocycloadditions: is this system catalytic? How does the G-quadruplex pre-organize reactive cinnamate groups on the periphery of the structure? What drives the regio- and stereoselectivity of the reaction? To answer

the above questions, we synthesized and characterized a new guanosine derivative, 5′-*meta*-methoxycinnamoyl-2′,3′-isopropylidene guanosine (G **29**) (**Figure 4.1**). Self-assembly and reactivity of [G **29**]$_{16}$•3K^{+}3I^{-} were studied by 1D and 2D ^{1}H NMR, mass spectrometry, X-ray crystallography, and computational studies. G-quadruplexes formed from G **29** were investigated for catalytic turnover.

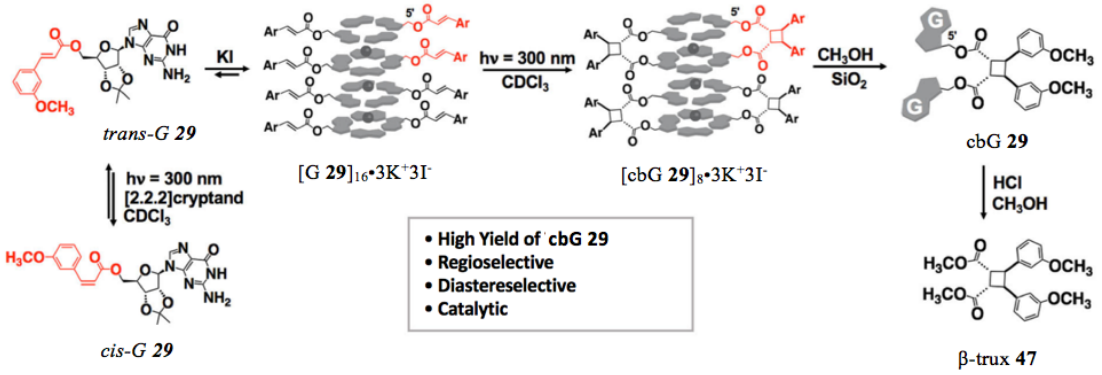

Figure 4.1. *trans*-5′-*meta*-Methoxycinnamate-2′, 3′-isopropylidine guanosine G **29** and KI form a H-bonded G-quadruplex [G **29**]$_{16}$•3K^{+}3I^{-} that undergoes [2+2] photocycloaddition to give [**cbG 29**]$_{8}$•3K^{+}3I^{-} containing cyclobutane **cbG 29**. When excess [2.2.2]-cryptand is added, in order to sequester K^{+}, irradiaton of G **29** gives only isomerization about the C=C π-bond resulting in a mixture of *trans*-G **29** and *cis*-G **29.** Cyclobutane β-truxinate derivative (**cbG 29**), can be isolated and further reacted to give β-trux **47**.

4.2 Background and Hypothesis: Preorganization and Template-Directed Synthesis of Reactive Olefins on Periphery of G-quadruplex Structure

Self-assembly processes allow for quick and efficient organization of reactive groups. Supramolecular templating relies on non-covalent interactions to orient reactants for formation of new covalent bonds.[113-117] This non-covalent templating

strategy can efficiently align reactive units to undergo stereoselective transformations. Supramolecular templating would be even more valuable if products were able to exchange with reactants, so that the process becomes catalytic. In this chapter, we examine the G-quadruplex as a supramolecular scaffold for templating the spatially demanding [2+2] photocycloaddition of G **29** (**Scheme 4.1**).[63]

Guanosine derivatives, in the presence of K^+ form H-bonded G_4-quartets.[29] The G_4-quartets then stack to give G-quadruplexes made of multiple G_4-quartet layers occupied with stabilizing cations. The rigid $([G]_4 \bullet K^+])_n$ core can induce the 5′-sidechains to adopt well-defined conformations. In **Chapter 2** we described $[G\ \mathbf{21}]_{16} \bullet 3K^+$ hexadecamers made from 5′-benzoyl G **21** analogs that have extensive interlayer H-bonds and π-π interactions on the assembly's exterior. We hypothesized that the G-quadruplex could act as a supramolecular template and pre-organize reactive groups for organic reactions. We reasoned that the interlayer separations of ca. ~3.3 Å would be ideal to template the [2+2] photocycloaddition of 5′-cinnamate esters radiating from the G-quadruplex. We envisioned that attaching reactive olefins to the 5′-sidechain might align the olefins for photodimerization and would enable facile release of the cyclobutane product after formation. We also postulated that the [2+2] process might be catalytic, since G monomers are in dynamic exchange with G-quadruplex subunits. We studied 5′-*meta*-methoxy cinnamate G **29**, since *meta*-methoxy cinnamic acid does not photodimerize either in the solid-state or in solution.[118]

As discussed in **Chapter 3**, truxinate cyclobutanes are found in natural products and synthetic drugs.[86,89-92] These bioactive compounds can be prepared by [2+2] photocycloadditions of alkenes. Cyclization is most efficient when 2 C=C bonds align in parallel, with reacting atoms held less than 4.2 Å apart.[83,84] If the alkenes are dispersed in solution, cyclobutane formation is usually disfavored and the major photoreaction is *trans-cis* isomerization about the C=C double bond. Often, [2+2] cycloaddition occurs better in the solid-state than in solution, especially if the alkene crystallizes so that the topological requirements for dimerization are satisfied. But, solid-state reactions suffer if the crystal degrades during irradiation.[83-85,93]

Synthetic methods that enable high yields of [2+2] cycloaddition in solution are particularly valuable. Templating strategies enable [2+2] photocycloaddition in solution.[100,119] One approach is to covalently tether 2 alkenes, so that the C=C π bonds populate spatial conformations that can dimerize.[97-99] Another approach is to use non-covalent interactions to organize C=C bonds for reaction.[100-106] Molecular containers can facilitate [2+2] photocycloaddition of alkenes, often with good regioselectivity and stereoselectivity.[101-103] The host sequesters alkenes so that they dimerize upon irradiation. Sometimes, these reactions are catalytic as cyclobutane product exchanges with reactants, enabling turnover. Intermolecular H bonding of 2 alkenes to a template can also trigger [2+2] cycloaddition of cinnamate esters in solution, and some of these H-bonding templates have catalytic turnover.[104,105] Our goal was to use the G-

quadruplex, a robust H-bonded assembly, as a supramolecular template to pre-organize multiple cinnamates for catalytic photodimerization in dilute solution.

4.3 Supramolecular Templating and G-Quadruplex Promoted Synthesis

Supramolecular templating makes use of non-covalent interactions to align and control the reactivity of compounds. Supramolecular synthesis can be used to synthesize challenging target compounds and mechanically interlocked molecules.[113] One example of a supramolecular templated synthetic method is the Na^+ templated formation of crown ethers by Pederson, who was subsequently awarded the Nobel prize for his contribution to chemistry.[115] Pederson took advantage of ion-dipole interactions between the ether oxygens of an ethylene oxide chain and a central sodium cation to template the annulation of a series of benzo crown ethers in good yields (**Figure 4.2.A**).[115] Using a similar reaction strategy, Sauvage utilized a metal chelation template strategy to promote the formation of a mechanically interlocked catenane **48.**[116] A copper (I) ion was used to form a coordination complex between two phenanthroline derivatives, intertwined ring segments were then covalently locked to form a two-ring mechanically interlocked catenane (**Figure 4.2.B**).

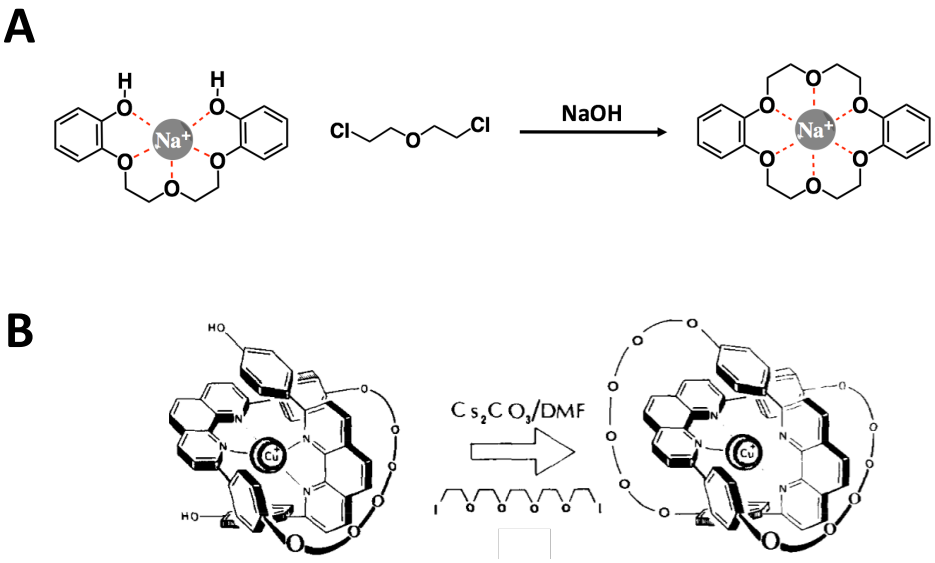

Figure 4.2. Supramolecular templating of A) the synthesis of dibenzo-18-crown-6-ether using Na^+•ether ion-dipole interactions to template ring closure.[115] B) The synthesis of a phenanthroline catenane **48** templated by Cu^+ coordination to interdigitate the reactants before catenation.[116]

G-quadruplex self-assembly has also been utilized to template spatially controlled organic reactions. The Davis group synthesized a lipophilic guanosine derivative, 5′-(3,5-bis(allyloxy)) benzoyl-2′,3′-isopropylidene guanosine G **19**, incorporating a reactive allyloxy alkene group at the 5′-position. When self-assembled, the 5′-bis(allyloxy)guanosine G-quadruplex [G **19**]$_{16}$•3K^+ was covalently captured through olefin metathesis between olefins on neighboring G_4-quartets. The resulting covalently captured quadruplexes were found to function as transmembrane ion channels in phospholipid vesicles (**Figure 4.3**).[61]

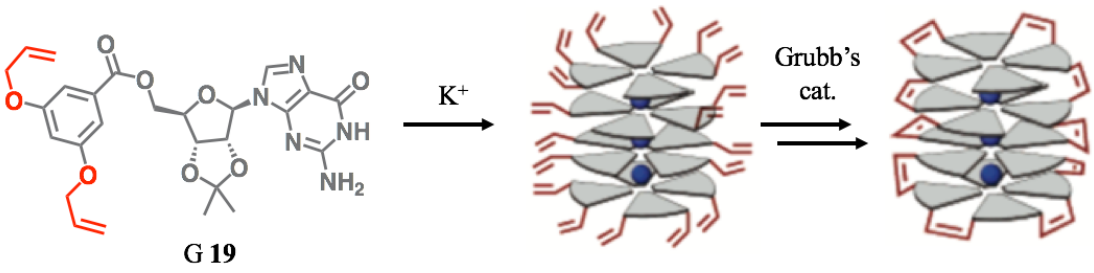

Figure 4.3. Supramolecular templating using the G-quadruplex. Self-assembly of [G **19**]$_{16}$•3K^{+}3I^{-} enabled an olefin metathesis reaction that covalently locked the G-quadruplex structure.[61]

The G-quadruplex has also been found to template photodimerization reactions in naturally occurring G4 rich DNA sequences. Su *et al.* found that a G rich telomeric DNA strand (**Tel22** = 5′-AGGGTTAGGGTTAGGGTTAGGG-3′) self-assembled into G-quadruplexes that templated the [2+2] photocycloaddition of thymine dimers. The basket type G-quadruplexes shown in **Figure 4.4** promoted the cycloaddition of two thymidine nucleotides in neighboring strands.[120]

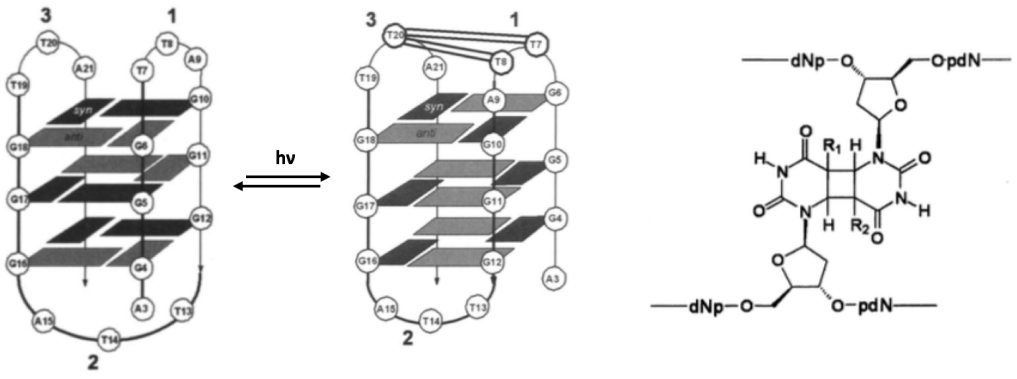

Figure 4.4. G-quadruplex templated photodimerization of thymine in G-rich DNA.[120]

The central core of lipophilic G-quadruplexes can also template photochemical reactions. Previous work found that 1) a light catalyzed *cis/trans* isomerization can control assembly and disassembly of G-quadruplexes,[121] and 2) C8-modified analogs undergo [2+2] photocycloaddition within the G-quadruplex core.[62] The Rivera group covalently modified a lipophilic guanosine derivative (dG **20**) at the C8 position with a photoreactive chalconyl group, which upon self-assembly and irradiation with ultraviolet light (365 nm) underwent a photocycloaddition reaction (**Figure 4.5)**. This photocycloaddition reaction modulated G-quadruplex molecularity in solution, switching assemblies from G_{16}-hexadecamers to G_{12}-dodecamers.

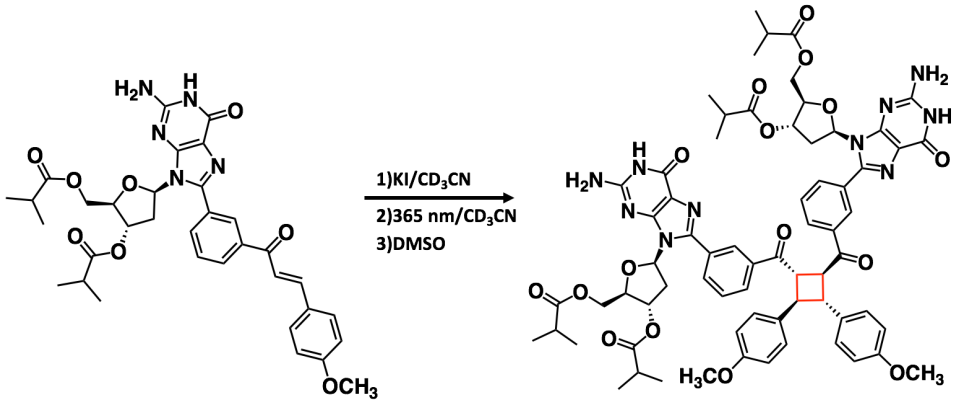

Figure 4.5. G-quadruplex templating on the core of the G-quadruplex. Chalconyl photocycloaddition templated by a lipophilic G-quadruplex.[62]

Gaining motivation from these previous examples we sought to perform a synthetically useful photocycloaddition reaction at the 5′-position of a lipophilic guanosine derivative using G **29**. Herein, we describe a templating/covalent capture strategy that enables photochemical formation of 8 cyclobutanes in one non-covalent

assembly at the periphery of the G-quadruplex structure. We report that *trans*-5′-(3-methoxycinnamoyl)-2′,3′-isopropylidene guanosine (**G 29**) and KI self-assemble in solution to give a complex, [G **29**]$_{16}$•3K$^+$3I$^-$, where C=C π bonds in neighboring G$_4$-quartets are aligned directly on top of one another and separated by 3.3 Å, enabling [2+2] photocycloaddition in solution. Irradiation of [G **29**]$_{16}$•3K$^+$3I$^-$ in solution forms new C-C σ bonds, giving [**cbG 29**]$_8$ •3K$^+$3I$^-$, a species with 8 subunits of cyclobutane **cbG 29** (**Figure 4.1**). Cyclobutane **cbG 29** is made in high yield (>90 %) by exposing a dilute solution of [G **29**]$_{16}$•3K$^+$3I$^-$ to light, either from a lamp or the sun. This templating/covalent capture approach enables regio- and stereoselective synthesis of **cbG 29**. Importantly, this [2+2] photocycloaddition is catalytic in K$^+$ since the reactant **G 29** and product **cbG 29** are in dynamic equilibrium with G-quadruplexes, and QM/MM calculations reveal that incorporation of **G 29** into the G-quadruplex is favored over incorporation of cyclobutane **cbG 29**.[63]

4.4 Synthesis of 5′-*meta*-Methoxycinnamoyl-2′, 3′-Isopropylidene Guanosine G 29

We began by synthesizing 5′-*meta*-methoxycinnamoyl-2′, 3′-isopropylidene guanosine G **29**. To perform this synthesis, we used 1-ethyl-3-(3-dimethylaminopropyl)carbodimide (EDC) to couple a carboxylic acid to the 5′-position of a protected 2′,3′-isopropylidne guanosine (IspG) on a 1.00 g scale (**Figure 4.6**) . The use of EDC coupling versus the acid chloride decreased side product formation. When using the highly reactive acid chloride the diacylated N2, O5′-diacyl product can form. Additionally, EDC is water soluble and easily removed from the completed reaction

through a series of H_2O washes, thus eliminating timely column purifications. **G 29** was triturated with hot isopropanol, and the remaining solid was isolated as a white powder in 86.9 % yield.

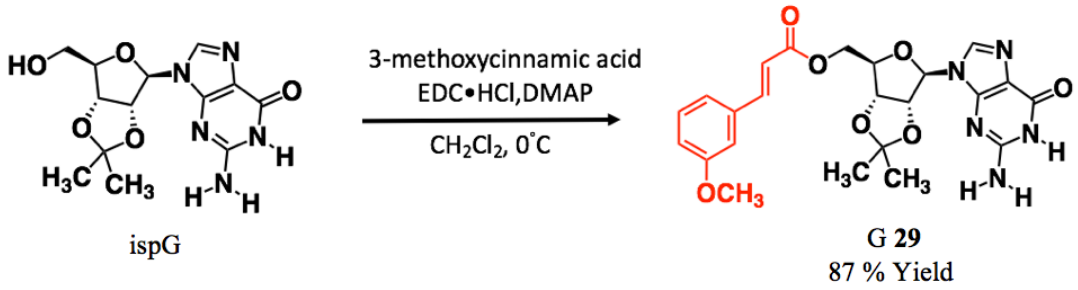

Figure 4.6. Synthesis of 5′-*meta*-methoxycinnamoyl-2′,3′-isopropylidene guanosine G **29.**

4.5 UV-Vis Spectroscopy of 5′-*meta*-Methoxycinnamoyl-2′, 3′- Isopropylidene Guanosine G 29

We examined the photochemical properties of monomeric *trans*-G **29** in $CDCl_3$. UV-vis spectroscopy showed a band with λ_{max} of 285 nm extending to 315 nm, due to the π-π^* transition for 5′-cinnamate (**Figure 4.7**). The UV-Vis spectra of G **29** is a combination of the 2′, 3′-isopropylidene guanosine **IspG** and 3-methoxycinnamic acid (***m*MeOCA**) spectrum. All irradiation experiments performed later in this chapter use 300 nm wavelength ultraviolet light where the cinnamate ester absorbs, but the **IspG** unit does not absorb.

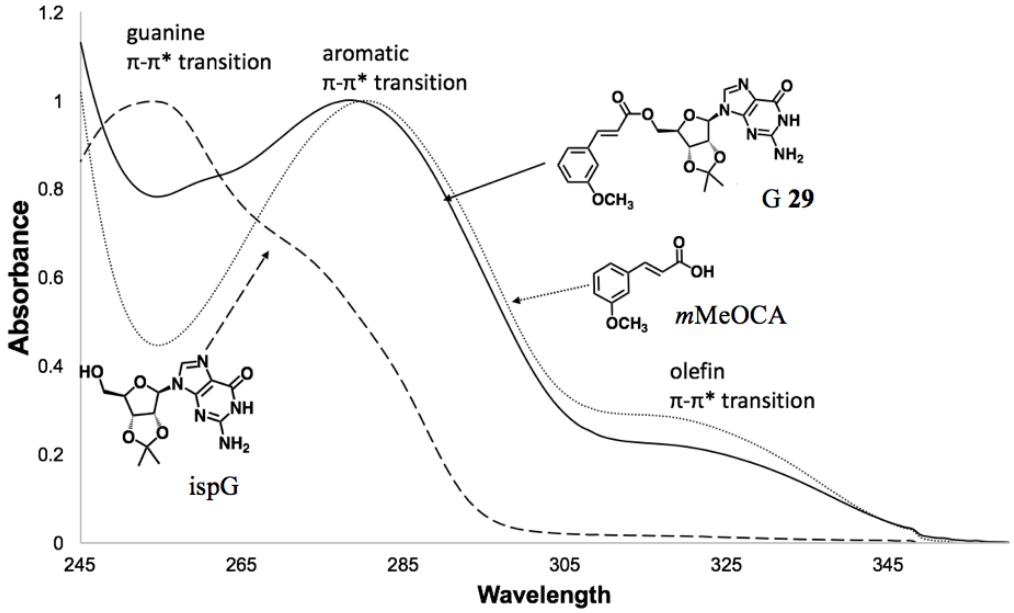

Figure 4.7. Normalized UV-Vis spectra of 2′,3′-isopropylidene guanosine **IspG** (72.9 μM)**,** 3-methoxycinnamic acid ***m*MeOCA** (79.7 μM), and *trans*-5′-(3-methoxy)cinnamoyl-2′,3′-isopropylidene guanosine **G 29** (72.7 μM).

4.6 Photoisomerization of 5′-*meta*-Methoxycinnamoyl-2′, 3′-Isopropylidene Guanosine G12

After examining the UV-vis absorbance, we turned our attention towards the photoreactivity of G **29**. Monomeric G **29** did not dimerize when irradiated in solution. To ensure there were no G-quadruplex assemblies present during irradiation excess [2.2.2]-cryptand was added to sequester any rogue Na^+ or K^+ cations. When a solution of *trans*-G **29** (10 mM) and cryptand (140 mM) in $CDCl_3$ was irradiated for 24 h with 300 nm light we observed, by ^1H NMR analysis, only isomerization to give a 56:44

photostationary mix of *trans*-G **29** and *cis*-G **29** (**Figure 4.8**). With no cations available to form G-quadruplexes, there was no [2+2] cycloaddition of G **29**.

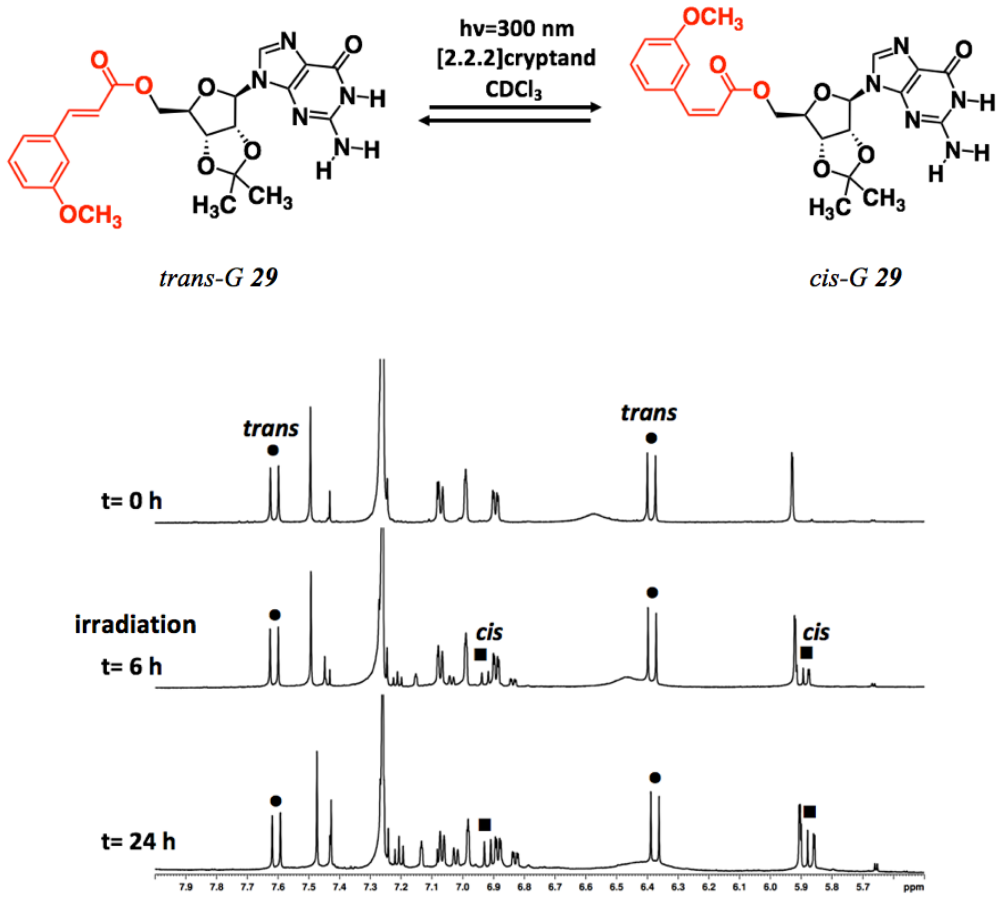

Figure 4.8. Top) Illustration of the photoisomerization of 5′-*meta*-methoxycinnamoyl-2′, 3′-isopropylidene guanosine G **29**. Bottom) A series of ^{1}H NMR spectra of the photoisomerization of G **29** (10 mM) highlighting the aromatic and olefin region at t = 0 h, 6 h, and 24 h in $CDCl_3$. [2.2.2] Cryptand (140 mM) was added to prevent G-qudruplex formation. *trans*-G **29** (•) and *cis*-G **29** (■).

4.7 G-Quadruplex Self-Assembly of 5′-*meta*-Methoxycinnamoyl-2′,3′-Isopropylidne G 29

The guanosine derivative 5′-(3-methoxy)cinnamoyl-2′, 3′-isopropylidene guanosine G **29** (10 mM) formed a D4-symmetric hexadecamer [G **29**]$_{16}$•3K^{+}3I^{-} (0.625 mM) in the presence of 1 equiv. of KI (10 mM). We characterized the self-assembly of G **29** by mass spectrometry (**Figure 4.9**), ^{1}H NMR, CD spectroscopy, and X-ray crystallography. [G **29**]$_{16}$•3K^{+}3I^{-} was identified based on splitting of ^{1}H NMR signals into pairs of equal intensity (**Figure 4.10**). Formation of the hexadecameric G-quadruplex was further supported by ESI-MS, showing a major, triply charged peak at 2617.4 m/z, indicating a molecular weight of 7852.2 for [G **29**]$_{16}$•3K^{+}3I^{-}.

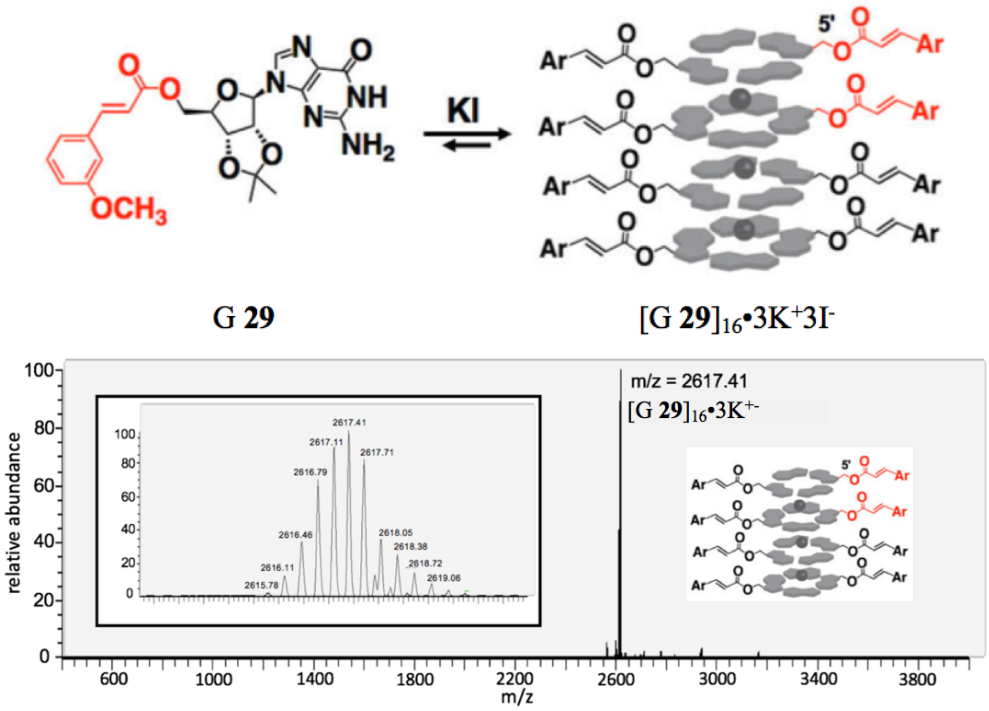

Figure 4.9. Top) Illustration of the self-assembly of [G **29**]$_{16}$•**3K^{+}3I^{-}**. Bottom) ESI mass spectrum of [G **29**]$_{16}$•3K^{+}3I^{-} (0.625 mM) in $CDCl_3$.

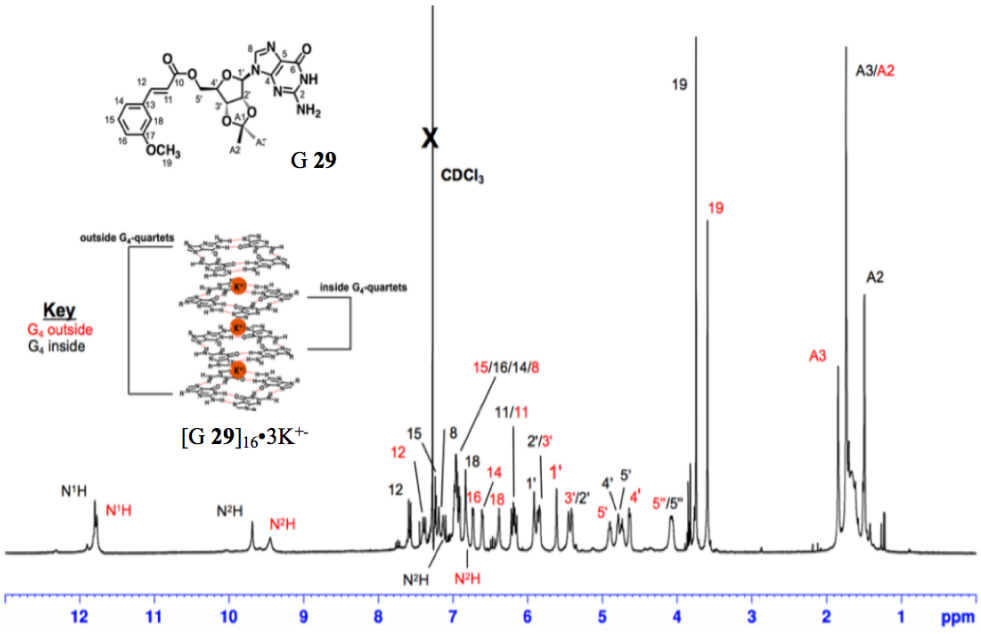

Figure 4.10. ^{1}H NMR spectrum of the self-assembly of G **29** (10 mM) in the presence of 1 eq. KI (10 mM) in $CDCl_3$ at 25 °C. Evidence for [G **29**]$_{16}$•3K^{+}3I^{-} formation is shown by the characteristic splitting of ^{1}H NMR signals into two sets of resonances that exist in a 1:1 ratio.

Nuclear Overhasuer effect spectroscopy was used to further characterize the G-quadruplex assemblies. Characteristic NOE signals between the 5′ protons and the exocyclic N^{2}H amino protons for the G$_{16}$-hexadecamer formation were observed (**Figure 4.11**). These signals provide evidence for interlayer H bonding interactions between the 5′-carbonyl of one G$_4$-quartet with the neighboring layers exocyclic N^{2}H amine protons, as was seen with the 5′-benzoyl G **21** derivative (refer to **Chapter 2**).[33] We also observed interlayer NOE interactions between the olefinic protons of one G$_4$-quartet layer with the adjacent quartet layer. This is significant because it is consistent

with close contacts between C=C bonds in the "outer" and "inner" G_4-quartets, which is required for the [2+2] photocycloaddition to occur (**Figure 4.12**).

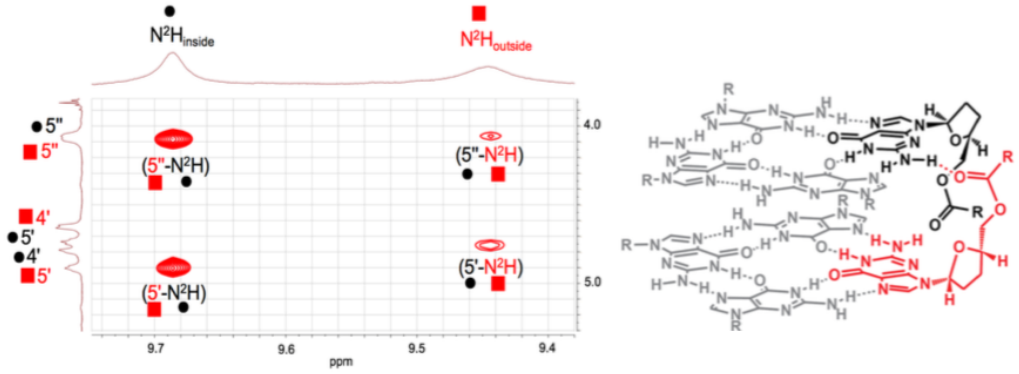

Figure 4.11. ^{1}H-^{1}H NOE spectrum highlighting the interlayer interactions between the 5′ protons and the exocyclic N^2H amino protons of [G **29**]$_{16}$•3K$^+$3I$^-$(0.625 mM in $CDCl_3$ at 25 °C). This result provides evidence for interlayer H bonding interactions between the 5′-carbonyl and the exocyclic amine.

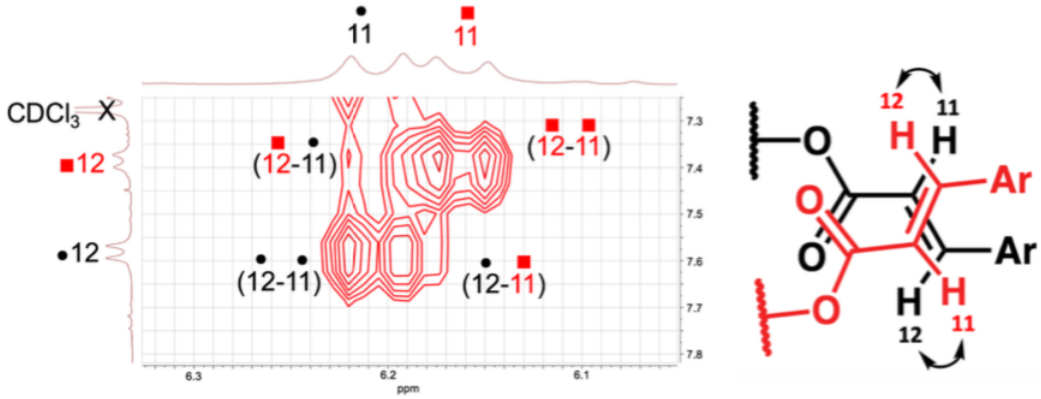

Figure 4.12. ^{1}H-^{1}H NOE spectrum highlighting the interlayer interactions between neighboring olefinic protons in [G **29**]$_{16}$•3K$^+$3I$^-$ (0.625 mM in $CDCl_3$ at 25 °C).

4.8 X-Ray Crystal Structure of $[G\ \mathbf{29}]_{16}\bullet 3K^{+}3I^{-}$

Crystals of $[G\ \mathbf{29}]_{16}\bullet 3K^{+}3I^{-}$ were grown by vapor diffusion of Et_2O into a vial containing $[G\ \mathbf{29}]_{16}\bullet 3K^{+}3I^{-}$ (0.625 mM in $CDCl_3$ at -6 ℃). After two weeks crystals had formed. X-ray diffraction of single crystals confirmed that 16 units of G **29** and 3 equivalents of KI form a D_4-symmetric hexadecamer. The G-quadruplex core and most 5′-cinnamate sidechains were well defined, whereas the aryl rings and some cinnamate sidechains were disordered. In terms of its H-bonded core, the solid-state structure of $[G\ \mathbf{29}]_{16}\bullet 3K^{+}3I^{-}$ is similar to other G-quadruplex structures.[33,41] Importantly, X-ray data revealed that 5′-ester carbonyls from one G_4-quartet form H-bonds with exocyclic amines (N^2H_B donor) projecting from neighboring G_4-quartets (**Figure 4.13**). These N^2H_B•••O=C interlayer H-bonds clamp together G_4-quartets in $[G\ \mathbf{29}]_{16}\bullet 3K^{+}3I^{-}$ so that C=C bonds from the "outer" layer stack on C=C bonds from the "inner" layer (**Figure 4.14A**). Thus, olefinic carbons at C1 of one layer and C1′ of the next layer are separated by just 3.3 Å (**Figure 4.14B**). This orientation of alkenes in $[G\ \mathbf{29}]_{16}\bullet 3K^{+}3I^{-}$ would predict formation of a symmetrical *syn* head-to-head dimer upon photoirradiation.

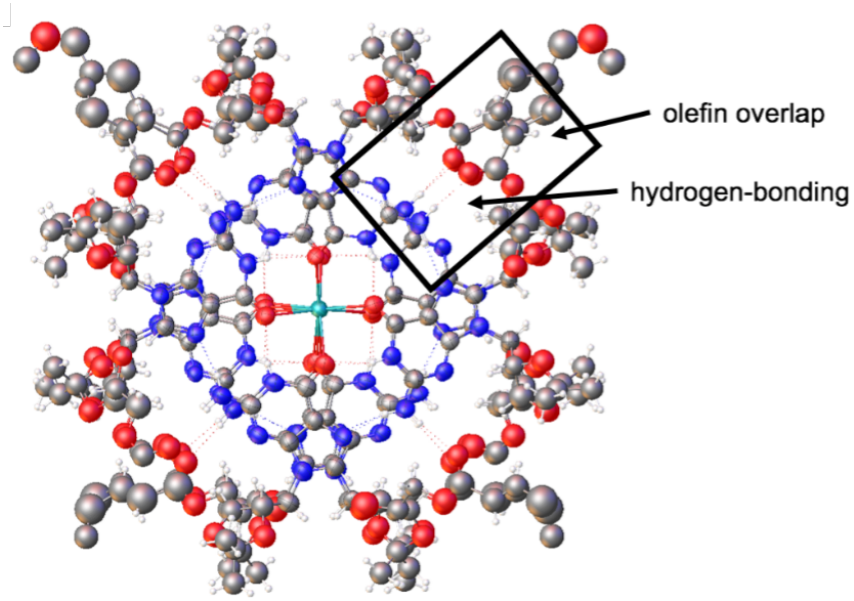

Figure 4.13. Top-view of X-ray crystal structure of [G **29**]$_{16}$•3K^{+}3I^{-}. The highlighted region shows the alignment of the olefins on the periphery of the structure in neighboring layers. This overlap is required for [2+2] cycloaddition to occur. In addition to the olefin overlap, there are hydrogen-bonding interaction between the 5′-carbonyl and exocyclic N^{2}H-amino protons that help to pre-organize the alkene groups for photochemistry.

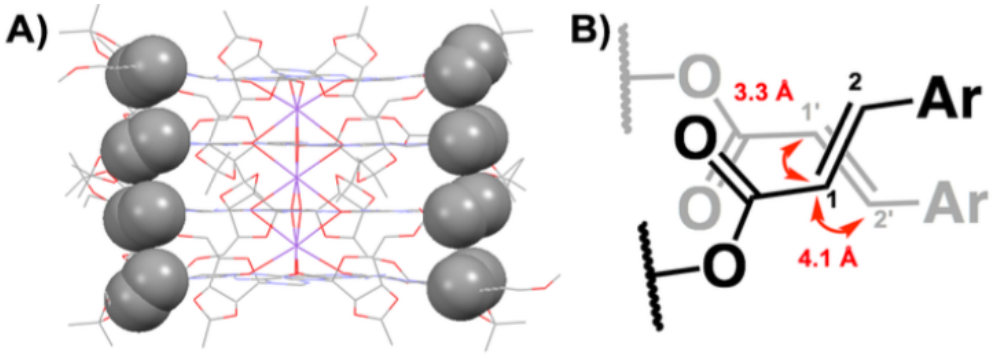

Figure 4.14. A) X-ray structure of [G **29**]$_{16}$•3K^{+}3I^{-}. View highlights stacked C=C bonds (space-filling. B) Illustration of stacked olefins. Formation of a σ-bond between C1 and C1′ (3.3 Å distance) upon photoirradiation leads to regioselective formation of β-truxinate **cbG 29**.

4.9 Computational Modeling of [G **29**]$_8$•K^+: A Simplified Model to Explain the Reactivity of [G **29**]$_{16}$•$3K^+3I^-$

Because the aryl rings and some C=C bonds were disordered in the X-ray structure of [G **29**]$_{16}$•$3K^+3I^-$, ONIOM (our own n-layered integrated molecular orbital and molecular mechanics) calculations were performed to fill in structural ambiguities.[122] Wes Lee used a hybrid density functional (WB97XD) in combination with a semi-empirical method (PM6),[123,124] to optimize the structure of a [G **29**]$_8$•K^+ fragment. The ONIOM (QM:MM) approach, combining the accuracy of DFT calculations with the lower computational cost of molecular mechanics, has been used to calculate geometry for a DNA G-quadruplex.[125,126]

Due to the many atoms in [G **29**]$_{16}$•$3K^+3I^-$, we computed structures for G_8•K^+ octamers that contain 2 (rather than 4) G_4-quartet layers. Since it is D_4-symmetric the 2 G_8•K^+ octamers that make up [G **29**]$_{16}$•$3K^+3I^-$ are identical, so we reasoned that analysis of an octamer would help better understand the structure of [G **29**]$_{16}$•$3K^+3I^-$. The computed model for octamer [G **29**]$_8$•K^+, which provided insights lacking from the X-ray structure, revealed that the 3-methoxy aryl rings do not π-stack. Other aspects of the calculated model agreed with the X-ray structure for [G **29**]$_{16}$•$3K^+3I^-$. First, interlayer H-bonds between 5′-ester carbonyls and exocyclic amino protons (N^2H_B donor) were similar. Second, the C=C bonds from the "outer" G_4-layer stack on C=C bonds from the "inner" G_4-layer with *s*-cis conformations in both crystal structure and calculated model.

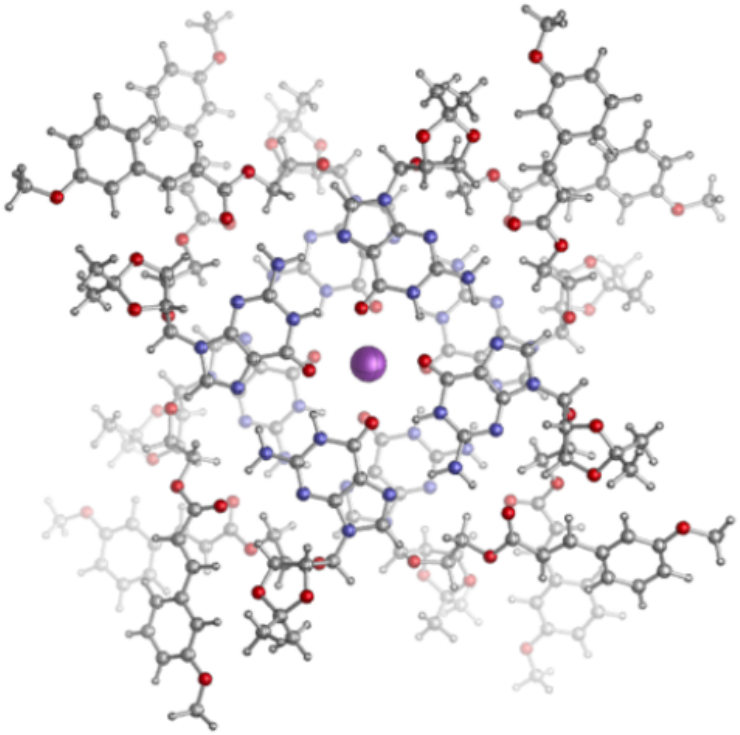

Figure 4.15. Energy minimized structure of [**G 29**]$_8$•K^+ using the ONIOM method. The calculated structure exhibits similar features to the X-ray crystal structure of [G **29**]$_{16}$•3K^+3I^-; showing interlayer H-bonding and alignment of peripheral olefins, as depicted in **Figure 4.13**.

4.10 Photocycloaddition of 5′-*meta*-Methoxycinnamoyl-2′, 3′-Isopropylidene Guanosine G 29

The photochemical reactivity of G **29** changed dramatically when KI was added to a solution of *trans*-G **29**, as a single cyclobutane stereoisomer **cbG 29** formed upon irradiation with 300 nm light. As described below, formation of β-truxinate **cbG 29**, which occurs via a net head-to-head and syn dimerization of stacked *trans* olefins, requires a templating K^+ cation. Irradiation of a 0.625 mM solution of [G **29**]$_{16}$•3K^+3I^-

in $CDCl_3$ (10 mM of **G 29**) resulted in a significant broadening of ^1H NMR signals, likely due to formation of mixed G-quadruplexes containing G **29** and cyclobutane **cbG 29**. This broadening made it difficult to monitor reaction progress by ^1H NMR in $CDCl_3$ (**Figure 4.16**).

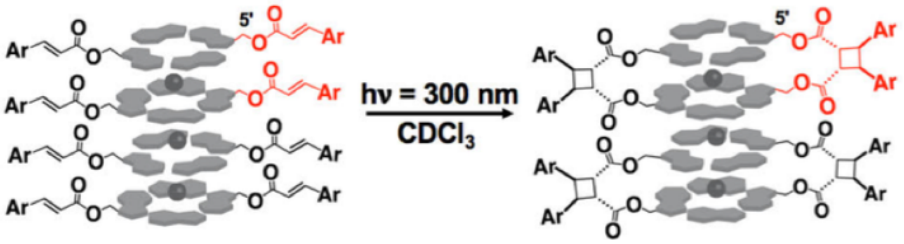

[G **29**]$_{16}$•3K$^+$3I$^-$ [cbG **29**]$_8$•3K$^+$3I$^-$

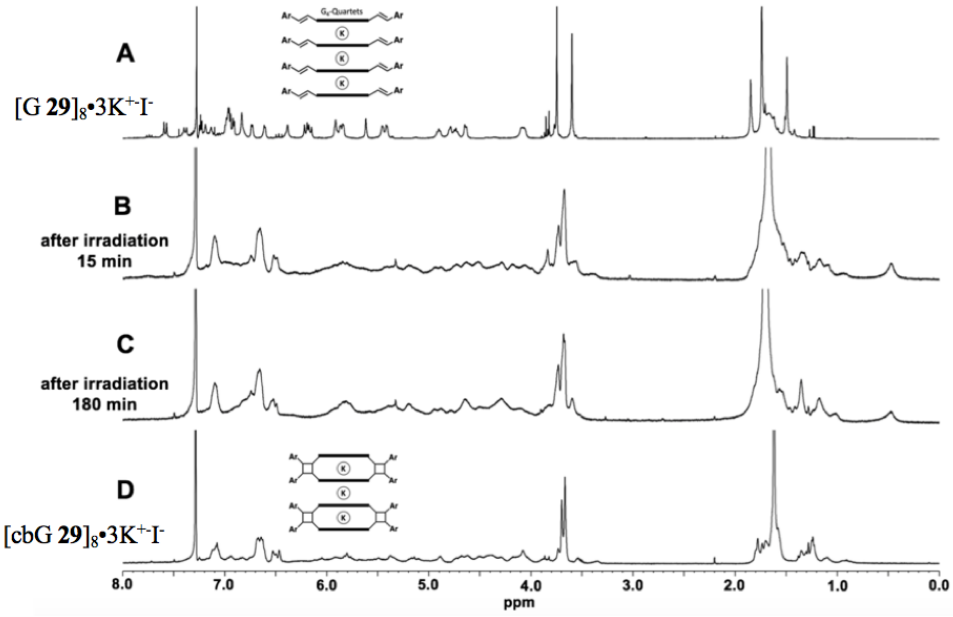

Figure 4.16. A) ^1H NMR spectrum of [G **29**]$_{16}$•3K$^+$3I$^-$ (0.625 mM) in $CDCl_3$. B) ^1H NMR spectrum of the reaction after 15 min photoirradiation of [G **29**]$_{16}$•3K$^+$3I$^-$ (0.625 mM) in $CDCl_3$. A broadening of signals is observed as assemblies containing statistical mixtures of *trans*-G **29**, *cis*-G **29**, and **cbG 29** form. C) ^1H NMR spectrum of the reaction mixture after 180 min of photoirradiation of [G **29**]$_{16}$•3K$^+$3I$^-$ (0.625 mM) in $CDCl_3$. D) ^1H NMR spectrum of a solution of 5 mM **cbG 29** in the presence of 10 mM KI in $CDCl_3$.

The [2+2] photoreaction was followed in $CDCl_3$ using CD spectroscopy, a chiral UV-vis absorbance technique that is a sensitive probe of helical structures, as well as other secondary and tertiary structures of bio-molecules.[127,128] **Figure 4.17** shows the transformation of the CD spectra for [G **29**]$_{16}$•3K$^+$3I$^-$ into a new CD signature upon irradiation. The starting [G **29**]$_{16}$•3K$^+$3I$^-$ has 2 intense positive bands, one at 260 nm for stacked G_4-quartets and one at 307 nm for cinnamate's π-bond, which clearly senses the core's helical chirality. Importantly, the spectrum of the photoproduct (t=180 min) did not show cinnamate's CD band at 307 nm, indicating that all C=C π bonds in [G **29**]$_{16}$•3K$^+$3I$^-$ reacted to produce a new G-quadruplex [**cbG 29**]$_8$•3K$^+$3I$^-$, with its own distinct CD signature being a negative exciton centered at 280 nm. ESI-MS of this new complex showed a major signal for a triply charged species at 2617.58 m/z, consistent with the structure of [**cbG 29**]$_8$•3K$^+$ (mw 7852.7) (**Figure 4.18**).

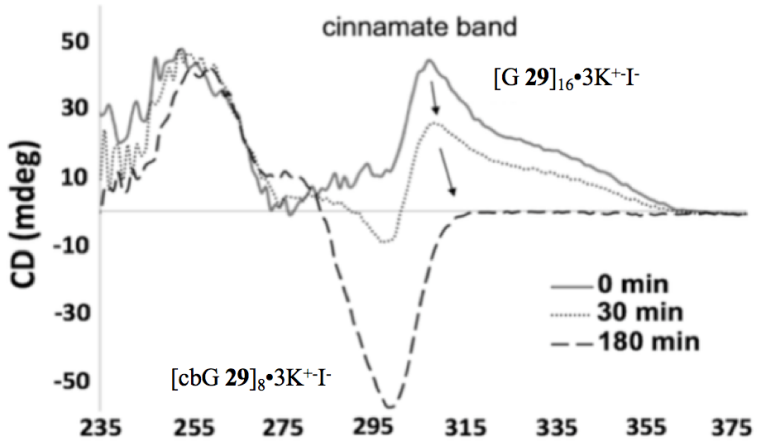

Figure 4.17. Circular dichroism spectra monitoring the reaction progress of the photocycloaddition of a solution of [G **29**]$_{16}$•3K^{+}3I^{-} (0.625 mM) in $CDCl_3$. Reaction aliquots were taken and diluted to a final concentration of 12.5 μM in $CDCl_3$ at 25 °C. An induced CD signal is present at 307 nm for the conjugated olefin of *trans*-G **29**. The induced signal is undetectable after 180 min. As the reaction progresses the olefin undergoes [2+2] photocycloaddition resulting in loss of the CD signal for [G **29**]$_{16}$•3K^{+}3I^{-} and formation of a new signal for [**cbG 29**]$_8$•3K^{+}3I^{-}.

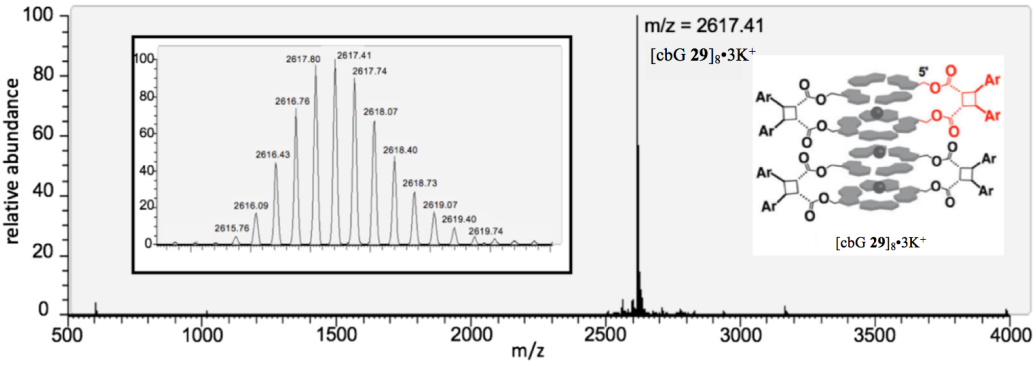

Figure 4.18. ESI mass spectrum of [**cbG 29**]$_8$•3K^{+}3I^{-} (0.625 mM) showing a triply-charged species at 2617.41 m/z corresponding to a molecular weight equal to 7852.23 g mol^{-1}.

To follow the real-time photocycloaddition of [G **29**]$_{16}$•3K^{+}3I^{-} in $CDCl_3$ by ^{1}H NMR, aliquots were removed, $CDCl_3$ was evaporated and the residue dissolved in DMSO-d_6, a solvent that breaks up H-bonded assemblies. Chemical shifts of cinnamate's *meta*-OCH_3 distinguished competing reactions, isomerization of *trans*-G

29 to *cis*-G **29** and [2+2] cycloaddition to give cyclobutanes. **Figure 4.19** shows that after 1 h most of *trans* cinnamate G **29** had been converted into a new compound that was not *cis* isomer G **29**. After 6 h, photoreaction was complete, with formation of greater than 92% of β-truxinate cyclobutane **cbG 29**, a compound whose structure we characterized by ^{1}H NMR and ^{13}C NMR and mass spectrometry. We confirmed the identity of photoproduct **cbG 29** by converting it to the known dimethyl ester β-trux **47** (**Figure 4.20**).[103]

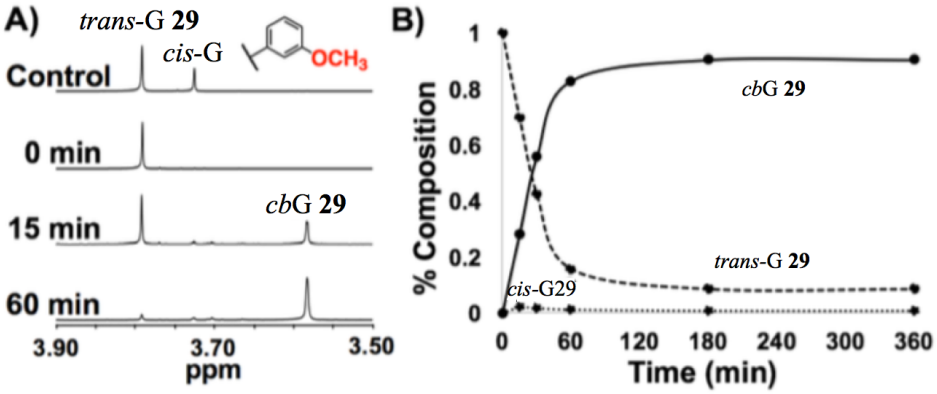

Figure 4.19. A) ^{1}H NMR spectra of the *meta* –OCH_3 protons during irradiation of [G **29**]$_{16}$•3K^{+}3I^{-}. The top spectrum is a control experiment performed in DMSO-d$_6$ showing that irradiation of monomeric *trans*-G **29** gives only *cis*-G **29**. Irradiation of [G **29**]$_{16}$•3K^{+}3I^{-} leads to cyclobutane **cbG 29**. B) Graph showing production of cyclobutane **cbG 29** upon photoirradiation of [G **29**]$_{16}$•3K^{+}3I^{-}.

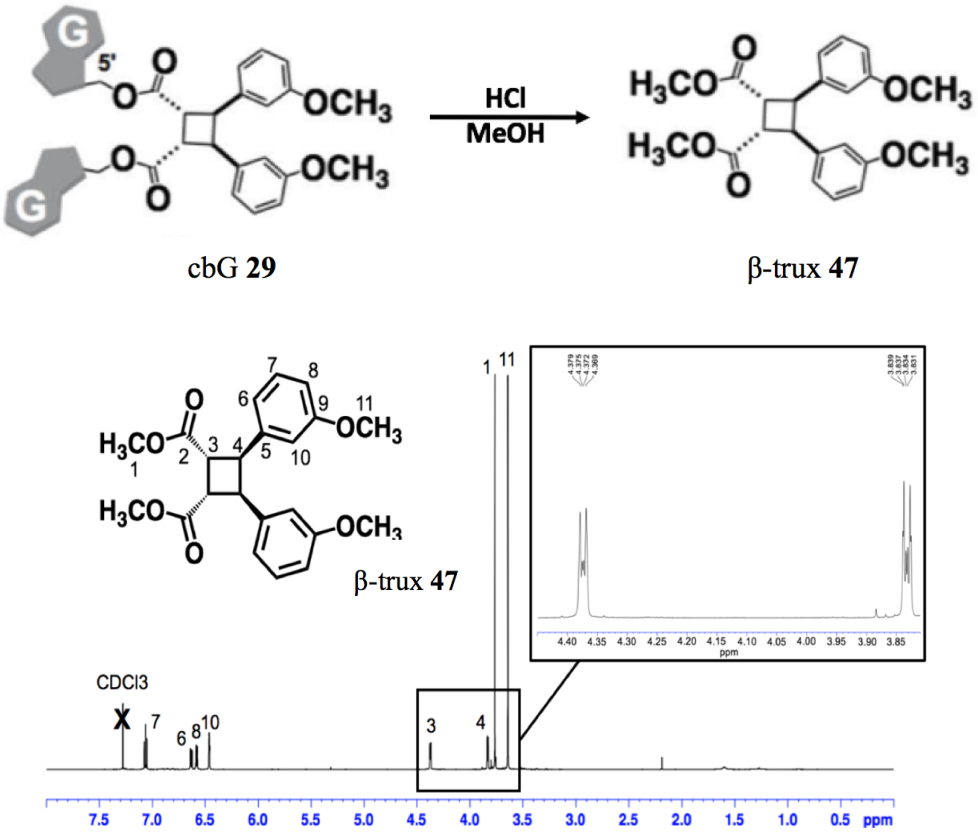

Figure 4.20. ^{1}H NMR spectrum of β-truxinate methyl ester β-trux **47** in $CDCl_3$.

4.11 Photocycloaddition of 5′-*meta*-Methoxycinnamoyl-2′, 3′-Isopropylidene Guanosine G 29 Using the Sun as a Light Source

With an eye towards a greener approach we decided to perform the photocycloaddition reaction using the sun as the UV light source. Cycloaddition templated by [**G 29**]$_{16}$•3K^{+}3I^{-} (0.625 mM in 1 mL $CDCl_3$) gave a high yield (> 90%) of cyclobutane **cbG 29** when performed in sunlight (**Figure 4.21**). The reaction was performed on May 3rd, 2018 in College Park, on a sunny day with a UV index of

approximately 8. The reaction was carried out on the roof of a nearby building in a location unimpeded by shade (shown in the photograph in **Figure 4.21A**). The reaction was monitored by ^{1}H NMR at 0 min, 30 min, 60 min, 180 min, and 360 min. The reaction was complete by 360 min.

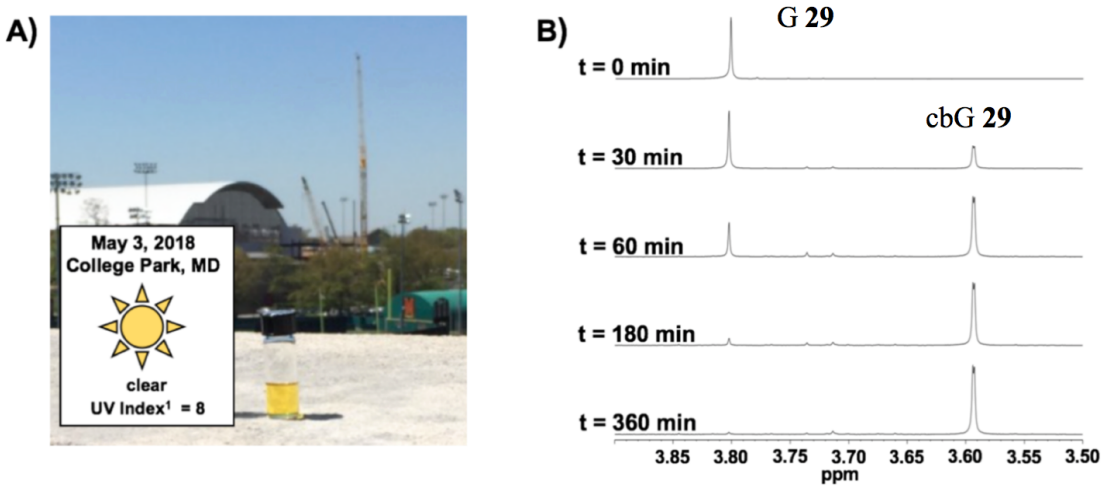

Figure 4.21. A) Photograph showing the [2+2] photocycloaddition carried out in sunlight. The vial contains [G **29**]$_{16}$•3K^{+}3I^{-} (10 mM in CDCl3) to **cbG 29**. The photoreaction took place at the University of Maryland, College Park, MD on May 3rd, 2018. The weather for the day was clear with a predicted UV index of 8 for the Washington D.C. region. The irradiation took place from 11:00 AM to 5:00 PM. B) A series of ^{1}H NMR spectra monitoring the photocycloaddition of [G **29**]$_{16}$•3K+3I- to **cbG 29**. Due to signal broadening in CDCl3 aliquots of the reaction mixture were taken out, the solvent was evaporated, and the sample was re-dissolved in DMSO-d_6 to take ^{1}H NMR.

4.12 Mechanistic Study of the [G 29]$_{16}$•3K^{+}3I^{-} Promoted [2+2] Photocycloaddition Reaction using Computational Methods

To 1) understand the selective formation of cyclobutane **cbG 29** and 2) compare relative stabilities of assemblies containing cinnamate G **29** and cyclobutane G **29** we

carried out high-level computations with the ONIOM method ((M06-2X/6-31+G(d,p):B3LYP/6-31G(d)-in $CHCl_3$ (CPCM)//WB97XD-6-31G(d):PM6). **Figure 4.22** shows energetics of self-assembly intermediates on a path leading to cyclobutane **cbG 29**. The lowest energy complex ($\mathbf{A}_{cis:cis}$) adopts an *s-cis* conformation about each 5′-cinnamate. If concerted photodimerization of pre-organized C=C olefins, which adopt a crisscross orientation, were to occur from this G $\mathbf{A}_{cis:cis}$ complex it would predict formation of a 1,3-disubstituted cyclobutane. Experimentally, only β-truxinate **cbG 29**, a *cis*-1,2-diester, is formed upon irradiation of $[G\ \mathbf{29}]_{16}\bullet 3K^{+}3I^{-}$. Concerted formation of β-truxinate **cbG 29** requires one of the reacting esters to adopt an s-*trans* conformation. Structure $\mathbf{A}_{trans:cis}$, where 1 of 4 pairs of alkenes stacks in a parallel orientation, had a relative energy just 0.1 kcal mol^{-1} above G $\mathbf{A}_{cis:cis}$. From the G $\mathbf{29}_{trans:cis}$ intermediate, photocycloaddition leads to formation of $\mathbf{A}_{1,2\text{-}syn}$, an intermediate with a relative energy of +3.0 kcal. Release of β-truxinate **cbG 29** from $\mathbf{A}_{1,2\text{-}syn}$ and incorporation of 2 equiv. of *trans*-G **29** would regenerate the G $\mathbf{A}_{cis:cis}$ complex. If stacked olefins were to react directly out of the lowest-energy conformation ($\mathbf{A}_{cis:cis}$) to form $\mathbf{A}_{1,2\text{-}syn}$, it would suggest a step-wise mechanism where initial σ-bond formation occurs between C1 and C1′ to give a biradical. Subsequent σ-bond rotation and coupling of the 2 benzyl radicals (C2 and C2′) would form the cyclobutane in G-quadruplex $\mathbf{A}_{1,2\text{-}syn}$. Alternatively, as pictured in **Figure 4.22**, one 5′-cinnamate sidechain could adopt a conformation that aligns reactive C=C π bonds so that they are oriented face-to-face ($\mathbf{A}_{trans:cis}$). This G $\mathbf{A}_{trans:cis}$ species could undergo a concerted cycloaddition to give $\mathbf{A}_{1,2\text{-}syn}$. Regardless of the mechanism, either concerted or stepwise, the consequence of pre-organization of

5′-cinnamate esters in the G-quadruplex is a highly regio- and stereoselective [2+2] photocycloaddition.

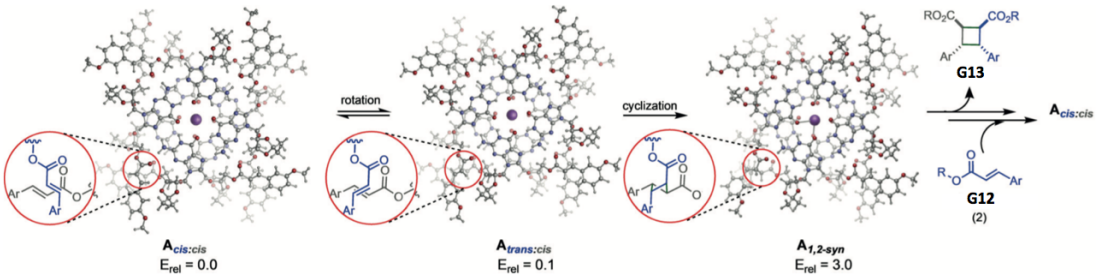

Figure 4.22. A proposed pathway for [2+2] photocycloaddition of trans 1 to give β-truxinate **cbG 29**, as templated by the G-quadruplex. Using the ONIOM method, optimized structures and energies were calculated for a series of $G_8 \cdot K+$ octamers. This particular pathway involves bond rotation of a cinnamate ester in G $\mathbf{A}_{cis:cis}$ to give G $\mathbf{A}_{trans:cis}$, which undergoes concerted [2+2] photocycloaddition, to give cyclobutane-containing $\mathbf{A}_{1,2\text{-}syn}$. Exchange of *trans*-G **29** with β-truxinate **cbG 29** in $\mathbf{A}_{1,2\text{-}syn}$ would make this process catalytic. Figure generated by Wes Lee and Dr.Osvaldo Gutierrez.

Energy calculations were performed on [**cbG 29**]$_4$•K^+ an analogous structure for the G-quadruplex of [**cbG 29**]$_8$•$3K^+$, the G-quadruplex formed by the [2+2] photocycloaddition product. Computations suggest that formation of 4 cyclobutane rings significantly destabilized this [**cbG 29**]$_4$•K^+ assembly relative to [G **29**]$_8$•K^+. This thermodynamic destabilization indicated to us that this system might be catalytic. We hypothesized that catalytic turnover might take place in the G-quadruplex. The cyclobutane G-quadruplex showed a distorted G_4-quartet that might lead to easier disassembly of the G-quadruplex and incorporation of new monomeric G **29** units to reform the reactive [G **29**]$_{16}$•$3K^+3I^-$ complex (**Figure 4.23**).

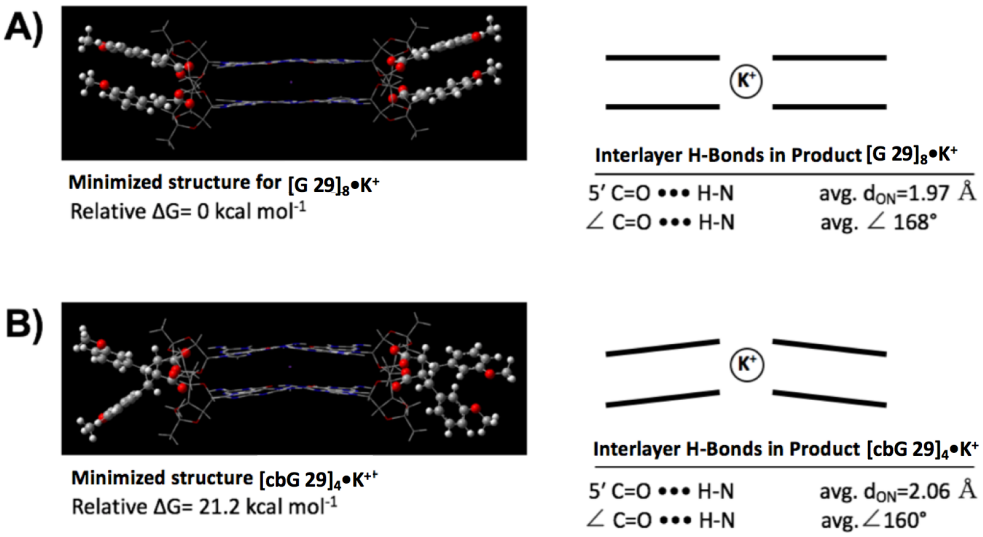

Figure 4.23. A) Minimized energy structure for [G **29**]$_8$•K^+. The G_4-quartets are planar. B) Minimized energy structures for [**cbG 29**]$_4$•K^+. The G_4-quartets are distorted out of the plane. The relative free energy of 21.2 kcal mol^{-1} indicates that cyclobutane **cbG 29** formation destabilizes the assembly.

4.13 Catalytic Turnover of the [G 29]$_{16}$•3K^+3I^- Templated [2+2] Photocycloaddition

Since computations indicated that **G29** cyclobutane formation destabilizes the G-quadruplex, we reasoned that the system could be catalytic in K^+ if cinnamate G **29** in solution were to expel cyclobutane **cbG 29** from the assembly (**Figure 4.24**). We tested for catalysis by monitoring [2+2] cycloaddition of *trans*-G **29** to **cbG 29** under conditions with insufficient K^+ to fully complex *trans*-G **29** (**Figure 4.25** and **Figure 4.26**). We conducted these reactions on a relatively large scale (194 mg of **G 29** in 40 mL of $CHCl_3$), so that a) ratios of G **29** (mw 483.4) and KI (mw 166) could be determined by weight and b) we could demonstrate the synthetic utility of this process.

The figure shows that photocycloaddition is sensitive to K^+ concentration. Addition of excess K^+ (1:1 KI to G **29**) gave a relatively fast cycloaddition (>90% yield of **cbG 29** after 6 h). The [2+2] cycloaddition was slower, but still gave high yields of **cbG 29**, for a sample with a 1:64 ratio of KI to G **29**. Initially, the reaction mixture was heterogeneous, but became clear as insoluble G **29** was converted into soluble **cbG 29.** The reaction with a 1:64 ratio of KI to G **29** gave ~90% yield of product, indicating that the photocycloaddition is catalytic in K^+.

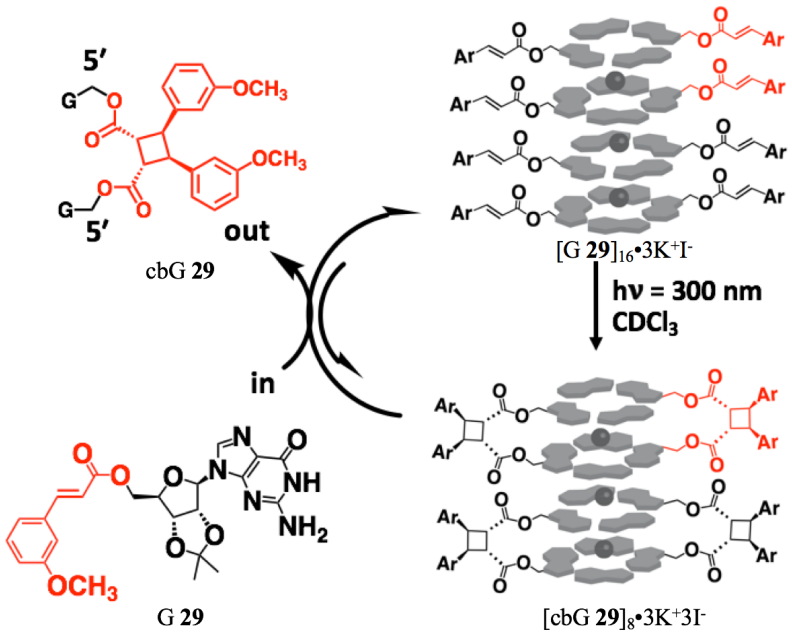

Figure 4.24. Illustration showing the proposed [2+2] photocycloaddition catalytic turnover templated by $[G\ \mathbf{29}]_{16}\bullet 3K^+3I^-$. In the presence of K^+, G **29** self-assembles into $[G\ \mathbf{29}]_{16}\bullet 3K^+3I^-$. Irradiation of $[G\ \mathbf{29}]_{16}\bullet 3K^+3I^-$ results in the formation of cbG **29**$^-$. The final step in the turnover is the departure of cbG **29** from the G-quadruplex and re-insertion of G **29**.

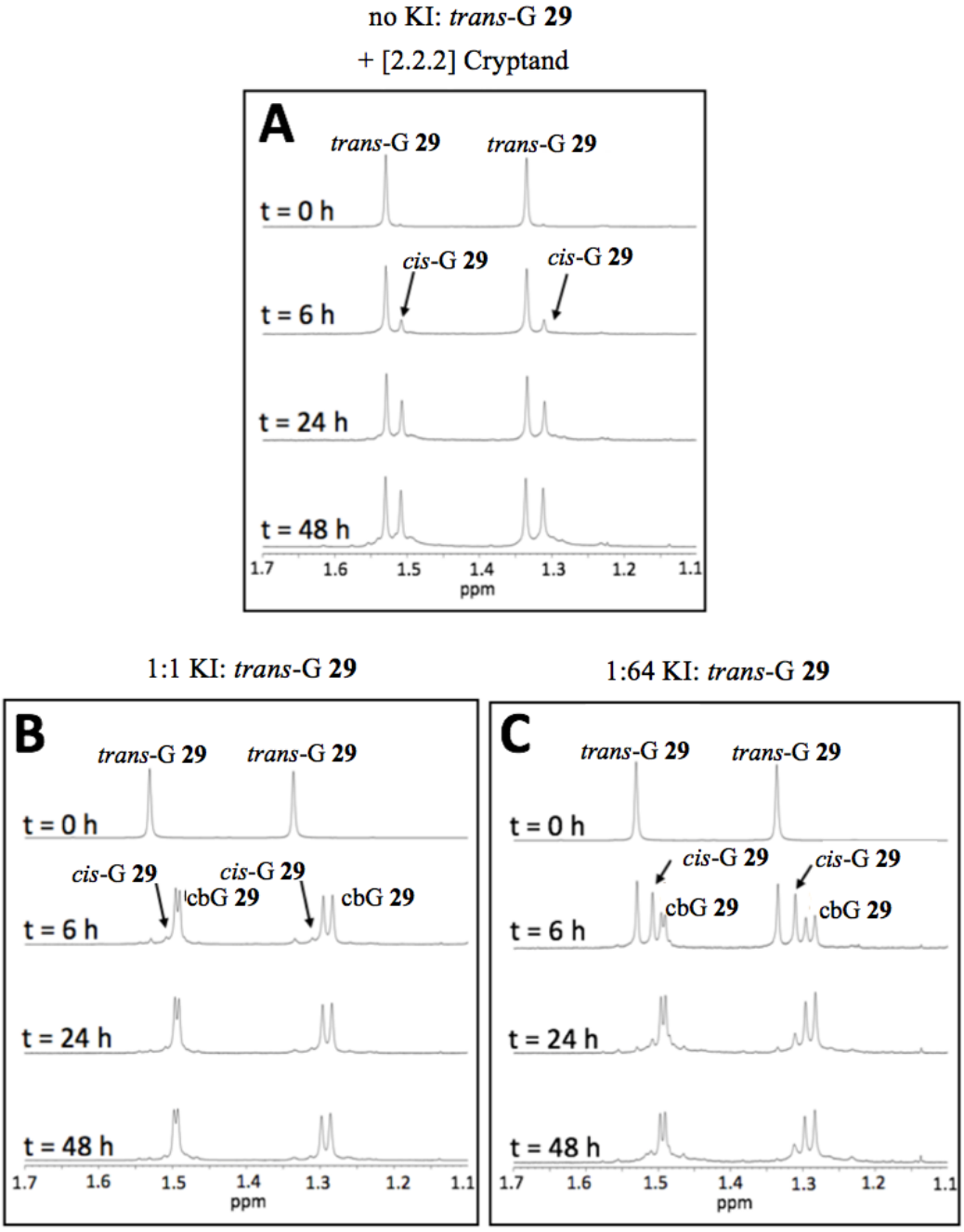

Figure 4.25. A series of ^{1}H NMR spectra monitoring the acetonide protons for the [2+2] photocycloaddition of *trans*-G **29** to diguanosyl β-truxinate **cbG 29** in the presence of varying stoichiometric amounts of KI. To monitor the reaction progress aliquots were taken from the reaction mixtures, solvent evaporated, and redissolved in DMSO-d_6 at t=0 h, 6 h, 24 h, and 48 h.

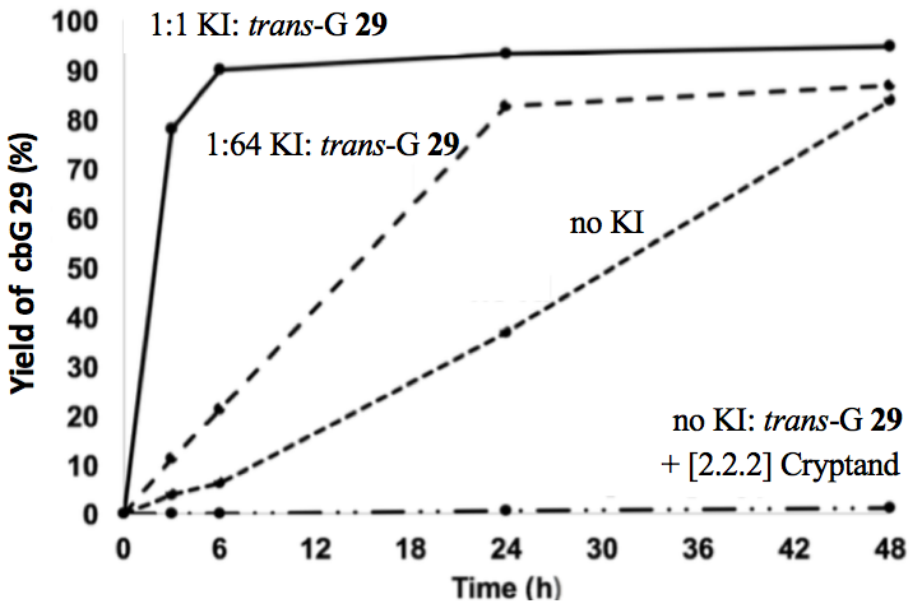

Figure 4.26. Graph showing production of **cbG 29** as a function of irradiation time. Reactions were performed by continuous irradiation (hν=300 nm) of samples containing G **29** (193.6 mg, 10 mM) in 40 mL of $CDCl_3$ with various amounts of KI. The control experiment contained [2.2.2] cryptand (140 mM) to sequester and adventitious cations. Aliquots were removed at different times, the solvent was evaporated, and the residue was dissolved in DMSO-d_6 for subsequent NMR analysis.

We were perplexed by a control experiment wherein cycloaddition of cinnamate G **29** to give **cbG 29** occurred even when no KI was added (**Figure 4.26**). We suspected that production of **cbG 29** under these conditions was due to the ability of G **29** to scavenge adventitious Na^+ or K^+ from solvent or glassware to form photo-reactive G-quadruplex [G **29**]$_{16}$•3M^+. Our hypothesis was supported by comparing elemental analyses of freshly prepared G **29** with material subjected to the sample preparation protocol used prior to irradiation, a process that involves 1) suspending G **29** in $CDCl_3$, 2) sonication and 3) overnight stirring in $CDCl_3$. Elemental analysis of purified G **29** indicated a Na^+:G **29** ratio of 1:157 and a K^+:G **29** ratio of 1:820, as

shown in the **Table 4.1**. The concentration of these cations increased after the sample preparation protocol, showing a Na^+: G **29** ratio of 1:55 and a K^+: G **29** ratio of 1:431. Our hypothesis that adventitious cations template formation of reactive G-quadruplexes was supported by an experiment wherein excess [2.2.2]-cryptand (140 mM) was added to a suspension of G **29** (10 mM) in $CDCl_3$. Photoirradiation of that sample for 48 h showed no formation of cyclobutane **cbG 29**. Overall, this data (**Table 4.1**) allows us to conclude that the [2+2] photocycloaddition of cinnamate G **29** is catalytic with regard to K^+. An individual cation enables multiple turnovers of guanosine 5′-cinnamate G **29** to give high yields of diguanosylcyclobutane **cbG 29**.

Sample	Molar Ratios			Ratio of K^+ and Na^+ Ions: *trans*-G 29		
	K^+	Na^+	G 29	K^+:G 29	Na^+:G 29	Total K^+ & Na^+:G 29
No Manipulation	1	5.2	820.1	1:820	1:158	1:132
Manipulated	1	7.8	431.2	1:431	1:55	1:49

Table 4.1. Table summarizing elemental analysis results for trans G **29** before and after sample manipulation. The purified trans G **29** sample contained trace amounts of Na^+ and K^+ , most likely introduced through general handling of materials. The manipulated sample had increased amounts of Na^+ and K^+, most likely introduced from the solvent and glassware used for the photoreactions.

4.14 Conclusion

We have demonstrated that the self-assembled G-quadruplex enables regio- and stereoselective formation of cyclobutanes, in dilute solution, by organizing 5′-

cinnamate esters for [2+2] photocycloaddition. The templating K^+ cation is required for photocycloaddition; without K^+ cinnamate ester G **29** undergoes only *trans-cis* isomerization upon photo-irradiation. Because of the pre-organization of 5′-cinnamate side-chains in the G-quadruple, cyclobutane **cbG 29** is produced in high yields (> 90%) and with excellent regio- and diastereoselectivity (one product formed). Importantly, this photocycloaddition is catalytic in K^+, since reactants and products can readily exchange between solution and G-quadruplex assembly.

4.15 Closing Remarks

The G-quadruplex is a unique system. The guanosine monomer is easily modified allowing for the incorporation of new functionality to the assembly. My work has focused on the study of G-quadruplexes assemblies with alterations made to the 5′-position of guanosine. There is still much more work to be done to fully elucidate how other synthetic alterations impact the self-assembly of the G-quadruplex. With an increased understanding of structure and stability of the G-quadruplex, new assemblies can be built with intriguing new properties and functionalities.

I have explored using the G-quadruplexes to promote spatially restricted [2+2] cycloaddition reactions. There is still a lot of room to advance this work and translate this method to other reactions. G4-DNA G-quadruplexes have been shown to catalyze stereoselective Michael-additions, Diels-Alder reactions, and oxidation reactions. There is not much literature on reactive lipophilic G-quadruplexes, making this a

potentially lucrative area for novel research. Other photochemical cycloadditions could be explored, such as the synthesis of ladderanes. Organocatalytic groups, such as proline, could be tethered to the G-quadruplex to promote stereocontrolled aldol reactions. Metal chelating groups could be added to the G-quadruplex to use the chiral microenvironment of the assembly to promote stereocontrolled reactions. It is an exciting area of research and I look forward to clever advancements made in this field.

Chapter 5. Experimental and References

5.1 General Experimental

General Information: UV-vis experiments were performed on a Cary 100 Bio UV-vis spectrometer at 25 °C in a 1 cm path-length quartz cuvette. CD experiments were performed on a Jasco J-810 spectropolarimeter at 25 °C. All CD experiments were performed using a 100-mm quartz cuvette purchased from Hellma Analytics. ^{1}H NMR was performed using a Bruker AV-III 600 MHz instrument. ^{13}C NMR was performed using a Bruker DRX-500 MHz instrument. ^{19}F NMR was performed using a Bruker AV-400 MHz instrument. Deuterated solvents were purchased from Cambridge Isotopes Lab. ESI-MS experiments were performed on a JEOL AccuTOF-CS Spectrometer or ThermoFisher Orbitrap Fusion Lumos Tribrid spectrometer. Computational models were made using Gaussian09 and computations were performed using the Deepthought2-HOC super computer at the University of Maryland. Photochemical reactions were performed in a Southern New England Ultraviolet Company Rayonet RMR-600 Photochemical Reactor light box using 300 nm bulbs (a total of 8 bulbs) from S.N.E. Ultraviolet Co. Elemental analysis samples were ran by Galbraith Laboratories. Chemicals and solvents were purchased from Acros, Sigma-Aldrich, Alfa Aesar, Fisher, Santa Cruz Biotechnology or Carbosynth and used without further purification.

5.2 Experimental Procedures for Chapter 2-Controlling the Molecularity and Stability of H-Bonded G-Quadruplexes by Modulating the Structure's Periphery

5.2.1 Synthesis of Compounds in Chapter 2

5′-(Benzoyl)-2′,3′-Isopropylidene Guanosine G 21: To a suspension of 2′,3′-isopropylidene guanosine (1.00 g, 3.1 mmol). DMAP (20 mg), and trimethylamine (0.86 mL, 6.2 mmol) in CH_3CN (38 mL) was added benzoyl chloride (0.53 mL, 4.6 mmol). The mixture was stirred for 16 h, after which TLC analysis (9:1 CH_2Cl_2:MeOH) indicated that the reaction was complete. The reaction mixture was concentrated *in vacuo* to give a white solid. The resulting solid was triturated with MeOH, filtered and vacuum dried to give G **21** as a white powder (0.462 g, 35%).

^{1}H NMR (400 MHz, DMSO-d_6) δ: 10.75 (s, 1H, N^{1}H), 7.94-7.91 (m, 2H, H11), 7.85 (s, 1H, H8), 7.69-7.64 (t, J=7.4 Hz, 1H, H13), 7.52 (dd, J=7.6 Hz, 2H, H12), 6.58 (s, 2H, N^{2}H), 6.06 (d, J=1.9 Hz, 1H, H1′), 5.33-5.26 (m, 2H, H3′ and H2′), 4.55 (dd, J= 3.0, 10.2 Hz, 1H, H5′), 4.44-4.37 (m, 2H, H5′′ and H4′), 1.54 (s, 3H, HA2/HA3), 1.35 (s, 3H, HA2/HA3); ^{13}C NMR (125 MHz, DMSO d_6 δ: 165.85 (C9), 157.10 (C6), 154.13 (C2), 150.89 (C4), 136.54 (C8), 133.88 (C13), 129.74 (C10), 129.66 (C11), 129.16 (C12), 117.45 (C1A), 113.83 (C5), 88.83 (C1′), 84.63 (C4′), 84.18 (C2′), 81.52 (C3′), 65.09 (C5′), 27.46 and 25.89 (CA2 and CA3) ESI-MS ($M+H^+$): 428.16.

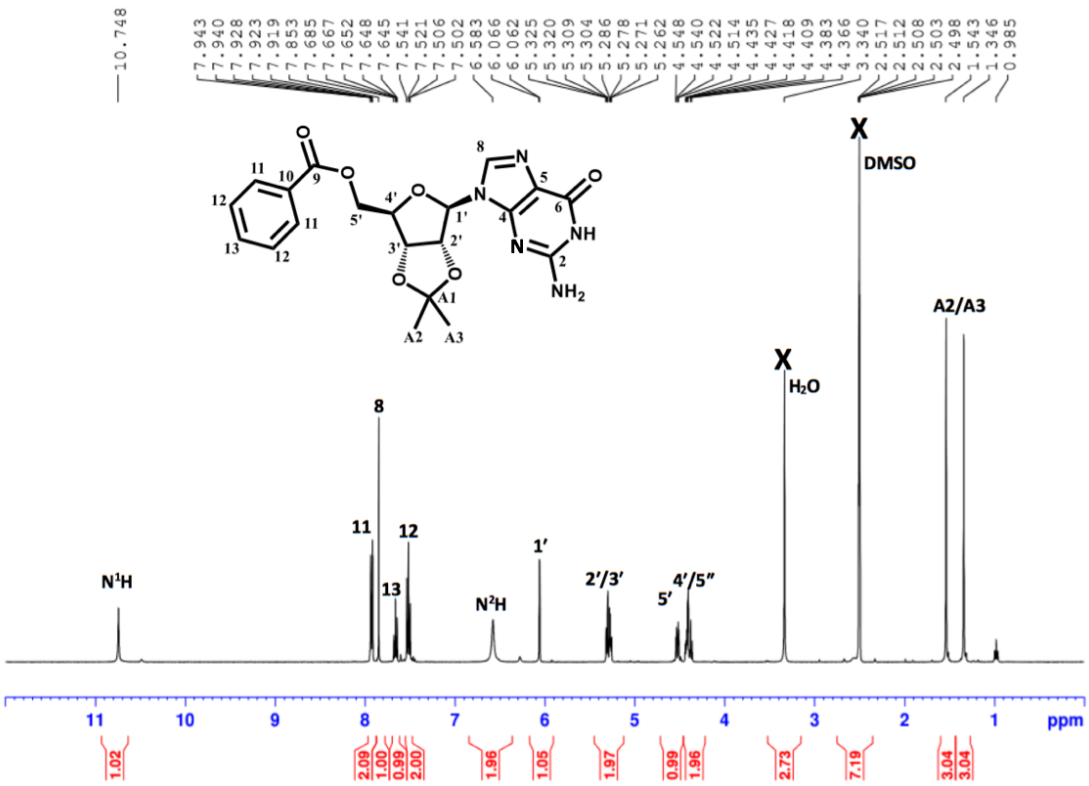

Figure 5.1. ^{1}H NMR of 5′-benzoyl-2′,3′-isopropylidene guanosine G **21** in DMSO-d_6.

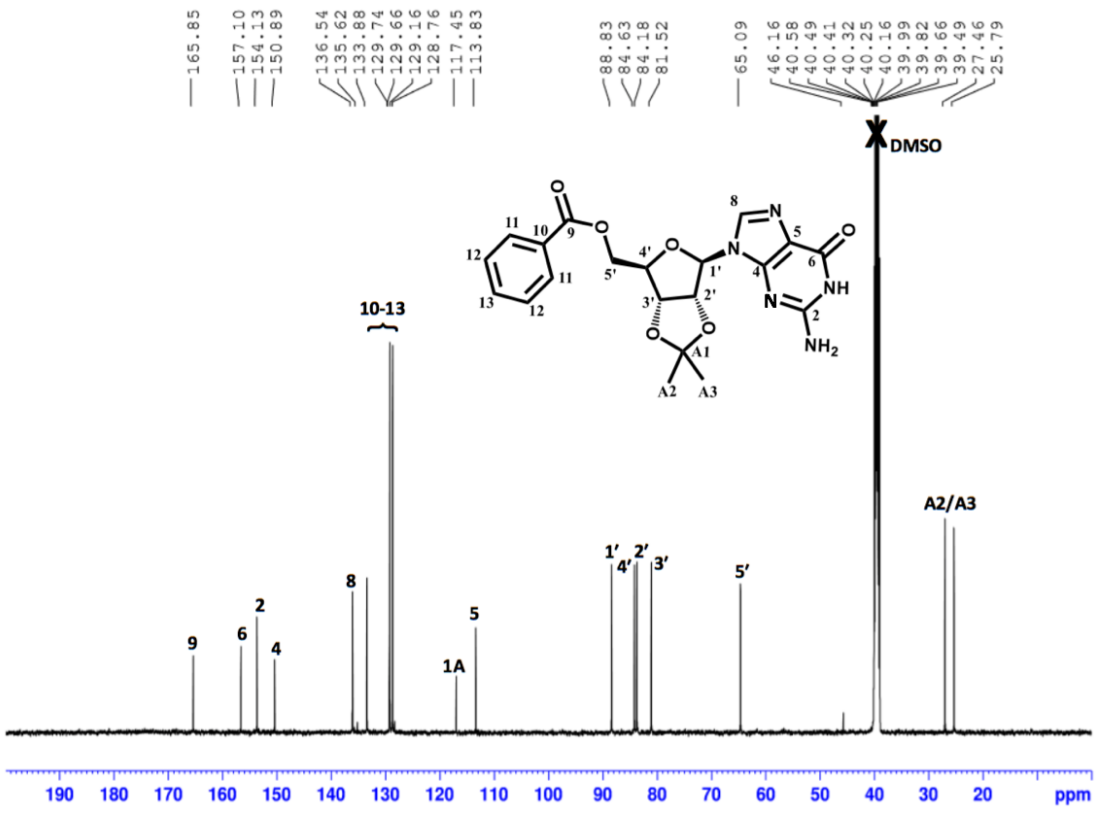

Figure 5.2. ^{13}C NMR of 5′-benzoyl-2′,3′-isopropylidene guanosine G **21** in DMSO-d_6.

5′-(4-Nitrobenzoyl)-2′,3′-Isopropylidene Guanosine G 22: To a suspension of 2′,3′-isopropylidene guanosine (0.50 g, 1.55 mmol), DMAP (15 mg), and triethylamine (0.65 mL, 4.6 mmol) in CH_3CN (18 mL) was added 4-nitrobenzoyl chloride (0.575 g, 3.1 mmol). The reaction mixture stirred for 4 h, after which time tlc analysis (9:1 CH_2Cl_2: MeOH) indicated the reaction was complete. The reaction mixture was concentrated *in vacuo* to give a white solid. Column chromatography on silica gel (95:5 CH_2Cl_2:MeOH) gave G **22** as a white solid. The solid was washed with water and vacuum dried to give G **22** as a white powder (0.209 g, 28.4%).

^{1}H NMR (400 MHz, DMSO-d_6) δ:10.72 (s, 1H, N_1H), 8.34-8.31 (m, 2H, H11 or H12), 8.16-8.13 (m, 2H, H11 or H12), 7.85 (s, 1H, H8), 6.5 (s, 2H, N^2H), 6.07 (d, J=1.4 Hz, 1H, H1′), 5.32 (m, 2H, H2′ and H3′), 4.61-4.60 (dd, J=5.4 Hz, 9.4 Hz, 1H, H5′), 4.46-4.44 (m, 2H, H5′′ and H4′), 1.55 (s, 3H, HA2 or HA3), 1.35 (s, HA2 or HA3) ^{13}C NMR (125 MHZ, DMSO-D_6) δ: 164.41 (C9), 157.06 (C6), 154.09 (C2), 150.84 (C4), 150.73 (C13), 136.64 (C8), 135.18 (C10), 131.14 (C12), 124.22 (C1), 117.50 (CA1), 113.82 (C5), 88.90 (C1′), 84.57 (C4′), 84.15 (C2′), 81.40 (C3′), 65.77 (C5′), 27.47 and 25.82 (CA2 and CA3) ESI-MS: ($M+H^+$)= 473.14.

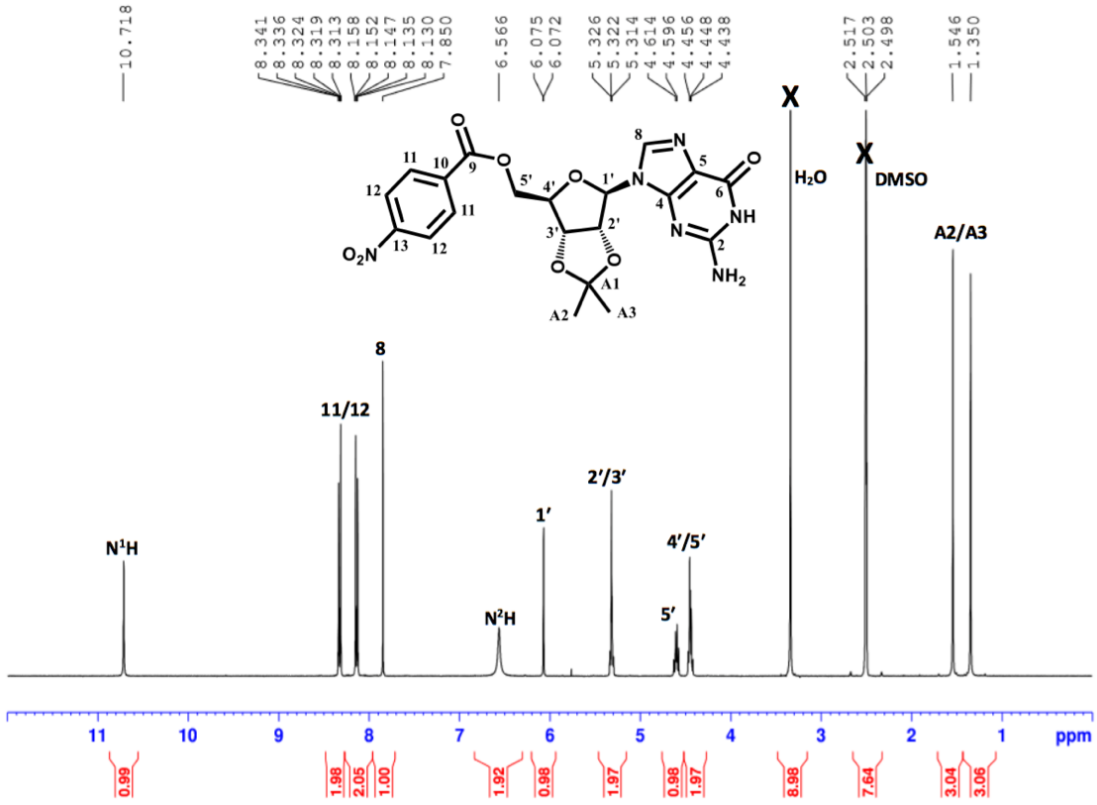

Figure 5.3. ^{1}H NMR of 5′-*para*-nitrobenzoyl-2′,3′-isopropylidene guanosine G **22** in DMSO-d_6.

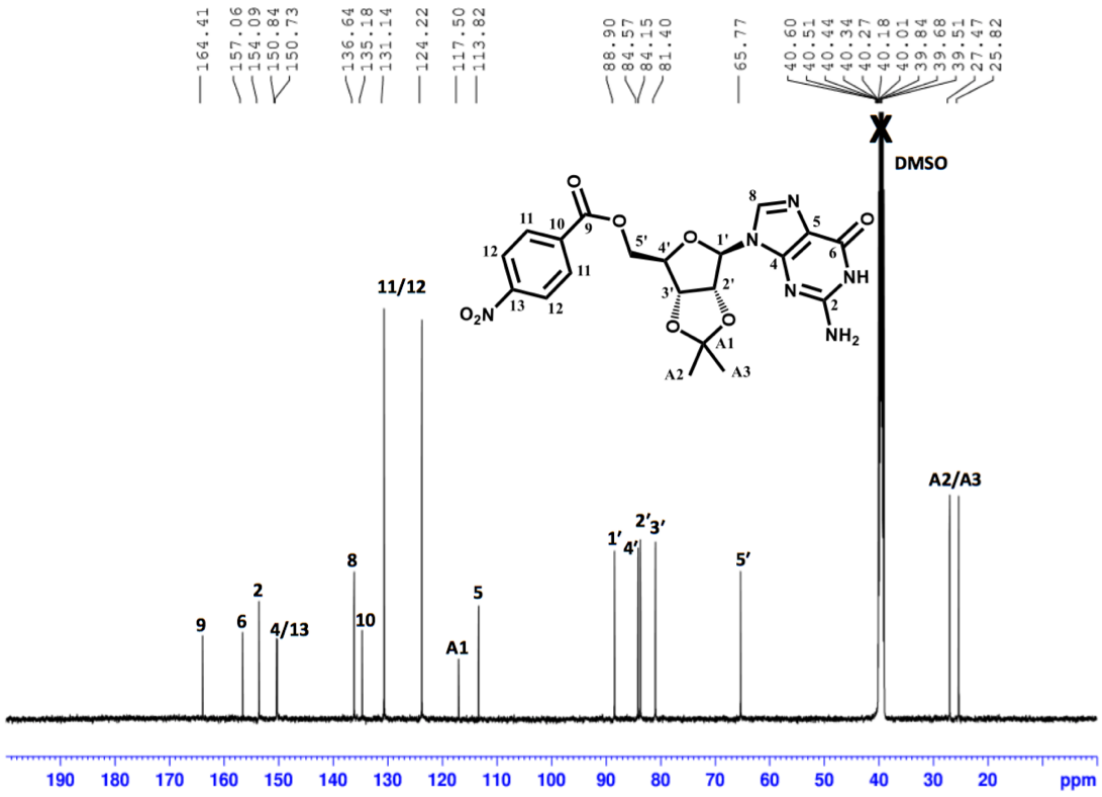

Figure 5.4. ^{13}C NMR of 5′-*para*-nitrobenzoyl-2′,3′-isopropylidene guanosine G **22** in DMSO-d_6.

5′-(4-Methoxybenzoyl)-2′,3′-Isopropylidene Guanosine G 23: To a suspension of 2′,3′-isopropylidene guanosine (1.00 g, 3.1 mmol), DMAP (27 mg), and trimethylamine (1.94 mL, 13.9 mmol) in CH_3CN (18 mL) was added 4-methoxybenzoyl chloride (1.05 mL, 7.7 mmol). The mixture was stirred for 4 h, after which tlc analysis (9:1 CH_2Cl_2:MeOH) indicated the reaction was complete. The reaction mixture was concentrated *in vacuo* to give a white solid. The resulting solid

was triturated with MeOH, filtered and vacuum dried to give G **23** as a white powder (0.532 g, 37.5%)

^{1}H NMR (400 MHz, DMSO-d_6) δ: 10.72 (s, 1H, N^{1}H), 7.88-7.86 (d, J=8.9 Hz, 2H, H11 or H12), 7.84 (s, 1H, H8), 7.04-7.01 (d, J=8.9 Hz, 2H, H11 or H12), 6.56 (s, 2H, N^{2}H$_2$), 6.04 (d, J=2 Hz, 1H, H1′), 5.31-5.29 (dd, J=2.0, 6.3 Hz, 1H, H2′), 5.24 (dd, J=3.6, 6.3 Hz, 1H, H3′), 4.50 (dd, J=4.1 , 11.1 Hz, 1H, H5′), 4.40-4.31 (dt, J=3.7, 7.5 Hz, 1H, H4′), 4.33 (dd, J=6.6, 11.1 Hz, 1H, H5′′), 3.83 (s, 3H, H14), 1.53 (s, 3H, HA2), 1.34 (s, 3H, HA3) ^{13}C NMR (125 MHz, DMSO-d_6) δ: 165.51 (C9), 163.70 (C13), 157.09 (C6), 154.12 (C2), 150.91 (C4), 136.50 (C8), 131.80 (C11), 120.98 (C10), 117.45 (CA1), 114.44 (C12), 113.83 (C5), 88.82 (C1′), 84.65 (C4′), 84.15 (C2′), 81.52 (C3′), 64.76 (C5′), 55.95 (C14), 27.46 and 25.79 (CA2 and CA3) ESI MS: (M+H^{+})=458.17.

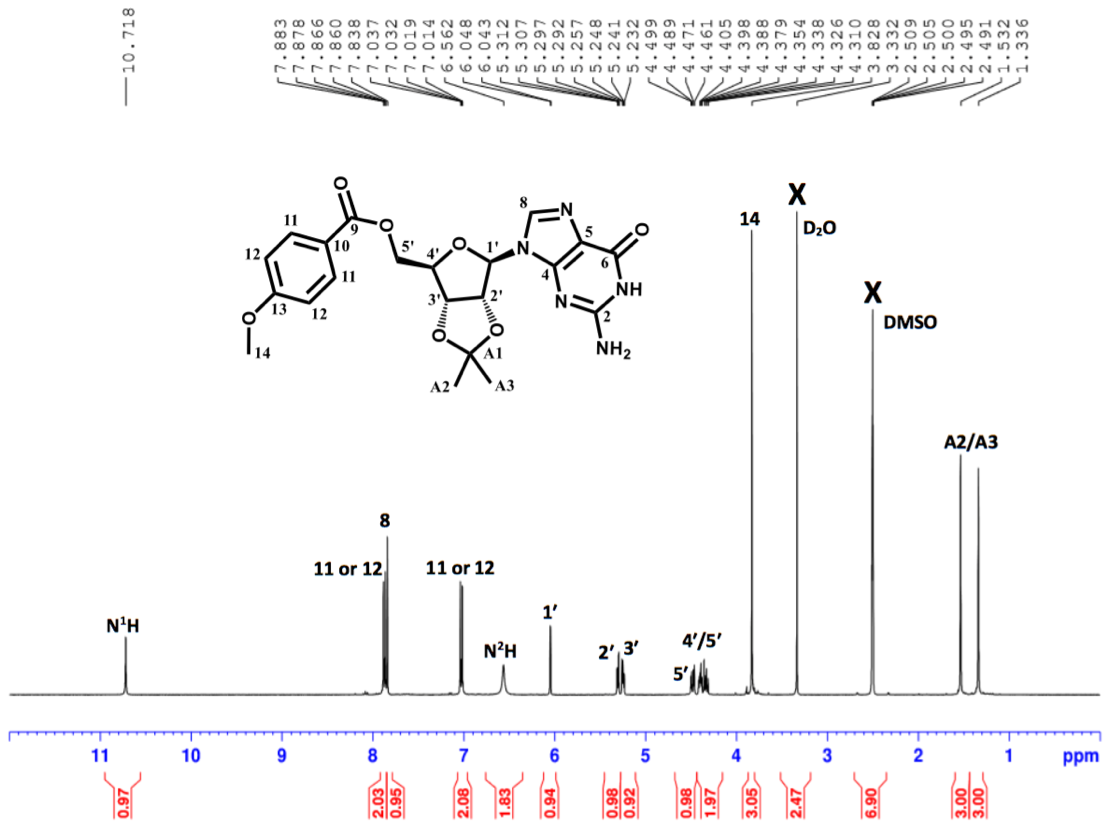

Figure 5.5. ^{1}H NMR of 5′-*para*-methoxybenzoyl-2′,3′-isopropylidene guanosine G **23** in DMSO-d_6.

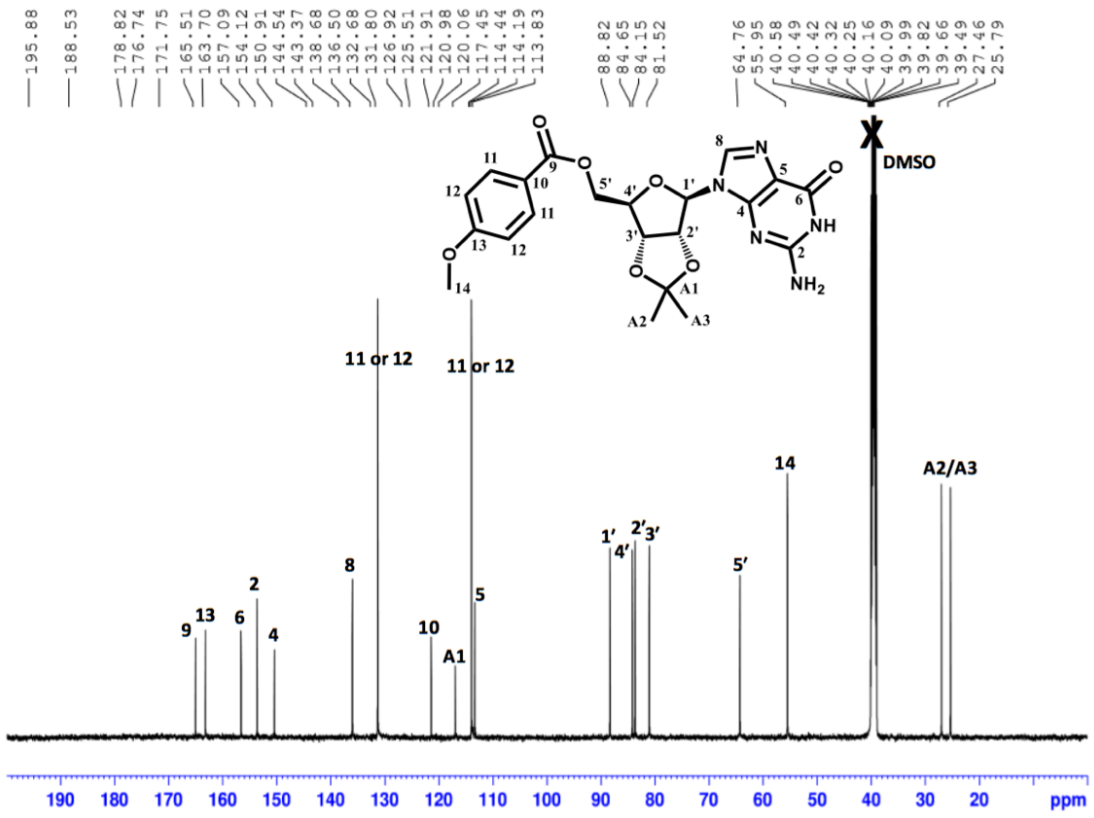

Figure 5.6. ^{13}C NMR of 5′-*para*-methoxybenzoyl-2′,3′-isopropylidene guanosine G **32** in DMSO-d_6.

5′-(2-Naphthoyl)-2′,3′-Isopropylidene Guanosine G24: To a suspension of 2′, 3′-isopropylidene guanosine (0.50 g, 1.5 mmol), DMAP (20 mg), and triethylamine (0.97 mL, 6.9 mmol) in CH_3CN (18 mL) was added 2-naphthoyl chloride (0.59 g, 3.1 mmol). The reaction mixture was allowed to stir for 4 h, after which time tlc analysis (9:1 CH_2Cl_2:MeOH) indicated the reaction was complete. The product G **24** precipitated out of the action mixture as a white powder and was collected by vacuum filtration. The precipitate was washed with water and vacuum dried to give G **24 a**s a white powder (0.217 g, 29.5%).

^{1}H NMR (400 MHz, DMSO-d_6) δ:10.73 (s, 1H, N^{1}H), 8.58 (t, J=1.0 Hz, 1H), 8.13-8.11 (m, 1H), 8.04 (t, J=7.8 Hz, 2H), 7.96 (dd, J=1.7, 8.6 Hz, 1H), 7.88 (s, 1H, H8), 7.70-7.60 (m, 2H), 6.58 (s, 2H, N^{2}H$_2$), 6.09 (d, J=1.1 Hz, 1H, H1′), 5.31 (m, 2H, H2′ and H3′), 4.62 (dd, J=7.7 Hz, 7.8 Hz, 1H, H5′), 4.48-4.45 (m, 2H, H4′ and H5′′), 1.55 (s, 3H, HA2 or HA3), 1.35 (s, 3H, HA2 or HA3); ^{13}C NMR (125 MHz, DMSO-d_6) δ: 166.0 (C9), 157.10 (C6), 154.15 (C2), 150.91 (C4), 136.54, 135.54, 132.45, 131.09, 129.78, 129.10, 128.82, 128.12, 127.42, 127.05, 125.22, 117.48 (CA1), 113.85 (C5), 88.89 (C1′), 84.82 (C4′), 84.29 (C2′), 81.56 (C3′), 65.39 (C5′), 27.48 and 25.81(CA2 and CA3).

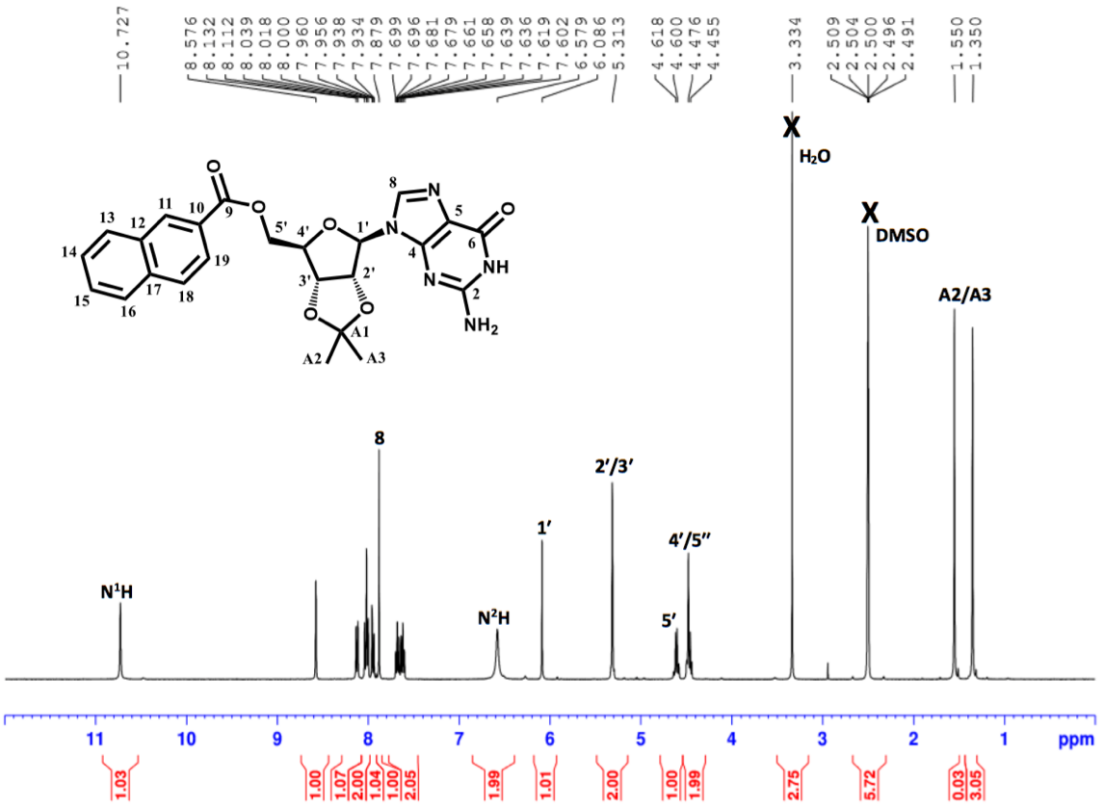

Figure 5.7. ^{1}H NMR of 5′-(2-naphthoyl)-2′,3′-isopropylidene guanosine G **24** in DMSO-d_6

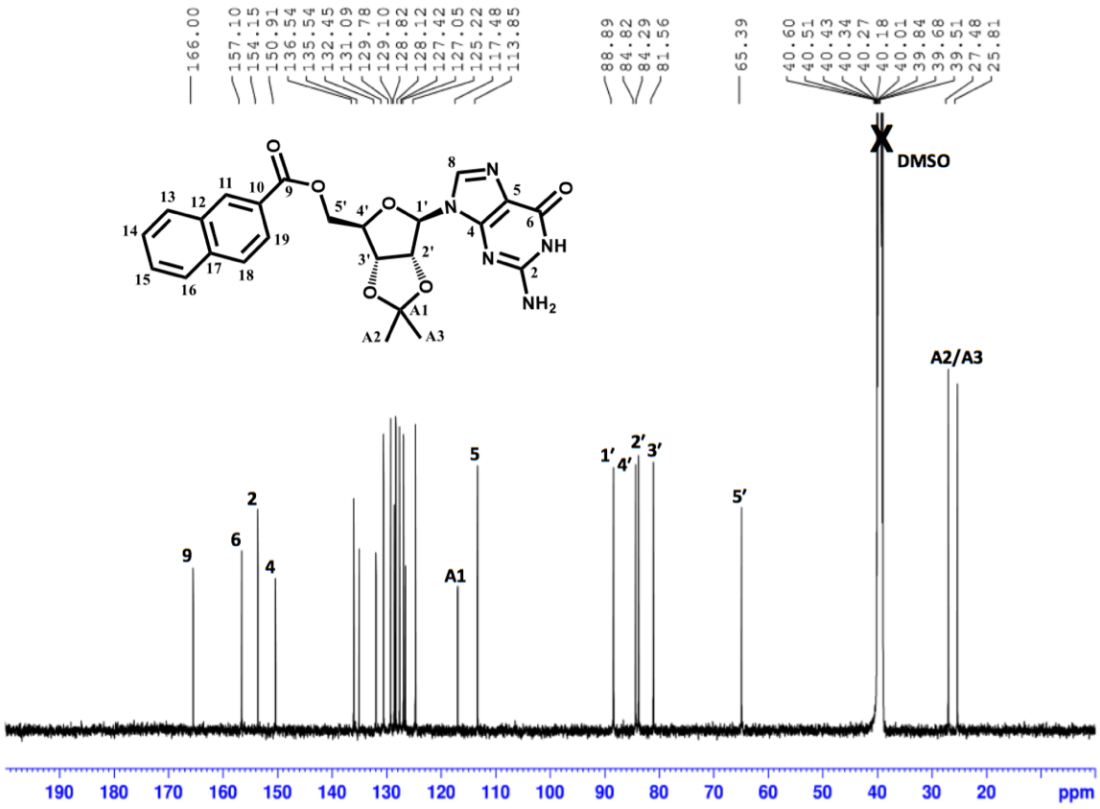

Figure 5.8. ^{13}C NMR of 5′-(2-naphthoyl)-2′,3′-isopropylidene guanosine G **24** in DMSO-d_6.

5′-(2,3,4,5,6)Pentafluorobenzyol-2′, 3′-Isopropylidene Guanosine G 25: To a suspension of 2′, 3′-isopropylidene guanosine (0.51 g, 1.55 mmol), DMAP (15 mg), and trimethylamine (0.43 mL, 3.0 mmol) in CH_3CN (18 mL) was added (2,3,4,5,6)-pentafluorobenzoyl chloride (0.33 mL, 2.3 mmol). The reaction mixture was allowed

to stir for 2 h, after which time tlc analysis (9:1 CH_2Cl_2:MeOH) indicated the reaction was complete. The reaction mixture was concentrated *in vacuo* to give a yellow solid. Column chromatography on silica gel (95:5 CH_2Cl_2:MeOH) gave G **25** as a white solid. The solid was washed with water and vacuum dried to give G **25** as a white powder (0.236 g, 29.5%).

^{1}H NMR (400 MHz, DMSO-d_6) δ: 10.69 (s, 1H, N^{1}H), 7.80(s, 1H, H8), 6.51 (s, 2H, N^{2}H), 6.04 (d, J=1.6 Hz, 1H, H1′), 5.30 (dd, 1.6, 6.1 Hz, 1H, H2′), 5.22(dd, 3.6, 6.1 Hz, 1H, H3′) 4.62 (dd, 3.9,11.8 Hz, 1H, H5′), 4.48(dd, 6.6, 11.9 Hz, 1H, H5′′), 4.39 (m, 1H, H4′) ; ^{13}C NMR (125 MHz, DMSO-d_6) δ: 158.06 (C9), 156.56 (C6), 153.53 (C2), 150.29(C4), 145.93(C11), 143.82(C13), 138.30(C12), 136.08(C8), 116.93(A1), 113.22(C5), 106.93(C10), 88.67(C1′), 84.06(C4′), 83.62(C2′), 80.93(C3′), 66.12(C5′), 26.92 and 25.26(CA2 and CA3); ^{19}F NMR (376 MHz, DMSO-d_6) δ: -138.95 (m, 2F, F11), -148.73 (tt, 1F, F13), -161.09 (m, 2F, F12) ; ESI MS: ($M+H^+$)=518.01.

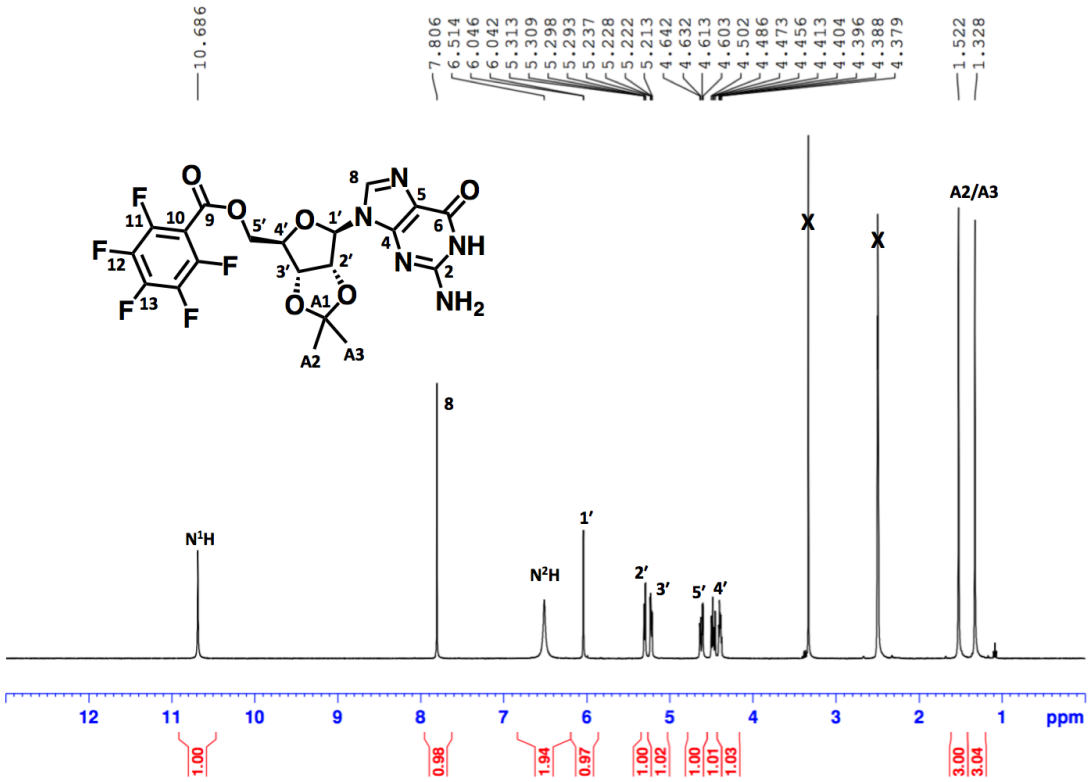

Figure 5.9. ^{1}H NMR of 5′-(2,3,4,5,6)-pentafluorobenzoyl-2′,3′-isopropylidene guanosine G **25** in DMSO-d_6.

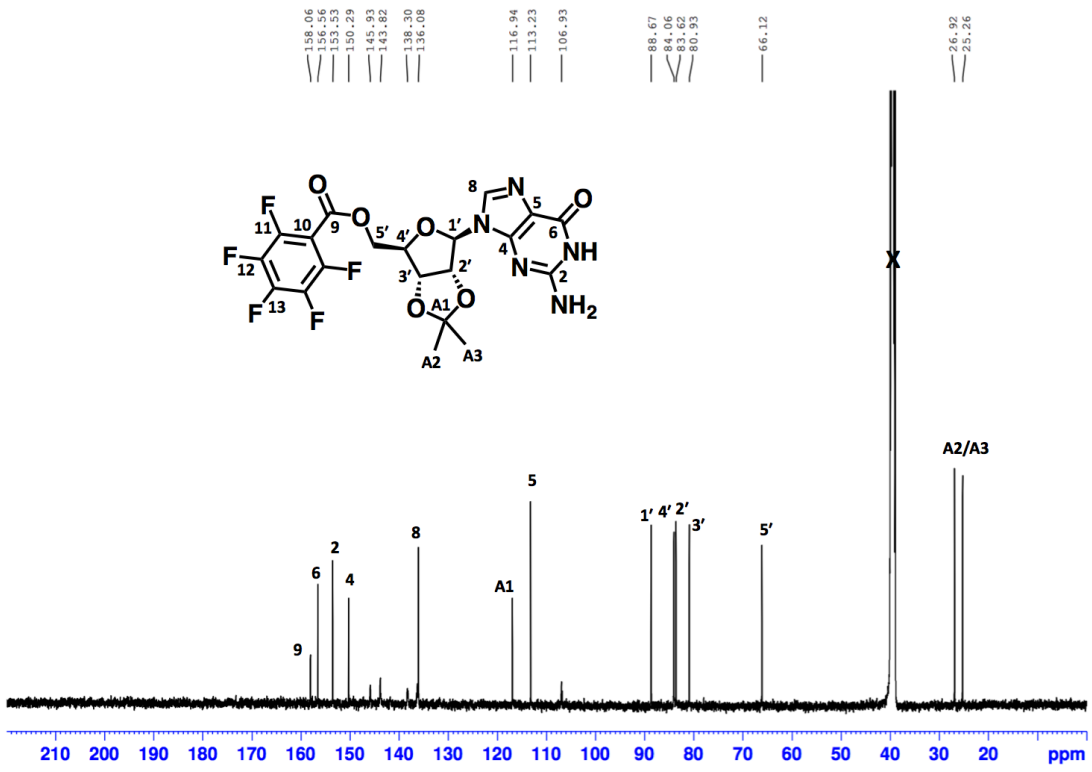

Figure 5.10. ^{13}C NMR of 5′-(2,3,4,5,6)-pentafluorobenzoyl-2′,3′-isopropylidene guanosine G **25** in DMSO-d_6.

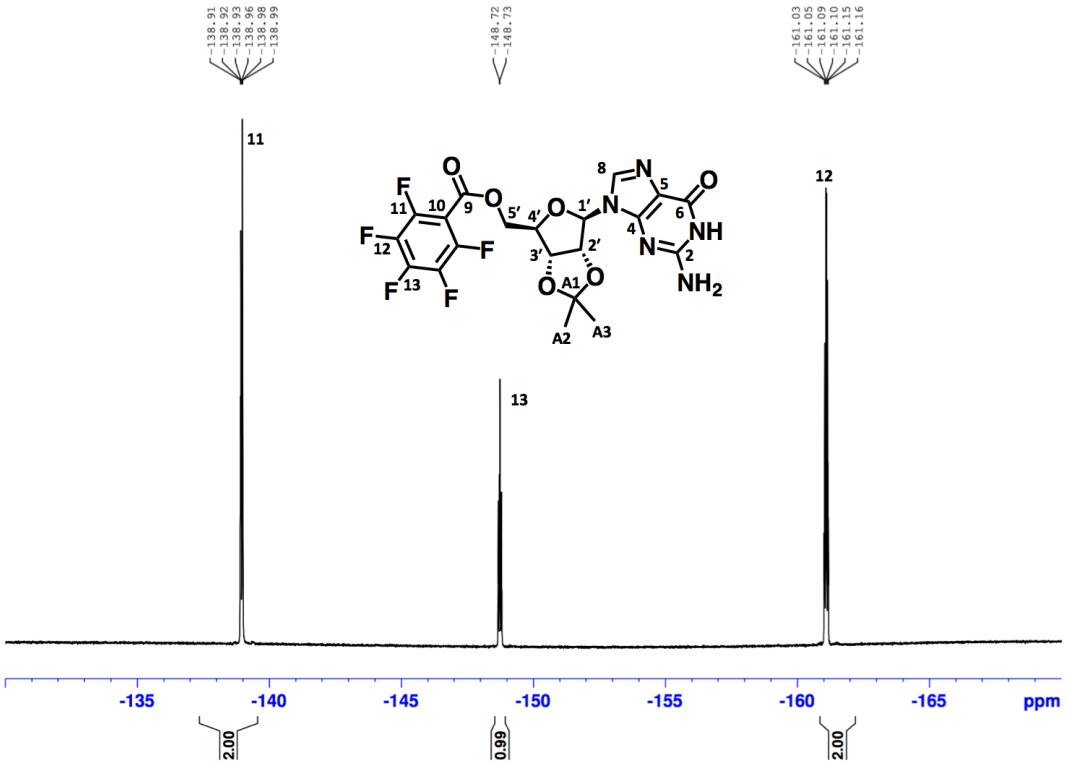

Figure 5.11. ^{19}F NMR of 5′-(2,3,4,5,6)-pentafluorobenzoyl-2′,3′-isopropylidene guanosine G **25** in DMSO-d_6.

5.2.2. General Procedure for the Formation of G-Quadruplex Octamers $[G]_8 \bullet K^+I^-$ and Hexadecamers $[G]_{16} \bullet 3K^+3I^-$ in Chapter 2

Potassium iodide (0.100 g, 0.602 mmol) was dissolved in H_2O (1 mL) to give a stock solution of 0.602 M KI. Aliquots of the aqueous KI stock solution were added to a scintillation vial (2.1 µL to prepare octamer $[G]_8 \bullet K^+I^-$ or 4.2 µL for hexadecamer $[G]_{16} \bullet 3K^+3I^-$) and placed in an oven for 1 h to evaporate the H_2O. A 0.625 mM solution of hexadecamer $[G]_{16} \bullet 3K^+3I^-$ or a 1.25 mM solution of octamer $[G]_8 \bullet K^+I^-$ was prepared in either CD_3CN (1 mL) or $CDCl_3$ (1 mL) by adding 10 µmol of guanosine derivative

to the vial containing the appropriate amount of KI, sonicating for one h, and then stirring overnight. The resulting complexes were confirmed by ^{1}H NMR analysis by their characteristic spectra, ESI-MS, or X-ray crystallography. The D_4-symmetric octamers $[G]_8 \bullet K^+I^-$ give a single set of ^{1}H NMR signals and the D4-symmetric hexadecamers $[G]_{16} \bullet 3K^+3I^-$ give two sets of ^{1}H NMR signals of equal intensity, one set for the outer G-quartets and one set for the inner G-quartets.

5.2.3 Mixed 5′-Benzoyl-2′,3′-Isopropylidene Guanosine G 21 and 5′-(2,3,4,5,6) Pentafluorobenzoyl-2′, 3′-Isopropylidene Guanosine G 25 G-Quadruplex Experiments

Potassium iodide (0.100 g, 0.602 mmol) was dissolved in H_2O (1 mL) to give a stock solution of 0.602 M KI. Aliquots of the aqueous KI stock solution were added to a scintillation vial (2.1 μL to prepare octamer $[G]_8 \bullet K^+I^-$ or 4.2 μL for hexadecamer $[G]_{16} \bullet 3K^+3I^-$) and placed in an oven for 1 h to evaporate the H2O. The vials were taken out of the oven, allowed to cool to room temperature, and equimolar amounts of G **21** and G **25** were added to the vials. A 0.625 mM solution of mixed G_{16}-hexadecamer complexes or a 1.25 mM solution of mixed G_8-octamer complexes was prepared in $CDCl_3$ (1 mL) by adding equimolar amounts of G **21** (2.1 mg, 5 μmol) and G **25** (2.6mg, 5 μmol) to the vial containing the appropriate amount of KI, sonicating for one h, and then stirring overnight. The resulting complexes were examined by ^{1}H NMR and ESI-MS.

5.2.4 G-Quadruplex Thermodynamic Stability ^{1}H NMR Studies Using DMSO-d_6 Titrations

G_{16}-hexadecamers of [G **21**]$_{16}$•3K^+3I^-, [G **23**]$_{16}$•3K^+3I^-, or [G **24**]$_{16}$•3K^+3I^- (0.625 mM) in CD_3CN were prepared as described in **Section 5.2.2**. A 0.5 mL aliquot of the G_{16}-hexadecamer solution was placed in an NMR tube. To perform the titration, aliquots of DMSO-d_6 were added directly to the NMR tube containing the G_{16}-quadruplex solution (0.625 mM, 0.5 mL), the NMR tube was inverted 3X and allowed to sit for 10 min before acquiring ^{1}H NMR spectrum. ^{1}H NMR spectroscopy was used to monitor the [G]$_{16}$•3K^+3I^-:G monomer ratio as DMSO-d_6 was titrated into each sample. The DMSO-d_6 titrations were performed at v/v % DMSO-d_6/CD_3 CN (volume of DMSO-d_6): 5.6 % (30 μL), 9.1 % (50 μL), 16.7 % (100 μL), 20 % (125 μL), 25.9 % (175 μL), and 31.9 % DMSO-d_6 (225 μL).The ^{1}H NMR titration experiments were performed in CD_3CN, primarily because the self-assemblies are not as thermodynamically stable in the more polar CD_3CN over the nonpolar $CDCl_3$. Additionally, better resolution of the N^{1}H NMR resonances is observed in CD_3CN over $CDCl_3$.

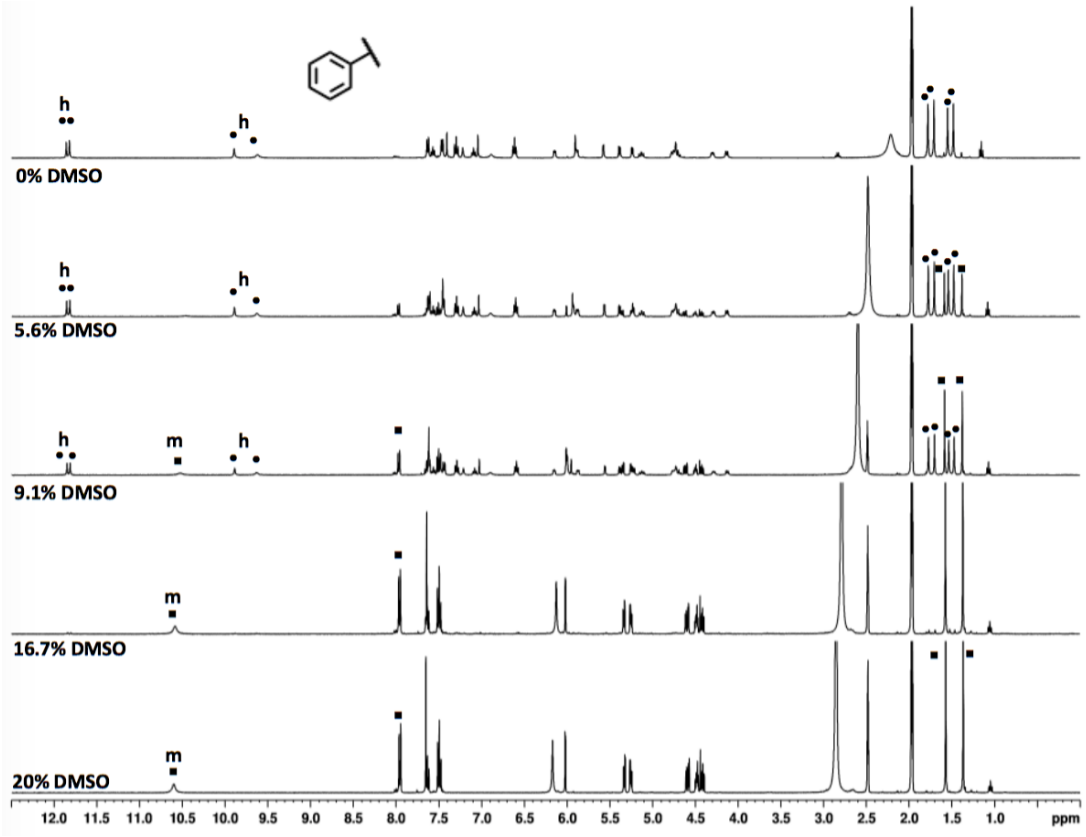

Figure 5.12. DMSO-d_6 titration of [G **21**]$_{16}$•3K$^+$3I$^-$. Hexadecamer (•,h); Monomer (■,m).

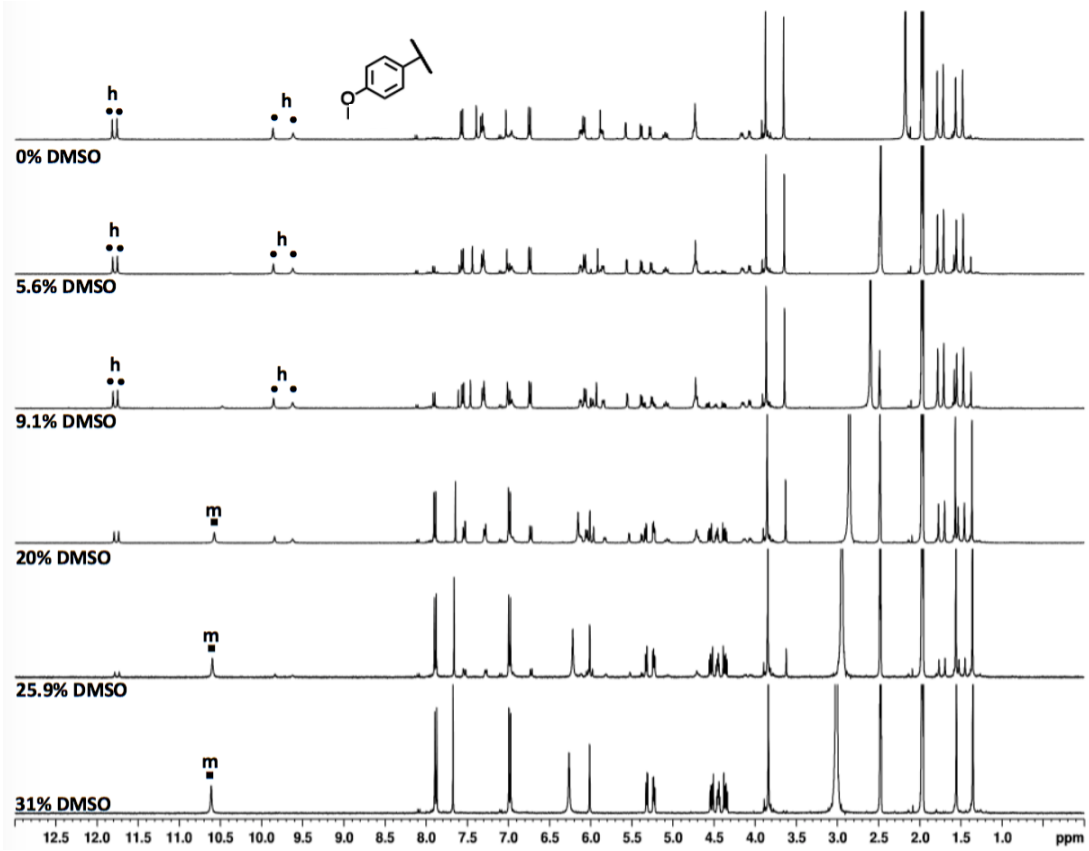

Figure 5.13. DMSO-d_6 titration of [G **23**]$_{16}$•3K$^+$3I$^-$. Hexadecamer (•,h); Monomer (■,m).

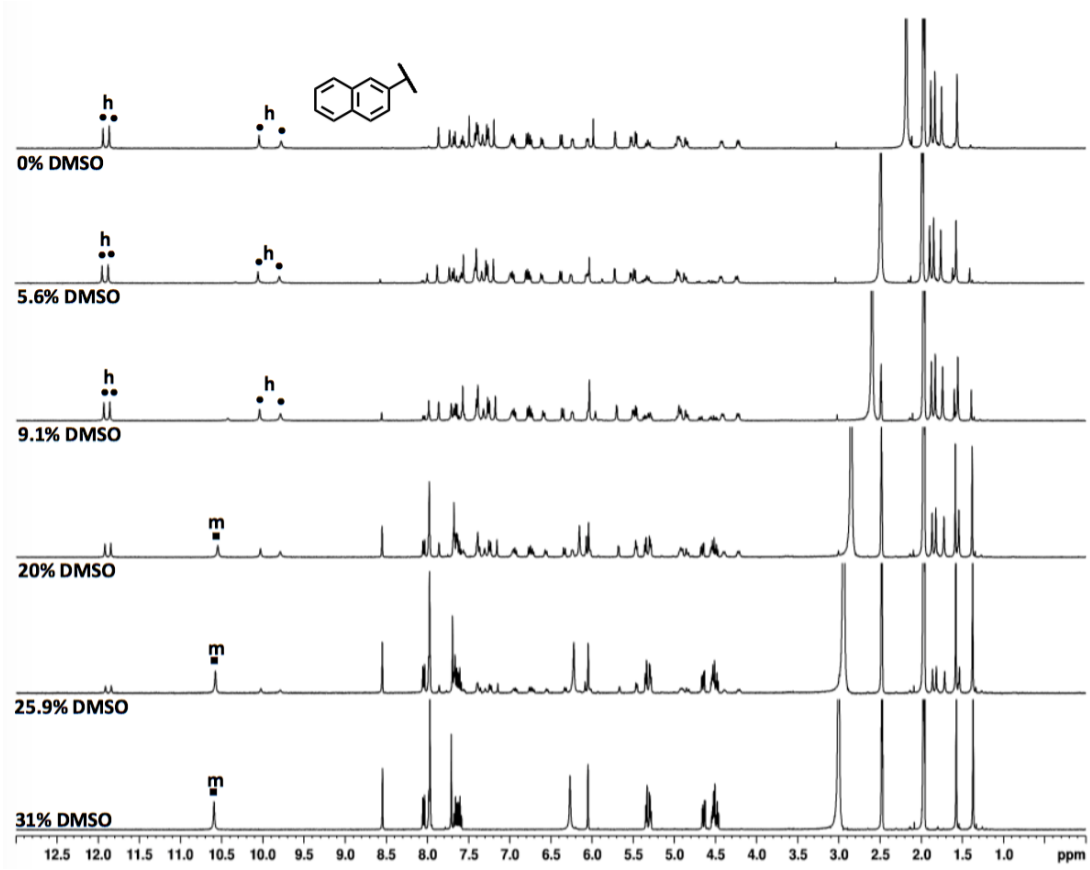

Figure 5.14. DMSO-d_6 titration of [G **24**]$_{16}$•3K$^+$3I$^-$. Hexadecamer (•,h); Monomer (■,m).

5.2.5 G-Quadruplex H/D Kinetic Stability ^{1}H NMR Studies

G_{16}-hexadecamers of [G **21**]$_{16}$•3K$^+$3I$^-$, [G **23**]$_{16}$•3K$^+$3I$^-$, or [G **24**]$_{16}$•3K$^+$3I$^-$ (0.625 mM) in CD_3CN were prepared as described in **Section 5.2.2**. A 0.5 mL aliquot of each G-quadruplex solution was allocated to separate NMR tubes. D_2O (10 µL) was added directly to the NMR tubes containing the G-quadruplex solution (0.625 mM, 0.5 mL), the NMR tube was inverted 3X, vortexed for 10 s, and placed into the NMR

spectrometer. ^{1}H NMR spectroscopy was used to monitor G-quadruplex N^{1}H and N^{2}H H/D exchange over time. We decided to carry out the H/D exchange ^{1}H NMR experiments in CD_3CN for 3 reasons: 1) better signal resolution for the 2 amide N^{1}H protons in CD_3CN; 2) CD_3CN, unlike $CDCl_3$, is miscible with D_2O, which greatly facilitated the H/D exchange experiments and 3) because the hexadecamers are less stable in CD_3CN, than in $CDCl_3$, we could better detect differences in kinetic stabilities in the for the hexadecamers made from G **21**, G **23**, and G **24**.

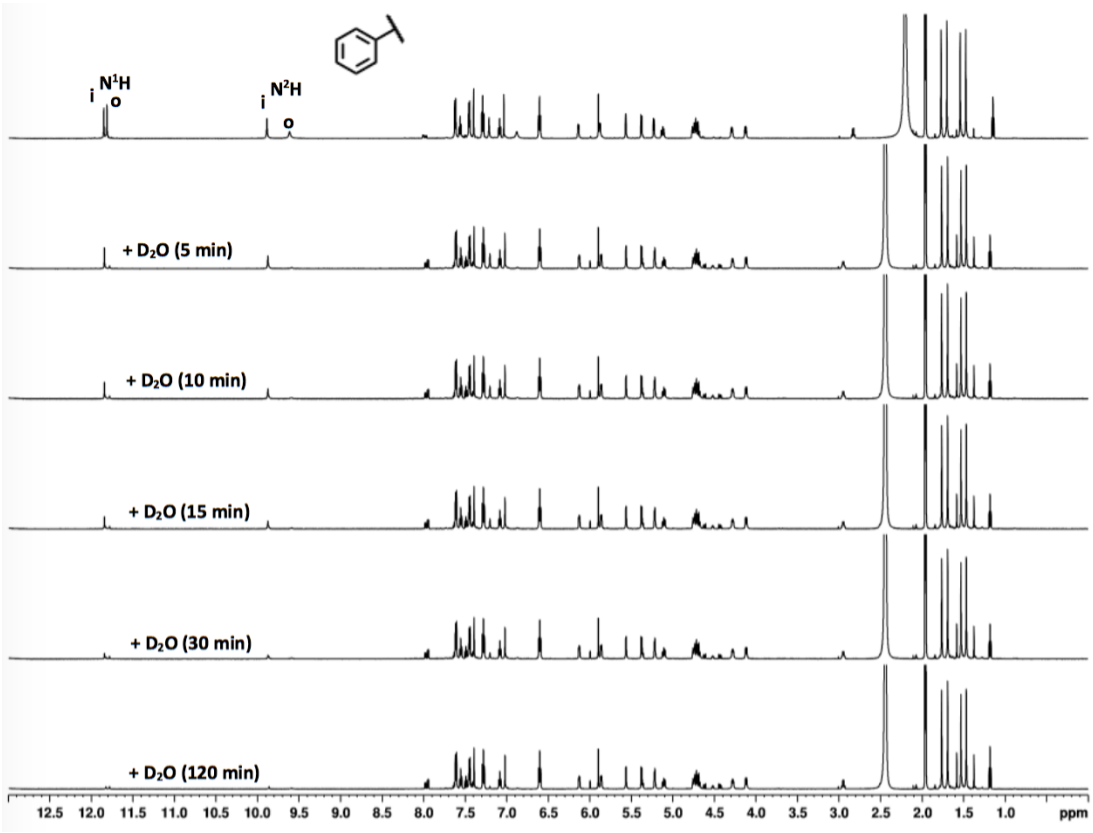

Figure 5.15. Full spectra for the H/D exchange of amide N^{1}H and amino N^{2}H protons of [G **21**]$_{16}$•3K^{+}3I^{-}.

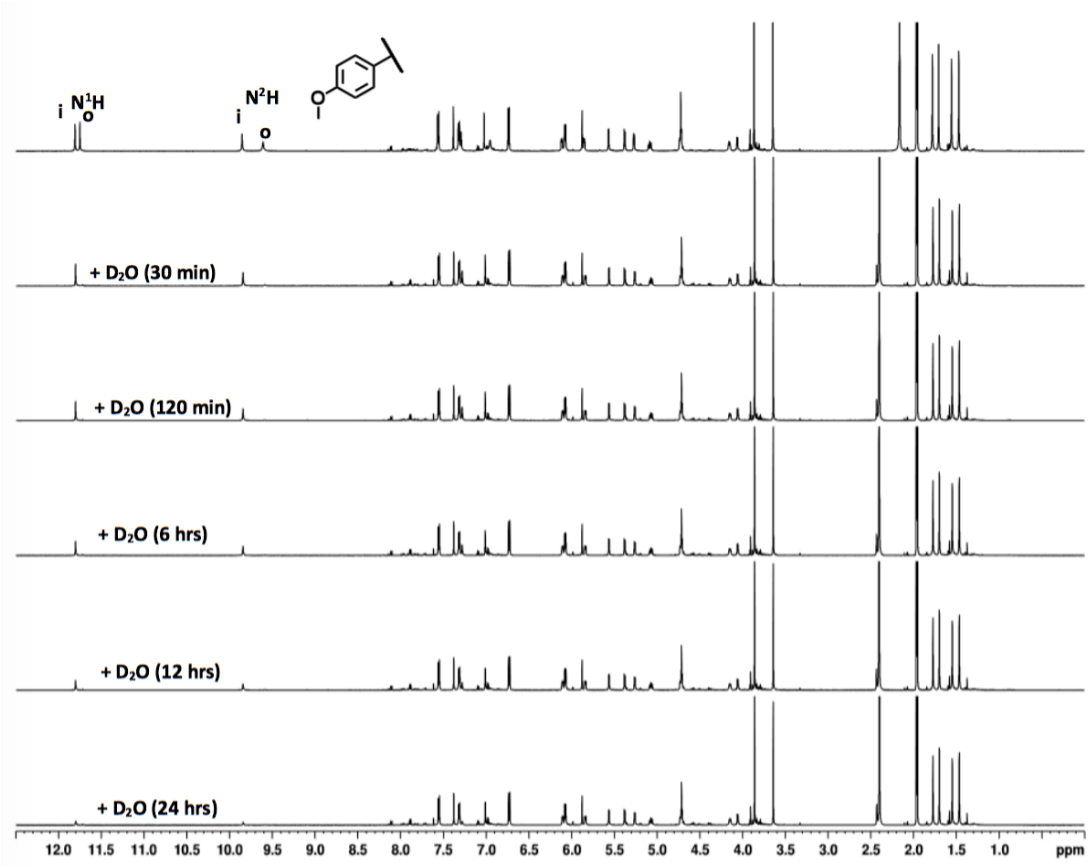

Figure 5.16. Full spectra for the H/D exchange of amide N^1H and amino N^2H protons of [G **23**]$_{16}$•3K^+3I^-.

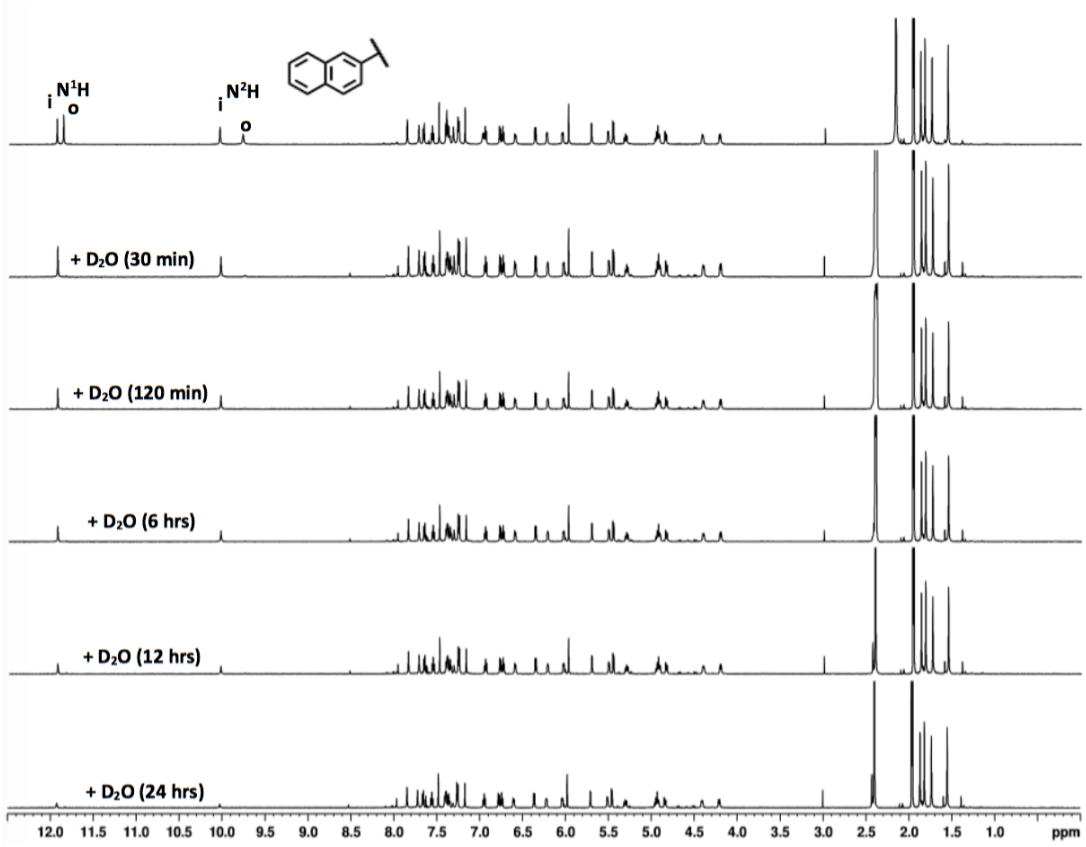

Figure 5.17. Full spectra for the H/D exchange of amide N^1H and amino N^2H protons of [G **24**]$_{16}$•3K$^+$3I$^-$.

5.2.6 Crystallization of Hexadecamer [G 21]$_{16}$•3K$^+$3I$^-$

To a solution of [G **21**]$_{16}$•3K$^+$3I$^-$ (0.625 mM) in $CDCl_3$ (0.50 mL) was added benzene-d_6 (50 μL) as a co-crystallization solvent. The scintillation vial containing this solution was then placed upright, without the lid, into a clean jar that contained Et_2O (5 mL). The jar was capped and stored in a freezer at -6 °C. Yellow, cube-shaped crystals formed after 72 h. Subsequent X-ray analysis showed them to be hexadecamer [G **21**]$_{16}$•3K$^+$3I$^-$. Crystal Structure data for [G **21**]$_{16}$•3K$^+$3I$^-$ has been deposited with the

Cambridge Crystallographic Data Centre as CCDC-1495606.

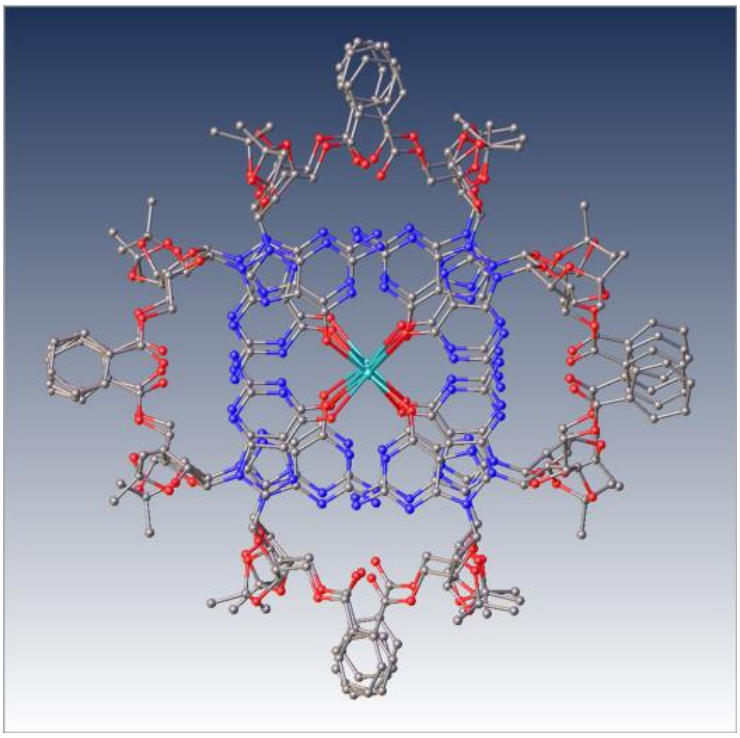

5.3 Experimental Procedures for Chapter 3-Utilizing the G-Quadruplex as a Scaffold for [2+2] Photocycloaddition Reactions of Lipophilic 5′-Cinnamate Modified Guanosines

5.3.1 Synthesis of Compounds in Chapter 3

Synthesis of Trans-5′-Cinnamoyl-2′, 3′-Isopropylidene Guanosine (G 26): 2′, 3′-Isopropylidene guanosine (1.42 g, 4.39 mmol), DMAP (0.269 g, 2.20 mmol), and cinnamic acid (0.653 g, 4.39 mmol) were added to a 250-mL round-bottom flask containing CH_2Cl_2 (120 mL). The round-bottom flask was wrapped with aluminum foil

to protect the reaction mixture from light. To the resulting suspension, DCC (1.09 g, 5.27 mmol) was added. The mixture was stirred for 16 h at ambient temperature. Tlc analysis (9:1 CH_2Cl_2:MeOH) indicated that the reaction had not gone to completion after 16 h. Additional cinnamic acid (0.653 g, 2.20mmol) and DCC (1.09 g, 5.27 mmol) was added to the flask and the resulting solution was stirred for an additional 24 h, after which time tlc analysis indicated that the reaction was complete. The reaction mixture was concentrated *in vacuo* to afford a white solid. The solid was re-suspended in cold CH_3CN (150 mL) and vacuum filtered. The remaining precipitate was washed with cold CH_3CN (3 X 50 mL). The resulting filtrate was then concentrated *in vacuo* to give a white solid. Column chromatography on silica gel (95:5 CH_2Cl_2:MeOH) gave G **26** as a white solid. The solid was washed with H_2O (3 X 100 mL), isolated by vacuum filtration, and vacuum dried to give G **26** as a white powder (1.56 g, 78.3 %).

^{1}H NMR (600 MHz, DMSO-d6) δ: 101.72 (s, 1H, N^{1}H), 7.89 (s, 1H, H8), 7.71 (dd, 2.26, 6.2 Hz, 2H, H13), 7.63 (d, J=15.8 Hz, 1H, H11), 7.44-7.41 (m, 2H, H14 & H15), 6.64 (d, J=15.8 Hz, 1H, H10), 6.57 (s, 2H, N^{2}H), 6.03 (d, 2.1 Hz, 1H, H1′), 5.31 (dd, 2.1, 6.1 Hz, 1H, H2′), 5.19 (dd, 3.6, 6.1 Hz, 1H, H3′), 4.40 (dd, 4.54, 11.2 Hz, 1H, H5′), 4.36 (m, 1H, H4′), 4.26 (dd, 6.1, 11.2 Hz, 1H, H5′′), 1.54 (s, 1H, HA2 or HA3), 1.35 (s, 3H, HA2 or HA3); ^{13}C NMR (125 MHz, DMSO-d_6) δ: 166.32 (C9), 157.10 (C6), 154.14 (C2), 150.97 (C4), 145.44 (C11), 136. 51 (C8), 134.36 (C12), 130.99 (C14), 129.34 (C15), 128.83 (C13), 117.99 (C10), 117.39 (C5), 113.75 (CA1), 88.83 (C1′),

84.57 (C4′), 84.06 (C2′), 81.57 (C3′), 64.70 (C5′), 27.47 (CA2/CA3), 25.77 (CA2/CA3); ESI-MS ($M+H^+$): 454.07.

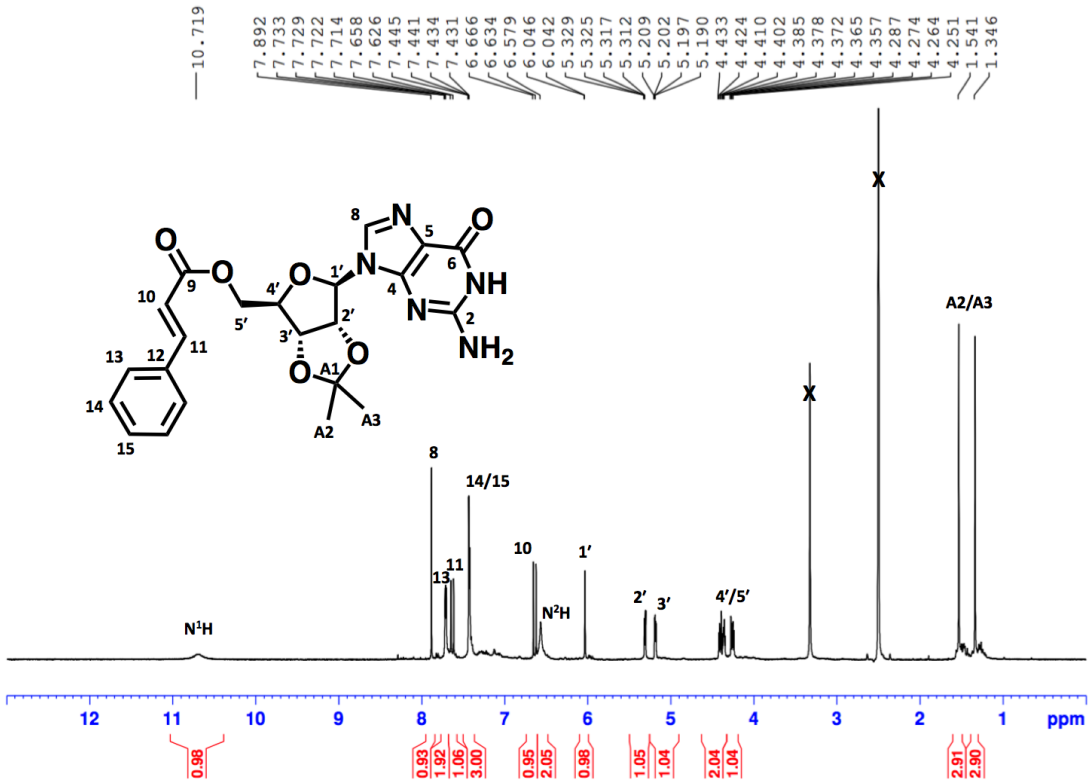

Figure 5.18. ^{1}H NMR of 5′-cinnamoyl-2′,3′-isopropylidene guanosine G **26** in DMSO-d_6

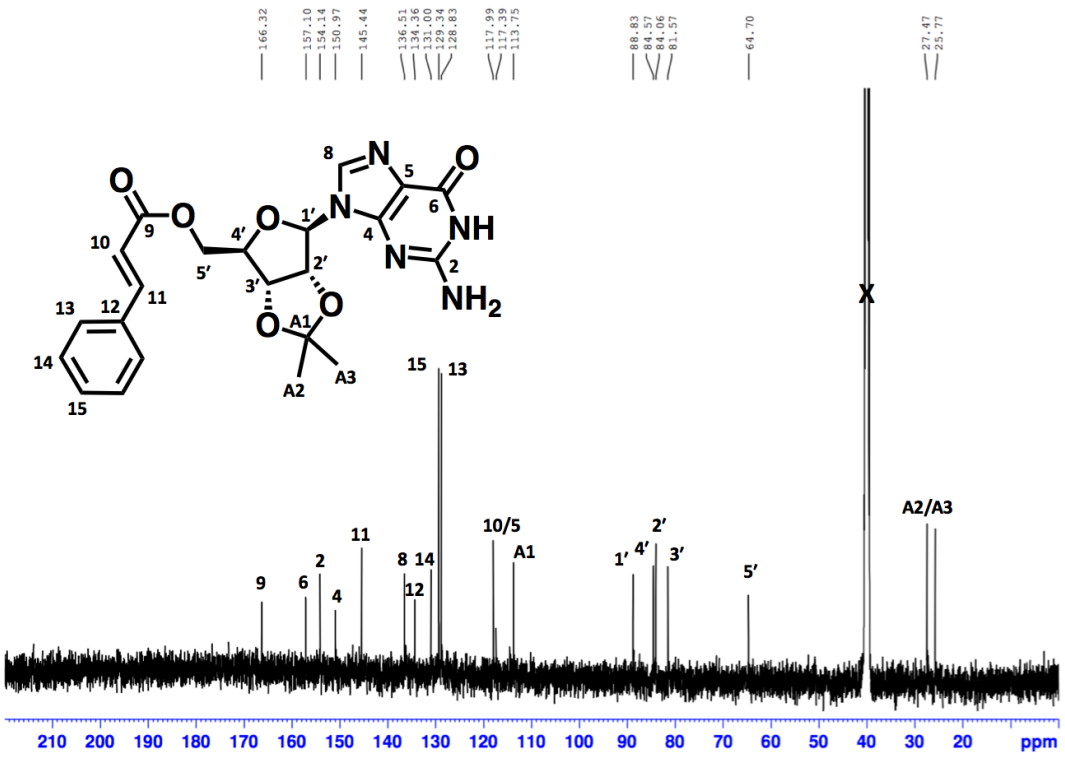

Figure 5.19. ^{13}C NMR of 5′-cinnamoyl-2′,3′-isopropylidene guanosine G **26** in DMSO-d_6

Synthesis of Trans-5′-(2-Methoxy)-Cinnamoyl-2′, 3′-Isopropylidene Guanosine (G 27): 2′, 3′-Isopropylidene guanosine (0.668 g, 2.10 mmol), DMAP (0.126 g, 1.05 mmol), and 2-methoxycinnamic acid (0.368 g, 2.1 mmol) were added to a 100-mL round-bottom flask containing CH_2Cl_2 (50 mL). The round-bottom flask was wrapped with aluminum foil to protect the reaction mixture from light. To the resulting suspension, DCC (0.512 g, 2.48 mmol) was added. The mixture was stirred for 16 h at ambient temperature, after which Tlc analysis (9:1 CH_2Cl_2:MeOH) indicated that the reaction was near completion. The reaction mixture was concentrated *in vacuo* to afford

a white solid. The solid was re-suspended in cold CH_3CN (50 mL) and vacuum filtered. The remaining precipitate was washed with cold CH_3CN (3 X 25 mL). The resulting filtrate was then concentrated *in vacuo* to give a white solid. Column chromatography (95:5 CH_2Cl_2:MeOH) on silica gel gave G **27** as a white solid. The solid was washed with H_2O (3 X 100 mL), isolated by vacuum filtration, and vacuum dried to give G **27** as a white powder (0.447 g, 44.7 %).

^{1}H NMR (600 MHz, DMSO-d_6) δ: 10.64 (s, 1H, N^{1}H), 7.88 (s, 1H, H8), 7.86 (d, J=16.1 Hz, 1H, H11), 7.71 (dd, J=1.8, 7.9 Hz, 1H, H17), 7.42 (td, 1.8, 7.9, 8.4 Hz, 1H, H15), 7.10 (d, 8.4 Hz, 1H, H14), 6.99 (t, 7.9, 7.6 Hz, 1H, H16), 6.6. (d, J=16.1 Hz, 1H, H10), 6.57 (s, 2H, N^{2}H), 6.03 (d, J=2.1 Hz, 1H, H1′), 5.29 (dd, 2.1, 6.20 Hz, 1H, H2′), 5.18 (dd, J=3.5, 6.2 Hz, 1H, H3′), 4.39 (dd, J=4.3, 11.1 Hz, 1H, H5′), 4.35 (m, 1H, H4′), 4.25 (dd, 6.6, 11.1 Hz, 1 H, H5′′), 3.87 (s, 3H, H18), 1.53 (s, 3H,A2/A3), 1.33 (s, 3H, A2/A3); ^{13}C NMR (125 MHz, DMSO-d_6) δ: 166.66 (C9), 158.36 (C13), 157.10 (C6), 154.12 (C2), 150.95 (C4), 140.25 (C11), 136.49 (C8), 132.63 (C12), 129.20 (C17), 122.55 (C15), 121.15 (C14), 117.99 (C16), 117.37 (C5), 113.75 (CA1), 112.21 (C10), 88.78 (C1′), 84.59 (C4′), 84.08 (C2′), 81.59 (C3′), 64.66 (C5′), 56.10 (C18), 27.46 (CA2/CA3), 25.75 (CA2/CA3) ESI-MS ($M+H^+$): 484.08.

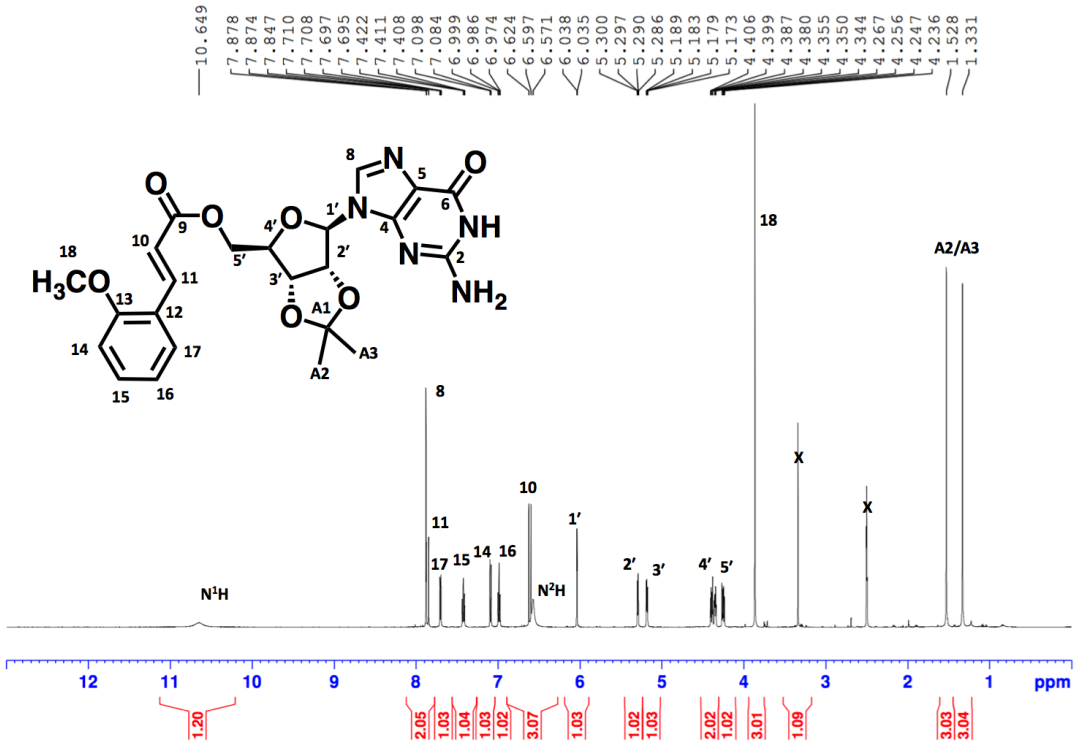

Figure 5.20. ^{1}H NMR of 5′-(2-methoxy)-cinnamoyl-2′,3′-isopropylidene guanosine G **27** in DMSO-d_6.

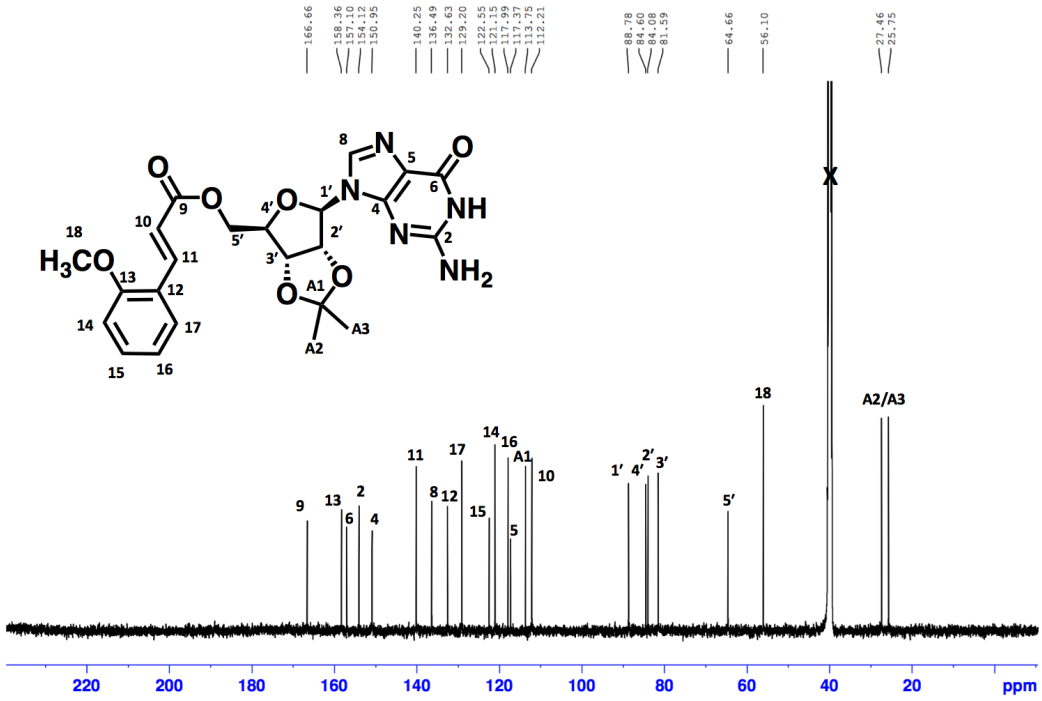

Figure 5.21. ^{13}C NMR of 5′-(2-methoxy)-cinnamoyl-2′,3′-isopropylidene guanosine G **27** in DMSO-d_6.

Synthesis of Trans-5′-(4-Methoxy)-Cinnamoyl-2′,3′-Isopropylidene Guanosine (G 28): 2′,3′-Isopropylidene guanosine (0.500 g, 1.55 mmol), DMAP (0.094 g, 0.77 mmol), and 4-methoxycinnamic acid (0.550 g, 3.10 mmol) were added to a 250-mL round-bottom flask containing CH_2Cl_2 (50 mL). The round-bottom flask was wrapped with aluminum foil to protect the reaction mixture from light. To the resulting suspension, EDC•HCl (0.440 g, 2.30 mmol) was added. The mixture was stirred for 16 h at ambient temperature, after which time everything had dissolved. Tlc analysis (9:1 CH2Cl2:MeOH) indicated that the reaction had not gone to completion after 16 h.

Additional 4-methoxycinnamic acid (0.550 g, 3.10 mmol) and EDC•HCl (0.440 g, 2.30 mmol) was added to the flask and the resulting solution was stirred for an additional 24 h, after which time tlc analysis indicated that the reaction was complete. The reaction mixture was concentrated *in vacuo* to afford a white solid. The solid was re-dissolved in $CHCl_3$ (50 mL) and the solution was washed with H_2O (3 X 50 mL). The organic phase was separated and concentrated *in vacuo* to afford an off-white solid. The solid was triturated with hot isopropanol (50 mL), allowed to cool to room temperature, and isolated by vacuum filtration. The resulting solid was washed with distilled water and then dried to give G **28** as a white powder (0.545 g, 72.8 %).

^{1}H NMR (600 MHz, DMSO-d_6) δ: 10.71 (s, 1H, N^{1}H), 7.88 (s, 1H, H8), 7.67 (d, 8.6 Hz, 2H, H13), 7.58 (d, 16.1 Hz, 1H, H11), 6.97 (d, J=8.6 Hz, 2H, H14), 6.56 (s, 2H, N^{2}H), 6.48 (d, J=16.1 Hz, 1H, H10), 6.03 (d, J=1.9 Hz, 1H, H1′), 5.31 (dd, 1.9,6.2 Hz, 1H, H2′), 5.17 (dd, 3.1, 6.2 Hz, 1H, H3′), 4.41-4.32 (m, 2H, H4′/H5′′), 4.22 (dd, J=5.8,10.7 Hz, 1H, H5′), 3.79 (s, 3H, H16), 1.52 (s, 3H, HA2/HA3), 1.33 (s, 3H, HA2/HA3); ^{13}C NMR (125 MHz, DMSO-d_6) δ: 166.58 (C9), 161.67 (C15), 157.10 (C6), 154.12 (C2), 150.97(C4), 154.24 (C11), 136.51(C8), 130.64 (C13), 126.98 (C12), 117.39 (C5), 115.22 (C10), 114.81 (C14), 113.74 (CA1), 88.83(C1′), 84.61(C4′), 84.05(C2′), 81.59(C3′), 64.51(C5′), 55.76(C16), 27.46(A2/A3), 25.76(A2/A3) ; ESI-MS (M+H^{+}): 484.08.

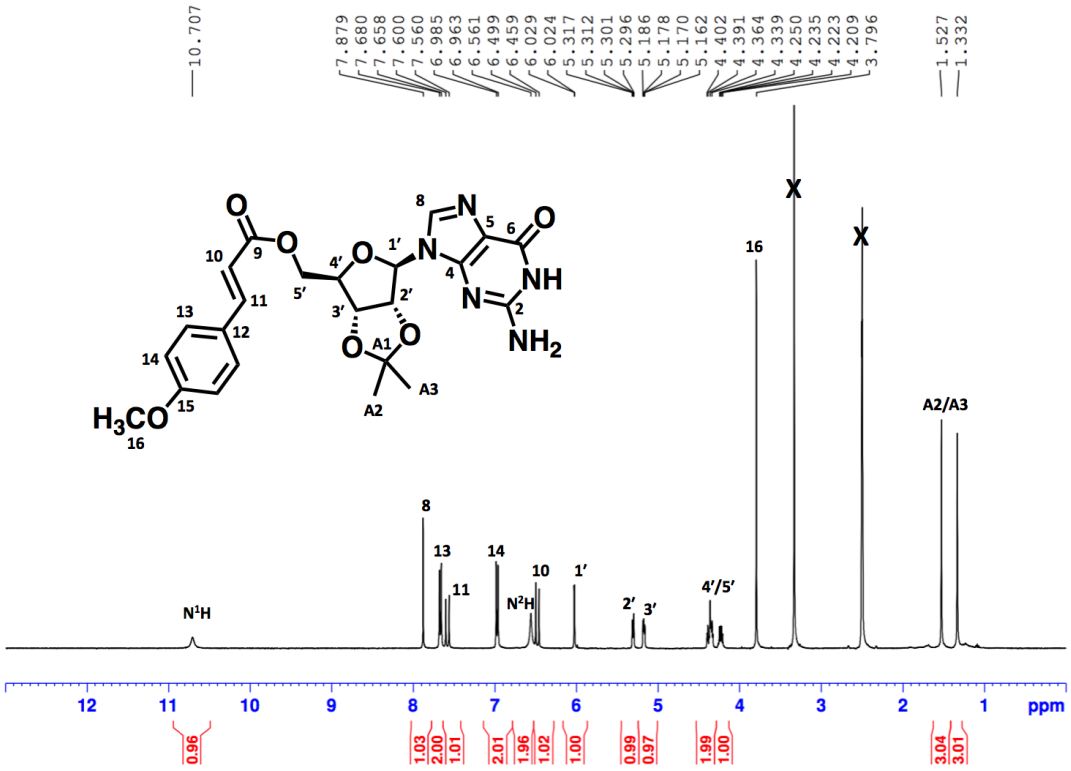

Figure 5.22. ^{1}H NMR of 5′-(4-methoxy)cinnamoyl-2′,3′-isopropylidene guanosine G **28** in DMSO-d_6.

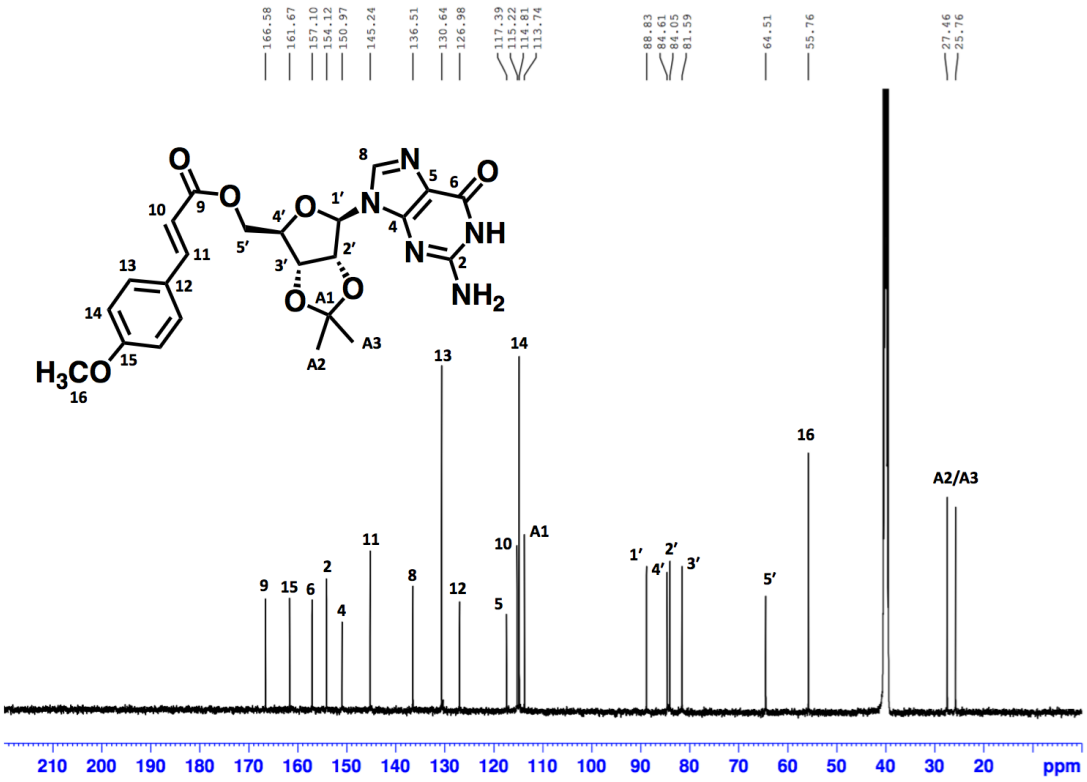

Figure 5.23. ^{13}C NMR of 5′-(4-methoxy)cinnamoyl-2′,3′-isopropylidene guanosine G **28** in DMSO-d_6.

5.3.2 Photoisomerization Reactions for Chapter 3

Photoisomerization of 5′-Cinnamoyl-2′,3′-Isopropylidene Guanosine (G 26) in DMSO-d_6: 5′-Cinnamoyl-2′,3′-isopropylidene guanosine G **26** (4.5 mg, 10.0 μmol) was added to a 4-mL vial containing DMSO-d_6 (1.00 mL). G **26** completely dissolved. The vial was placed in a Rayonet RMR-600 photochemical reactor and irradiated using 300 nm wavelength bulbs. Aliquots were taken out and analyzed at 0 min, 30 min, 60

min, and 360 min. A photostationary state was achieved within 360 min, resulting in 50 % *trans*-G **26**: 50% *cis*-G **26**, as determined by ^{1}H NMR integration.

Photoisomerization of 5′-Cinnamoyl-2′,3′-Isopropylidene Guanosine (G 26) in CD_3CN: 5′-Cinnamoyl-2′,3′-isopropylidene guanosine G **26** (4.5 mg, 10.0 μmol) and [2.2.2]cryptand (15.1 mg, 80 μmol) were added to a 4-mL vial containing CD_3CN (1.0 mL). The vial was placed in a Rayonet RMR-600 photochemical reactor and irradiated using 300 nm wavelength bulbs. Aliquots were taken out and analyzed at 0 min, 10 min, 30 min, and 60 min. A photostationary state was achieved within 60 min, resulting in 50 % *trans*-G **26**: 50% *cis*-**G 26**, as determined by ^{1}H NMR integration.

Photoisomerization of 5′-(2 –Methoxy)-Cinnamoyl-2′,3′-Isopropylidene Guanosine G 27: 5′-(2-Methoxycinnamoyl-2′,3′-isopropylidene guanosine G **27** (4.8 mg, 10.0 μmol) was added to a 4-mL vial containing DMSO-d_6 (1.00 mL). G **27** completely dissolved. The vial was placed in a Rayonet RMR-600 photochemical reactor and irradiated using 300 nm wavelength bulbs. Aliquots were taken out and analyzed at 0 min, 30 min, 60 min, and 360 min. A photostationary state was achieved within 360 min, resulting in 34 % *trans*-G **27**: 66% *cis*-G **27**, as determined by ^{1}H NMR integration.

Photoisomerization of 5′-(4-Methoxy)-Cinnamoyl-2′,3′-Isopropylidene Guanosine G 28: 5′-(4-Methoxycinnamoyl-2′,3′-isopropylidene guanosine G **28** (4.8 mg, 10.0 μmol)

was added to a 4-mL vial containing DMSO-d_6 (1.00 mL). G **28** completely dissolved. The vial was placed in a Rayonet RMR-600 photochemical reactor and irradiated using 300 nm wavelength bulbs. Aliquots were taken out and analyzed at 0 min, 30 min, 60 min, and 360 min. A photostationary state was achieved within 360 min, resulting in 45 % *trans* G **28**: 55% *cis* G **28**, as determined by ^{1}H NMR integration.

5.3.3 Self-Assembly of G_{16}-Hexadecamers for Photocycloaddition Reactions

Self-Assembly of a 5′-Cinnamoyl-2′,3′-Isopropylidine Guanosine G_{16}-Hexadecamer $[G\ 26]_{16}\bullet 3K^+3I^-$: Potassium iodide (0.100 g, 0.602 mmol) was dissolved in H_2O (1 mL) to give a stock solution of 0.602 M KI. An aliquot of the aqueous KI stock solution (16.8 μL) was added to a 4-mL vial and placed in a glass-drying oven for 1 h at 160 °C to evaporate the H_2O. A 0.625 mM solution of hexadecamer [G **26**]$_{16}\bullet 3K^+3I^-$ was prepared in $CDCl_3$ (1 mL) by adding *trans* G **26** (4.5 mg, 10.0 μmol) to the vial containing KI, sonicating for 1 h, and then stirring for 16 h. The vial was wrapped with aluminum foil to protect the reaction mixture from light. The resulting G_{16}-hexadecamer [G **26**]$_{16}\bullet 3K^+3I^-$ was confirmed by ^{1}H NMR.

Self-Assembly of a 5′-(2-Methoxy)-Cinnamoyl-2′,3′-Isopropylidine Guanosine G_{16}-Hexadecamer $[G\ 27]_{16}\bullet 3K^+3I^-$: Potassium iodide (0.100 g, 0.602 mmol) was dissolved in H_2O (1 mL) to give a stock solution of 0.602 M KI. An aliquot of the aqueous KI

stock solution (16.8 μL) was added to a 4-mL vial and placed in a glass-drying oven for 1 h at 160 °C to evaporate the H_2O. A 0.625 mM solution of hexadecamer [G **27**]$_{16}$•3K$^+$3I$^-$ was prepared in $CDCl_3$ (1 mL) by adding *trans*-G **27** (4.8 mg, 10.0 μmol) to the vial containing KI, sonicating for 1 h, and then stirring for 16 h. The vial was wrapped with aluminum foil to protect the reaction mixture from light. The resulting G_{16}-hexadecamer [G **27**]$_{16}$•3K$^+$3I$^-$ was confirmed by ^{1}H NMR.

Self-Assembly of a 5′-(4-Methoxy)-Cinnamoyl-2′,3′-Isopropylidine Guanosine G_{16}-Hexadecamer [G 28]$_{16}$•3K$^+$3I$^-$: Potassium iodide (0.100 g, 0.602 mmol) was dissolved in H_2O (1 mL) to give a stock solution of 0.602 M KI. An aliquot of the aqueous KI stock solution (16.8 μL) was added to a 4-mL vial and placed in a glass-drying oven for 1 h at 160 °C to evaporate the H_2O. A 0.625 mM solution of hexadecamer [G **28**]$_{16}$•3K$^+$3I$^-$ was prepared in $CDCl_3$ (1 mL) by adding *trans* G **28** (4.8 mg, 10.0 μmol) to the vial containing KI, sonicating for 1 h, and then stirring for 16 h. The vial was wrapped with aluminum foil to protect the reaction mixture from light. The resulting G_{16}-hexadecamer [G **28**]$_{16}$•3K$^+$3I$^-$ was confirmed by ^{1}H NMR.

5.3.4 General Procedure for the Small-Scale [2+2] Photocycloaddition Reaction of [G 26]$_{16}$•3K$^+$3I$^-$, [G 27]$_{16}$•3K$^+$3I$^-$, and [G 28]$_{16}$•3K$^+$3I

G_{16}-quadruplexes of [G **26**]$_{16}$•3K$^+$3I$^-$, [G **27**]$_{16}$•3K$^+$3I$^-$, or [G **28**]$_{16}$•3K$^+$3I$^-$ were prepared as described in **Section 5.3.3**. The vial had the aluminum foil removed and

was placed in a Rayonet RMR-600 photochemical reactor and irradiated using 300 nm wavelength bulbs. Reaction aliquots were taken at t = 15 min, 30 min, 1 h, 3 h, 6 h, and 24 h, the solvent was removed, and the remaining residue was re-dissolved in DMSO-d_6 for ^{1}H-NMR analyses.

5.3.5 Transesterification and Characterization of the [2+2] Photocycloaddition Reaction Products

Transesterification of [G 26]$_{16}$•3K$^+$3I$^-$ Photocycloaddition Product: Potassium iodide (30 mg, 0.18 mmol) was added to a 20-mL vial containing $CHCl_3$ (18 mL). The flask was wrapped with aluminum foil to protect the reaction mixture from light until the sample was ready for irradiation. *Trans*-G **26** (81.0 mg, 0.18 mmol) was added to the flask, sonicated for 1 h, and then stirred for 16 h to prepare a G-quadruplex solution (0.625 mM [G **26**]$_{16}$•3K$^+$3I$^-$). The flask had the foil removed and was placed in a Rayonet RMR-600 photochemical reactor and irradiated using 300 nm wavelength bulbs. The sample was irradiated for 24 h, after which time ^{1}H NMR analysis showed almost full conversion to the guanosine cyclobutane product. The reaction mixture was transferred to a 50-mL round-bottom flask, concentrated *in vacuo* and re-dissolved in MeOH (18 mL). Concentrated 12 M HCl (1 mL, 12 mmol) was added to the solution and the resulting solution was refluxed for 24 h, after which time tlc analysis (95:5 CH_2Cl_2:MeOH) showed the reaction was complete. The solution was concentrated *in*

vacuo, dissolved in CH_2Cl_2, and washed with a saturated sodium bicarbonate solution. The organic layer was isolated and purified by column chromatography on silica gel (95:5 CH_2Cl_2:CH_3OH) to afford the methyl esters as a colorless oil (16 mg, 55.2 %).

^{1}H NMR (600 MHz, DMSO-d_6) δ: 7.35-7.28 (m, 3H, δ and ε aromatic H), 7.10 (t, J=7.2,8.0 Hz, 4H, β7), 7.05 (t, J=7.2, 7.8, 2H, β8), 6.92 (d, J= 8.0 Hz, 4H, β6), 4.40 (dd, J=2.3,3.6 Hz, 2H, β3), 4.00 (t, 8.7, 9.7 Hz, 0.4H, ε3), 3.85 (dd, J=2.3, 3.5 Hz, 2H, β4), 3.75 (s, 6H, β1), 3.75(s, δ1 or ε1), 3.74(s, δ1 or ε1), 3.49 (dd, J=3.2, 5.2 Hz, 0.4H, δ4), 3.29 (t, 6.5 Hz, 8.7 Hz, 0.4 H, ε4); ^{13}C NMR (125 MHz, DMSO-d_6) δ: 172.83 (C2), 138. 44 (C5), 127.95 (C6), 127.72 (C7), 126.31 (C8), 52.07 (C3), 44.89 (C1), 43.24 (C4).

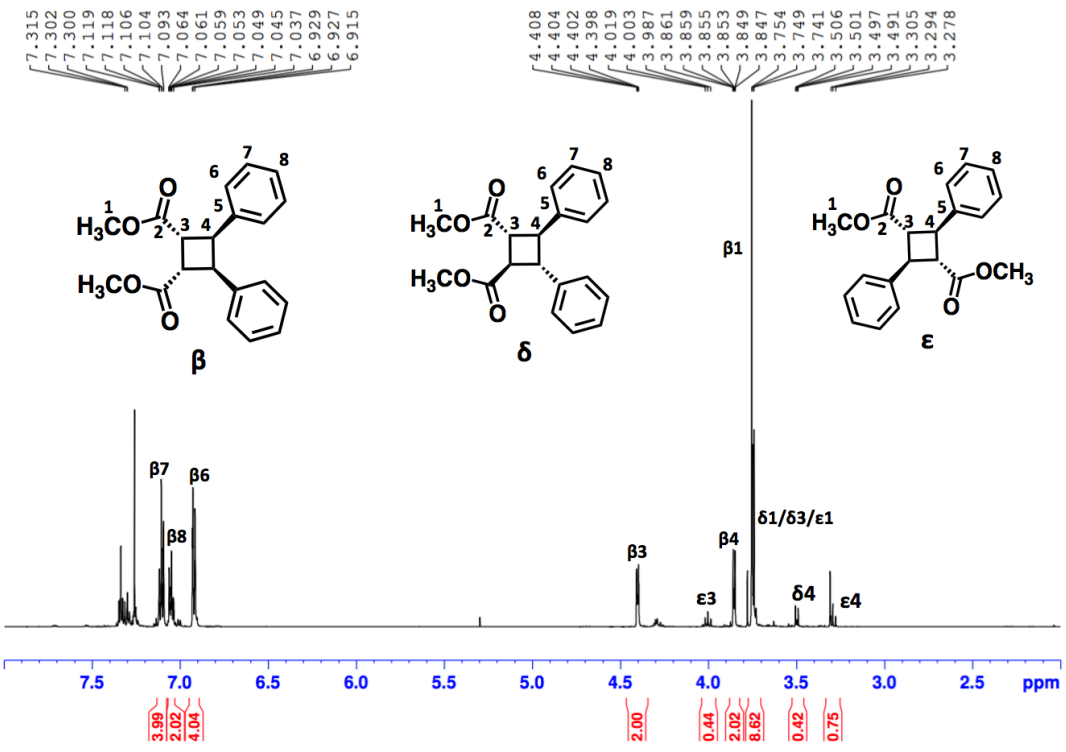

Figure 5.24. ^{1}H NMR of the transesterified cyclobutane products formed during the photoreaction of [G **26**]$_{16}$•3K^{+}3I^{-} in $CDCl_3$. β-truxinate, δ-truxinate, and ε-truxillates formed during the irradiation of [G **26**]$_{16}$•3K^{+}3I^{-}.

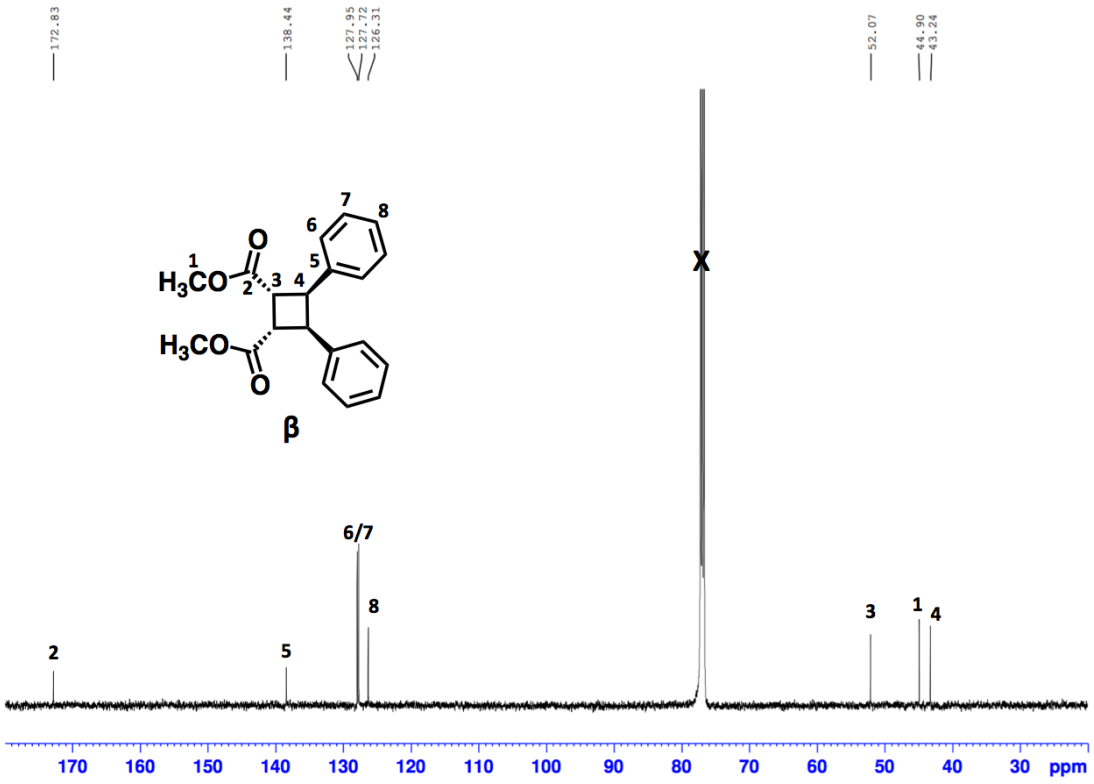

Figure 5.25. ^{13}C NMR of the transesterified cyclobutane products formed during the photoreaction of [G **26**]$_{16}$•3K^{+}3I^{-} in $CDCl_3$.

Transesterification of [G 27]$_{16}$•3K^{+}3I^{-} Photocycloaddition Product: Potassium iodide (30 mg, 0.18 mmol) was added to a 20-mL vial containing $CHCl_3$ (18 mL). The flask was wrapped with aluminum foil to protect the reaction mixture from light until the sample was ready for irradiation. *trans*-G **26** (87.0 mg, 0.18 mmol) was added to the flask, sonicated for 1 h, and then stirred for 16 h to prepare a G-quadruplex solution (0.625 mM [G **26**]$_{16}$•3K^{+}3I^{-}). The flask had the foil removed and was placed in a

Rayonet RMR-600 photochemical reactor and irradiated using 300 nm wavelength bulbs. The sample was irradiated for 24 h, after which time ^{1}H NMR analysis showed almost full conversion to the cyclobutane product. The reaction mixture was transferred to a 50-mL round-bottom flask, concentrated *in vacuo* and re-dissolved in MeOH (18 mL). Concentrated 12 M HCl (1 mL, 12 mmol) was added to the solution and the resulting solution was refluxed for 24 h, after which time tlc analysis (95:5 CH_2Cl_2:MeOH) showed the reaction was complete. The solution was concentrated *in vacuo,* dissolved in CH_2Cl_2, and rinsed with a saturated sodium bicarbonate solution. The organic layer was isolated and purified by column chromatography on silica gel (95:5 CH_2Cl_2:CH_3OH) afforded the methyl esters as a colorless oil (22.8 mg, 67.1%).

^{1}H NMR (600 MHz, DMSO-d_6) δ: 7.27 (dd, J=1.6, 7.4 Hz, ωH6), 7.20 (td, J=1.7, 7.7, 8.1 Hz, 0.5H, ωH8), 7.01 (td, J=1.7, 7.8, 8.1 Hz, 2H, μH6), 6.97 (dd, J= 1.6, 7.6 Hz, 2 H, μH7), 6.91 (td, J=1.1, 7.4, 7.7 Hz, 0.5H, ωH7), 6.82 (dd, J=1.1, 8.1 Hz, 0.5H, ωH9), 6.73 (td, J=1.1, 7.6, 7.8 Hz, 2H, μH7), 6.53 (dd, 0.9, 8.1 Hz, 2H, μH9),4.58 (dd, J=2.5, 3.7 Hz, 2H, μH3), 4.16 (dd, J=3.6, 5.4 Hz, 0.5H, ωH3), 3.99 (dd, 2.5, 3.6 Hz, 2H, μH4), 3.73 (s, 6H, μH1), 3.73 (s, 3H, ωH1/10), 3.52 (s, 6H, μH10), 3.32 (dd, J= 3.6, 5.4 Hz, 0.5H, ωH4); ^{13}C NMR (125 MHz, DMSO-d_6) δ: 173.68 (ωC2), 173.37 (μC2), 157.41 (μC11), 157.09 (ωC11), 129.47 (μC6), 128.15 (ωC6), 127.83 (μC5), 127.67 (ωC5), 127.46 (μC8), 127.29 (ωC8), 120.44 (μC9), 119.46 (ωC9)109.58 (ωC7), 54.64 (ωC10), 51.84 (ωC3), 45.29 (μC1), 42.34 (ωC1), 40.67 (ωC4), 40.55 (μC4).

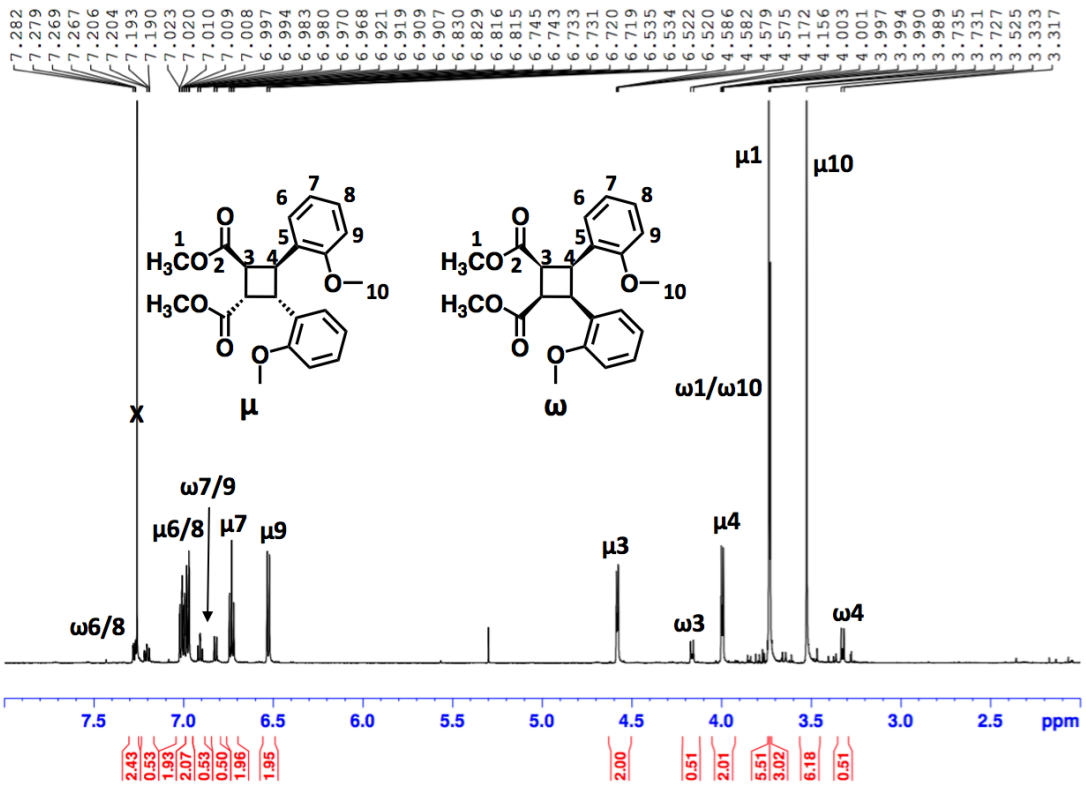

Figure 5.26. ^{1}H NMR of the transesterified cyclobutane products formed during the photoreaction of [G **27**]$_{16}$•3K^{+}3I^{-} in $CDCl_3$.μ-truxinate **44** and ω-truxinates **45** formed during the irradiation of [G **27**]$_{16}$•3K^{+}3I^{-}.

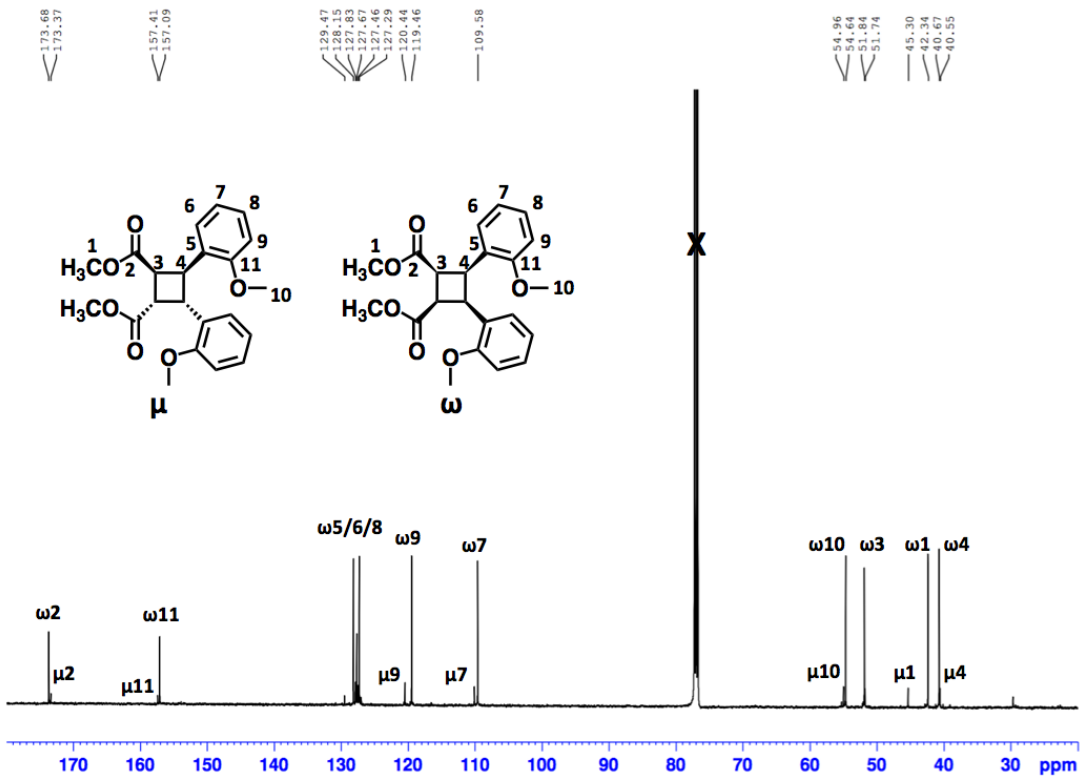

Figure 5.27. ^{13}C NMR of the transesterified cyclobutane products formed during the photoreaction of [G **27**]$_{16}$•3K^{+}3I^{-} in $CDCl_3$.

Transesterification of [G 28]$_{16}$•3K^{+}3I^{-} Photocycloaddition Product: Potassium iodide (30 mg, 0.18 mmol) was added to a 20-mL vial containing $CHCl_3$ (18 mL). The flask was wrapped with aluminum foil to protect the reaction mixture from light until the sample was ready for irradiation. *Trans*-G **28** (87.0 mg, 0.18 mmol) was added to the flask, sonicated for 1 h, and then stirred for 16 h to prepare a G-quadruplex solution (0.625 mM [G **28**]$_{16}$•3K^{+}3I^{-}). The flask had the foil removed and was placed in a Rayonet RMR-600 photochemical reactor and irradiated using 300 nm wavelength

bulbs. The sample was irradiated for 24 h, after which time ^{1}H NMR analysis showed almost full conversion to the cyclobutane product. The reaction mixture was transferred to a 50-mL round-bottom flask, concentrated *in vacuo* and re-dissolved in MeOH (18 mL). Concentrated 12 M HCl (1 mL, 12 mmol) was added to the solution and the resulting solution was refluxed for 24 h, after which time tlc analysis (95:5 CH_2Cl_2:MeOH) showed the reaction was complete. The solution was concentrated *in vacuo,* dissolved in CH_2Cl_2, and rinsed with a saturated sodium bicarbonate solution. The organic layer was isolated and purified by column chromatography on silica gel (95:5 CH_2Cl_2:CH_3OH) afforded the methyl esters β-trux **46** as a colorless oil (14.6 mg, 42.2%).

^{1}H NMR (600 MHz, DMSO-d_6) δ: 6.83 (d, J=8.6 Hz, 4H, H6), 6.67 (d, J=8.6 Hz, 4H, H7), 4.29 (dd, J=2.3, 3.4 Hz, 2H, H3), 3.76 (dd, 2.3, 3.4 Hz, 2H, H4), 3.74 (s, 6H, H1), 3.71 (s, 6H, H) ^{13}C NMR (125 MHz, DMSO-d_6) δ:172.96 (C2), 158.01 (C8), 130.70 (C5), 128.79 (C6), 113.44 (C7), 55.07 (C9), 52.01 (C3), 44.30 (C1), 43.56 (C4).

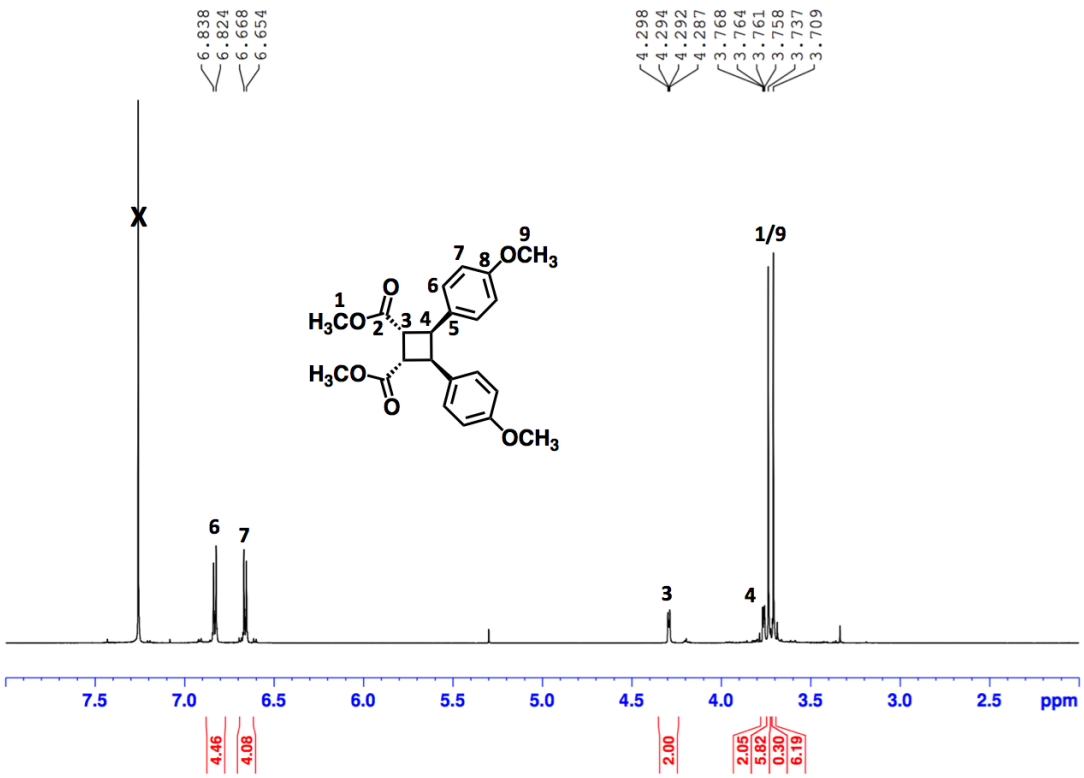

Figure 5.28. ^{1}H NMR of the transesterified cyclobutane products formed during the photoreaction of [G **28**]$_{16}$•3K^{+}3I^{-} in $CDCl_3$. β-truxinate formed during the irradiation of [G **28**]$_{16}$•3K^{+}3I^{-}.

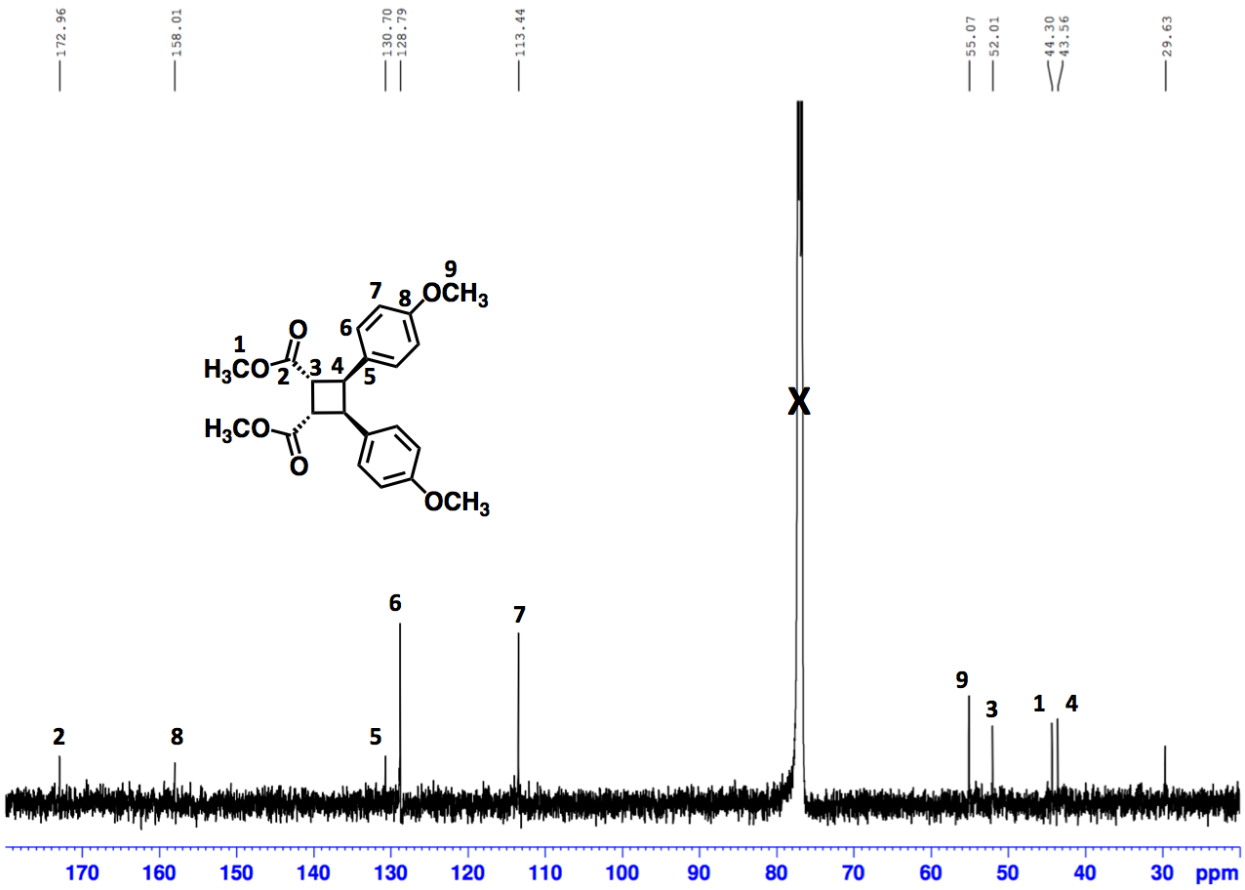

Figure 5.29. ^{1}H NMR of the transesterified cyclobutane products formed during the photoreaction of [G **28**]$_{16}$•3K^{+}3I^{-} in $CDCl_3$.

5.4 Chapter 4 Experimental- A Highly Regioselective and Stereoselective [2+2]Photocycloaddition of 5′-*meta*-Methoxycinnamoyl-2′,3′-Isopropylidene Guanosine

5.4.1 Synthesis of Compounds in Chapter 4

Synthesis of Trans-5′-(3-Methoxy)-Cinnamoyl-2′, 3′-Isopropylidene Guanosine (G 29)：2′, 3′-Isopropylidene guanosine (1.00 g, 3.09 mmol), DMAP (0.196 g, 1.60

mmol), and 3-methoxycinnamic acid (1.10 g, 6.28 mmol) were added to a 250-mL round-bottom flask containing CH_2Cl_2 (140 mL). The round-bottom flask was wrapped with aluminum foil to protect the reaction mixture from light. To the resulting suspension, EDC•HCl (1.78 g, 9.28 mmol) was added. The mixture was stirred for 16 h at ambient temperature, after which time everything had dissolved. Tlc analysis (9:1 CH_2Cl_2:MeOH) indicated that the reaction had not gone to completion after 16 h. Additional 3-methoxycinnamic acid (1.10 g, 6.28 mmol) and EDC•HCl (1.78 g, 9.28 mmol) was added to the flask and the resulting solution was stirred for an additional 24 h, after which time tlc analysis indicated that the reaction was complete. The reaction mixture was concentrated *in vacuo* to afford a yellow solid. The solid was re-dissolved in $CHCl_3$ (100 mL) and the solution was washed with H_2O (3 X 100 mL). The organic phase was separated and concentrated *in vacuo* to afford an off-white solid. The solid was triturated with hot isopropanol (100 mL), allowed to cool to room temperature, and isolated by vacuum filtration. The resulting solid was washed with distilled water and then dried to give *trans*-G **29** as a white powder (1.30 g, 86.9 %).

^{1}H NMR (600 MHz, DMSO-d$_6$) δ: 10.73 (s, 1H, N^{1}H), 7.90 (s, 1H, H8), 7.61 (d, *J*= 16.0 Hz, 1H, H12), 7.37-7.21 (m, 3H, H14/H15/H18), 7.01 (dd, *J*=8.1, 2.6 Hz, 1H, H16), 6.68 (d, *J*=16.0 Hz, H11), 6.57 (s, 2H, N^{2}H), 6.05(d, *J*= 2.1 Hz, 1H, H1'), 5.32 (dd, *J*= 6.2, 2.2 Hz, 1H, H2′), 5.20 (dd, *J*=6.2, 3.5 Hz, 1H, H3′), 4.41 (dd, *J*=11.6, 4.2

Hz, 1H, H5′), 4.37 (m, 1H, H4′), 4.26 (dd, *J*=11.6, 6.7 Hz, 1H, H5″), 3.80 (s, 3H, H19), 1.54 (s, 3H, A3), 1.35 (s, 3H, A2); ^{13}C NMR (125 MHz, DMSO-d6) δ: 166.33 (C10), 160.02 (C17), 157. 09 (C6), 154. 12 (C2), 150.96 (C4), 145.40 (C12), 136.54 (C8), 135.76 (C13), 130.36 (C14), 121.48 (C18), 118.32 (C11), 117.37 (C5), 117.17(C16), 113.74 (CA1), 113.38 (C15), 88.78 (C1′), 84.60 (C4′), 84.05 (C2′), 81.56 (C3′), 64.71 (C5′), 55.68 (19), 27.46 (CA3), 25.76 (CA2); ESI- MS (M+H$^+$): 484.22 g mol^{-1}

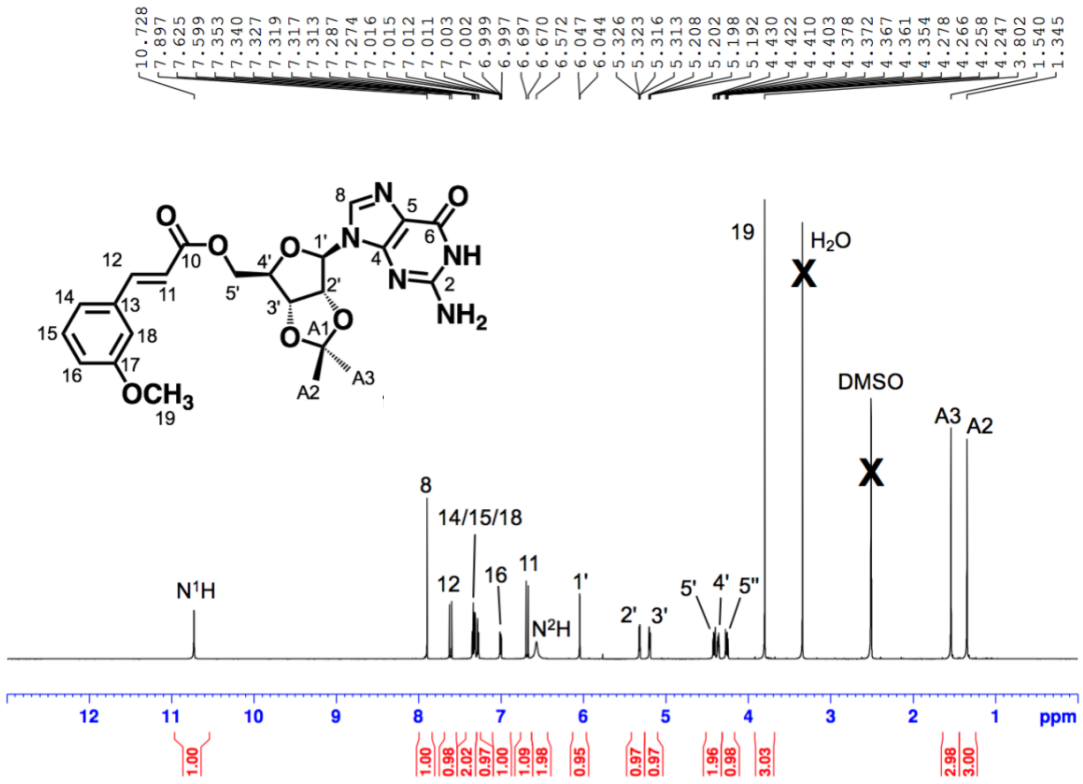

Figures 5.30. ^{1}H NMR of 5′-(3-methoxy)cinnamoyl-2′,3′-isopropylidene guanosine G **29** in DMSO-d$_6$.

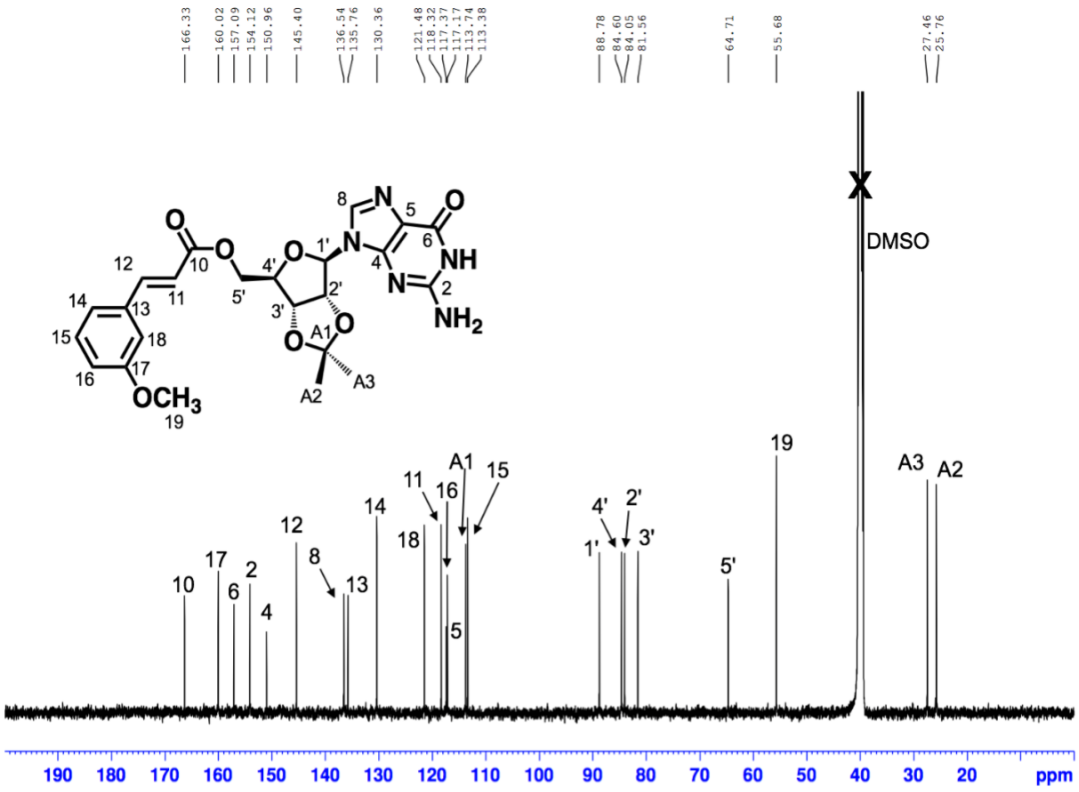

Figures 5.31. ^{13}C NMR of 5′-(4-methoxy)cinnamoyl-2′,3′-isopropylidene guanosine G **29** in DMSO-d_6.

5.4.2 Photoisomerization of 5′-(3-Methoxy)Cinnamoyl-2′,3′-Isopropylidne Guanosine

6.4.2 Photoisomerization of 5′-(3-Methoxycinnamoyl-2′,3′-Isopropylidene Guanosine) G29

Trans-G **29** (4.8 mg, 10.0 µmol) and [2.2.2] cryptand (37.6 mg, 140 µmol) were added to a 4-mL vial containing $CDCl_3$ (1.00 mL) to give a suspension. The vial was

wrapped with aluminum foil to protect the reaction mixture from light until the sample was ready for irradiation. This mixture was sonicated for 1 h and then stirred for 16 h. ^{1}H NMR analysis of the suspension after 24 h showed monomeric *trans* **1**. The vial containing the suspension had the foil removed and was placed in a Rayonet RMR-600 photochemical reactor and irradiated using 300 nm wavelength bulbs. Aliquots were taken and analyzed at 0 min, 15 min, 30 min, 60 min, and 180 min. A photostationary state was achieved within 60 min, resulting in 55.8 % *trans*-G **29**: 44.2% *cis*-G **29**, as determined by ^{1}H NMR integration.

5.4.3 Formation of [G 29]$_{16}$•3K$^+$3I$^-$ Hexadecamers for Photocycloaddition Studies

Potassium iodide (0.100 g, 0.602 mmol) was dissolved in H_2O (1 mL) to give a stock solution of 0.602 M KI. An aliquot of the aqueous KI stock solution (19.2 μL) was added to a 4-mL vial and placed in a glass-drying oven for 1 h at 160 °C to evaporate the H_2O. A 0.625 mM solution of hexadecamer [G **29**]$_{16}$•3K$^+$3I$^-$ was prepared in $CDCl_3$ (1 mL) by adding *trans* G **29** (4.8 mg, 10.0 μmol) to the vial containing KI, sonicating for 1 h, and then stirring for 16 h. The vial was wrapped with aluminum foil to protect the reaction mixture from light. The resulting G_{16}-hexadecamer [G **29**]$_{16}$•3K$^+$3I$^-$ was confirmed by ^{1}H NMR and ESI-MS.

5.4.4 Small-Scale [2+2] Photocycloaddition Reaction of $[G27]_{16}•3K^{+}3I^{-}$

A G_{16}-quadruplex of $[G\ \mathbf{29}]_{16}•3K^{+}3I^{-}$(0.625 mM) was prepared as described in **Section 5.3.3**. The vial had the aluminum foil removed and was placed in a Rayonet RMR-600 photochemical reactor and irradiated using 300 nm wavelength bulbs. To analyze the [2+2] photocycloaddition reaction, aliquots were taken at t = 15 min, 30 min, 1 h, 3 h, 6 h, and 24 h, the solvent was removed, and the remaining residue was re-dissolved in DMSO-d_6 for ^{1}H-NMR analyses.

5.4.5 Transesterification of $[G\ 29]_{16}•3K^{+}3I^{-}$Photocyloaddition Product

Potassium iodide (68.7 mg, 0.41 mmol) was added to a 150-mL round-bottom flask containing $CHCl_3$ (41.0 mL). The flask was wrapped with aluminum foil to protect the reaction mixture from light until the sample was ready for irradiation. *Trans*-G **29** (0.200 g, 0.41 mmol) was added to the flask, sonicated for 1 h, and then stirred for 16 h to prepare a G-quadruplex solution (0.625 mM $[G\ \mathbf{29}]16•3K^{+}3I^{-}$). The flask had the foil removed and was placed in a Rayonet RMR-600 photochemical reactor and irradiated using 300 nm wavelength bulbs. This solution was irradiated for 24 h, after which time ^{1}H NMR analysis showed almost full conversion to 3. The reaction mixture was concentrated *in vacuo* and dissolved in MeOH (20

mL). Concentrated 12 M HCl (34 μL, 0.41 mmol) was added to the solution to bring the total concentration of HCl to 20 mM and the resulting solution was refluxed for 24 h, after which tlc analysis (95:5 CH_2Cl_2:CH_3OH) and ^1H NMR showed the reaction was complete. The solution was concentrated *in vacuo*, dissolved in $CHCl_3$ (10 mL) and washed with water (3 X 50 mL). The organic layer was isolated and concentrated *in vacuo*. Purification by column chromatography on silica gel (95:5 CH_2Cl_2:CH_3OH) afforded β-trux **47** as a yellow oil. (63.0 mg, 79.1 %).

^1H NMR (600 MHz, $CDCl_3$) δ: 7.10-7.02 (m, 2H, H7), 6.63 (ddd, *J*= 8.3, 2.6, 0.9 HZ, 2H,H8), 6.58 (ddd, *J*= 7.6, 1.7, 0.9 Hz, 2 H, H6), 6.46 (dd, *J* = 2.6, 1.7 Hz, 2H, H10), 4.40-4.35 (dd, *J*= 3.8, 2.2 Hz, 2H, H3), 3.86-3.78(m, *J*= 3.8, 2.2, 1.06 Hz, 2H, H4), 3.76 (s, 6H,H1), 3.64 (s, 6H, H11); ^{13}C NMR (125 MHz, $CDCl_3$) δ: 172.75 (C2), 159.30 (C9), 140.08 (C5), 128.94 (C7), 120.10 (C6), 113.56 (C8), 112.09 (C10), 55.03 (C3), 52.07 (C4), 44.86 (C1), 43.32 (C11) ; ESI-MS ($M+H^+$): 385.17 g mol^{-1}; EI-MS m/z 384.21 (M+,1); 192.14 (100); 161.11 (38), 113.06 (8).

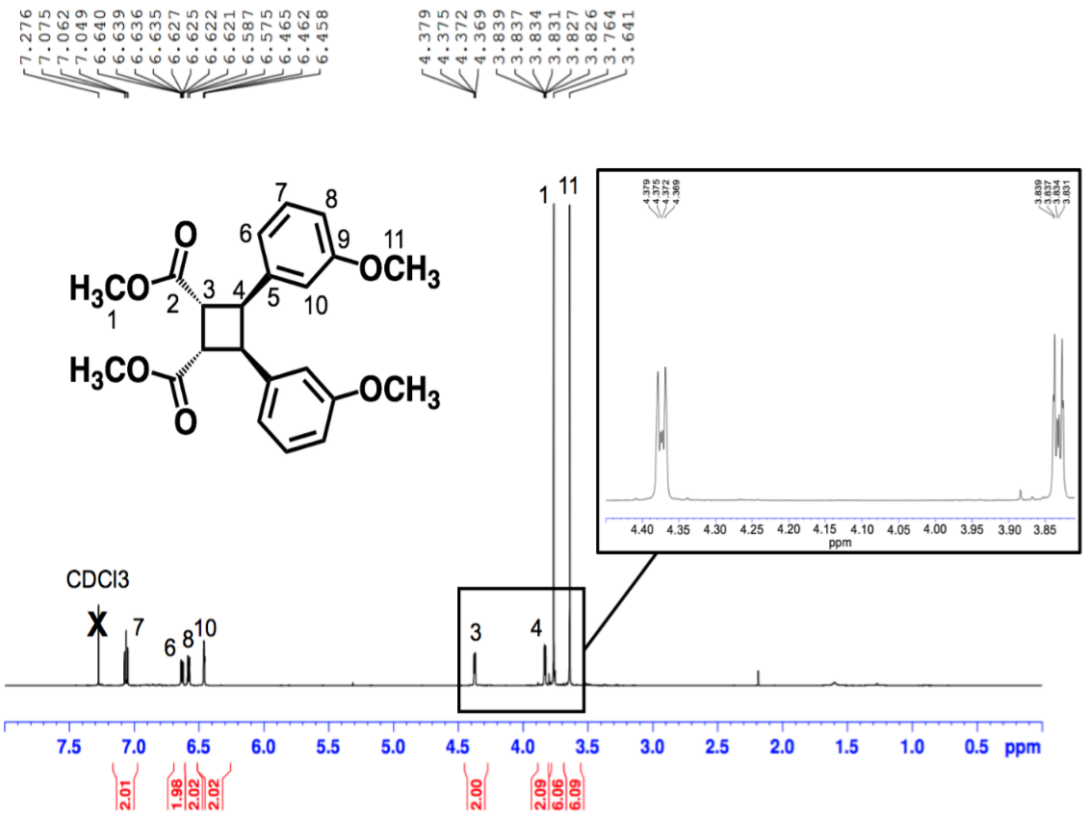

Figure 5.32. ^{1}H NMR of the transesterified cyclobutane products **47** formed during the photoreaction of [G **29**]$_{16}$•3K^{+}3I^{-} in $CDCl_3$. β-truxinate formed during the irradiation of [G **29**]$_{16}$•3K^{+}3I^{-}.

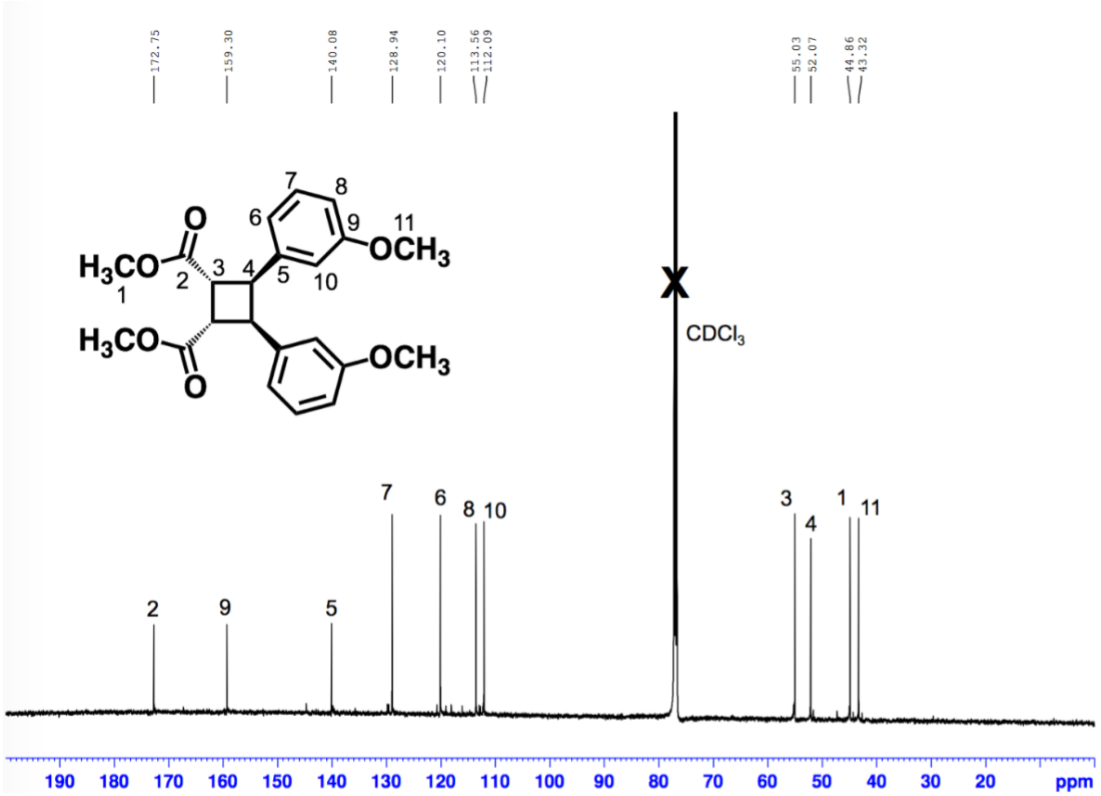

Figure 5.33. ^{1}H NMR of the transesterified cyclobutane products **47** formed during the photoreaction of [G **29**]$_{16}$•3K^{+}3I^{-} in $CDCl_3$.

5.4.6 Crystallization of Hexadecamer [G 29]$_{16}$•3K^{+}3I^{-}

A solution of [G **29**]$_{16}$•3K^{+}3I^{-} (0.313 mM) in $CDCl_3$ (0.5 mL) was prepared in a 4-mL vial. The vial was then placed, with the lid slightly unscrewed, into a clean jar that contained Et_2O (2 mL). The jar was capped and stored in a -6 ℃ freezer. Yellow, cube-shaped crystals formed after two weeks at -6 ℃. Subsequent X-ray analysis showed the crystals to be hexadecamer [G **29**]16•3K^{+}3I^{-}. The crystal structure is deposited at Cambridge Crystallographic Data Centre: CCDC #1869119.

5.4.7 [2+2] Photocycloaddition Reaction of [G 29]$_{16}$•3K$^+$3I$^-$ Using Sunlight as the UV-Source

A G$_{16}$-quadruplex of [G **29**]$_{16}$•3K$^+$3I$^-$(0.625 mM) was prepared as described in **Section 5.3.3**. The vial had the aluminum foil removed and was placed outside at the University of Maryland-College Park on May 3rd, 2018. The weather was clear with a predicted UV-Index of 8 for the Washington D.C. region. The irradiation took place from 11:00 AM to 5:00 PM. To analyze the [2+2] photocycloaddition reactions aliquots were taken at t = 15 min, 30 min, 60 min, 180 min, and 360 m, the solvent was removed, and the remaining residue was re-dissolved in DMSO-d$_6$ for ^{1}H-NMR analyses.

5.4.8 Experimental Section for Catalysis Experiments with Varying Amounts of KI

Samples were prepared with varying stoichiometric ratios of KI: *trans*-G **29** (1:1 KI: *trans*-G **29**, 1:64 KI: *tran*-G **29**, and 0:1 KI: *trans*-G **29**). An additional sample was prepared as a control that contained no added KI, *trans*-G **29 ,** and [2.2.2] cryptand to sequester cationic impurities. The sample vials were wrapped with aluminum foil to protect the reaction mixture from light until the samples were ready for irradiation. For each sample, *trans*-G **29** (193.4 mg, 0.400 mmol) was added to $CHCl_3$ (40 mL) in a 45-mL glass container. KI was weighed out on an analytical balance (1.0 mg, 6.25 μmol for 1:64 KI: *trans*-**G 29**; 66.4 mg, 400 μmol for 1:1 KI: *trans*-**G 29**) and added to the glass vial containing *trans*-**G 29**, sonicated for 1 h, and then stirred for 16 h. To the

control sample no KI was added, but instead [2.2.2] cryptand (2.1 g, 5.6 mmol) was added. The foil was removed and the vials were placed in a Rayonet RMR-600 photochemical reactor and irradiated using 300 nm wavelength bulbs. Reaction aliquots were taken out at 0 h, 6 h, 24 h, and 48 h, solvent evaporated and re-dissolved in DMSO-d_6 to monitor the reaction by ^{1}H NMR. The results are shown in **Figure 4.25**.

5.4.9 Sample Preparation for Elemental Analysis

Two samples were prepared and sent to Galbraith Laboratories for elemental analysis to determine if Na^+ and K^+ impurities were present due to sample handling and preparation. The elemental analysis that was performed used inductively coupled plasma atomic emission spectroscopy (ICP-AES). Sample 1 contained purified *trans* G **29** before any sample manipulation. It was placed in a 4-mL glass vial, wrapped in aluminum foil and shipped to Galbraith. Sample 2 was exposed to $CHCl_3$ and a "clean" 45 mL glass vial, similar to the vial that was used for catalysis experiments described above on page S35, to determine if the solvent or glassware used for the photoreactions introduces Na^+ and K^+ impurities. The manipulation procedure was as follows: a 10 mM solution of *trans*-G **29** (96.7 mg, 0.200 mmol) was prepared in 20 mL $CHCl_3$ in a 45 mL glass vial, sonicated for 1 h, and then stirred for 16 h. The solvent was evaporated and the samples were sent off for elemental analysis.

5.4.10 Computational Methods and Results

All optimizations on [G **29**]$_8$•K^+ and related structures were carried out using the 2-layer QM/MM ONIOM method,[1] as implemented in Gaussian09.[2] As depicted below in **Figure 5.37** the *high layer* region (QM portion) consisted of the 5′-(3-methoxycinnamoyl) sidechains containing the reactive C=C p bonds and this region was modeled using a DFT functional constructed to account for dispersion interactions (wB97XD)[3] with a 6-31g(d) basis. The *low layer* region (MM portion), which consisted of the G$_8$•K^+ octamer, was treated using a semi-empirical PM6 method.[4] Vibrational frequencies were computed at the same level to obtain enthalpic and free energy corrections at 298 K and to characterize the minima (zero imaginary frequencies). This QM/MM ONIOM method provided excellent agreement with X-ray structural information (see manuscript). To refine energetics, we carried out single-point energy calculations using the ONIOM method with hybrid DFT functionals for both low (rB3LYP/6-31G(d)) and high (rM06- 2X/6-31+G (d,p)) layers in a polarizable continuum solvent ($CHCl_3$) with CPCM as a solvation model,[5] to account for the condensed phase effects. Similar methods have been recently used to model related DNA G-quadruplexes.[6] Structural figures were generated using CLYview.[7]

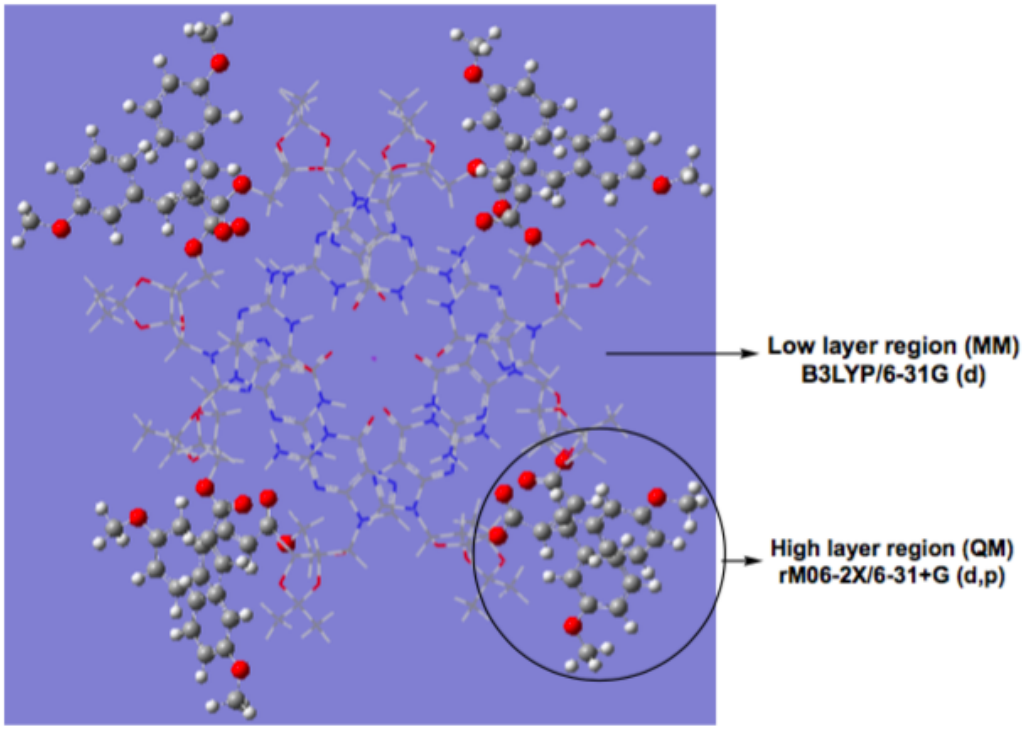

Figure 5.34. Illustration of how the QM/MM ONIOM method was applied to the computation of structure for [G **29**]$_8$•K^+I^-. The 5′-(3-methoxycinnamoyl) sidechains, circled and shown in ball and stick format, was used as the *high layer* region, with QM calculation being used. The [G **29**]$_8$•K^+I^- core, depicted in wireframe, was calculated as the *low layer* region, using molecular mechanics.

Computational Methods References:

1. (a) Chung, L. W.; Hirao, H.; Li, X.; Morokuma, K. WIREs Comput. Mol. Sci. 2012, 2, 327−350. (b) Vreven, T.; Byun, K. S.; Komáromi, I.; Dapprich, S.; Montgomery, J. A.; Morokuma, K.; Frisch, M. J. J. Chem. Theory Comput. 2006, 2, 815−826. (c) Vreven, T.; Morokuma, K. J. Comput. Chem. 2000, 21, 1419−1432. (d) Chung, L. W.; Sameera, W. M. C.; Ramozzi, R.; Page, A. J.; Hatanaka, M.; Petrova, G. P.; Harris, T. V.; Li, X.; Ke, Z.; Liu, F.; Li, H. B.; Ding, L.; Morokuma, K. Chem. Rev. 2015, 115, 5678−5796.

2. Gaussian 09, Revision E.01, M. J. Frisch, G. W. Trucks, H. B. Schlegel, G. E. Scuseria, M. A. Robb, J. R. Cheeseman, G. Scalmani, V. Barone, B. Mennucci, G. A. Petersson, H. Nakatsuji, M. Caricato, X. Li, H. P. Hratchian, A. F. Izmaylov, J. Bloino, G. Zheng, J. L. Sonnenberg, M. Hada, M. Ehara, K. Toyota, R. Fukuda, J. Hasegawa, M. Ishida, T. Nakajima, Y. Honda, O. Kitao, H. Nakai, T. Vreven, J. A. Montgomery, Jr., J. E. Peralta, F. Ogliaro, M. Bearpark, J. J. Heyd, E. Brothers, K. N. Kudin, V. N. Staroverov, T.Keith, R. Kobayashi, J. Normand, K. Raghavachari, A. Rendell, J. C. Burant, S. S. Iyengar, J. Tomasi, M. Cossi, N. Rega, J. M. Millam, M. Klene, J. E. Knox, J. B. Cross, V. Bakken, C. Adamo, J. Jaramillo, R. Gomperts, R. E. Stratmann, O. Yazyev, A. J. Austin, R. Cammi, C. Pomelli, J. W. Ochterski, R. L. Martin, K. Morokuma, V. G. Zakrzewski, G. A. Voth, P. Salvador, J. J. Dannenberg, S. Dapprich, A. D. Daniels, O. Farkas, J. B. Foresman, J. V. Ortiz, J. Cioslowski, and D. J. Fox, Gaussian, Inc., Wallingford CT, 2013.

3. Chai, J.-D.; Head-Gordon, M. J. Chem. Phys. 2008, 128, 084106

4. J. J. P. Stewart, J. Mol. Model. 2007, 13, 1173-1213.

5. Takano, Y.; Houk, K. N. J. Chem. Theory Comput. 2005, 1, 70-77. 6. K. Gkionis, H. Kruse, J. Sponer, J. Chem. Theory Comput. 2016, 12, 2000-2016 and references therein.

6. CYLview, 1.0b; Legault, C. Y., Université de Sherbrooke, 2009 (http://www.cylview.org)

References

1. Giorgi, T.; Grepioni, F.; Manet, I.; Mariano, P.; Masiero, S.; Mezzina, E.; Pierracini, S.; Saturni, L.; Spada, G.P.; Gottarelli, G. "Gel-Like Lyomesophases Formed in Organic Solvents by Self-Assembled Guanine Ribbons." *Chem. Eur. J.* **2002**, 8, 2143-2152.

2. Gellert, M.; Lipsett, M.N. Davies, D.R. "Helix Formation by Guanylic Acid." *Proc. N. A. S.* **1962**, 48, 2013-2018.

3. Fresco, J.R.; Massoulie, J. "Polynucleotides. V. Helix-Coil Transition of Polyriboguanylic Acid." *J. Am. Chem. Soc.* **1963**, 85, 1352-1353.

4. Pinnavaia, T.J. Marshall, C.L.; Mettler, C.M.; Fisk, C.L.; Miles, H.T.; Becker, E.D. "Alkali Metal Ion Specificity in the Solution Ordering of a Nucleotide, 5′-Guanosine Monophosphate." *J. Am. Chem. Soc.* **1978**, 100, 3625-3627.

5. Pinnavaia, T.J.; Miles, H.T.; Becker, E.D. "Self-Assembled 5′-Guanosine Monophosphate. Nuclear Magnetic Resonance Evidence for a Regular, Ordered Structure and Slow Chemical Exchange." *J. Am. Chem. Soc.* **1975**, 97, 7198-7200.

6. Gottarelli, G.; Masiero, S.; Spada, G.P. "Self-Assembly in Organic Solvents of Deoxyguanosine Derivative Induced by Alkali Metal Picrates." *Chem. Commun.* **1995**, 2555-2557.

7. Davis, J.T. Tirumala, S.; Jensen, J.R.; Radler, E.; Fabris, D. "Self-Assembled Ionophores from Isoguanosine." *J. Org. Chem.* **1995**, 60, 4167-4176.

8. Monchaud, D.; Teulade-Fichou, M. "A Hitchhiker's Guide to G-Quadruplex Ligands." *Org. Biomol. Chem.* **2008**, 6, 627-636.

9. Balasubramanian, S.; Hurley, L.H.; Neidle, S. "Targeting G-Quadruplexes in Gene Promoters: A Novel Anticancer Strategy?" *Nat. Rev. Drug Discov.* **2011**, 10, 261-275.

10. Ohnmacht, S.A.; Neidle, S. "Small-Molecule Quadruplex-Targeted Drug Discovery." *Biorg. Med. Chem. Lett.* **2014**, 24, 2602-2612.

11. Rhodes, D.; Lipps, H.J.; "G-Quadruplexes and Their Regulatory Roles in Biology." *Nucleic Acids. Res.* **2015**, 43, 8627-8637.

12. Rastogi, S.; Zhang, D.; Davis, J.T. "The Natural Product Prodigiosin Binds G-Quadruplex DNA." *Supramol. Chem.* **2015**, 28, 18-28.

13. Wu, G.; Kwan, I.C.M. "Helical Structure of Disodium 5′-Guanosine Monophosphate Self-Assembly in Neutral Solution." *J. Am. Chem. Soc.* **2006**, 131, 3180-3182.

14. Mudronova, K.; Rimal, V.; Mojzes, P. "Effect of Ribose Versus 2′-Deoxyribose Residue in Guanosine 5′-Monophosphates on Formation of G-Quartets Stabilized by Potassium and Sodium Cations." *Vibration Spectroscopy.* **2015**, 82, 60-65.

15. Zhang, Z.; Kim, S.; Gaffney, B.L.; Jones, R.A. "Polymorphism of the Signaling Molecule c-di-GMP." *J. Am. Chem. Soc.* **2006**,128, 7015-7024.

16. Phan, A.T.; Kuryavyi, V.; Luu, K.N.; Patel, D.J. Neidle, S.; Balusabramanian, S. "Structural Diversity of G-Quadruplex Scaffolds." *Quadruplex Nucleic Acids,* **2006**, Cambridge, UKRSC publishing (pg.81-99)

17. Phan, A.T.; Kuryavyi, V.; Burge, S.; Neidle, S.; Patel, D. "Structure of an Unprecedented G-Quadruplex Scaffold in the Human *c-kit* Promoter." *J. Am. Chem. Soc.* **2007**, 129, 4386-4392.

18. Phan, A.T.; Kuryavyi, V.; Luu, K.N.; Patel, D.J. "Structure of Two Intramolecular G-Quadruplexes Formed by Natural Human Telomere Sequences in K^+ Solution." *Nucleic Acids Res.* **2007**, 35, 6517-6525.

19. Lu, K.N.; Phan, A.T.; Kuryavyi, V.; Lacroix, L.; Patel, D.J. "Structure of the Human Telomere in K^+ Solution: An Intramolecular (3+1) G-Quadruplex Scaffold." *J. Am. Chem. Soc.* **2006**, 128, 9963-9970.

20. Adrian, M.; Heddi, B.; Phan, A.T. "NMR Spectroscopy of G-Quadruplexes." *Methods*, **2012**, 57, 11-24.

21. McCallum, J.; Amare, S.; Nolan, R. "G-Octamer Formation from N^9-Modified Guanine Derivatives." *Nucleosides, Nucleotides, and Nucleic Acids.* **2010**, 29, 801-808.

22. Ghoussoub, A.; Lehn, J. "Dynamic Sol-Gel Interconversion by Reversible Cation Binding and G-Quartet Based Supramolecular Polymers." *Chem. Commun.* **2005**, 5763-5765.

23. Gubala, V.; Betancourt, J.; Rivera, J.M. "Expanding the Hoogsteen Edge of a 2′-Deoxyguanosine: Consequences for G-Quadruplex Formation." *Org. Lett.* **2004**, 6, 4735-4738.

24. Garcia-Arriaga, M.; Hobley, G.; Rivera, J.M. "Structural Studies of Supramolecular G-Quadruplexes Formed from 8-Aryl-2′-Deoxyguanosine Derivatives." *J. Org. Chem.* **2016**, 81, 6026-6035.

25. Gubala, V.; Rivera-Sanchez, M.C.; Hobley, G.; Rivera, J.M. "The Impact of 8-Aryl- and 8-Heteroaryl-2′-Deoxyguanosine Derivatives on G-Quadruplex Formation." *Nucleic Acid Symposium Series.* **2007**, 51, 39-40.

26. He, Y.; Zhang, Y.; Wojtas, L.; Akhmedov, N.G.; Thai, D.; Wang, H. ; Li, X.; Guo, H.; Shi, X. "Construction of a Cross-Layer Linked G-Octamer *via* Conformational Control: A Stable G-Quadruplex in H-Bond Competitive Solvents." *Chem. Sci.* **2019**, advanced article.

27. Kaucher, M.S.; Davis, J.T. "N2, C8-Disubstituted Guanosine Derivatives Can Form G-Quartets." *Tetrahedron Lett.* **2006**, 47, 6381-6384.

28. Martic, S.; Liu, X.; Wang, S.; Wu, G. "Self-Assembly of N^2-Modified Guanosine Derivatives: Formation of Discrete Octamers." *Chem. Eur. J.* **2008**, 14, 1196-1204.

29. Davis, J.T.; Spada, G.P. "Supramolecular Architectures Generated by Self-Assembly of Guanosine Derivatives." *Chem. Soc. Rev.* **2007**, 36, 296-313.

30. Peters, G.M.; Skala, L.P.; Plank, T.N.; Hyman, B.J.; Reddy, G.N.M.; Marsh, A.; Brown, S.P.; Davis, J.T. "A G_4•K^+ Hydrogel Stabilized by an Anion". *J. Am. Chem. Soc.* **2014**, 136, 12596-12599.

31. Peters, G.M.; Skala, L.P.; Plank, T.N.; Oh, H.; Reddy, G.N.M.; Marsh, A.; Brown, S.P.; Raghavan, S.R.; Davis, J.T. "G4-Quartet•M^+ Borate Hydrogels." *J. Am. Chem. Soc.* **2015**, 137, 5819-5827.

32. Xiao, S.; Davis, J.T. "A G_4•K^+ Hydrogel Made from 5′-Hydrazinoguanosine for Remediation of α,β-Unsaturated Carbonyls." *Chem. Commun.* **2018**, 54, 11300-11303.

33. Sutyak, K.B.; Zavalij, P.Y.; Robinson, M.L.; Davis, J.T. "Controlling Molecularity and Stability of Hydrogen Bonded G-Quadruplexes by Modulating the Structures Periphery." *Chem. Commun.* **2016**, 52, 11112-11115.

34. Sen, D.; Gilbert, W. "A Sodium-Potassium Switch in the Formation of Four-Stranded G4-DNA." *Nature*. **1990**, 344, 410-414.

35. Ma, L.; Iezzi, M.; Kaucher, M.S.; Lam, Y.; Davis, J.T. "Cation Exchange in Lipophilic G-Quadruplexes: Not All Ion Binding Sites are Equal." *J. Am. Chem. Soc.* **2006**, 128, 15269-15277.

36. Bhattachryya, D.; Arachilage, G.M.; Basu, S. "Metal Cations in G-Quadruplex Folding and Stability." *Front. Chem.* **2016**, 38, 1-14.

37. Shi, X.; Fettinger, J.C.; Davis, J.T. "Ion-Pair Recognition by Nucleoside Self-Assembly: Guanosine Hexadecamers Bind Cations and Anions." *Angew. Chem. Int. Ed.* **2001**, 40, 2827-2831.

38. Chen, F. "Sr^{2+} Facilitate Intramolecular G-Quadruplex Formation of Telomeric Sequences." *Biochem.* **1992**, 31, 3769-3776.

39. Martin-Hidalgo, M.; Rivera, J.M. "Metallo-Responsive Switching Between Hexadecameric and Octameric Supramolecular G-Quadruplexes." *Chem. Commun.* **2011**, 47, 12485-12487.

40. Shi, X.; Fettinger, J.C.; Davis, J.T. "Homochiral G-Quadruplexes with Ba^{2+} but Not with K^{+}: The Cation Programs Enantiomeric Recognition." *J. Am. Chem. Soc.* **2001**, 123, 6738-6739.

41. Kotch, F.W.; Fettinger, J.C.; Davis, J.T. "A Lead-Filled G-Quadruplex: Insight into the G-Quartet's Selectivity for Pb^{2+} over K^{+}." *Org. Lett.* **2000**, 2, 3277-3280.

42. Basu, S.; Szewczak, A.A.; Cocco, M.; Strobel, S.A. "Direct Detection of Monovalent Metal Ion Binding to a DNA G-Quartet by ^{205}Tl NMR." *J. Am. Chem. Soc.* **2000**, 122, 3240-3241.

43. Gill, M.L.; Strobel, S.A.; Loria, J.P. "Crystalization and Characterization of the Thallium Form of the *Oxytrychia nova* G-Quadruplex." *Nucleic Acids Res.* **2006**, 34,4506-4514.

44. Kwan, I.C.M.;She, Y.; Wu, G. "Trivalent Lanthanide Metal Ions Promote Formation of Stacking G-Quartets." *Chem. Commun.* **2007**, 4286-4288.

45. Galezowska, E.; Gluszynska, A.; Juskowiak, B. "Luminescence Study of G-Quadruplex Formation in the Presence of Tb^{3+} Ion." *J. Inorg. Biochem.* **2007**, 101, 678-685.

46. Shi, X.; Mullaugh, K.M.; Fettinger, J.C.; Jiang, Y.; Hofstadler, S.A.; Davis, J.T. "Lipophilic G-Quadruplexes are Self-Assembled Ion Pair Receptors and the Bound Anion Modulates the Kinetic Stability of these Compounds." *J. Am. Chem. Soc.* **2003**, 125, 10830-10841.

47. Davis, J.T.; Kaucher, M.S.; Kotch, F.W.; Iezzi, M.A.; Clover, B.C.; Mullaugh, K.M. "Kinetic Control in Non-Covalent Synthesis: Regioselective Ligand Exchange in a Hydrogen Bonded Assembly." *Org. Lett.* **2004**, 6, 4265-4268.

48. González-Rodríguez, D.; van Dongen, J.L.V.; Lutz, M.; Spek, A.L.; Schenning, A.P.H.J.; Meijer, E.W. "G-Quadruplex Self-Assembly Regulated by Coulombic Interactions." *Nature Chem.* **2009**, 1, 151-155.

49. Fadaei, E.; Martín-Arroyo, M.; Tafazzoli, M.; González-Rodríguez, D. "Thermodynamic and Kinetic Stabilities of G-Quadruplexes in Apolar Solvents." *Org. Lett.* **2017**, 19, 460-463.

50. Dingley, A.J.; Peterson, R.D.; Grzesiak, S.; Feigon, J. "Characterization of the Cation and Temperature Dependence of DNA G-Quadruplex Hydrogen Bond Properties Using High-Resolution NMR." *J. Am. Chem. Soc.* **2005**, 127, 14466-14472.

51. Rachwal, P.A.; Fox, K.R. "Quadruplex Melting." *Methods*, **2007**, 43, 291-301.

52. Harraz, D.M.; Davis, J.T. "A Self-Assembled Peroxidase from 5′-GMP and Heme." *Chem. Commun.* **2018**, 54, 1587-1590.

53. Travascio, P.; Li, Y.; Sen, D. "DNA-Enhanced Peroxidase Activity of a DNA Aptamer-Hemin Complex." *Chem. Biol.* **1998**, 5, 505-517.

54. Poon, L.C.; Methot, S.P.; Morabi-Pazooki, W.; Pio, F.; Bennet, A.J.; Sen, D. "Guanine Rich-RNAs and DNAs that Bind Heme Robustly Catalyze Oxygen Transfer Reactions." *J. Am. Chem. Soc.* **2011**, 133, 1877-1884.

55. Golub, E.; Freeman, R.; Willner, I. "Hemin/G-Quadruplex-Catalyzed Aerobic Oxidation of Thiols to Disulfides: Application of the Process for the Development of Sensors and Aptasensors and for Probing Acetylcholine Esterase Activity." *Anal. Chem.* **2013**, 85, 12126-12133.

56. Roe, S.; Ritson, D.J.; Garner, T.; Searle, M.; Moses, J.E. "Tunable DNA-Based Asymmetric Catalysis Using a G-Quadruplex Supramolecular Assembly." *Chem. Commun.* **2010**, 46, 4309-4311.

57. Cheng, M.; Li, Y.; Zhou, J.; Jia, G.; Lu, S.; Yang, Y.; Li, C. "Enantioselective Sulfoxidation Reaction Catalyzed by a G-Quadruplex Metalloenzyme." *Chem. Commun.* **2016**, 52, 9644-9647.

58. Wang, C.; Jia, G.; Zhou, J.; Li, Y; Liu, Y.; Lu, S.; Li, C. "Enantioselective Diels-Alder Reactions with G-Quadruplex DNA-Based Catalysts." *Angew. Chem. Int. Ed.* **2012**, 51, 9352-9355.

59. Tang, Z.; Gonçalves, D.P.N.; Wieland, M.; Marx, A.; Hartig, J.S. "Novel DNA Catalysts Based on G-Quadruplex Recognition." *ChemBioChem* .**2008**, 9, 1061-1064.

60. Wang, C.; Li, Y.; Jia, G.; Liu, Y.; Lu, S.; Li, C. "Enantioselective Friedel-Crafts Reactions in Water Catalyzed by a Human Telomeric G-Quadruplex Metalloenzyme." *Chem. Commun.* **2012**, 48, 6232-6234.

61. Kaucher, M.S.; Harrel, W.A.; Davis, J.T. "A Unimolecular G-Quadruplex that Functions as a Synthetic Transmembrane Na^+ Transporter." *J. Am. Chem. Soc.* **2005**, 128, 38-39.

62. Rivera, J.M.; Silva-Brenes, D. "A Photoresponsive Supramolecular G-Quadruplex." *Org. Lett.* **2013**, 15, 2350-2353.

63. Sutyak, K.B.; Lee, W.; Zavalij, P.Y.; Gutierrez, O.; Davis, J.T. "Templating and Catalyzing [2+2] Photocycloadditions in Solution Using a Dynamic G-Quadruplex." *Angew. Chem. Int. Ed.* **2019**, 57, 17146-17150.

64. Sreenivasachary, N.; Lehn, J.M. "Gelation-Driven Component Selection in the Generation of Constitutional Dynamic Hydrogels Based of Guanine Quartet Formation" *Proc. Natl. Acad. Sci. U. S. A.* **2005**, 102, 5938.

65. Likhitsup, A.; Yu, S.; Ng,Y.H.; Chai, C.L; Tam, E.K.W. "Controlled Polymerization and Self-Assembly of a Supramolecular Star Polymer with a Guanosine Quadruplex Core." *Chem. Commun.* **2009**, 4070.

66. Abet, V.; Evans, R.; Guibbal, F.; Caldarelli, S.; Rodriguez, R. "Modular Construction of Dynamic Nucleodendrimers." *Angew. Chem., Int. Ed.* **2014**, 53, 4862.

67. Nikan, M.; Sherman, J.C. "Template –Assembled Synthetic G-Quartets (TASQs)." *Angew. Chem. Int. Ed.* **2008**, 47, 4900.

68. Murat, P.; Cressend, D.; Spinelli, N.; Van der Heyden, A; Labb, P.; Dumy, P.; Defrancq, E. "A Novel Conformationally Constrained Parallel G Quadruplex." *ChemBioChem.* **2008**, 9, 2588.

69. Stefan, L.; Guedin, A; Amrane, S.; Smith, N.; Denat, F.; Mergny, J.L.; Monchaud, D. “DOTASQ as a Prototype of Nature-Inspired G-Quadruplex Ligand.” *Chem. Commun.* **2011**, 47, 4992

70. Masiero, S.; Gottarelli, G.; Pieraccini, S.”G-Quartets as a Self-Assembled for Circular Porphyrin Arrays.” *Chem. Commun.* **2000**, 1995.

71. Graziano, C.; Masiero, S.; Pieraccini, S.; Lucarini, M.; Spada, G.P. “A Cation-Directed Switch of Intermolecular Spin-Spin Interactions of Guanosine Derivatives Functionalized with Open-Shell Units.” *Org. Lett.* **2008**, 10, 1739.

72. Spada, G.P; Lena,S.; Masiero,S.; Pieraccini, S.; Surinand, M.; Samori,P. “Guanosine-Based Hydrogen-Bonded Scaffolds: Controlling the Assembly of Oligothiophenes.” *Adv. Mater.* **2008**, 20, 2433.

73. Kumar, Y.P; Das, R.N.; Kumar, S.; Schutte, O.M.; Steinem, C.; Dash, J. “Triazole-Tailored Guanosine Dinucleosides as Biomimetic Ion Channels to Modulate Transmembrane Potential.” *Chem. – Eur. J.* **2014**, 20, 3023.

74. Ma, L.; Melegari, M.; Colombini, M.; and Davis, J.T. “Large and Stable Transemembrane Pores from Guanosine-Bile Acid Conjugates.” *J. Am. Chem. Soc.* **2008**, 130, 2938.

75. Forman, S.L; Fettinger, J.C.; Pieraccini, S.; Gottarelli, G.; Davis, J.T. “Toward Artificial Ion Channels: A Lipophilic G-Quadruplex.” *J. Am. Chem. Soc.* **2000**, 122, 4060.

76. Wong, A.; Fettinger, J.C.; Forman, S.L.; Davis; J.T.; Wu, G. “The Sodium Ions Inside a Lipophilic G-Quadruplex Channel as Probed by Solid-State 23Na NMR.” *J. Am. Chem. Soc.* **20**02, 124, 742.

77. Mammen, M.; Simanek, E.E.; Whitesides, G.M. “Predicting the Relative Stabilities of Multiparticle Hydrogen-Bonded Aggregates Based on the Number of Hydrogen Bonds and the Number of Particles and Measuring these Stabilities with Titrations Using Dimethyl Sulfoxide.” *J. Am. Chem. Soc.* **1996**, 118, 12614.

78. Yang, L.; Brazier, J.B.; Hubbard, T.A.; Rogers, D.M.; Cockroft, S.L. "Can Dispersion Forces Govern Aromatic Stacking in an Organic Solvent?" *Angew. Chem., Int. Ed.* **2016**, 55, 912.

79. Patrick, C.R.; Prosser, G.S. "A Molecular Complex of Benzene and Hexafluorobenzene." *Nature.* **1960**, 187, 1021-1021.

80. Wheeler, S.E. "Local Nature of Substituent Effects in Stacking Interactions." *J. Am. Chem. Soc*. **2011**, 133, 10262-10274.

81. West, A.P.; Mecozzi, S.; Dougherty, D.A. "Theoretical Studies of the Supramolecular Synthon Benzene • • • Hexafluorobenzene." *J. Phys. Org. Chem.* **1997**, 10, 347-350.

82. Tsuzuki, S.; Uchimaru, T.; Mikami, M. "Intermolecular Interactions between Hexafluorobenzene and Benzene: Ab Initio Calculations Including CCSD(T) Level Electron Correlation Correction." *J. Phys. Chem. A*. **2006**, 110, 2027-2033.

83. Cohen, M.D.; Schmidt, G.M.J. "Topochemistry. I. A Survey." *J. Chem. Soc.* **1964**, 1996-2000.

84. Schmidt, G.M.J."Topochemistry. III. The Crystal Chemistry of Some Trans-Cinnamic Acids." *J. Chem. Soc.* **1964**, 2014-2021.

85. Poplata, S.; Tröster, A.; Zou, Y.Q.; Bach, T. "Recent Advances in the Synthesis of Cyclobutanes by Olefin [2+2] Photocycloaddition Reactions." *Chem. Rev.* **2016**, 116, 9748-9756.

86. Dembitsky, V.M. "Bioactive Cyclobutane-Containing Alkaloids." *J. Nat. Med.* **2008**, 62, 1-33.

87. Hanley, A.B.; Russel, W.R.; Chesson, A. "Formation of Substituted Truxillic and Truxinic Acids in Plant Cell Walls." *Phytochem*. **1993**, 33, 957.

88. Carnachan, S.M.; Harris, P. "Ferulic Acid is Bound to the Primary Cell Walls of all Gymnosperm Families." *Biochem. Sys. Eco.* **2000**, 28, 865.

89. 89) Nakamura, M.; Chi, Y.; Yan, W.; Yonezowa, A.; Nakasugi, Y.; Yoshizawa, T.; Hashimoto, F.; Kinjo, J.; Nohara, T.; Sakurada, S. "Structure-Antinociceptive Activity Studies of Incarvillateine a Monoterpene Alkaloid from Incarvillea Sinensis." *Planta Med.* **2001**, 67, 114.

90. Carmignani, M.; Volpe, A.R.; Monache, F.D.; Botta, B.; Espinal, R.; De Bonnevaux, S.C.; De Luca, C.; Botta, M.; Corelli, F.; Tafi, A.; Ripanti, G.; Monache, G.D. "Novel Hypotensive Agents from Verbesin caracasana. 6. Synthesis and Pharmacology of Caracasandiamide." *J. Med. Chem*. **1999**, 42, 3116.

91. Tsai, I; Lee, F.; Wu, C.; Duh, C.; Ishikawa, T.; Chen, J.; Chen, Y.; Seki, H.; Chen, I. "New Cytotoxic Cyclobutanoid Amides, a New Furanoid Lignan and Anti-Platelet Aggregation Constituents from Piper arborescens." *Planta Med.* **2005**, 71, 535.

92. Fujiwara, A.; Nishi, M.; Yoshida, S.; Hasegawa, M.; Yasuma, C.; Ryo, A.; Suzuki, Y. "Eucommicin A, a β-truxinate Lignan from Euccomia ulmoides, is a Selective Inhibitor of Cancer Stem Cells." *Phytochem.* **2016**, 122, 139.

93. MacGillvray, L.R. "Organic Synthesis in the Solid-State via Hydrogen-Bond-Drive-Self-Assembly." *J. Org. Chem.* **2008**, 73, 3311-3317.

94. 94) Coates, G.W.; Dunn, A.R.; Henling, L.M.; Ziller, J.W.; Lobkovsky, E.B.; Grubbs, R.B. "Phenyl-Perfluorophenyl Stacking interactions: Topochemical [2+2] Photodimerization and Photopolymerization of Olefinic Compounds." *J. Am. Chem. Soc.* **1998**, 3641-3649.

95. Sharma, C.V.K.; Panneerselvam, K.; Shimoni, L.; Katz, H.; Carrel, H.L.; Desiraju, G.R. "3-(3',5'-Dinitrophenyl)-4-(2',5'-Dimethoxyphenyl)Cyclobutane- 1,2-Dicarboxylic Acid: Engineered Topochemical Synthesis and Molecular and Supramolecular Properties." *Chem. Mater.* **1994**, 6, 1282-1292.

96. Ito, Y.; Borecka, B.; Trotter, J.; Scheffer, J.R.; "Control of Solid-State Photodimerization of trans-Cinnamic Acid by Double Salt Formation with Diamines." *Tet. Lett.* **1995**, 36, 6083-6086.

97. Zitt, H.; Dix, I.; Hopf, H; Jones, P.G. "4,15-Diamino[2.2]Paracyclophane, A Reusable Template for Topochemical Reaction Control in Solution." *Eur. J. Org. Chem.* **2002**, 2298-2307.

98. Ghosn, M.W.; Wolf, C. "Stereocontrolled Photodimerization with Congested 1,8-Bis(4′-Anilino)Napthalene Templates." *J. Org. Chem.* **2010**, 75, 6653-6659.

99. Yuasa, H.; Nakatani, M.; Hashimoto, H. "Exploitation of Sugar Ring Flipping for a Hinge-Type Tether Assisting a [2+2]Cycloaddition." *Org. Biomol. Chem.* **2006**, 4, 3694-3702.

100. Bibal, B.; Mongin, C.; Bassani, D.M. "Template Effects and Supramolecular Control of Photoreactions in Solution." *Chem. Soc. Rev*. **2014**, 43, 4179-4198.

101. Pattabiraman, M.; Kaanumalle, L.S.; Natarajan, A.; Ramamurthy, V. "Regioselective Photodimerization of Cinnamic Acids in Water: Templation with Cucurbiturils." *Langmuir.* **2006**, 22- 7605-7609.

102. Pattabiraman, M.; Natarajan, A.; Kaanumalle, L.S.; Ramamurthy, V. "Templating Photodimerization of Trans-Cinnamic Acids with Cucurbit[8]uril and γ-Cyclodextrin." *Org. Lett.* **2005**, 7, 529-532.

103. Karthikeyan, S.; Ramamurthy, V. "Templating Photodimerization of Trans-Cinnamic Acid Esters with a Water-Soluble Pd Nanocage." *J.Org. Chem.* **2007**, 72, 452-458.

104. Beak, P.; Ziegler, J.M. "Molecular Organization by Hydrogen Bonding: Juxtaposition of Remote Double Bonds for Photocyclization in a 2-Pyridone Dimer." *J. Org. Chem.* **1981**, 46, 619-624.

105. Bassani, D.M.; Darcos, V.; Mahony, S.; Desvergne, J. "Supramolecular Catalysis of Olefin [2+2] Photodimerization." *J. Am. Chem. Soc.* **2000**, 122, 8795-8796.

106. Telmesani, R.; Park, S.H.; Lynch-Colameta, T., Beeler, A. "[2+2] Photocycloaddition of Cinnamates in Flow and Development of Thiourea Catalyst." *Angew. Chem. Int. Ed.* **2015**, 54, 11521-11525.

107. Kaucher, M.S.; Lam, Y.; Pieraccini, S.; Gottarelli, G.; Davis, J.T. "Using Diffusion NMR to Characterize Guanosine Self-Association: Insights into Structure and Mechanism." *Chem. Eur. J.* **2005**, 11, 164-173.

108. Pagire, S.K.; Hossain, A.; Traub, L.; Kerris, S.; Reiser, O. "Photosensitized Regioselective [2+2] Cycloaddition of Cinnamates and Related Alkenes." *Chem. Commun.* **2017**, 53, 12072-12075.

109. Lei, T.; Zhou, C.; Huang, M.; Zhao, L.; Yang, B.; Ye, C.; Xiao, H.; Meng, Q.; Ramamurthy, V.; Tung, C.; Wu, L. "General and Efficient Intermolecular [2+2] Photodimerization of Chalcones and Cinnamic Acid Derivatives in Solution Through Visible-Light Catalysts." *Angew. Chem. Int. Ed.* **2017**, 56, 15407-15410.

110. Telmesani, R.; White, J.A.H.; Beeler, A.B. "Liquid-Liquid Slug-Flow-Accelerated [2+2]Photocycloaddition of Cinnamates." *ChemPhotochem.* **2018**, 2, 865-869.

111. D'Auria, M.; Vantaggia, A. "Photochemical Dimerization of Methoxy Substituted Cinnamic Acid Methyl Esters." *Tetrahedron.* **1992**, 48, 2523-2528.

112. Lei, T.; Zhou, C.; Wei, X.; Yang, B.; Chen, B.; Tung, C.; Wu, L.; "Construction of Cyclobutanes by Multicomponent Cascade Reactions in Homogeneous Solution Through Visible-Light Catalysis." *Chem. Eur. J.* **2019**, 25, 879-884.

113. Beves, J.E.; Blight, B.A.; Campbell, C.J.; Leigh, D.A.; McBurney, R.T. "Strategies and Tactics for the Metal-Directed Synthesis of Rotaxanes, Knots, Catenanes, and Higher Order Links." *Angew. Chem. Int. Ed.* **2011**, 50, 9260-9327.

114. Wang, W.; Wang, Y.X..; Yang, H. "Supramolecular Transformations Within Discrete Coordination-Driven Supramolecular Architectures." *Chem. Soc. Rev.,* **2016**, 45, 2656-2693.

115. Pederson, C.J. "Cyclic Polyethers and Their Complexes with Metal Salts." *J. Am. Chem. Soc.* **1967**, 89, 7017-7036.

116. Dietrich-Buchecker, C.O.; Sauvage, J.P. "A Novel Family of Molecules-The Metallocatenanes." *Tetrahedron Lett.* **1983**, 24, 5095-5098.

117. Neuhaus, P.; Cnossen, A.; Gong, J.Q.; Herz, L.M.; Anderson, H.L. ”A Molecular Nanotube with Three-Dimensional π-Conjugation.” *Angew. Chem. Int. Ed.* **2015**, 54, 7344-7348.

118. Cohen, M.D.; Schmidt, G.M.J. “Topochemistry. II. The Photochemistry of Trans-Cinnamic Acids.” *J. Chem. Soc.* **1964**, 2000-2013.

119. Gan, M.; Yu, J.; Wang, Y.; Han, Y. “Template-Directed Photochemical [2 + 2] Cycloaddition in Crystalline Materials: A Useful Tool to Access Cyclobutane Derivatives.” *Cryst. Growth Des.* **2018**, 18, 533-565.

120. Su, D.G.T.; Fang, H.; Gross, M.L. Taylor, J.A. “Photocrosslinking of Human Telomeric G-Quadruplex Loops by Anti Cyclobutane Thymine Dimer Formation.” *PNAS*. **2009**, 106, 12861-12866.

121. Lena, S.; Neviani, P.; Masiero, S.; Pieraccini, S.; Spada, G.P. Triggering of Guanosine Self-Assembly by Light. *Angew. Chem. Int. Ed.* **2010**, 49, 3657-3660.

122. Chung, L.W.; Sameera, W.M.C.; Ramozzi, R.; Page, A.J.; Hatanaka, M.; Petrova, G.P.; Harris, T.V.; Li, X.; Ke, Z.; Liu, F.; Li, H.; Ding, L.; Morokuma, K. “The ONIOM Method and Its Applications.” *Chem. Rev.* **2015**, 115, 12, 5678-5796.

123. Chai, J.; Head-Gordon, M. ”Long-Range Corrected Hybrid Density Functional Theory Functionals with Damped Atom-Atom Dispersion Corrections.” *Phys. Chem. Chem. Phys.,* **2008**, 10, 6615-6620.

124. Stewart, J.J.P. “Optimization of Parameters for Semi-Empirical Methods V. Modification of NDDO Approximations and Applications to 70 Elements.” *J. Mol. Model.* **2007**, 13, 1173-1213.

125. Gkionis, K.; Kruse, H.; Sponer, J. “ Derivation of Relaible Geometries in QM Calculations of DNA Structures: Explicit Solvent QM/MM and Restrained Implicit Solvent QM Optimizations of G-Quadruplexes.” J. *Chem. Theory Comput.* **2016**, 12, 2000−2016.

126. Ho, J.; Newcomer, M.B; Ragain, C.M.; Gascon, J.A.; Batista, E.R.; Loria, J.P; Batista, V.S. "MoD-QM/MM Structural Refinement Method: Characterization of Hydrogen Bonding in the Oxytricha nova G-Quadruplex" *J. Chem. Theory Comput*. **2014**, 10, 5125-5135.

127. Masiero, S.; Trotta, R.; Pieraccini, S.; De Tito, S.; Perone, R.; Randazzo, A.; Spada, G.P. "A non-empirical chromophoric interpretation of CD spectra of DNA G-quadruplex structures" *Org. Biomol. Chem.* **2010**, 8, 2683-2692.

128. M. Marusic, J. Plavec, "The Effect of DNA Sequence Directionality on G-Quadruplex Folding" *Angew. Chem. Int. Ed.* **2015**, 54, 11171-11179.